2014

Contributions to the understanding of harmonics, flicker and voltage unbalance management in future electricity distribution networks

Devinda Perera
University of Wollongong

School of Electrical, Computer and Telecommunication Engineering

Contributions to the Understanding of Harmonics, Flicker and Voltage Unbalance Management in Future Electricity Distribution Networks

Devinda Perera, BSc(Eng)

Supervisors

Prof. Sarath Perera, Dr. Philip Ciufo & Dr. Lasantha Meegahapola

This thesis is presented as part of the requirements for the

Award of the Degree of

Doctor of Philosophy

of the

University of Wollongong

March 2014

Dedicated to my parents...

Certification

I, Devinda Perera, declare that this thesis, submitted in fulfilment of the requirements for the award of Doctor of Philosophy, in the School of Electrical, Computer and Telecommunications Engineering, University of Wollongong, is entirely my own work unless otherwise referenced or acknowledged. This manuscript has not been submitted for qualifications at any other academic institute.

Devinda Perera

Date: 31 March 2014

Abstract

The connection of electromagnetically disturbing installations, including new forms of generating systems, to power distribution networks continue to increase. As a result, managing the network electromagnetic compatibility (EMC) within stipulated limits has become a major challenge to distribution network service providers (DNSPs). Therefore, the availability of a set of guidelines and recommendations based on well researched engineering practices would facilitate DNSPs in the provision of adequate supply quality to customers connected to the distribution networks. Accordingly, the International Electrotechnical Committee (IEC) has released a series of standards and technical reports to address the management of EMC in distribution networks.

Despite the availability of these standards and technical reports, there remain inadequacies in these documents as well as gaps in the existing knowledge in relation to management of EMC, where further refinements and contributions are required. These inadequacies and gaps must be addressed in order for DNSPs to properly manage EMC in distribution networks.

The low frequency EMC concerns addressed in this Thesis include harmonics, voltage fluctuations and flicker, and voltage unbalance (VU). The focus of this Thesis is to investigate the management of these key EMC issues in future distribution networks.

The recently published IEC Technical Report IEC 61000-3-14, provides power quality (PQ) emission limits for large disturbing installations connected to low voltage (LV) distribution networks. Noting that harmonic voltages in networks arise due to both large installations and smaller installations (whose harmonic current emission levels are governed by equipment standards), IEC 61000-3-14 proposes an additional factor, which is referred to as a 'reduction factor'. This factor represents the fraction of the contribution to global emission allowance from the harmonic current emissions of smaller installations. IEC 61000-3-14 recommends that DNSPs

determine these reduction factors considering the prevailing system conditions in their networks. The analyses presented in this Thesis show that the establishment of a universal value (network independent) for the reduction factor is not advisable, as it depends on a number of variables which are unique to the distribution network under consideration. This difficulty undermines the applicability of the IEC approach in relation to practical LV networks.

Furthermore, a number of methodologies that exist in the current technical literature in relation to the assessment of harmonic current emission limits for disturbing installations connected to the public LV network are closely examined, emphasising the strengths and weaknesses of each approach. A comparative study using test LV distribution networks is conducted. The study shows that, though underlying philosophies and data requirements for each of the investigated methodologies vary significantly, they provide emission limits for each individual installation which are not too dissimilar.

In relation to VU, application of the IEC methodologies may or may not lead to a conservative emission allocation, especially in complex radial networks. An alternative VU emission allocation methodology based on the constrained bus voltage (CBV) method is proposed in this Thesis. The theoretical bases for the formulation of the CBV methodology are presented together with several application examples. The CBV methodology is shown to be superior in comparison to the VU allocation methodology presented in IEC Technical Reports, as the former enables the network VU absorption capacity to be fully utilised.

Compared to both IEC and CBV methodologies, the novel VU emission allocation procedure presented in this Thesis that is based on the concept of voltage droop (VD), provides a simplistic, less computationally and data intensive technique.

In addition to harmonics and VU, voltage fluctuations and flicker are expected to become a major concern for DNSPs due to integration of intermittent and fluctuating renewable energy generators (REGs) to the distribution networks where little

or no knowledge exists in relation to the contributions made by such sources to the network. The impacts of REGs with different control modes (i.e. power factor control operation, voltage control mode and reactive power dispatch mode) on voltage fluctuations and flicker are examined in this Thesis. In addition, the attenuation characteristics of distribution system loads and their impact on flicker levels in the distribution network are also investigated. The results demonstrate that flicker emission characteristics of REGs are influenced negatively by the reactive power control strategy employed and the flicker attenuation characteristics are influenced by the various load types connected to the distribution feeder. This is an aspect which has not been recognised in existing literature. The outcomes of the study emphasises the need for adequate planning by DNSPs in relation to voltage fluctuations and flicker, before connecting REGs to the distribution network that have the capability to control the power factor or voltage.

This Thesis also examines the PQ characteristics of small single-phase photovoltaic inverter (PVI) systems, with the objective of establishing realistic information relevant to their PQ impacts on the distribution network, as such knowledge is not widely available and will be useful for DNSPs in managing their networks. This is achieved by conducting controlled laboratory experiments using an experimental test setup based on IEC recommendations from which the harmonics and flicker emission levels have been generally observed to be within stipulated limits, however, some PVIs exceeded the emission limits for even harmonics.

Acknowledgements

I wish to express my sincere appreciation to many people who have helped me throughout my PhD candidature at University of Wollongong.

I would like to pay my greatest gratitude and appreciation to my principal supervisor, Professor Sarath Perera of University of Wollongong (UoW), for providing me the opportunity to pursue postgraduate studies at the University of Wollongong and the support given throughout the study period in many ways. Sincere gratitude hereby extended to my co-supervisors Dr. Philip Ciufo and Dr. Lasantha Meegahapola for valuable guidance and encouragement extended to me.

Special thanks go to Sean Elphick and Dr. Vic Smith of the Australian Power Quality and Reliability Centre, for their generous technical support provided in setting up the laboratory experiments. Also, the personal and administrative support provided by Jacqueline Adriaanse, Kim Griffin, Sasha Nikolic, Roslyn Causer-Temby, Raina Lewis, Gerrard Drury, members of the Illawara Committee for International Students of University of Wollongong, and all the Technical Staff of School of Electrical, Computer and Telecommunication Engineering, University of Wollongong are acknowledged with gratitude.

I would like to thank Dr. Nishad Mendis and Dr. Upuli Jayatunga for the support given during my candidature. Thanks also go to my fellow graduate students Brian Perera, Amila Wickramasinghe and Dothinka Ranamuka for their valuable input to my research work.

Last but not least, I would like to thank my parents, Charles Perera and Janet Rosa, my wife, Athmi Jayawardena and rest of my family for their unconditional love and continuous support. I would not have been able to complete this thesis without you.

List of Principal Symbols and Abbreviations

CBV	constrained bus voltage
CUF	current unbalance factor
DG	distributed generators
DFIG	doubly-fed induction generator
DNSP	distribution network service provider
EHV	extra high voltage
EMC	electromagnetic compatibility
FSIG	fixed speed induction generators
HV	high voltage
IEC	International Electrotechnical Commission
IEEE	Institute of Electrical and Electronics Engineers
LV	low voltage
LVUR	line voltage unbalance rate
MV	medium voltage
NECA	National Electricity Code Australia
NEMA	National Electrical Manufacturer's Association
PCC	point of common coupling
PMSG	permanent magnet synchronous generators
POC	point of connection
POE	point of evaluation
PQ	power quality
PV	photovoltaic
PVI	photovoltaic inverter
PVUR	phase voltage unbalance rate
REG	renewable energy generators
RMS	root mean square
VD	voltage droop
VU	voltage unbalance
VUF	voltage unbalance factor
a, b, c	refer to the three phases
α	summation law exponent

β	summation law exponent for small installations
$\boldsymbol{CUF_{L_x}}$	complex current unbalance factor of the load x
CUF_{L_x}	magnitude of the current unbalance factor of the load x
D	magnitude of the resulting disturbance
D_i	magnitudes of the individual emission levels to be combined
D_s	PQ disturbance emission in the voltage level s
D_s^{total}	resultant PQ disturbance emission in the voltage level s
D_{us}	PQ disturbance emission transferred to voltage s from upstream network
$\boldsymbol{\Delta I_x}$	change in the current of a load x (phasor)
ΔI_x	change in the current of a load x
ΔP	active power change
ΔQ	reactive power change
$\boldsymbol{\Delta V_x}$	voltage change at the busbar x (phasor)
ΔV_x	magnitude of voltage change at the busbar x
E_{D_i}	PQ disturbance emission allocation for installation i
$E_{Ih:i}$	harmonic current emission limit for the installation i
$E_{I_2:i}$	negative-sequence current emission limit for the installation i
$E_{u:i}$	VU emission limit for the installation i
f_b	fundamental frequency
f_m	modulation frequency
γ	influence factor
$G_{D:s}$	maximum allowable global emission allowance at voltage level s
$G_{h:s}$	maximum acceptable global contribution of harmonic voltage to the voltage level s
$G_{u:s}$	maximum acceptable global contribution of VU to the voltage level s
I_1	RMS current of the fundamental component
I_h	RMS current of the h^{th} harmonic component
I_L	RMS load current
$I_{L:x}$	RMS load current of the installation x (based on agreed power)
$I_{1:x}$	positive-sequence current of the load x
$I_{2:x}$	negative-sequence current of the load x
IM	three-phase induction motor load

k_D	PQ disturbance allocation constant
k_h	harmonic allocation constant
k_m	ratio between the rated motor load (in MVA) and the total load (in MVA) supplied by an LV system
k_u	VU allocation constant
K_{hB}	reduction factor for harmonics
K_{uB}	reduction factor for VU
K_{uE}	reduction factor to account for system asymmetries
L_s	PQ disturbance planning level at voltage level s
$L_{h:s}$	harmonic planning level at voltage level s
L_{us}	PQ disturbance planning level at upstream network to voltage level s
$L_{u:s}$	VU planning level at voltage level s
m	modulation depth
P_{lt}	long-term flicker severity
P_{st}	short-term flicker severity
$P_{st:x}$	short-term flicker severity at busbar x
ϕ	power factor
R_x	Thévenin resistance at the PCC of the installation x
s	any sub-system (S = HV, MV, LV)
S_t	total system capacity of the MV/LV considered network
S_x	apparent power/agreed power of the installation connected to busbar x
$S_{OS:i}$	harmonic load of the installation i
$S_{sc:x}$	short-circuit capacity at any busbar x/ short-circuit capacity at the PCC of load x
$S_{t:s}$	total system capacity of the voltage level s
$T_{D:x-y}$	PQ disturbance transfer coefficient from x to y
$T_{\Delta V:x-y}$	voltage fluctuation transfer coefficient from x to y
$T_{h:x-y}$	harmonic transfer coefficient from x to y
$T_{u:x-y}$	VU transfer coefficient from x to y

$T_{P\text{st}:x-y}$	flicker transfer coefficient from x to y
TDD_I	current total demand distortion
THD_V	voltage total harmonic distortion
THD_I	current total harmonic distortion
θ	$\arctan(\frac{\Delta Q}{\Delta P}))$
U_1	positive-sequence voltage
U_2	negative-sequence voltage
$U_{1:x}$	positive-sequence voltage at busbar x
$U_{1:x}$	negative-sequence voltage at busbar x
$U_{1,\text{droop}}$	system positive-sequence voltage droop
$U_{1,\text{droop}:i}$	positive-sequence voltage droop of installation i
φ	grid impedance angle
V_1	RMS voltage of the fundamental component
V_h	RMS voltage of the h^{th} harmonic component
V_p	amplitude of the fundamental voltage
$\boldsymbol{V_x}$	steady state voltage phasor at the busbar x
V_x	magnitude of the steady state voltage at the busbar x
V_{ab}, V_{bc}, and V_{ca}	magnitudes of RMS line-line voltages
$\boldsymbol{V_{ab}}$, $\boldsymbol{V_{bc}}$, and $\boldsymbol{V_{ca}}$	RMS line-line voltage phasors
$V_{h:x}^{\text{total}}$	total harmonic voltage at the busbar x
V_{droop}	system voltage droop
$V_{\text{droop}:i}$	load voltage droop of installation i
$V_{h:\text{x}}(S_t)$	global contribution of all installations, to the harmonic voltage of order h at the busbar x
VUF_x^{total}	magnitude resultant VUF at the x^{th} busbar
$\boldsymbol{VUF_x}$	complex VUF caused by the unbalanced installations connected to the busbar x or complex VUF at the busbar x
VUF_x	magnitude of the VUF caused by the unbalanced installations connected to the busbar x or magnitude VUF at the busbar x
$VUF_{x\|IM}$	VUF at the busbar x, when an induction motor is in operating in the adjacent busbar

$x_{1:x}$	fundamental reactance at the POC of the installation x
X_x	Thévenin reactance at the POC of the installation x
Z_B	modulus of the short-circuit impedance of the system at the LV substation busbar
Z_x	modulus of the short-circuit impedance of the system at the POC/POE of the installation x
Z_L	steady-state impedance of the load
Z_S	impedance of the supply system
$Z_{h:B}$	modulus of the harmonic impedance at the LV busbar
$Z_{h:x}$	modulus of the harmonic impedance at busbar x
$Z_{hF1:i}$	modulus of the harmonic impedance at the POE of the customer installation i, connected to feeder F1
$Z_{11:x-y}$	positive-sequence impedance between x and y busbars
$Z_{21:x-y}$	negative-sequence positive-sequence coupling impedance between x and y busbars
$Z_{22:x-y}$	negative-sequence impedance between x and y busbars
Z'_L	dynamic impedance of the load to small voltage fluctuations

Publications Arising from the Thesis

1. D. Perera, S. Perera, P. Ciufo, and V.J. Gosbell. Comparison of Methodologies for Assessment of Harmonic Current Emission Limits for Large Installations Connected to LV Networks. In *Proc.* 15th *Int. Conf. Harmonics and Quality of Power (ICHQP 2012)*, pp.328-335, June 2012.

2. D. Perera, L. Meegahapola, S. Perera, and P. Ciufol. Flicker Propagation Analysis in Distribution Networks with Embedded Generation. In *Proc. Int. Conf. Power System Technology (POWERCON 2012)*, pp.1-6, Oct. 2012.

3. D. Perera, P. Ciufo, L. G. Meegahapola, and S. Perera. Power Quality Emission Assessment of Photovoltaic Inverters based on IEC Technical Report 61000-3-15:2011. In *Proc. Australasian Universities Power Engineering Conference (AUPEC 2013)*, Sept. 2013.

4. D. Perera, L. Meegahapola, S. Perera, and P. Ciufo. Characterisation of Flicker Emission and Propagation in Distribution Networks with Bi-directional Power Flows. *Renewable Energy*, Vol. 63, pp.172-180, March 2014.

5. D. Perera, P. Ciufo, S. Perera and L. Meegahapola. Voltage Unbalance Emission Allocation Using Constrained Bus Voltage Method in Radial Distribution Networks. In 16th *Int. Conf. Harmonics and Quality of Power (ICHQP 2014)*, pp.273-277, May 2014.

Table of Contents

List of Figures

List of Tables

Chapter 1

Introduction

1.1 Statement of the Problem

The proliferation of electromagnetically disturbing installations, including embedded generation systems, have led to increasing concerns on the deterioration of electromagnetic compatibility (EMC) in distribution networks [1, 2]. This is partly because the current disturbance levels caused by existing installations have already taken up the network disturbance absorption capacity. Thus, any further connection of disturbing installations might lead to the exceedance of stipulated EMC limits. This uncertainty associated with the growth of disturbing installations in distribution networks, emphasises the requirement for recommendations based on well researched engineering practices in relation to the management of network EMC.

The International Electrotechnical Committee (IEC) has published a series of standards and technical reports which provide guidelines to network operators, equipment manufacturers and system owners on the coordination of low frequency disturbances in the electrical power system [2–10]. The low frequency EMC concerns (which are more commonly termed as power quality (PQ) concerns) addressed in these technical reports include harmonics, voltage fluctuations and flicker, and voltage unbalance (VU). The IEC Technical Reports IEC 61000-3-6, IEC 61000-3-7, and IEC 61000-3-13 address PQ coordination with regard to high voltage (HV)

and medium voltage (MV) networks, whereas IEC 61000-3-14 offers guidelines for low voltage (LV) distribution networks. In addition, the IEC has recently published IEC 31000-3-15 as a supplement to equipment standards which specifically addresses the emission requirements for individual distributed generators (DGs). The general approach for the PQ disturbance coordination process as described in these technical reports, is to apportion the network PQ disturbance absorption capability to disturbing installations (loads and generators) by providing a disturbance emission allocation. Despite the availability of these standards and technical reports, there remains inadequacies in these documents as well as gaps in the existing knowledge in relation to management of PQ, where further refinements and contributions are required. The focus of this Thesis is to address these inadequacies and gaps, and facilitate DNSPs in the management of PQ in distribution networks[1].

The IEC Technical Report IEC 61000-3-14 provides guidelines for the assessment of emission limits of PQ disturbances for large disturbing installations including DGs connected to LV distribution networks. In the case of harmonics, the harmonic voltages in a network arise not only due to large installations, but also due to the smaller installations (e.g. domestic equipments, PV systems) whose harmonic current emission levels are governed by respective equipment standards. Therefore, apportioning the total harmonic absorption capacity of an LV network to large installations only, can lead to higher harmonic voltage levels which exceed stipulated limits. Hence, IEC 61000-3-14 proposes an additional factor referred as the 'reduction factor' in the allocation process, which considers the contribution from harmonic current emissions of smaller installations to the total harmonic voltage in the distribution network. Despite the mathematical explanations given in the Technical Report with regard to the proposed approach, no attempts have been made to investigate its applicability in practical LV distribution networks. Hence, additional work is required, including benchmarking the IEC 61000-3-14 methodology against other harmonic emission

[1]In the context of this Thesis, the distributed generators (DGs) and embedded generators refer to generation sources that are connected to the distribution network, including renewable energy generators (REGs) as well as conventional generators.

allocation practices in use, in order to justify the proposed approach.

In addition to harmonics, VU is also expected to become a major concern to distribution network service providers (DNSPs) [1]. IEC Technical Reports IEC 61000-3-13 and IEC 61000-3-14 address the coordination of VU in MV and LV distribution networks respectively. The approach given in these Technical Reports follows the same principles as harmonic emission allocation with regard to radial distribution networks, where system inherent asymmetries such as distribution line asymmetries are negligible. VU is known to attenuate when propagating from upstream networks to downstream networks and vice-versa [11]. The attenuation characteristics of VU largely depend on the type of loads connected to the distribution network. Although the attenuation when VU is propagating from upstream network to downstream networks is addressed in IEC technical reports through the introduction of a transfer coefficient, any attenuation that occurs when VU is transferring from downstream to the upstream network, at the same voltage levels, has not been taken into consideration. Thus, with regard to radial distribution networks, the proposed methodologies may lead to stringent emission limits for individual installations, while underutilising the VU emission absorption capacity of the network. Hence, the contribution towards the development of an approach to assess the VU attenuation and propagation in radial distribution networks will further facilitate the VU emission allocation process.

The constrained bus voltage method (CBV) is investigated in established technical literature [12, 13] as an alternative to IEC methodologies for allocation of harmonics and flicker emission levels to individual installations in radial distribution networks, considering attenuation aspects. With the methodologies developed to assess VU attenuation and propagation with regard to radial distribution networks, a possibility exists to extend the concept of CBV to radial MV and LV distribution networks to coordinate VU. However, the main disadvantage with the CBV method is that it is data intensive and requires that the VA capacity and the short-circuit capacity at the point of connection (POC) of all present and future loads connected

to the distribution network be known. Alternatively, a novel method based on the concept voltage droop (VD) is proposed in [14–16] for harmonic emission allocation, which focuses on minimising the data requirements and ease of application. The philosophy of the VD method is that the harmonic voltage at the extremity of the power system is limited by the maximum VD of the power system. Following a similar philosophy, the VD concept should be able to be applied for VU emission allocation. However, the theoretical work required to extend the VD method for VU emission allocation has yet to be developed. In addition, the applicability of IEC, CBV and VD methodologies, in relation to VU emission allocation for DGs needs to be investigated.

In relation to coordination of voltage fluctuations and flicker in distribution networks, the emission allocation methodologies are given in IEC Technical Reports IEC 61000-3-7 and IEC 61000-3-14. Similar to harmonics and VU, these methodologies have been mainly developed considering distribution system loads and unidirectional power flows in the distribution networks. With the increasing penetration levels of intermittent and fluctuating renewable energy generating systems in distribution networks, and the resulting bidirectional power flows, flicker levels in the network can be affected. In addition, the reactive power control strategy implemented in these renewable energy generators (REGs) can also influence the flicker levels in distribution networks [17]. These additional complexities that arise due to the connection of REGs and their effects in relation to voltage fluctuations and flicker, require further investigations.

In addition to large REG installations, the proliferation of small, single-phase photovoltaic inverter (PVI) systems in LV distribution networks can also lead to degraded quality of supply to customers [1]. The increase in the penetration level of PVIs in a distribution network happens over time, resulting in the connection of PVIs with various technologies that have different PQ characteristics. PQ characteristics of equipment including PVIs are generally examined using PQ emission tests as proposed by relevant IEC standards. Such experiments will provide valuable insight

into the PQ behaviour of equipment and will facilitate DNSPs in assessing the impact of these equipment and in the overall management of PQ in the distribution network. In spite of various field measurements and simulation work carried out in relation to PQ disturbances emission from PVIs in the established technical literature [18–20], only limited research outcomes are available in the public domain [21] in which controlled PQ emission tests are carried out using a standard networks to investigate the PQ behaviour of PVIs. Hence, further efforts are required in terms of PQ research, to characterise the PQ behaviour of PVIs using laboratory experiments.

1.2 Research Objectives and Methodologies

The aim of the current research is to bridge the gap between the existing knowledge in relation to PQ disturbance management in radial distribution networks, with an emphasis on the integration of embedded generation. The PQ disturbances addressed in this Thesis include harmonics, voltage fluctuations and flicker, and VU. The key objectives include:

- Examination of PQ disturbance emission allocation methodologies given in IEC standards and technical reports in relation to the availability of PQ disturbance absorption capacity for integration of DGs.
- Development of the theoretical bases in relation to attenuation and propagation aspects of VU and flicker in radial distribution networks with embedded generation.
- Investigation of the PQ behaviour of small scale PV systems in relation to harmonics and flicker.

The theoretical bases to the harmonic emission allocation methodology given in the IEC Technical Report IEC 61000-3-14 are established using a radial multi-feeder distribution network. The outcomes of the proposed methodology are compared against other emission allocation methodologies by considering two case studies,

followed by a discussion in relation to exceedance of stipulated limits and availability of additional absorption capacity for integration of DGs.

Analysis of the attenuation and propagation of VU is accomplished by the development of appropriate mathematical models, that are verified using unbalanced load flow analyses. The impact of induction motor loads has been incorporated in the analyses. Based on the outcomes, a revised VU emission allocation methodology based on the concept of CBV is proposed. In addition, the mathematical bases in relation to VD method for VU emission allocation are examined. The application of the proposed methodologies is demonstrated using models of radial multi-feeder distribution networks at MV and LV levels.

Investigations in to flicker propagation and attenuation is achieved by considering a REG connected to a distribution feeder. Mathematical models are developed incorporating reactive power control strategies of the generators. Theoretical bases which describe the behaviour of different load types, including constant power loads and constant current loads, under fluctuating voltage conditions are developed. Verifications of the outcomes are achieved using a simulation model of a wind farm consisting doubly-fed induction generators (DFIGs) connected to an MV distribution feeder.

Finally, the PQ behaviour of PVIs in relation to harmonics and flicker are examined using a standard test setup as given by the IEC 61000-3-15. The test setup is later modified to replicate a radial LV distribution network, in order to investigate the attenuation characteristic of multiple PVI systems.

1.3 Outline of the Thesis

A brief summary of the contents of the remaining chapters of this Thesis is provided here;

Chapter 2: In this chapter, a literature review and the background information

required to carry out the work given in this Thesis is presented. The definitions, sources and impacts of harmonics, voltage fluctuations and flicker, and VU are briefly discussed, emphasising the requirements for PQ disturbance management. The key aspects of the PQ disturbance coordination process, including the PQ disturbance emission allocation process proposed in IEC documents, are presented. Alternative PQ disturbance emission allocation methodologies discussed in various other technical reports and standards are examined, followed by a discussion on PQ disturbance attenuation and propagation. This chapter also briefly discusses the existing knowledge on the impacts of embedded generation on PQ in distribution networks.

Chapter 3: The harmonic emission allocation methodology given in IEC Technical Report IEC 61000-3-14, including the concept of a 'reduction factor', is closely examined in this chapter. A number of case studies are conducted with regard to harmonic emission allocation using test radial LV distribution networks, and the outcomes are compared against other emission allocation techniques.

Chapter 4: The mathematical models to investigate the attenuation and propagation of VU when transferring from downstream to upstream at the same voltage level are developed, forming the theoretical basis for Chapter 5. The models are verified using unbalanced load flow analyses. A statistical approach to estimate the VU in the presence of multiple unbalanced installations is presented. A methodology to quantify the VU attenuation provided by three-phase induction motor installations is proposed.

Chapter 5: The extension of the CBV methodology for VU emission allocation in radial distribution networks where system inherent asymmetries are negligible is discussed. A number of case studies are presented to illustrate the applicability of the proposed method. A new emission allocation methodology based on the concept of VD is also proposed as a less data intensive alternative to IEC and CBV methodologies. Results established using the proposed methodologies are compared

against those established by the IEC methodologies for MV and LV distribution networks.

Chapter 6: The chapter describes flicker emission and propagation in a distribution network with REGs. The impact of reactive power control strategies employed in REG with regard to flicker emission and propagation is analysed using mathematical models. The outcomes are verified employing a simulation model of a wind farm consisting DFIGs connected to a radial distribution feeder. Mathematical models are developed to characterise the attenuation aspects of different load types. The impact of distribution system loads on flicker emission from REG and flicker propagation in the distribution network are analysed and verified using simulation models.

Chapter 7: The harmonic and flicker emission from PVIs are examined using a laboratory test setup. A series of PQ emission assessment tests proposed by IEC 61000-3-15 are conducted on individual PVIs, and results are examined in relation to compliance with stipulated limits by the same standard. The laboratory experimental setup is then extended, in order to investigate the PQ attenuation characteristics of multiple PVIs.

Chapter 8: This chapter summarises the significant outcomes from this Thesis and makes recommendations and suggestions for future work.

Chapter 2

Literature Review

2.1 Introduction

This chapter presents a brief introduction to the main PQ problems investigated in this Thesis. Section 2.2 presents definition of harmonics, voltage fluctuations and flicker, and VU respectively. Sources and impacts of PQ disturbances are discussed in Section 2.3 and Section 2.4 respectively. Section 2.5 introduces the concept of compatibility levels and planning levels which are employed by the IEC to coordinate PQ disturbances in power systems. An overview of the relevant standards on the assessment and allocation of emission limits for disturbing installations is presented in Section 2.6. A generalised methodology for PQ disturbance emission allocation given in IEC Technical Reports is reviewed in Section 2.7, emphasising the relevance of PQ disturbance transfer coefficients. The deficiencies in the current IEC emission allocation process is explained in Section 2.8, followed by a discussion on alternative PQ emission allocation methodologies, which have been developed to address those concerns. A critical review on PQ disturbance propagation and attenuation in power systems is presented in Section 2.9. Finally, a discussion in relation to the impacts of renewable power generation on PQ in distribution networks are presented in Section 2.10, forming the basis for Chapter 6 and Chapter 7. The chapter is summarised in Section 2.11.

2.2 Power Quality Definitions

PQ problems are defined as "any power problem manifested in voltage, current or frequency deviations that results in failure or mal-operation of customer and utility equipment" [22]. PQ disturbances can be broadly classified into two categories as follows [23]:

- Variations - A characteristic of voltage or current which is never exactly equal to its nominal or desired value. Examples include harmonics, inter-harmonics, voltage fluctuations and VU.
- Events - A significant deviation of voltage or current from its normal or ideal wave shape is called an 'event'. Examples include interruptions, voltage swells and voltage sags.

Variations are monitored continuously over a period of time, whereas events are monitored using a triggering mechanism which records the desired property once a set value is exceeded [23].

The focus of this Thesis is on three PQ problems which are classified as variations; harmonics, voltage fluctuations and flicker, and VU. In the following sections, definitions of the PQ disturbances investigated in this Thesis are presented.

2.2.1 Harmonics

Power system harmonics are defined as "sinusoidal voltages and currents at frequencies that are integer multiples of the fundamental frequency" [22]. When harmonic voltages or currents are present, the resultant waveform will deviate from its sinusoidal shape. In the case of electrical power systems the fundamental frequency is either 50 Hz or 60 Hz. Hence, the harmonic frequencies will appear as integer multiples of 50 Hz (100 Hz, 150 Hz, 250 Hz, etc.) or integer multiples of 60 Hz (120 Hz, 180 Hz, 300 Hz, etc.).

Distortion in the voltage waveform is characterised by total harmonic distortion, THD_V, which is defined as root mean square (RMS) of harmonics expressed as a percentage of the fundamental component as given in (2.1):

$$THD_V = \frac{\sqrt{\sum_{h=2}^{h_{\max}} V_h^2}}{V_1} \tag{2.1}$$

where; V_h is the RMS voltage of the h^{th} harmonic component, V_1 is the RMS voltage of the fundamental component and $h_{\max}$ is the highest harmonic order of interest. Similarly, the current total harmonic distortion can be defined as (2.2):

$$THD_I = \frac{\sqrt{\sum_{h=2}^{h_{\max}} I_h^2}}{I_1} \tag{2.2}$$

where; I_h is the RMS current of the h^{th} harmonic component and I_1 is the RMS current of the fundamental component.

In case of harmonic currents, fundamental current may fall to a value close to zero under certain circumstances [22], resulting in large values for THD_I. Hence, the distortion in the current waveform is generally characterised by total demand distortion, TDD_I, which is defined as the RMS of the current harmonics expressed as a percentage of the RMS load current. The general expression for TDD for harmonic currents is given in (2.3):

$$TDD_I = \frac{\sqrt{\sum_{h=2}^{h_{\max}} I_h^2}}{I_L} \tag{2.3}$$

where; I_h is the RMS current of the h^{th} harmonic component and I_L is the RMS load current.

2.2.2 Voltage Fluctuations and Flicker

According to the International Electrotechnical Vocabulary (IEV 161-08-05) [24], voltage fluctuations are defined as "a series of voltage changes or a continuous variation of the RMS or peak value of the voltage". Such voltage changes can lead

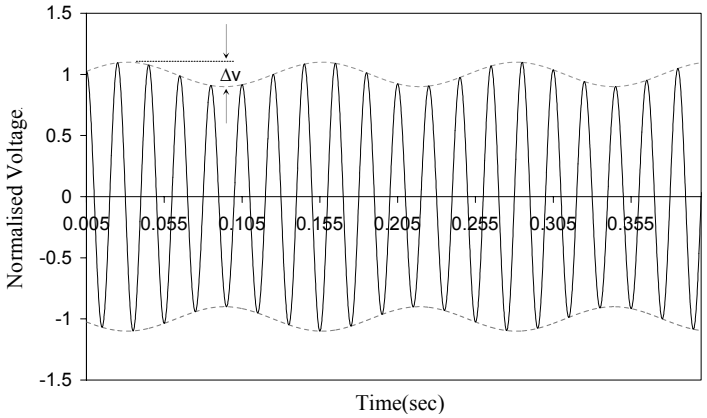

Figure 2.1: Sinusoidal voltage fluctuations due to amplitude modulation of fundamental frequency with a single modulating component

to variations in the illumination intensity of electric lighting devices leading to the phenomenon referred to as lamp flicker.

The IEV 161-08-05 defines flicker as "the impression of unsteadiness of visual sensation induced by a light stimulus whose illuminance or spectral distribution fluctuates with time". As the impression of visual sensation may vary from person to person, flicker can be considered as a physiological quantity rather than simply a physical quantity. As flicker is induced by voltage fluctuations, these two terms are used interchangeably [25, 26] to describe the overall PQ disturbance.

Fig. 2.1 illustrates the voltage fluctuations arising from sinusoidal amplitude modulation, a classical case considered in flicker studies. The corresponding instantaneous voltage, $v(t)$, can be expressed as:

$$v(t) = V_p[1 + m\sin(2\pi f_m t)]\cos(2\pi f_b t) \tag{2.4}$$

where; V_p is the amplitude (nominal) of the fundamental ac voltage, f_b is the fundamental frequency, f_m is the modulation frequency, $m = \Delta v/2V_p$ is the modulation depth and Δv is the magnitude of voltage fluctuation.

The key parameters that determine the perceptibility of flicker can be identified as magnitude (Δv) and the frequency (f_m) of voltage fluctuations. Flicker frequencies in the range of 0.05-35 Hz can lead to perceptible flicker [26, 27], where 8.8 Hz

is the most sensitive flicker frequency to the human eye. At this frequency, Δv as small as 0.25% would be sufficient to produce perceptible flicker [27, 28].

The severity of flicker is measured using two indices; short-term flicker severity index, P_{st}, and long-term flicker severity index, P_{lt}, using the IEC flickermeter [27]. The short-term flicker severity index is calculated using measurements over a period of 10 minutes and is used to evaluate the severity of disturbances that exist for relatively short time periods. The long-term flicker severity is established using measurements over 2 hours using 12 consecutive values of P_{st} and is suitable for measuring the severity of disturbances that exist over a longer period of time. The threshold value of P_{st} for perceptibility is unity.

2.2.3 Voltage Unbalance

The International Electrotechnical Vocabulary (IEV 161-08-09) defines VU as a condition in poly-phase electric power systems in which the magnitudes of the fundamental phase voltages and/or the associated phase angles of separation are not equal. In three-phase power systems, VU can exist in two forms, either as negative-sequence unbalance or zero-sequence unbalance.

In electrical networks with a path for the flow of zero-sequence currents such as in grounded-neutral systems, the presence of zero-sequence voltage can become an issue [29, 30]. However, such issues can be easily mitigated through proper system design and maintenance [5,31]. In addition, zero-sequence unbalance does not affect ungrounded-neutral systems and dual-phase installations. In contrast, the negative-sequence voltage can propagate through all power system components similar to the positive-sequence voltage and is a major concern for DNSPs [32]. Thus, it is a common practice to associate VU with the negative-sequence VU.

The severity of VU is characterised by a voltage unbalance factor (VUF), which is defined as the modulus of the ratio of the fundamental negative-sequence voltage component, U_2, to positive-sequence voltage component, U_1. The general expression

for VUF is given in (2.5):

$$VUF = \left|\frac{U_2}{U_1}\right| = \frac{|\boldsymbol{V_{ab}} + a^2\boldsymbol{V_{bc}} + a\boldsymbol{V_{ca}}|}{|\boldsymbol{V_{ab}} + a\boldsymbol{V_{bc}} + a^2\boldsymbol{V_{ca}}|} \tag{2.5}$$

where; $\boldsymbol{V_{ab}}$, $\boldsymbol{V_{bc}}$, and $\boldsymbol{V_{ca}}$ are RMS line-line voltage phasors and $a = 1\angle 120^o$.

A practical approach for establishing the VUF using the three fundamental line-line RMS voltage magnitudes is given in (2.6) [33]:

$$VUF = \sqrt{\frac{1 - \sqrt{3 - 6\epsilon}}{1 + \sqrt{3 - 6\epsilon}}} \tag{2.6}$$

where;

$$\epsilon = \frac{V_{ab}^4 + V_{bc}^4 + V_{ca}^4}{(V_{ab}^2 + V_{bc}^2 + V_{ca}^2)^2}$$

V_{ab}, V_{bc} and V_{ca} are the magnitudes of the fundamental line-line RMS voltages.

The VUF definition in (2.5) is established using only the magnitudes of the ratio $\frac{U_2}{U_1}$. However, it is possible to incorporate the phase angle information to the definition of VUF. The resulting complex VUF has been used for analysis of VU in power systems in [34, 35].

Alternative definitions for VU also exist, which are proposed by National Electrical Manufacturer's Association (NEMA) [36] and Institute of Electrical and Electronics Engineers (IEEE) [37]. For completeness, The NEMA definition which is known as 'line voltage unbalance rate' (LVUR), and the IEEE definition which is known as 'phase voltage unbalance rate' (PVUR) are given in (2.7) and (2.8) respectively.

$$LVUR = \frac{\text{Maximum voltage deviation from the average line-line voltage}}{\text{Average line-line voltage}} \tag{2.7}$$

$$PVUR = \frac{\text{Maximum voltage deviation from the average phase voltage}}{\text{Average phase voltage}} \tag{2.8}$$

2.3 Sources of Power Quality Disturbances in Distribution Networks

Harmonic voltages are generated in power system due to non-linear loads drawing non-sinusoidal currents from the network [25]. Non-linear loads include saturated magnetic circuits (e.g. power transformers, rotating machines) and power electronic converters. Power electronic converters are one of the major harmonic contributors in LV networks. More common power converters include switch mode power supplies, inverters, and rectifiers [38].

Voltage fluctuations and flicker are mainly caused by large intermittent loads such as electric arc furnaces (EAFs), which are normally supplied through dedicated feeders connected to HV or MV busbars. The rapid variation in the active and reactive power drawn by an EAF can lead voltage fluctuations in the low voltage side of the installation transformer. Such voltage fluctuations could also be reflected on to the HV side, and then transferred to distribution networks. The causes of flicker in distribution networks are fluctuating loads such as HVAC applications (electrical heating systems, compressors used in cooling systems, heat pumps, air conditioning systems), electrical machines with alternating torque (wood and metal workshop machines, welding machines, drilling machines, sawing mills), and electrical ovens [39].

The presence of large single-phase and double-phase loads (e.g. LV appliances, electric traction motors [40,41], induction furnaces) and their instant demand changes are identified to cause VU in distribution networks [42]. Network asymmetries (unsymmetrical line impedances and transformers) are also known contributors for VU [43–48].

The rapid growth of REGs such as wind generation systems and photovoltaic systems are also attributed to degrading PQ in distribution networks [1,10]. Further details with regard to the impacts of REGs on network PQ will be presented in Section 2.10.

2.4 Effects of Power Quality Disturbances

The PQ disturbances discussed in Section 2.2 can have both short-term and long-term effects on distribution systems and connected customer loads. While short-term effects result in immediate damage and equipment malfunction, long-term term effects can lead to reduced life span of equipment due to thermal stress.

Harmonic voltage distortion can significantly impact the performance of rotating machinery. Harmonic voltages would cause harmonic fluxes which do not contribute to useful motor torque and induce high frequency currents in the rotor. The effects are decreased efficiency along with heating, vibration and high pitch noise [39,49,50]. The performance of transformers is affected due to current harmonics which cause copper and stray flux losses, and voltage harmonics which cause additional iron losses [39]. Harmonics are also a major cause of dielectric stresses in capacitor banks, causing additional heating and leading to premature failures [51, 52]. In addition, capacitors, together with the supply source and load inductance, can form resonant circuits, in which harmonic currents and voltages can be multiplied. The resulting voltages can cause damage to capacitors and other equipment. High peak voltages resulting from harmonic distortions can cause insulation breakdown in cables, hence, disruption of supply. Harmonic interference with sensitive equipment such as protective relays, metering devices, control circuits and communication circuits can experience malfunction and component failure [38].

The main effect of rapid voltage fluctuation is lamp flicker. Voltage fluctuations with magnitude variation of range 0.9-1.1 pu with frequencies 0.5-35 Hz can lead to lamp flicker, which can be irritating to human eye [27]. In addition, recent investigations into effects of regular voltage fluctuations in relation to rectifier filter capacitors indicate that voltage fluctuations can result in significant increase in the capacitor RMS current, which leads to the undesirable effects of raising the electrolytic capacitor temperature and thus, accelerating the ageing process [53].

Excessive VU is known for producing additional heating in both stator and rotor

windings in induction motors, leading to a reduction in the efficiency [32, 54–56]. When an induction motor is exposed to unbalanced voltages, the negative-sequence voltage component produces an air gap flux which rotates against the air gap flux produced by positive-sequence voltages, resulting in the reduction of the motor torque. In addition, increased motor vibration and noise can be experienced [32]. Therefore, NEMA Standard MG 1-1993 [32] and Australian Standard 1359.31-1997 [57] recommend derating of the motor power, based on the degree of VU. Furthermore, static power converters produce characteristic and uncharacteristic harmonics in the presence of VU [32, 58]. For example, power electronic converters with uncontrolled diode rectifier front-ends (e.g. adjustable speed drives [32, 59]) produce uncharacteristic triplen harmonics in addition to the characteristic harmonics in the input current in the presence of supply VU. Other power system components such as synchronous generators, transmission overhead lines and cables, and transformers can also be affected by VU. Similar to induction motors, synchronous generators can also be subjected to excessive heating leading to increased losses and possible damage to structural components [60]. The flow of negative-sequence currents in overhead lines, cables, and transformers increases power losses, lowering their capacity [11, 61].

2.5 Limits for Power Quality Disturbances

As discussed in Section 2.4, PQ disturbances have short-term and long-term adverse effects on customer and power system equipment. The long-term effects are not often visible to DNSPs or customers until failures of the equipment occur, which often requires costly repairs or replacements. Therefore, both customers and DNSPs are required to be proactive in their approach to maintain network PQ at desired levels. In this regard, the IEC has defined a set of reference limits for each PQ disturbance type, which can be used by DNSPs to maintain EMC in their respective networks. The EMC is defined as the ability of an equipment or system to

function satisfactorily in its electromagnetic environment without introducing intolerable electromagnetic disturbances in to that environment. Two different limits are defined as compatibility levels and planning levels. Sections 2.5.1 and 2.5.2 provides a brief description of these limits and their importance to DNSPs and customers.

2.5.1 Compatibility Levels

In the EMC coordination process for power systems, the compatibility between system disturbance levels and equipment immunity levels is ensured by providing reference values known as compatibility levels [62]. Equipment must be designed to ensure immunity to the disturbance at least up to the compatibility level, and DNSPs are required to maintain the disturbances at or below the compatibility levels.

Due to the stochastic nature of PQ phenomena, compatibility levels are generally determined based on the 95% probability of disturbances in the entire power system. Fig. 2.2 illustrates the relationship between system disturbances, immunity and compatibility levels.

The IEC compatibility standards IEC 61000-2-2 [62] and IEC 61000-2-12 [63] provide the harmonics, voltage fluctuations and flicker, and VU compatibility levels in MV and LV networks respectively. The compatibility levels are given in terms of both short-term and long-term effects. Table 2.1 provides harmonic voltage compatibility levels for both MV and LV networks considering the long-term effects. The corresponding compatibility level for voltage total harmonic distortion is THD = 8%.

The compatibility limits for harmonics as given in Table 2.1 are specified considering the increase of the number of harmonic sources and the decrease of the proportion of purely resistive loads in relation to the overall load [62]. With reference to very short-term effects, the compatibility levels for individual harmonic components of the voltage are the values given in Table 2.1, multiplied by a factor k, where k is given as (2.9):

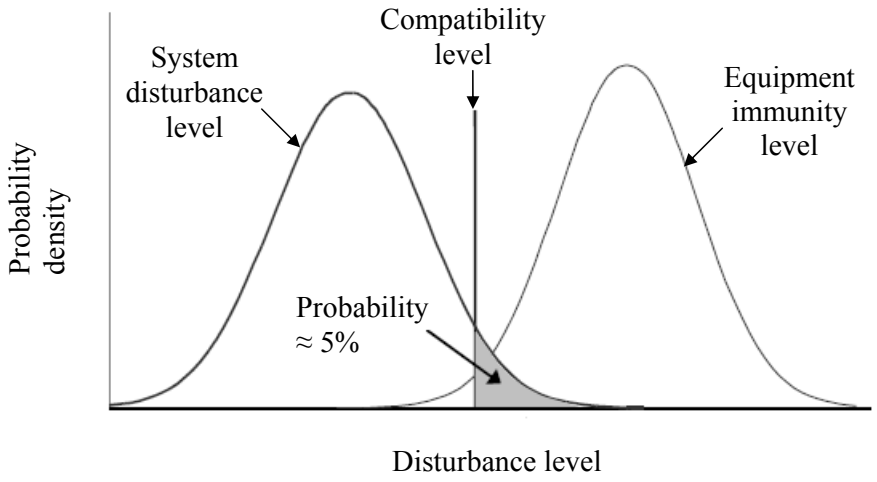

Figure 2.2: Statistical interpretation of the compatibility level (IEC 61000-2-2, IEC 61000-2-12) [62, 63]

$$k = 1.3 + \frac{0.7}{45} \times (h - 5) \tag{2.9}$$

where; h is the harmonic order. The corresponding compatibility level for the voltage total harmonic distortion is THD = 11%.

In relation to voltage fluctuations, voltage changes are limited to 3% of nominal supply voltage under normal circumstances for both MV and LV networks. However, step voltage changes exceeding 3% can occur infrequently on the public supply network. For flicker, the short-term and long-term flicker severity compatibility values are 1 and 0.8 respectively.

In the case of VU, IEC standards [62, 63] prescribe a VUF of 2% for both MV and LV networks. An excursion up to a VUF of 3% is allowed in some areas where predominantly single-phase loads are connected.

In addition to IEC compatibility level, various reference values are also prescribed under other national and international standards and are available in the established technical literature [38,64]. For example, Table 2.2 provides the maximum allowable harmonic distortion limits given by IEEE 519 [38].

Table 2.1: Harmonic voltage compatibility levels at both MV and LV networks [62, 63]

Odd harmonics Non-multiple of 3		Odd harmonics Multiple of 3		Even harmonics	
harmonic order h	harmonic voltage %	harmonic order h	harmonic voltage %	harmonic order h	harmonic voltage %
5	6	3	5	2	2
7	5	9	1.5	4	1
9	3.5	15	0.4	6	0.5
11	3	21	0.3	8	0.5
$17 \leq h \leq 49$	$2.27 \times \frac{17}{h} - 0.27$	$23 < h \leq 45$	0.2	$10 \leq h \leq 50$	$0.25 \times \frac{10}{h} + 0.25$

Table 2.2: Voltage distortion limits [38]

Bus Voltage at PCC	Individual Voltage Distortion (%)	Total Voltage Distortion THD (%)
69 kV and below	3.0	5.0
69.001 kV through 161 kV	1.5	2.5
161.001 kV and above	1.0	1.5

2.5.2 Planning Levels

Based on compatibility level values, planning level values are set for a particular voltage level by the body responsible for the planning and operation of the supply system. Setting of the planning levels is aimed at the coordination of PQ disturbances between various voltage levels such that the MV/LV compatibility level is not exceeded. Planning levels are considered as internal quality objectives of the respective system operators and depend on the structure of the network. Thus, only indicative values are provided in the technical literature [3, 65]. A statistical interpretation of the planning level is given in Fig. 2.3. Planning level values should always be equal to or lower than the compatibility level values.

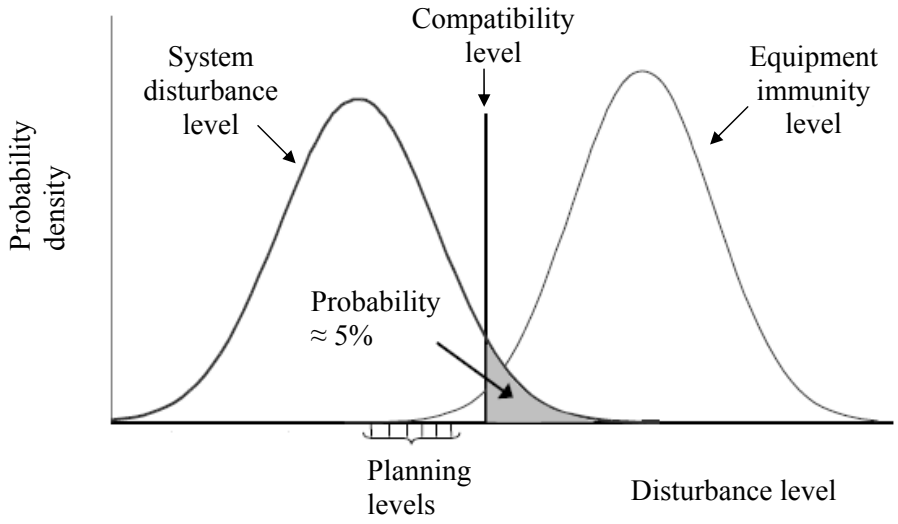

Figure 2.3: Statistical interpretation of the planning level (IEC 61000-2-2, IEC 61000-2-12) [11, 62, 63]

2.6 Power Quality Standards

In order to maintain the EMC in electrical power systems and to meet the compatibility and planning objectives, PQ disturbance emissions from individual installations and equipment need to be limited. The IEC has published a series of technical reports which provide guidelines for system operators and equipment manufacturers on the management of network PQ. These documents attempt to control the level of PQ disturbances by providing emission limits, such that if customers comply with the given limits, the net effect of all customer emissions will result in acceptable PQ disturbance level. The IEC EMC standards can be broadly classified into two categories; equipment standards and network standards/technical reports.

2.6.1 Equipment Standards

The equipment standards are developed with the objective of providing emission limits for customer equipment, so that when all equipment (which are also provided with a emission limits) operate simultaneously, the EMC can be ensured. The IEC standard IEC 61000-3-2 [6] provides harmonic current emission limits for equipment

with operating current up to 16 A. Equipment are classified into Classes A to D considering their operating characteristics, and emission limits are provided for each category. Harmonic current emission limits for equipment with input current higher than 16 A and less than 75 A are given in IEC 61000-3-12 [6]. Under IEC 61000-3-12, emission limits are derived based on the operating characteristics of the equipment and short-circuit ratio at the POC of the equipment. Similarly, voltage fluctuations and flicker emission limits for equipment with rated current up to 16 A and equipment with rated current higher than 16 A and less than 75 A are given in IEC 61000-3-3 [8] and IEC 61000-3-11 [9] respectively. In relation to VU, the responsibility of managing VU due to single-phase equipment falls with the system operator and consumers, hence, there is no separate standard for equipment.

In addition to equipment, small scale DGs are considered to be a source of PQ disturbance. Accordingly, the IEC has recently published a new Technical Report IEC 61000-3-15 [10] which focuses on provision of guiding principles on the assessment of low frequency electromagnetic immunity and emission requirements for dispersed generation systems up to 75 A. The PQ concerns addressed in this Technical Report include harmonics, inter harmonics, voltage fluctuations and flicker, VU, DC injections, short duration over voltages and switching frequency harmonics. In the case of harmonics, the emission limits are largely based on the IEC 61000-3-2 Class C (lighting) equipment limits, due to the commonality between such loads and DGs [10].

2.6.2 Network Standards

The primary objective of network standards is to provide guidance to system operators or owners on engineering practices, which will facilitate the provision of adequate service quality for all connected customers. The IEC Technical Reports IEC 61000-3-6 [3], IEC 61000-3-7 [4], and IEC 61000-3-13 [5] provide guiding principles on the assessment of emission limits for disturbing installations connected to

MV, HV and EHV power systems on harmonics, voltage fluctuations and flicker and VU respectively. In addition, IEC 61000-3-14 [2] focuses on the provision of emission limits for disturbing installations connected to LV distribution networks on harmonics, voltage fluctuations and flicker, and VU. The aforementioned technical reports [2–5] follow a three-stage emission allocation process, in coordinating the EMC in the power system. The three-stage emission allocation process will be explained in Section 2.7.

In addition to IEC standards and technical reports, some countries have their own national standards and recommended practices on coordination of PQ disturbances in power systems. Few of such technical reports and standards are listed here:

- "Technical Rules for the Assessment of Network Disturbances", is a technical report [66] used by DNSPs in Austria, Switzerland, Germany and Czech Republic, which provides emission limits for harmonics, voltage fluctuations, VU, inter harmonic voltages etc. for installations connected to MV and LV networks.

- IEEE 519-1992 "IEEE Recommended Practices and Requirements for Harmonic Control in Electrical Power Systems" was developed by the IEEE to provide guidance in the design of power system with non-linear loads. [38].

- HB 264 "Power Quality - recommendation for the application of AS/NZS 61000.3.6 and AS/NZS 61000.3.7" is used in Australia and provides recommendations for management of harmonics and flicker in MV distribution networks [65].

2.7 IEC Power Quality Disturbance Emission Coordination Process

Providing a PQ disturbance emission allocation for all loads connected to the power system is an integral part of the PQ emission disturbance coordination process. The general approach to the IEC methodology is presented in this section.

2.7.1 Emission Limits: Stages 1, 2, and 3

IEC Technical Reports [2–5] specify three stages governing the approval for the connection of disturbing installations to the power system.

- Stage 1 - simplified evaluation of disturbance emission

  Connection of small installations, which fulfill certain criteria, can be accepted without a detailed evaluation of their emission characteristics. For example, under the harmonic emission coordination methodology given IEC 61000-3-6, if an installation connected to MV, HV or EHV network meets the criteria given by (2.10), the connection is exempted from application of harmonic current emission limits.

$$\frac{S_i}{S_{sc:i}} \leq 0.1\% \tag{2.10}$$

  where; S_i is the agreed power of the consumer (MVA) and $S_{sc:i}$ is the short-circuit capacity at the point of common coupling (PCC) of the installation (MVA).

  Similar criteria exists for flicker and VU and are detailed in [4] and [5] respectively.

- Stage 2 - emission limits relative to actual system characteristics

  If an installation does not meet Stage 1 requirements, the installation is expected to comply with an emission limit imposed under the Stage 2 emission allocation process. The general approach of setting individual emission limits is discussed in Section 2.7.2.

- Stage 3 - acceptance of higher emission levels on a conditional basis

  Connection of an installation which would fail to comply with Stage 2 emission

limits can be conditionally accepted under some circumstances. This is particularly the case, when the parameters used under Stage 2 are conservative and there is some unused disturbance absorption capacity of the network that can be used on a temporary basis. Connection of an installation under Stage 3 will require conducting a detailed study to determine the pre-existing PQ disturbance levels and the expected contribution of the considered installation.

2.7.2 Development of Stage 2 Emission Limits

A detailed methodology for PQ emission disturbance allocation is presented under the Stage 2 in IEC technical reports [2–5]. The underlying philosophy of the Stage 2 methodology is that, when the system MVA capacity is utilised to its full extent and all connected installations inject their individual limits, the resultant emission level which arises at extremity of the network should be less than or equal to the planning level. The general approach for determining the emission limits to individual customers can be summarised as follows [11]:

- Application of a general summation law for combining emissions arising due to numerous sources of disturbances.
- Estimation of the maximum allowable global PQ disturbance emission capacity at the voltage level which the customer will be connected.
- Apportioning of the global emission allowance estimated to connected customers in an equitable manner.

General Summation Law

The resultant PQ disturbances due to multiple sources can be expressed as a vector summation of PQ disturbance emissions from each source. These vectors (magnitude and/or phase) of numerous installations are inherently random. A general summation law based on a statistical approach is proposed in [2–5] as a means for

calculation of disturbances levels caused by multiple sources. The summation law enables the calculation of resultant PQ disturbances, without the phase angle information. The resultant disturbance due to multiple sources based on the general summation law can be expressed as (2.11) [2–5]:

$$D = \sqrt[\alpha]{\sum D_i^{\alpha}} \tag{2.11}$$

where; D is the magnitude of the resulting disturbance, for considered aggregation of sources (probabilistic values) and D_i is the magnitudes of the individual emission levels to be combined. α is termed the summation exponent and mainly depends on following factors:

- The chosen probability for the actual values not to exceed the calculated value,
- The degree to which individual disturbance vary randomly in terms of magnitude and phase,
- The number of random variations considered (either the number of summated sources or the variation in time).

The value of the summation exponent for each type of PQ disturbance is listed in the respective IEC technical reports. For harmonic voltages, the value of the summation law exponent varies with harmonic order as shown by Table 2.3.

For flicker, the value of summation law exponent generally varies from 1 to 4, and depends on the main source which produces flicker emissions and the nature of coincidence of voltage fluctuations. In relation to VU, $\alpha = 1.4$ is selected as the summation law exponent, based on uniform distribution of random vectors with a random phase variation of 360 degrees and a magnitude range of 0.1 to 1.0 p.u [5].

Table 2.3: Recommended summation exponent values for harmonics [3]

Harmonic order	$h < 5$	$h \leq 10$	$h > 10$
α	1	1.4	2

Estimation of Global Emission Allowance

Evaluation of an emission limit for a single, disturbing installation connected to a voltage level s (thereafter called subsystem s) requires the determination of the 'maximum global emission allowance', $G_{D:s}$, which is the total particular PQ disturbance absorption capacity of the network at the voltage level s. The global emission in a particular subsystem is the emission arising due to the PQ disturbance sources that are connected to the considered subsystem and its downstream.

The total PQ disturbance emission at the subsystem s consists of the global emission in the particular system, D_s, and the PQ disturbance that propagates to the subsystem s from the upstream network, D_{us-s}. By combining these two emissions using the general summation law, the resultant disturbance level at the subsystem s, D_s^{total}, can be established as (2.12):

$$(D_s^{\text{total}})^\alpha = (D_s)^\alpha + (D_{us-s})^\alpha \tag{2.12}$$

PQ disturbances that propagate from an upstream network to the subsystem s, D_{us-s}, can be expressed as $D_{us-s} = T_{D:us-s} \cdot D_{us}$, where D_{us} is the global emission from all installations connected to the upstream network and $T_{D:us-s}$ is the PQ disturbance transfer coefficient from the upstream network to subsystem s. Typical values for the transfer coefficients for PQ disturbance types is given in the respective IEC technical reports. A detailed discussion on the estimation of PQ disturbance transfer coefficients is given in Section 2.9. Given that D_s and D_{us} are restricted by the planning level for the respective voltage level, the 'maximum allowable global emission allowance', $G_{D:s}$, can be calculated using (2.13):

$$G_{D:s} = \sqrt[\alpha]{(L_s)^\alpha - (T_{us-s}L_{us})^\alpha} \tag{2.13}$$

where; L_{us} and L_s are the planning levels for the upstream network and voltage level s respectively.

Apportioning of the Global Emission Allowance to an Individual Customer

Once the maximum allowable global emission limit has been determined, allocation of emission limits for individual installations, $E_{D:i}$, can be carried out based on the agreed power of consumer i, S_i, and the total supply capacity, $S_{t:s}$, of the voltage levels s. $E_{D:i}$ in its simplistic form is given by (2.14):

$$E_{D:i} = G_{D:s} \sqrt[\alpha]{\frac{S_i}{S_{t:s}}} \tag{2.14}$$

where; $S_{t:s}$ is the total MVA capacity of the voltage level s including provision for future load growth. Equation (2.14) is usually modified to represent the inherent characteristics of each PQ disturbance. For example, when allocating a VU emission limit for a customer connected to a HV or an MV network, (2.14) is modified to account for VU that arises due to the asymmetry of the supply system by incorporating an additional factor termed 'k_{uE} factor' [5]. Similarly, for harmonics and VU emission allocation for an installations connected to LV distribution network, an additional factor termed a 'reduction factor' is introduced to account for emissions caused by small installations [2]. These aspects will be discussed in subsequent chapters of this Thesis.

2.8 Alternative Emission Allocation Methodologies

Further examination of the IEC PQ disturbance emission allocation methodologies given in [2–5] reveals that the application of IEC methodologies even to a simple radial network, is a non-trivial task and requires the computation of several coefficients. In addition, investigations carried out in [65] have identified following issues with IEC approaches:

1. In relation to harmonic emission allocation in radial distribution networks, the methodology presented in IEC Technical Report IEC 61000-3-6 provides an

emission limit which is significantly higher for installations connected closer to the supply point (e.g. HV/MV transformer), compared to a installation (which has a same MVA capacity) that is connected at the end of the feeder.

2. In radial networks where fluctuating installations are distributed along the feeder, flicker levels can significantly attenuate when propagating from downstream to upstream of the network. However, such attenuation aspects are not taken into account in the flicker emission allocation methodologies given in IEC 61000-3-7. Hence, for radial distribution networks with parallel feeders, IEC 61000-3-7 methodology may provide conservative flicker emission limits and underutilised the flicker absorption capacity of the network. Similar observation can be made with respect to IEC 61000-3-13 and IEC 61000-3-14.

As a result, alternative PQ disturbance emission allocation methodologies have been developed to address aforementioned concerns associated with the IEC methodologies. Key objectives of these methodologies are reported in [11], and can be summarised as follows:

The PQ emission allocation methodology should:

- Ensure that the PQ disturbance levels at the extremity of the networks are within the compatibility limits set by [62, 63],
- Not distinguish between different types of customer installations, i.e. installations of equal MVA demand connected at a common busbar should receive equal emission limits,
- Be equitable in some sense, i.e. larger installations should be entitled to larger emission levels,
- Utilise as much of the network absorption capacity as possible.

In the following sections, two alternative PQ disturbance emission allocation methodologies developed by the Australian Power Quality and Reliability Centre at

the University of Wollongong are discussed.

2.8.1 Constrained Bus Voltage Method

An alternative harmonic emission allocation methodology called the Constrained Bus Voltage Method (CBV) has been proposed in [12]. In the CBV method, PQ disturbance levels at network busbars are explicitly forced to be at or below the set planning level when all loads inject their limits derived based on the new approach.

By employing the simple radial distribution network given in Fig. 2.4 where n disturbing installations are connected to the voltage level s, the general approach for the CBV method can be explained.

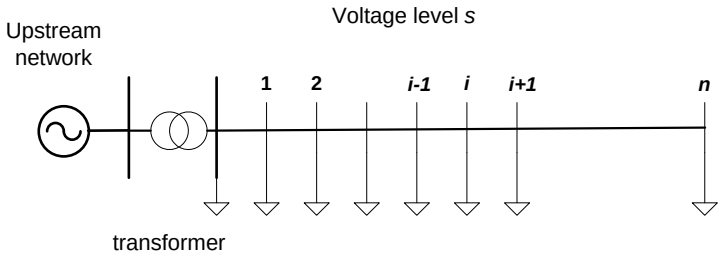

Figure 2.4: Radial distribution network with multiple installations

Assume that each installation i is allocated a PQ disturbance emission limit corresponding to its agreed power[1], S_i, as given by (2.15):

$$E_{D:i} = k_D \cdot f(S_i) \tag{2.15}$$

where; $E_{D:i}$ is the PQ emission limit for the installation i, $f(S_i)$ is a function of installation per-unit MVA capacity (also called as agreed power) and k_D is an allocation constant, that is yet to be determined. Considering the PQ disturbance attenuation and propagation characteristics, the total PQ disturbance at each busbar can be calculated as a function of k_D and $f(S_1)$ to $f(S_n)$ and PQ disturbances that propagate from the upstream network, D_{us-s}. The total PQ disturbance at

[1]The agreed power of the installation is considered to be equal to the apparent power of the installation.

each busbar, D_i^{total}, can be given by (2.16):

$$D_i^{\text{total}} = f(k_D, S_1, ..., S_n, D_{us-s}) \tag{2.16}$$

where; D_i^{total} is the total PQ disturbance level at the busbar i, S_1, ..., S_n are the MVA capacities of installations 1 to n, and D_{us-s} is the PQ disturbance that propagates from upstream network.

As the PQ disturbance level at each busbar should be less than the planning level for that voltage level, the allocation constant k_D can be calculated subject to the condition given by (2.17):

$$D_i^{\text{total}} \leq L_s \text{ for } i = 1, 2,..., \text{n} \tag{2.17}$$

where; L_s is the PQ disturbance planning level for that voltage level s. The allocation constant is dependent on network characteristics such as conductor impedance, transformer impedance, load distribution and network configuration [65]. Once, k_D is determined, the PQ disturbance emission allocation for installation i, $E_{D:i}$, can be calculated using (2.15).

One of the key drawbacks of the CBV methodology is that, in order to calculate the emission limits, the agreed power and the impedance at the POC of all present and future installations are required to be known in advance. However, such difficulties can be overcome by intuitive, good engineering judgment and planning [65].

The application of the CBV methodology in relation to harmonic emission allocation in a distribution network will be further discussed in Chapter 3, Section 3.4.4. The application of CBV methodology for flicker emission allocation and VU emission allocation in meshed networks, is given in [65] and [11] respectively.

2.8.2 Voltage Droop Method

A novel PQ disturbance emission allocation methodology based on the concept of voltage droop (VD) method is presented in [14, 16]. The main focus of the VD

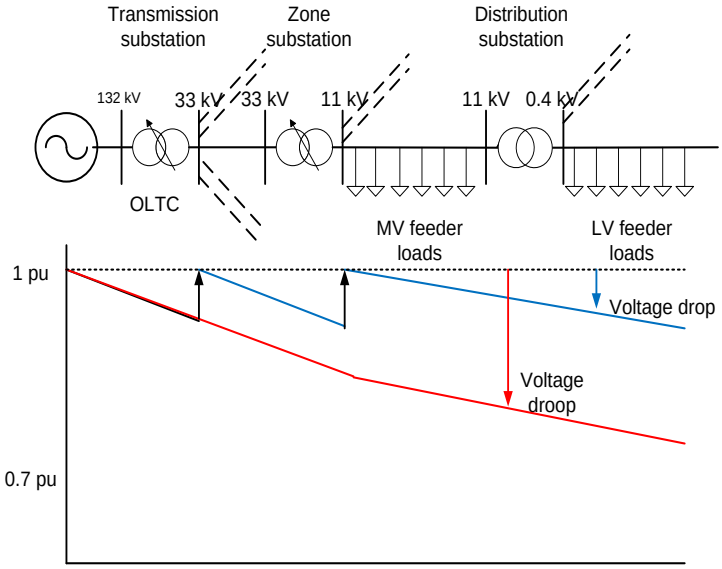

Figure 2.5: Distribution system voltage droop [14]

method is to provide a simple emission allocation process which requires minimal data and no assumptions [14, 16]. Considering the power system in Fig. 2.5, the concept of voltage droop can be explained.

When an installation is connected to the downstream LV network, a voltage drop can be experienced at the LV network and upstream network due to the interaction of the load current with system impedance. The summation of all voltage drops between the POC of the installation and transmission system which is represented by a Thévenin voltage source is termed as the 'voltage droop' of the installation.

When multiple loads are connected to the network, voltage drop between the last regulated MV busbar (11 kV in the example shown in Fig. 2.5) and the LV customers at the end of the system is generally restricted to 6-10%. The voltage drops further up in the network also need to be restricted to be within the tapping range of on load tap changing (OLTC) transformers. Typically, voltage drop in these parts of the system are restricted to 10% at each voltage level. The system voltage droop corresponds to the total voltage reduction between the transmission system which is represented by a Thévenin voltage source, and the network point being considered (i.e. LV feeder), when the network is loaded with multiple installations at each

voltage level. Hence, system VD is equal to the summation of all individual voltage drop components (i.e. voltage drop in LV network and voltage drop in upstream networks) in the network. For a typical Australian network, the value for system VD is found to be around 30% [14].

In the VD methodology for PQ disturbance emission allocation, each installation is provided with an emission allocation limit, which is a function of installation capacity and an allocation constant k_D. In general, the VD caused by the installation i, $V_{\text{droop},i}$, is also a function of the installation MVA capacity, S_i. Hence, the PQ disturbance caused by a single installation can be expressed as function of the VD caused by the same installation and the allocation constant k_D as given in (2.18):

$$E_{D:i} = f(k_D, V_{\text{droop},i}) \tag{2.18}$$

$E_{D:i}$ is the PQ emission limit for the installation i, $V_{\text{droop},i}$ is the VD caused by the installation i in per-unit, and k_D is an allocation constant, that is yet to be determined.

When aggregated across all loads, the net PQ disturbance level at the network is a function of the system VD. Considering the fact that the net PQ disturbance level of the network is constrained by the PQ disturbance planning level of the network and VD is constrained by the maximum allowed system VD (typically 30%), it is possible to evaluate the value of allocation constant k_D, hence, the emission allowance for each installation. The application of voltage droop methodology for harmonic emission allocation is discussed in Chapter 3, Section 3.4.2.

The objective of the VD method is to provide a pragmatic approach to provide PQ disturbance emission limits, rather than being mathematically exact. In [15], the error caused by the VD approach, when applied to typical Australian multi-feeder network is analysed, where an error of 20% is observed. Authors in [15] argues that such errors are justified, since, IEC methodologies require detailed modelling, but in practice much of data has to be guessed.

2.9 Power Quality Disturbance Attenuation and Propagation

The estimation of PQ disturbance propagation from an upstream network to a downstream network and vice versa is an integral part of the PQ emission allocation process discussed in Sections 2.7.2 and 2.8.1. While underestimation of the PQ disturbance propagation can lead to emissions exceeding set planning levels, overestimation can lead to conservative emission limits for individual customers. In addition, different load types such as constant power, constant current and induction motor loads can attenuate or exacerbate PQ disturbances. Thus, the accurate characterisation of PQ disturbance propagation and attenuation will facilitate the PQ disturbance emission allocation process.

There exist substantial research outcomes in relation to PQ disturbance propagation and attenuation. In the sections that follow, the existing knowledge with respect to harmonics, flicker and VU propagation and attenuation is reviewed.

2.9.1 Harmonics

Investigations into harmonic propagation and attenuation are reported in [67–69]. These studies are generally carried out using either frequency domain modelling using harmonic power flow programs or using time domain simulations. The frequency scan method can be identified as the most commonly used technique for harmonic analysis [70]. In the frequency scan method, the frequency response of a network seen at each bus or node is calculated by injecting a one per-unit sinusoidal current (or voltage) into the bus of interest. The main disadvantage of the frequency scan method is the inability to asses harmonic propagation in cases involving non-typical operating conditions such as partial loading of harmonic-producing devices, excessive harmonic voltage distortions and unbalanced network conditions. To overcome the aforementioned difficulties, the harmonic iteration method is proposed in [71,72] in which the harmonic sources are modelled as voltage dependent current sources.

In addition to the frequency domain approaches, time-domain simulation based on electromagnetic transient programs can be used [70]. However, time domain simulations lack the ability to incorporate load flow constraints such as constant power specification at load buses at the fundamental frequency. As a result of these studies, distribution system design (e.g. overhead lines vs underground cable lines, location of the transformer), parameters of the distribution system (e.g. conductor types), and load behaviour have been identified as main influence factors for harmonic propagation in distribution systems [73, 74]. In addition, transformer configuration (e.g. wye-delta) is also found to be a factor which determines harmonic propagation. For example, triplen harmonics are blocked by delta windings of power transformers [75].

2.9.2 Voltage Fluctuations and Flicker

Voltage fluctuations are generally caused by large disturbing loads, such as arc furnaces. Such disturbances are compensated at the premises by employing appropriate mitigation techniques (such as a static VAr compensator). Nevertheless, the possibility exists that disturbances propagate to downstream networks, leading to lamp flicker in LV distribution networks [76].

The propagation of flicker level at one location (A) with respect to another location (B) is quantified using the flicker transfer coefficient, $T_{P\mathrm{st}:A-B}$. This coefficient is determined by the ratio between the P_{st} values measured over the same period as given in (2.19) [77]:

$$T_{P\mathrm{st}:A-B} = \frac{P_{\mathrm{st}:B}}{P_{\mathrm{st}:A}} \tag{2.19}$$

Since, the performance of the flickermeter is linear for voltage fluctuations of identical waveform shapes, P_{st} can be assumed to be proportional to the relative voltage change ($\frac{\Delta V}{V}$). Thus, $T_{P\mathrm{st}:A-B}$ can be approximated by the ratio of relative voltage fluctuations at location A and B as given by (2.20):

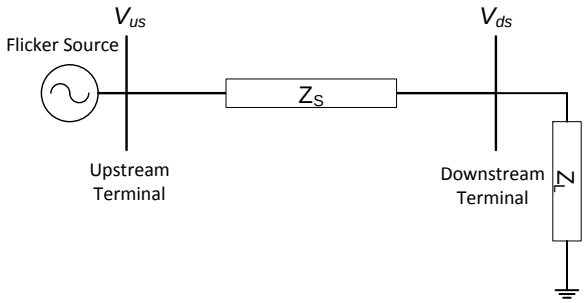

Figure 2.6: Radial power system

$$T_{P\text{st}:A-B} = \frac{\Delta V_B / V_B}{\Delta V_A / V_A} \tag{2.20}$$

where; V_A, V_B are the magnitudes of the steady-state voltages at point A and B respectively and, ΔV_A, ΔV_B are voltage fluctuations at point A and B respectively. For the radial network given in Fig. 2.6, two flicker transfer coefficients can be identified as; (1) downstream to upstream flicker transfer coefficient, $T_{P\text{st}:ds-us}$, and (b) upstream to downstream flicker transfer coefficient, $T_{P\text{st}:us-ds}$.

Investigations into flicker transfer from downstream to upstream in relation to radial networks are carried out in [78–80], where it is shown that the flicker transfer coefficient corresponds to the ratio of short-circuit capacities at the downstream to upstream network. In [81, 82], author argues that this approach may result in conservative values for flicker transfer coefficient, since the network resistance is neglected. Therefore, an evaluation process based on the current and voltage waveform measurements, which takes the network resistance in to account is proposed in [81].

In radial power systems, the upstream to downstream flicker transfer is dependent on downstream load composition [83]. Considering the radial distribution network in Fig 2.6, an expression for flicker transfer coefficient from upstream network to downstream network can be established as (2.21):

$$T_{P\text{st}:us-ds} \approx \frac{\left|\frac{\Delta V_{ds}}{V_{ds}}\right|}{\left|\frac{\Delta V_{us}}{V_{us}}\right|} = \frac{\left|1 + \frac{Z_s}{Z_L}\right|}{\left|1 + \frac{Z_s}{Z'_L}\right|} \tag{2.21}$$

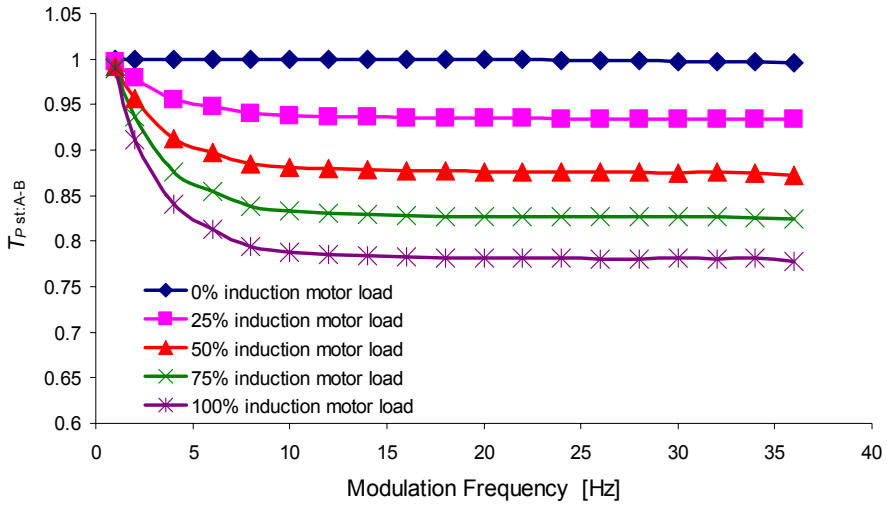

Figure 2.7: Variation of the flicker transfer coefficient with modulating frequency and the proportion of induction motor loading at the downstream location [76, 84]

where; V_{us}, V_{ds} are the magnitudes of the steady-state voltages at upstream and downstream terminals, ΔV_{us}, ΔV_{ds} are voltage fluctuations at upstream and downstream terminals, Z_L is the steady-state impedance of the load connected to the downstream terminal, Z'_L is the dynamic impedance of the load to small voltage fluctuations and Z_S is the impedance of the supply system (i.e. sum of the steady-state impedance of the transformers and the distribution line). For static components such as lighting and heating devices, the dynamic impedance is approximately equal to their steady-state impedances, which results in $T_{Pst:us-ds} \approx 1$. However, if the load consists of a significant proportion of induction motors, the combined dynamic load impedance would be relatively small compared to the corresponding steady state impedance [77], leading to a flicker transfer coefficient less than unity. Reference [76] provides a comprehensive understanding on the behaviour of induction motor loads subjected to regular voltage fluctuations and the dependency of the flicker transfer coefficient on modulation frequency. Fig. 2.7 illustrates the variation of the flicker transfer coefficient with modulation frequency and proportion of induction motor loading at the downstream network [84].

The modelling of HV to MV flicker propagation is also addressed in [84], where the flicker propagation is shown to be dependent on the type of distribution system

loads, composition of the load types, time constant of load responses and upstream impedance. In the absence of sufficient details and accurate information, a simplified model for flicker propagation from HV to MV network is proposed based on the loading level of the HV/MV transformer [84].

In comparison to radial distribution networks, the investigation of flicker propagation in interconnected systems is a non-trivial exercise due to the complexity that arises as result of interaction between various busbars. Three possible methods are reported in the established technical literature in relation to the analysis of propagation of flicker in interconnected networks. The simplified short-circuit method, which is proposed by IEC Technical Report IEC 61000-3-7 [4], is only valid for cases where a significant proportion of the sources contributing to short-circuit power at busbars, can be considered to be electrically independent. Alternatively, an impedance matrix method and load flow method have been proposed in [85].

2.9.3 Voltage Unbalance

Similar to voltage fluctuations and flicker, VU can also propagate from both upstream to downstream and downstream to upstream networks. VU propagation from an upstream network to a downstream network has been well addressed in the literature. Reference [5] reports that VU propagation from the MV to LV network, $T_{u:\mathrm{MV-LV}}$, is dependent on system and load characteristics and the downstream load composition, and can be estimated using (2.22):

$$T_{u:\mathrm{MV-LV}} = \frac{1}{1 + k_m \left(\frac{k_s - 1}{k_{sc-\mathrm{LV}} + 1} \right)} \tag{2.22}$$

where; k_m is the ratio between the rated motor load (in MVA) and the total load (in MVA) supplied by the downstream LV system, k_s is the ratio between the positive and negative-sequence (which is inductive) impedance of the aggregated motor load supplied by the LV system and $k_{sc-\mathrm{LV}}$ is the ratio between the short-circuit capacity

(in MVA) at the LV busbar and the total load (in MVA) supplied by the LV system.

Referring to (2.22), $T_{u:\mathrm{MV-LV}}$ can be observed to be less than unity when industrial load bases containing large proportions of mains connected three-phase induction motors are connected to the downstream network. VU propagation in the presence of passive loads are investigated in [86], where VU levels are shown to be exacerbated when constant current and constant power loads are connected to downstream networks.

Recent investigations into VU emission assessment have presented complex VUF based formulations which can be used to evaluate the VU emission contributions made by different sources of unbalance at the point of evaluation (POE) utilising snap-shot measurements of the power system for both radial and interconnected power systems. A generalised methodology for VU propagation is presented in [34, 35], where the effect of upstream source unbalance propagated to the POE has been separated from the VU emission at the POE.

2.10 Power Quality Disturbances due to Integration of Renewable Generation

2.10.1 Flicker Emission from Wind Generators

Voltage fluctuations leading to flicker have been identified as a key PQ problem associated with wind energy generators connected to distribution networks [1, 87, 88]. Wind farms which employ fixed speed induction generators (FSIG) are more susceptible to flicker due to power fluctuations arising as a result of variations in wind-speed, aerodynamic effects such as the tower shadow effect, yaw error and other mechanical properties of wind turbines [89–93]. A phenomenon known as 3P, in which the power output of the wind turbine oscillates at a frequency three times the blade turning speed is generally associated with the FSIGs [93, 94]. The oscillation occurs due to the wind shielding effect of each blade of a three blade

turbine as it passes the tower resulting in a reduction of about 20% of output power from the wind turbine. Wind farms which employ variable speed wind generator technologies such as doubly-fed induction generators (DFIG) and permanent magnet synchronous generators (PMSG) are considered to produce less flicker due to their capability to smooth 3P oscillations [95]. Field measurements and simulation models reported in [96–98] support the aforementioned observations in relation to variable speed wind generators. Nevertheless, flicker remains a PQ concern irrespective of generator technology, when wind generators are connected to distribution networks with low the short-circuit capacity [95].

A number of studies that have been conducted on flicker emission analysis [17, 95,99,100] in relation to wind generators are reported in technical literature. In [95], authors have identified wind speed, turbulence intensity, short-circuit ratio at the POC of the wind generator and grid impedance angles as pertinent factors which influence flicker emission from wind generators. In the case of fixed speed wind turbines, flicker emission is observed to increase with wind speed. For variable speed wind turbines, the flicker level increase with wind speed until the generator reaches its rated power. For higher wind speeds, the variable speed system will smooth out the power fluctuations, hence limiting the flicker emission [95]. In addition, higher turbulence intensity in the wind can lead to increased flicker emissions from wind generators [95].

In relation to flicker propagation from wind power generation, [101] presents a frequency domain model to investigate the flicker emission from a wind farm. Several case studies have been carried out using network models. The flicker levels at nodes with lower short-circuit power levels are observed to be relatively high, compared to the same at nodes with higher short-circuit power levels.

Modern wind generators such as DFIGs and PMSGs have proven reactive power capabilities [17, 102–104] which enable them to operate in various control modes such as power factor control and voltage control operation. In [17], the authors have

identified that the reactive power control strategy employed in the wind system can also influence the flicker emission from wind generators. The influence of wind and grid characteristics when wind farms are operating under power factor control mode, voltage control mode and reactive power dispatch mode are investigated in [17] using a simulation model of a wind farm. The study has shown that the wind generator control strategy influences flicker emission under different wind and network conditions. However, the theoretical bases explaining the flicker emission and propagation, when wind farms are operating in aforementioned control modes have not been developed. This will be the focus of the work undertaken in Chapter 6.

2.10.2 Impact of Roof Top Photovoltaic System on Distribution Network Power Quality

The proliferation of small scale PV generation systems in the LV distribution network can impact on the PQ in electrical networks [1, 10]. Some of the PQ problems discussed in the technical literature include steady-state voltage increase, harmonic and inter harmonic voltages, VU, and, flicker. In the following sections, a review of the established literature in relation to harmonics, voltage fluctuations and flicker caused by small scale PV systems is presented.

Harmonics

Photovoltaic systems can inject two distinct types of current harmonics to the distribution network. Higher order harmonics (e.g. switching frequency harmonics and associated side bands) can be injected to the distribution system due to switching operations of the power electronics [18]. In addition to switching order harmonics, low order harmonics can also be injected to the network due to the inability of the PV system switching control to produce a perfectly sinusoidal current. The control strategy employed in the PV inverter, the background distortion present at the POC and partial loading conditions [105–110] are identified as causes for low order

harmonic emissions.

The impact of harmonic currents produced by PV systems on the harmonic voltage distortion of the distribution network mainly depends on the impedance of the supply grid. Hence, PV systems connected to weak distribution networks (i.e. characterised by a low short-circuit capacity or high network supply impedance) can lead to an increase of the harmonic distortion of the network [1, 111].

Numerous studies have been conducted to investigate the impacts of PV system on harmonic emission in distribution networks. In [112–117], the increased harmonic distortion in the distribution network due to distributed PV systems is reported as a major concern. However, [1, 118] argue that the harmonic current emission (harmonic orders 5, 7, 11, 13, 17, 19, and triplen harmonics 3, 9 and 15) caused by modern PV inverter systems is smaller than the emissions by most consumer equipment, hence, increased voltage distortion due to PV systems is not substantial. However, significant increase in even harmonics, higher order triplen harmonics, and inter harmonics have been identified as a major PQ concern in [1, 18]. The cause of injection of even harmonics is investigated in [18] where it is found to be due to an unnecessarily large 2^{nd} harmonic component in the reference sine wave used to generate the switching pattern.

In addition, the harmonic emission due to multiple, identical PV systems is investigated in [18] where it is shown that the attenuation of harmonic voltages and currents are very limited, due to similar phase angles. In addition, a small amount of inverter-inverter interactions have also been identified, which can lead to an increase in harmonic emissions from each PV system.

Voltage Fluctuations and Flicker

Distribution networks may suffer from an increase in the levels of voltage fluctuations leading to flicker due to the integration of PV systems into distribution networks [10]. The problems associated with flicker are more likely to occur in situations where large

PV installations are connected to weak distribution networks (characterised by low short-circuit capacity) or when there are large numbers of parallel operated PV units operating in a localised areas (e.g. several roof top PV systems in a localised area).

Fast variations in solar irradiance and panel temperature due to passing clouds are reported as a cause in relation to flicker emission from PV systems. According to [1], a single PV panel can experience a reduction of 50% of its rated power during a period of 5 to 10 seconds, which is within the flicker frequency range. However, when a number of panels are spread over a distance of a few hundred metres (i.e. a low-voltage feeder), such changes take place in 30 - 60 seconds, which is beyond the flicker frequency range. Hence, the latter is not expected to cause an increase in the flicker levels in the network.

Inverter control characteristics have also been identified as potential contributors to flicker emission. In [1], a network impedance measurement which is performed every second by the PV inverter has been identified as a cause of flicker. In spite of the aforementioned concerns, flicker measurements carried out in [19, 118] conclude that the impacts of PV systems on flicker levels in distribution networks are minimal and well within the prescribed emission limits given in appropriate standards.

The increase in the penetration level of PV systems in a distribution network happens over time, resulting in the connection of PV systems with various technologies that have different PQ characteristics. Despite the number of studies as discussed previously, only limited research outcomes are available in the public domain [21] in which controlled experiments are carried out in a laboratory environment to investigate the harmonics and flicker behaviour of photovoltaic systems. Thus, the availability of realistic information through laboratory experiments in relation to harmonic and flicker performance of different types of PV systems, will further facilitate the DNSPs in understanding the impacts of PV systems. This aspect will be investigated in Chapter 7.

In addition to the aforementioned PQ concerns, networks can also be affected by

increased VU levels. Most PV systems are integrated into LV networks by means of a single-phase power electronic inverter unit. Large numbers of such units distributed along an LV distribution feeder can lead an increase in VU along the feeder [10]. Impact studies employing deterministic and stochastic models have been carried out in [119–121]. Results demonstrate that connection of PV installations in random location can cause an increase in VU in the network [121].

2.11 Chapter Summary

This chapter provided a review of existing knowledge in relation to three main PQ disturbances; harmonics, voltage fluctuations and flicker, and VU. The definitions, causes and impacts of each PQ disturbance were presented.

A discussion in relation to PQ disturbance emission allocation methodologies employed in various standards and technical reports was developed. A brief introduction to PQ disturbance propagation and attenuation were also presented.

The last section of the chapter covered the impact of distributed generation on PQ in distribution networks. Flicker emission from wind generators was discussed, emphasising the importance of the reactive power control strategy employed in such generator systems on flicker emission. A brief discussion on the impacts PV systems on network PQ was also presented.

Chapter 3

Comparative Analysis and Application of Harmonic Emission Allocation Methodologies

3.1 Introduction

Both appliances and installations with power electronic front-ends that draw harmonic currents are being increasingly connected to the power distribution network [22]. As a result of these harmonic currents and their interactions with network impedances, excessive harmonic voltages can develop that could adversely affect the performance of various customer and utility equipment. Thus, managing network harmonic voltage levels has become a key issue to DNSPs [2].

As discussed in Chapter 2, the harmonic current emission levels for equipment connected to the LV network are governed by product standards (e.g. IEC 61000-3-2 for equipment with rated up to current 16 A and IEC 61000-3-12 for equipment with rated current above 16 A to 75 A. The harmonic current emission levels for DGs with rated current up to 75 A are given by IEC 61000-3-15). Equipment that complies with these standards can be connected to the LV network without a detailed investigation. However, the connection of large installations and DGs to the

LV network are subject to the approval of DNSPs. Therefore, it is important that the DNSPs have carefully designed guidelines to assess large installations in relation to harmonic compatibility. A number of methodologies presently exist for the assessment of harmonic current emission limits for large installations connected to LV networks. Such applicable methodologies are detailed in the following technical reports, recommended practices and technical literature:

- IEC 61000-3-14:2011 Technical Report "Assessment of emission limits for the connection of disturbing installations to LV power systems" [2].
- "Technical Rules for the Assessment of Network Disturbances", Technical Report [66] which is used by DNSPs in Austria, Switzerland, Germany and Czech Republic.
- IEEE 519-1992 "IEEE Recommended Practices and Requirements for Harmonic Control in Electrical Power Systems" [38].
- "HB 264: Power Quality- recommended application of AS/NZS 36000.3.6 and AS/NZS 36000.3.7" [65].

In addition, the voltage droop (VD) approach [14] is currently being applied in Australia for harmonic emission allocation.

The main focus of this chapter is to examine the theoretical basis of the harmonic current emission allocation methodology presented in IEC 61000-3-14 and to investigate its applicability with regard to practical LV distribution networks. In addition, the IEC 61000-3-14 methodology will be benchmarked against other methodologies presented in aforementioned technical reports, standards and technical literature with regard to harmonic current limits, ease of application and data requirements.

This chapter is structured as follows. In Section 3.2, harmonic current emission allocation methodology presented in IEC 610000-3-14 is summarised. The theoretical basis of the concept of reduction factor, which is used in the IEC methodology is

presented in Section 3.3. Section 3.4 summarises the alternative methodologies for the assessment of harmonic current emission limits given by the Technical Report "Technical Rules for the Assessment of Network Disturbances", the VD method, IEEE 519 standard, and the CBV method respectively. Section 3.5 provides two application examples of these methodologies based on two LV distribution networks. Section 3.6 presents a critical discussion on the various methodologies. Section 3.7 summarises the work presented in the chapter emphasising the major conclusions.

3.2 Harmonic Emission Allocation Methodology Given in IEC 61000-3-14 [2]

The IEC 61000-3-14 provides a methodology for the assessment of harmonic current emission limits for individual installations connected to radial LV systems, based on the EMC concepts discussed in Section 2.5. A simplified scheme of a radial LV network, which will be used to illustrate the harmonic emission allocation process is given in Fig. 3.1. Three stages of evaluation which can be applied either in sequence or independently [2], are defined for the assessment of emission limits.

Stage 1: Small installations, such as residential houses, whose apparent power (VA) capacity, S_i, is less than the minimum value, $S_{\min}$, as defined by a DNSP, can be connected to the supply network without any further investigation. In such cases, the DNSP will rely on equipment standards [6,7] to limit the effects of harmonic emission on the network. Therefore, the selection of $S_{\min}$ is a compromise between limiting

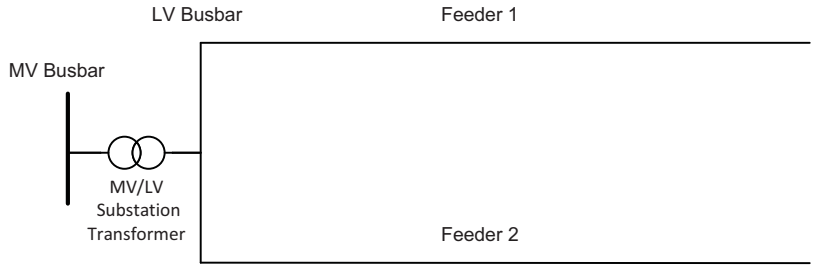

Figure 3.1: Simplified scheme of a radial LV system

the number of installations of which emissions need to be assessed and keeping the network harmonic emissions within acceptable limits. In addition, connection of an installation can be allowed under Stage 1, if the following conditions are met:

- The customer does not use power factor correction capacitors and/or harmonic filters,
- The ratio between the VA capacity of the installation (S_i) to short-circuit capacity at the POE ($S_{sc:i}$) is less than 1%,
- For each harmonic order, the harmonic current emission is smaller than the limit defined by the DNSP according to the network characteristics. The IEC 61000-3-14 does not provide procedures for evaluating the harmonic current emission limit. However, indicative values provided are given in Table 3.1 [2].

Table 3.1: Indicative values for harmonic current emission limits for Stage 1 assessment

Harmonic order (h)	3	5	7	9	11	13	$13 < h \leq 40$
Harmonic current emission limit as a % of rated current	4	5	5	1	3	3	$\frac{500}{h^2}$

Stage 2: For large installations ($S_i > S_{\min}$) that do not comply with Stage 1, higher harmonic current emission limits are allowed based on the network harmonic absorption capacity, the VA capacity of the installation and the network characteristics. The underlying concept of this approach is that, if the network is fully utilised to its capacity and if all installations inject up to their allocated limits, the net harmonic voltage level at the end of a feeder should be less than or equal to the chosen planning level.

Referring to Fig. 3.1, the total harmonic voltage at the LV level is the combination of harmonic voltages propagating from the upstream MV network and the contribution from the harmonic loads connected to the considered LV network.

Therefore, the maximum acceptable global contribution of harmonic voltage to the LV level, $G_{h:\mathrm{LV}}$, is given by (3.1) [2]:

$$G_{h:\mathrm{LV}} = \sqrt[\alpha]{L_{h:\mathrm{LV}}^{\alpha} - (T_{h:\mathrm{MV-LV}} L_{h:\mathrm{MV}})^{\alpha}} \tag{3.1}$$

where; $L_{h:\mathrm{MV}}$, $L_{h:\mathrm{LV}}$, $T_{h:\mathrm{MV-LV}}$ and α are the MV planning level, the LV planning level, the transfer coefficient from the upstream MV network to the LV network, and the summation law exponent for the h^{th} order harmonic respectively.

Noting that the harmonic voltage at the LV network arises due to both large installations and small installations, the individual current emission limits for a large installation can be established, subjected to the following two conditions:

1. The global contribution of all small and large installations to the harmonic voltage at any point of the network should not exceed $G_{h:\mathrm{LV}}$,

2. The global contribution of all small and large installations to the harmonic voltage at the substation LV busbar should not exceed maximum acceptable global contribution, $G_{h:B}$, value given by (3.2) [2]:

$$G_{h:B} = K_{hB} G_{h:\mathrm{LV}} \tag{3.2}$$

where; K_{hB} is a reduction factor which takes into account the contribution of harmonic voltage caused by small installations at the LV busbar. This factor is calculated by assuming that the entire network is fully loaded with small installations only and is given by (3.3) [2]:

$$K_{hB} = \frac{V_{h:\mathrm{B}}(S_t)}{\max(V_{h:\mathrm{LV}}(S_t))} \tag{3.3}$$

where; $V_{h:\mathrm{B}}(S_t)$ is the global contribution of all small installations, to the harmonic voltage of order h at the transformer LV busbar, and $\max(V_{h:\mathrm{LV}}(S_t))$ is the maximum value of the global contribution of all small installations, to

the harmonic voltage of order h at any point in the considered LV system.

A methodology for estimating K_{hB} is given in the IEC 61000-3-14 [2].

The fundamental assumption is that the percentages of small and large installations are generally not known in advance and depend highly on the LV system considered. Therefore, the emission limits for large installations will be defined so that a large installation can replace a set of small installations having the same global power without increasing harmonic voltage levels [2].

The harmonic current emission limit for an individual large installation, i, is given by (3.4) [2]. A detailed discussion, explaining the theoretical bases of (3.4) will be presented in Section 3.3.

$$E_{Ih:i} = \frac{V_n^2}{S_i} \cdot G_{h:LV} \sqrt[\alpha]{\frac{S_i}{S_t}} \min\left(\frac{K_{hB}}{Z_{h:B}}, \frac{1}{Z_{h:i}}\right) \tag{3.4}$$

where;

$E_{Ih:i}$ is the harmonic current emission limit for the installation i expressed as a percentage of the rated current of the installation,

V_n is the nominal phase-to-phase voltage of the LV network (V),

S_i is the VA capacity of the installation i (VA),

S_t is the total system VA capacity of the considered LV network (VA),

$Z_{h:B}$ is the modulus of the harmonic impedance at the LV busbar (Ω),

$Z_{h:i}$ is the modulus of the harmonic impedance at the POE of the customer installation i (Ω),

$\min(x, y)$ represents the minimum value of x and y.

The total system VA capacity, S_t, is usually selected as the VA capacity of the MV/LV transformer. When DGs are connected to the considered LV network, the VA capacity of the DG should be taken into account in determining the total system capacity, S_t. For instance, if an LV network has a 50% penetration level by

DG sources, S_t should be adjusted to be 150% of the MV/LV transformer capacity. This step ensures that some proportion of the system harmonic absorption capacity is available for harmonic current emission from DGs.

Stage 3: On some occasions, connection of an installation which fails to comply under Stage 2 is accepted at a higher emission level under a conditional basis. This is particularly the case, when the parameters used under Stage 2 are conservative and there is some unused disturbance absorption capacity of the network that can be used on a temporary basis. Connection of an installation under Stage 3 will require conducting a detailed study to determine the pre-existing harmonic levels and the expected contribution of the considered installation.

For the assessment of harmonic current emission limits under Stage 3, DG installations can be considered as disturbing installations. Correspondingly, S_t needs to be adjusted to take into account the presence of DG sources as in Stage 2.

3.3 Reduction Factor

3.3.1 Rationale of the Concept of Reduction Factor

A key concept introduced in IEC 61000-3-14 as presented in Section 3.2 is the reduction factor (K_{hB}). The reduction factor takes into account the harmonic current emission from small installations, for which the emission limits given in IEC 61000-3-14 do not apply, when allocating harmonic current emission limits for large installations. The importance of such a factor in the emission allocation process can be established by considering the LV network given in Fig. 3.1.

Assume that the MV/LV transformer has a capacity of 100 kVA and an impedance of $(0.037 + j0.060)\ \Omega$ referred to the LV side (i.e. $0.01 + j0.04$ pu). The network consists of two feeders, each 300 m long. Both phase and neutral conductor impedances are $(0.96 + j0.35)\ \Omega$/km [2]. Considering the 5^{th} harmonic, the maximum acceptable global contribution of harmonic voltage at the LV level, $G_{h:\text{LV}}$, can be calculated us-

ing (3.1). Assuming an MV planning level of 5%, an LV planning level of 6%, an MV to LV transfer coefficient of 1.0 and summation exponent of 1.4 [2], $G_{h:\mathrm{LV}}$ is calculated as 2.07%.

Consider the case of 20 small installations each with 2.5 kVA capacity, connected to each feeder and all installations are equally distributed along the feeder. The harmonic current emission from each small installation is estimated to be proportional to its apparent power and is given by (3.5) [2]:

$$E_{Ih:i} = A_h \sqrt[\beta]{S_i} \tag{3.5}$$

where; $E_{Ih:i}$ is the harmonic current emission from a small installation, S_i is the apparent power of the small installation calculated in per-unit, β is the summation law exponent for the small installation[1] and A_h is an allocation constant. The allocation constant is calculated under the assumption that when the network is fully loaded with small installations only (which are equally distributed along the feeder), the harmonic voltage contribution from all small installations to the harmonic voltage at the extremity[2] of the network is equal to $G_{h:\mathrm{LV}}$. For the given network, A_h for 5^{th} harmonic is calculated to be 0.071[3]. Therefore, the 5^{th} harmonic current emission from each small installation can be calculated using (3.5) and equals to 20.22% of its rated current. The contribution from all small installations to the harmonic voltages at the LV busbar, the end of Feeder 1 and the end of Feeder 2 are 1.33%, 2.07% and 2.07% respectively.

[1]Smaller installations such as houses have similar installed equipment and behaviour, leading to less diversity between their harmonic characteristics. Therefore, the phase angle diversity is expected to be less in small installations compared to large installations. As a result, the summation exponent proposed for for small installations, β, is generally lower than the summation exponent proposed for large installations, α [2]. The recommended values for β for different harmonic orders are given in IEC 61000-3-14. However, to simplify the analyses in this section, β for the 5^{th} harmonic is selected as 1.4.

[2]The extremity of the network is defined as the point in the network where the highest harmonic voltage would occur.

[3]The methodology for calculating the allocation constant, A_h, follows the same principles as the CBV approach discussed in Chapter 2, Section 2.8.1. Further discussion related to CBV approach is presented in Section 3.4.4. As discussed in Section 2.8.1, the allocation constant is dependent on network characteristics such as conductor impedance, transformer impedance, and network configuration. A_h for the network under consideration is calculated using a base of 100 kVA.

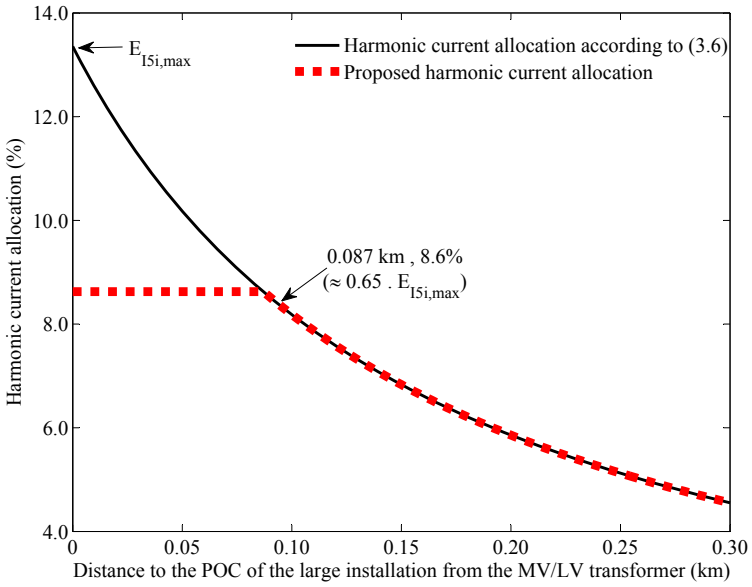

Figure 3.2: Harmonic current allocation for the large installation as a function of distance, l_i, from the LV busbar to the POC

Now, consider that all small installations connected to Feeder 2 are replaced by one large installation, with a capacity equal to the sum of all small installations in Feeder 2. The large installation is connected (l_i) km away from the LV busbar. For large installations, harmonic current emission allocation can be achieved by apportioning the $G_{h:\mathrm{LV}}$, based on the ratio of the installation VA capacity to the network VA capacity (i.e. the transformer capacity). The allowable harmonic current emission limit for the large installation, taking harmonic current diversity among loads into account is given by (3.6):

$$E_{Ih:i} = \frac{V_n^2}{S_i} \cdot \frac{1}{Z_{h:i}} G_{h:\mathrm{LV}} \sqrt[\alpha]{\frac{S_i}{S_t}} \tag{3.6}$$

Considering that $G_{h:\mathrm{LV}}$ equals to 2.07% (from (3.1)), S_i = 50 kVA and S_t = 100 kVA, a graphical representation of the harmonic current allocation for the large installation according to (3.6) (as a percentage of its rated current) as a function of l_i is given by the unbroken lines in Fig. 3.2. In addition, the resulting harmonic voltage at the ends of Feeder 1 and Feeder 2 from all installations (i.e. small installations and the large installation) connected to the LV network, as a function of l_i are given in Fig. 3.3 and Fig. 3.4 respectively using unbroken lines.

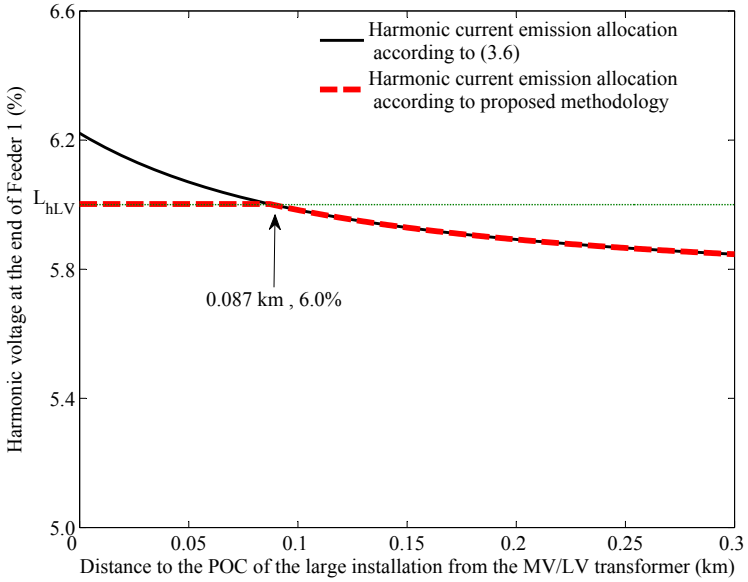

Figure 3.3: Harmonic voltage at the end of the Feeder 1 as a function of distance, l_i, from the LV busbar to the POC of the large installation connected to Feeder 2

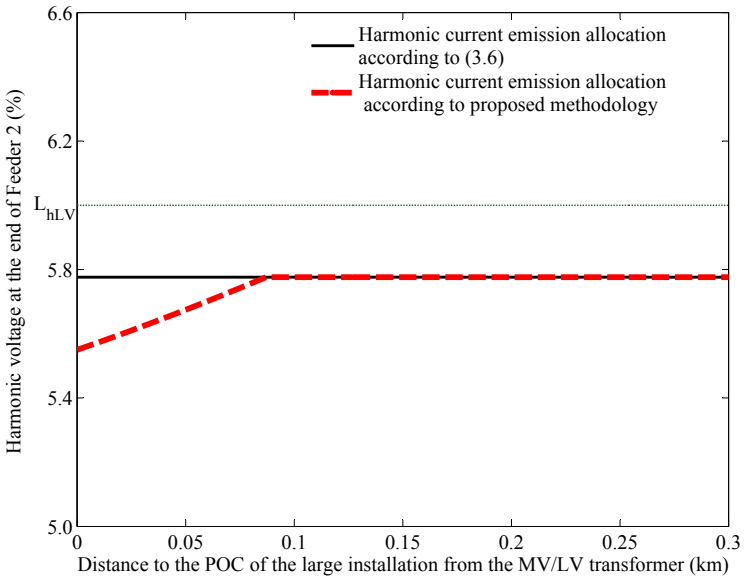

Figure 3.4: Harmonic voltage at the end of the Feeder 2 as a function of distance, l_i, from the LV busbar to the POC of the large installation connected to Feeder 2

Fig. 3.2 illustrates that the harmonic current allocation for the large installation reduces as the POC is varied along the feeder from the LV busbar to the end of Feeder 2. For instance, the harmonic current allocation of 13.2%, if the installation is connected to the LV terminal of the transformer (which is called $E_{5i,\max}$ hereafter) reduces to 4.6% if the installation is connected at the end of Feeder 2.

With reference to Fig. 3.3, $l_i = 0.087$ km can be observed as the critical point where the harmonic voltage at the and of Feeder 1 reaches the LV planning level. If $l_i < 0.087$ km, and if the harmonic current emission allocation for the large installation is carried out according to (3.6), Feeder 1 harmonic voltage will exceed the LV planning level. This is because, the harmonic current allocated to the large installation causes significantly higher harmonic voltage at the transformer LV terminal, which in turn increases the harmonic voltage at the end of Feeder 1. However, if $l_i \geq 0.087$ km, and the harmonic current emission allocation for large installation is carried out according to (3.6), Feeder 1 harmonic voltage will not exceed the LV planning level. Referring to Fig. 3.2, the corresponding harmonic emission allocation for the large installation when $l_i = 0.087$ km, can be found as 8.6% of rated current. Therefore, in order to maintain the Feeder 1 harmonic voltage within the LV planning level, harmonic current allocation for the large installation is proposed to be maintained at 8.6% (which is $0.65 \cdot E_{5i,max}$) if $l_i \leq 0.087$ km. For $l_i > 0.087$ km, the harmonic current emission allocation for large installation is required to be limited according to (3.6), in order to maintain the harmonic voltage of Feeder 2 within the $L_{h:\mathrm{LV}}$. The proposed harmonic current allocation levels for the large installation and corresponding harmonic voltages at the end of Feeders 1 and 2 are given in Fig. 3.2, Fig. 3.3 and Fig. 3.4 respectively using broken lines.

The constant 0.65 which was identified using Fig. 3.2 and Fig. 3.3, provides the fraction of $E_{5i,\max}$, that is allowed for the large installation, in order to maintain the network 5^{th} harmonic voltage at the end of Feeder 1 within the planning level. The mathematical analyses given in IEC 61000-3-14 shows that this constant (which is termed as the 'reduction factor, K_{hB}') can be approximated by the ratio of the

harmonic voltage contribution from all small loads to the harmonic voltage at the LV busbar (which is 1.33% for the network described in this section), and the harmonic voltage contribution from all small loads to the harmonic voltage at the end of Feeder 1 (which is 2.07% for the network described in this section), when the network is fully loaded with small installations only. A generic expression for the reduction factor when the networks consist of several feeders with unequal loading levels is given by (3.3). For brevity, (3.3) is repeated as follows:

$$K_{hB} = \frac{V_{h:B}(S_t)}{\max(V_{h:LV}(S_t))} \tag{3.7}$$

where; $V_{h:\mathrm{B}}(S_t)$ is the global contribution of all installations, to the harmonic voltage of order h at the transformer LV busbar, and $\max(V_{h:\mathrm{LV}}(S_t))$ is the maximum value of the global contribution of all installations, to the harmonic voltage of order h at any point in the considered LV system, when the network is fully loaded with small installations only.

The proposed harmonic current emission allocation in Fig. 3.2 can be achieved by replacing the term $\frac{1}{Z_{h:i}}$ in (3.6) with $\min(\frac{K_{hB}}{Z_{h:\mathrm{B}}}, \frac{1}{Z_{h:i}})$, leading to (3.4). The mathematical derivation of (3.4) is provided in IEC 61000-3-14.

With reference to (3.7), both $V_{h:B}(S_t)$ and $\max(V_{h:\mathrm{LV}}(S_t))$ can be shown to be proportional to the allocation constant for small installations, A_h. Therefore, the reduction factor in (3.7) is independent of A_h. As a result, the reduction factor will also be independent of the harmonic emission of small installations. Assuming an LV network with n number of feeders and contains only small installations, K_{hB} can also be calculated using (3.8) [2]:

$$K_{hB} = \frac{1}{\max\left[\sqrt[\beta]{1 - \frac{S_{Fj}}{S_t} + \sum_{k=1}^{m} \frac{S_{jk}}{S_t}\left(\frac{Z_{h:jk}}{Z_{h:\mathrm{B}}}\right)^{\beta}}\right]} \text{ for j =1,2,...,n} \tag{3.8}$$

where;

j is any feeder in the LV distribution network under consideration and $j = 1, 2, 3, ..., n$,

$Z_{h:\mathrm{B}}$ is the modulus of the harmonic impedance at the LV busbar (Ω),

S_t is the total system VA capacity of the considered LV network (VA),

S_{Fj} is the total VA capacity of all small installations connected to feeder j (VA),

m is the number of small installations connected to the feeder j,

k is any small installation that is connected feeder j, and $k = 1, 2, 3, ..., m.$,

$Z_{h:jk}$ is the harmonic impedance at the POE of the small installation k, which is connected to feeder j (Ω).

Referring to (3.8), the reader should note that the reduction factor will be dependent on network characteristics (i.e. number of feeders, network configuration, harmonic order, harmonic impedance of conductors and transformers) and the load distribution assumed in the network [2]. A sensitivity analyses with respect to the aforementioned parameters has been carried out in [2], assuming homogeneous conductors in the LV network. The salient factors are found to be the total system capacity, the number of feeders and the length of feeders. With respect to the harmonic order, the reduction factor is found to show only a slight variation in the case of non-triplen harmonics. The reduction factor for triplen harmonics is significantly less, compared to non-triplen harmonics due to the harmonic voltage drop in the neutral conductor. The reduction factor as a function of the length of the LV feeders, number of feeders and the capacity of MV/LV transformer is provided in a tabular form in [2].

The recommended approach for DNSPs to select the reduction factor is either by using the Tables given in Annex A of IEC 61000-3-14 or by application of (3.8). In order to apply (3.8) and accurately estimate the reduction factor, detailed knowledge with regard to the distribution of load in the network is required. In addition, difficulties also arise when the LV distribution network consists of LV feeders with spurs or when the network consists of number of different types of conductors, which is a situation in practical LV distribution networks. Under such situations, DNSPs need to calculate the reduction factor based on the fundamental principles described.

3.3.2 Dependency of Reduction Factor on Harmonic Current Injection from Small Installations

In both IEC 61000-3-14 and Section 3.3.1, the reduction factor is estimated subject to the condition that, when the network is fully loaded with small installations only, the harmonic voltage contribution from all small installations at the extremity of the network, is equal to $G_{h:\mathrm{LV}}$. With this assumption, each small installation in Section 3.3.1 was assumed to be injecting a 5^{th} harmonic current equal to 20.2% of its rated current. As the harmonic current allocation constant, A_h, is dependent on the characteristics of the network (i.e. the number of feeders, network configuration, harmonic impedance of conductors and transformers), the harmonic current allocation for small installations will also vary from one network to the other. This could lead to situations where the harmonic current emission assumed for small installations are significantly higher than what could occur in a practical distribution network. As the reduction factor (calculated according to (3.7) and (3.8)) is independent of the harmonic current emission from smaller installations, such situations are not reflected in the reduction factor calculation. Therefore, the application of the reduction factor for harmonic current emission allocation would unnecessarily restrict the harmonic emission limit for large installations. Similarly, the proposed approach may lead to situations where the harmonic current emission levels assumed for small installations are significantly lower than what could occur in a practical distribution network. As a result, higher emission limits are allowed for large installations, which could lead to harmonic voltages in the network that exceed the planning level.

In this section, the sensitivity of the reduction factor to the harmonic current emission assumed for small installations is investigated, employing the LV distribution network discussed in Section 3.3.1. The network consists of 10, 2.5 kVA small installations and a 50 kVA large installation which are connected to Feeder 1 and Feeder 2 respectively. Small installations are assumed to be equally distributed

along the Feeder 1, whereas the large installation is assumed to be connected to l_i km away from the LV busbar in Feeder 2. Four cases are considered. In the first two cases, the 5^{th} harmonic current emissions of small installations are assumed to be 17.5% and 22.5% of the rated current, and the corresponding reduction factor values are calculated following the principles given in Section 3.3.1. In the third case, the 5^{th} harmonic current emissions of small installations are assumed to be 10%, leading to a reduction factor of unity. In the fourth case, the 5^{th} harmonic current emissions of small installations are assumed to be 25% and it is shown that irrespective of the value used the for the reduction factor, the harmonic voltage in the distribution network will exceed the set planning level.

Consider the case where the harmonic current emission from small installations is 17.5% of rated current. The large installation connected to Feeder 2 is assumed to be injecting a harmonic current as given by (3.6). Fig. 3.5 illustrates the harmonic current emission allocation for the large installation and the corresponding harmonic voltage at the end of Feeder 1 as a function of l_i. Referring to Fig. 3.5 and Section 3.3.1, if the small installations are injecting 17.5% of their rated current, the maximum allowable harmonic current emission allocation for the large installation can be identified as 11.4% of its rated current (which is $0.85 \cdot E_{5i,\max}$), in order to maintain the Feeder 1 voltage within the planning level. Hence, the corresponding reduction factor would be 0.85. Similarly, Fig. 3.6 illustrates the harmonic current emission allocation for the large installation and the corresponding harmonic voltage at the end of Feeder 1 as a function of l_i, if the small installations are injecting 22.5% of harmonic current. The maximum allowable harmonic current emission allocation for the large installation can be found as 5.6% (which is $0.42 \cdot E_{5i,\max}$), which corresponds to a reduction factors of 0.42.

Fig. 3.7 and Fig. 3.8 illustrate the harmonic current emission allocation for the large installation and the corresponding harmonic voltage at the end of Feeder 1 as a function of l_i, when small installations are injecting harmonic current levels of 10% and 25% of their rated value. According to Fig. 3.7, the harmonic voltage at

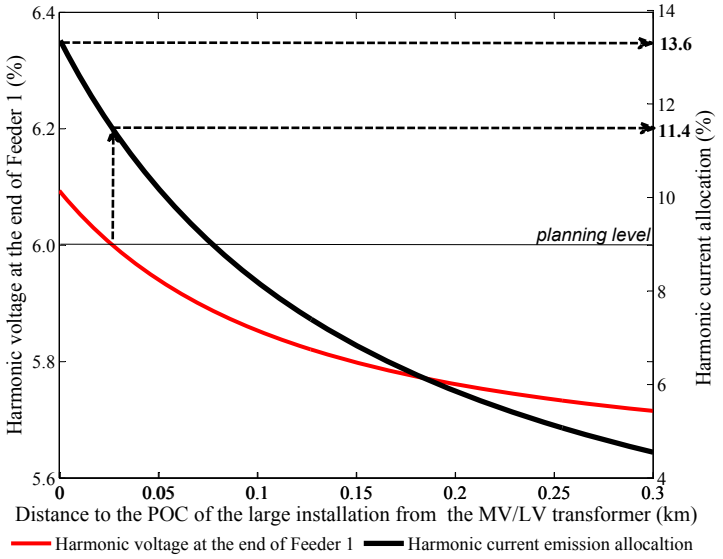

Figure 3.5: 5th harmonic voltage at the end of the Feeder 1 (when small installations are injecting harmonic current of 17.5% of its rated current) and harmonic current allocation for the large installation, as a function of distance from the LV busbar to the POC of the large installation in Feeder 2

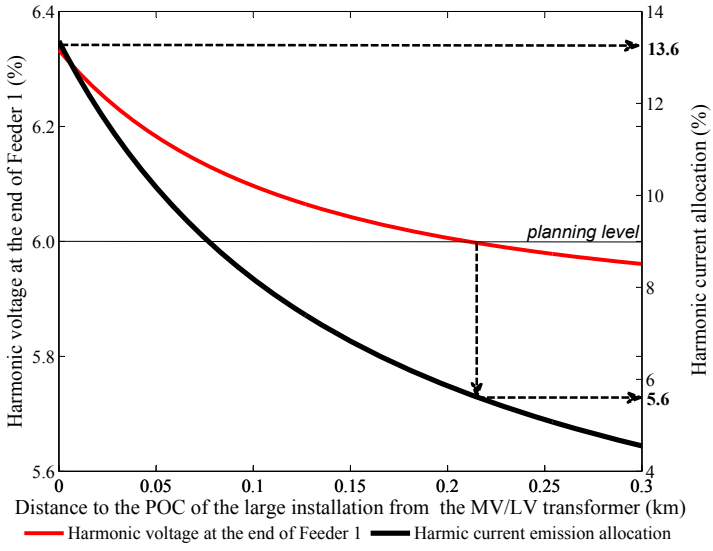

Figure 3.6: 5th harmonic voltage at the end of the Feeder 1 (when small installations are injecting harmonic current of 22.5% of its rated current) and harmonic current allocation for the large installation, as a function of distance from the LV busbar to the POC of the large installation in Feeder 2

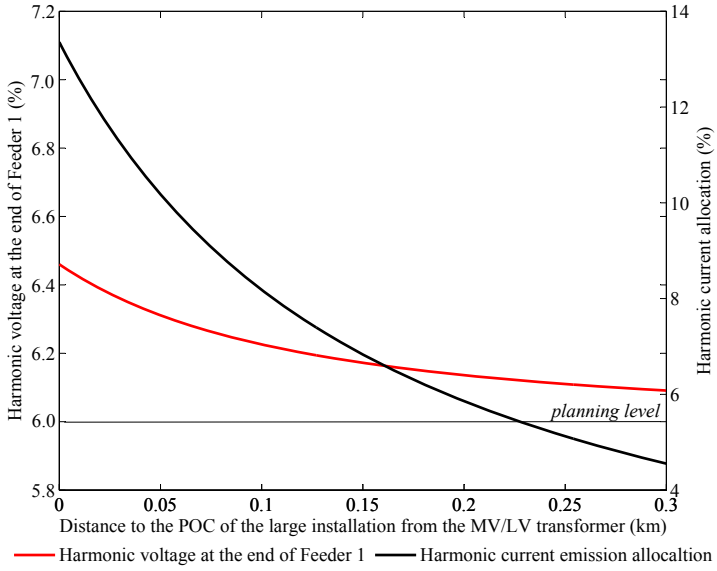

Figure 3.7: 5^{th} harmonic voltage at the end of the Feeder 1 (when small installations are injecting harmonic current of 10% of its rated current) and harmonic current allocation for the large installation, as a function of distance from the LV busbar to the POC of the large installation in Feeder 2

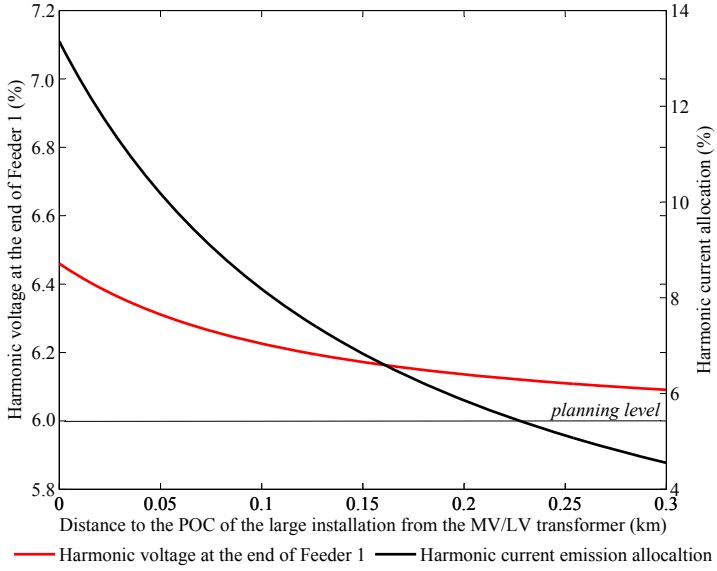

Figure 3.8: 5^{th} harmonic voltage at the end of the Feeder 1 (when small installations are injecting harmonic current of 25% of its rated current) and harmonic current allocation for the large installation, as a function of distance from the LV busbar to the POC of the large installation in Feeder 2

the end of Feeder 1 is less than the planning level, irrespective of the position of the large installation. Therefore, the maximum allowable harmonic current for the large installation will be 13.6%, which corresponds to a reduction factor of unity. However, when the harmonic current emissions from small installations are 25% of their rated current, the harmonic voltage at the end of the Feeder 1 exceeds the planning level, irrespective of the position of the large installation. Therefore, (3.6) cannot be used for harmonic current emission allocation for the large installation.

Fig. 3.9 illustrates the variation of the magnitude of the reduction factor for different levels of harmonic current injections from small installations for 3^{rd}, 5^{th} and 7^{th} harmonics for the given network. Accordingly, if the 5^{th} harmonic current injections from small installations are less than 15% of their rated current, the reduction factor would be unity. Similarly, if the 3^{rd} and 7^{th} harmonic injections from small installations are less than 5% and 10% respectively, the corresponding reduction factor would be unity. However, if the 3^{rd} and 7^{th} harmonic injections from small installations are greater than 12.5% and 17.5% respectively, the harmonic

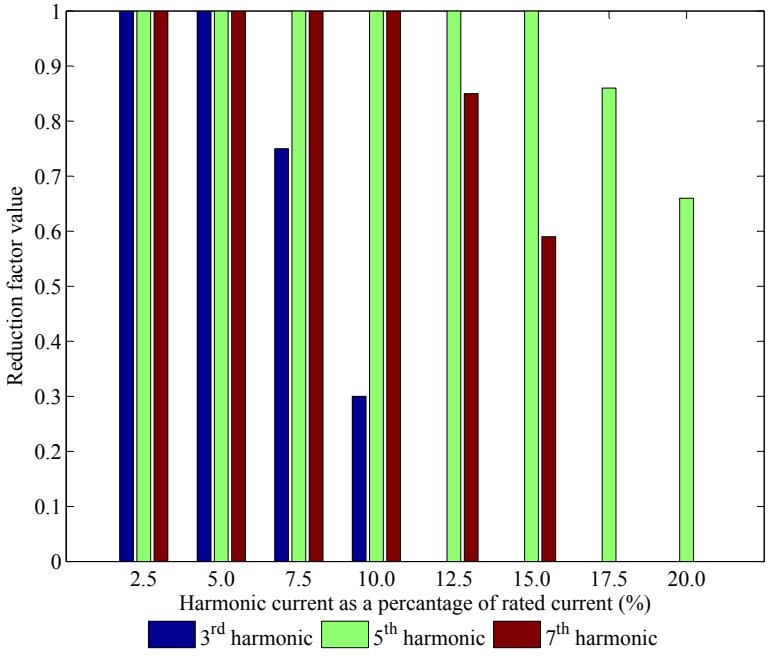

Figure 3.9: Variation of reduction factor value with harmonic current injection from small installations

voltage at the end of Feeder 1 exceeds the stipulated planning level, irrespective of the value used for reduction factor.

From this discussion, the reader should note that the reduction factor is dependent on the harmonic current emission from the small installations. As expected, the calculation of reduction factor and harmonic current emission allocation according to IEC approach might lead to the following extreme situations:

- Network voltage exceeding the LV planning level (as in the case when small installation harmonic emissions are assumed as 25%);
- Harmonic current emission allocation for a large installation is unnecessarily restricted (as in the case when small installation harmonic emission is assumed as 10%).

Therefore, an approach using a fixed harmonic emission for small installations based on field measurements is a better solution for calculating the reduction factor across different networks.

3.3.3 Reduction Factor for Network with Large Installations Only

A fundamental assumption made in the IEC harmonic current emission allocation methodology is that the percentages of small and large installations are generally not known in advance, and depend on the LV system considered [2]. In this section, the reduction factor is examined when all connected installations are classified as large installations, employing the LV network given in Fig. 3.1. In Feeder 1, n number of installations with VA capacities of $S_{F1:1}, ..., S_{F1:n}$ are connected. The harmonic impedance at the POC of each installation is $Z_{hF1:1}, ..., Z_{hF1:n}$ respectively. Similarly, m number of installations with VA capacities of $S_{F2:1}, ..., S_{F2:m}$ are connected to Feeder 2. The harmonic impedances at the POC of each installation is $Z_{hF2:1}, ..., Z_{hF2:m}$ respectively. If each installation is provided with a harmonic current emission limit based on (3.6), the harmonic voltage contribution from all in-

stallations to the harmonic voltage the end of Feeder 1, $V_{h:F1n}(S_t)$, can be expressed as (3.9):

$$V_{h:F1n}(S_t) = G_{h:\mathrm{LV}} \cdot \left[\sum_{i=1}^{n} \frac{S_{F1:i}}{S_t} + \sum_{j=1}^{m} (\frac{Z_{h:\mathrm{B}}}{Z_{h:F2j}})^{\alpha} \frac{S_{F2:j}}{S_t} \right]^{1/\alpha} \tag{3.9}$$

Since, $Z_{h:\mathrm{B}} \leq Z_{h:F2j}$ for all j=1,...,m,

$$V_{h:F1}(S_t) \leq G_{h:\mathrm{LV}} \cdot \left[\frac{\sum_{i=1}^{n} S_{F1:i} + \sum_{i=1}^{n} S_{F2:j}}{S_t} \right]^{1/\alpha} \tag{3.10}$$

Since $\sum_{i=1}^{n} S_{F1:i} + \sum_{j=1}^{n} S_{F2:j} \leq S_t$,

$$V_{h:F1}(S_t) \leq G_{h:\mathrm{LV}} \tag{3.11}$$

Similarly, the contribution from all loads connected at the LV network to the harmonic voltage at the end of Feeder 2, $V_{h:F2n}(S_t)$, can be shown to be:

$$V_{h:F2n}(S_t) \leq G_{h:\mathrm{LV}} \tag{3.12}$$

Equations (3.11) and (3.12) suggest that if all installations connected to the LV distribution network are classified as large installations, and harmonic emission allocation is carried out using (3.6), the harmonic voltage contribution from all loads to the harmonic voltage at the end of Feeder 1 and Feeder 2 would be less than or equal to $G_{h:\mathrm{LV}}$. Hence, the harmonic voltages at the end of Feeder 1 and Feeder 2 calculated using (3.1) will be within the planning level for the network. Therefore, if the network only consists of installations classified as large installations, the harmonic emission allocation can be carried out using (3.6). Alternatively, considering the fact that the term $\min(\frac{K_{hB}}{Z_{h:\mathrm{B}}}, \frac{1}{Z_{h:\mathrm{i}}})$ in (3.4) is equal to $\frac{1}{Z_{h:\mathrm{i}}}$ when $K_{hB} = 1$, it is possible to use (3.4) for harmonic current emission allocation for the network discussed using $K_{hB} = 1$. Therefore, if the network consists only of installations classified as large installations, the reduction factor would be considered as unity.

3.4 Alternative Harmonic Emission Allocation Methodologies

3.4.1 Technical Rules for the Assessment of Network Disturbances [66]

The Technical Report, Technical Rules for the Assessment of Network Disturbances [66] provides an alternative methodology for harmonic emission allocation for disturbing installations connected to LV networks. The methodology proposed in [66] follows the same philosophy as IEC 61000-3-14 (e.g. compatibility levels) [122, 123].

Assessment of emission limits for an installation is carried out in three steps:

Step 1: The ratio of the short-circuit capcity at the PCC, $S_{sc:i}$ (in kVA), to the agreed power of the installation, S_i (in kVA), is assessed. If $S_{sc:i}/S_i \geq 150$, the connection of the installation is automatically accepted and calculation of emission limits is not required.

Step 2: The ratio of the harmonic load, $S_{OS:i}$ (in kVA), to the agreed power of the installation, S_i, is determined. In order to determine $S_{OS:i}$, each load in the installation is grouped into one of the following three categories based on the total harmonic current distortion (THD_I);

1. Loads with $\text{THD}_\text{I} < 10\%$, are not considered in determining $S_{OS:i}$.
2. Loads with $10\% \leq \text{THD}_\text{I} \leq 25\%$, are classified as Group 1 and their capacity ($S_{\text{Gr.1}}$) is determined.
3. Loads with $\text{THD}_\text{I} > 25\%$, are classified as Group 2 and their capacity ($S_{\text{Gr.2}}$) is determined.

Considering the diversity of each load, the total $S_{OS:i}$ is calculated using (3.13) [66]:

$$S_{OS:i} = 0.5 \cdot S_{\text{Gr.1}} + S_{\text{Gr.2}} \tag{3.13}$$

Table 3.2: Proportionality factor values (p_h) for typical converter harmonics [66]

h	3	5	7	11	13	17	19	≥ 19
p_h	6 (18*)	15	10	5	4	2	1.5	1

$*$ p_h value for determining the harmonic current limit in the neutral conductor.

No distinction is made between the active power and the apparent power of the installation when determining $S_{OS:i}$ [66].

Step 3: The ratio of the harmonic load to the agreed power of the installation ($S_{OS:i}/S_i$) is examined subject to the following two conditions:

1. If $(S_{OS:i}/S_i) \leq 0.082 \cdot \sqrt{S_{sc:i}/S_i}$, the connection is approved and the calculation of emission limits is not required;

2. If $(S_{OS:i}/S_i) \geq 0.082 \cdot \sqrt{S_{sc:i}/S_i}$, remedial measures should be employed to limit the emission such that the allocation (which will be given by (3.14)) is not exceeded.

Emission allocation limit, $E_{Ih:i}$, in Amperes, for an installation i, is determined using (3.14) [66]:

$$\frac{E_{Ih:i}}{I_{L:i}} \leq \frac{p_h}{1000} \cdot \sqrt{\frac{S_{sc:i}}{S_i}} \tag{3.14}$$

where; $I_{L:i}$ is the rated current of the installation calculated based on the agreed power of the installation in Amperes (i.e. the VA rating of the installation). The proportionality factor, p_h, takes into account the permissible maximum harmonic voltage contribution at the transformer LV busbar for the h^{th} order harmonic. Typical values of p_h for converter specific harmonics are given in Table 3.2.

In addition, a total demand distortion factor (termed as the total harmonic factor in the Technical Report) ($\text{TDD}_{I:i}$) for the considered installation can be evaluated by (3.15) [66]:

$$\text{TDD}_{I:i} \leq \frac{20}{1000} \cdot \sqrt{\frac{S_{sc:i}}{S_i}} \tag{3.15}$$

For DGs, emission limits are required only if power in-feed takes place via power electronic front-ends. For such installations, 50% of the emission limit calculated using (3.14), are provided.

3.4.2 Voltage Droop Method

The VD method provides a harmonic allocation approach applicable to installations at both MV and LV levels [14, 16]. The philosophy of the VD method is that the h^{th} harmonic impedance of the network is h times the fundamental reactance. Thus, the h^{th} harmonic voltage drop contribution of an installation is proportional to the fundamental VD of that installation. Therefore, when aggregated across all installations, the maximum harmonic voltage in the network which would occur at the end of the most heavily loaded LV feeder, is proportional to h times the VD limit of the network [16]. This assumption will only be valid if the resistive component of the network impedance is negligible when compared to the reactive component of the network impedance. The data requirements for the application of this methodology are only the agreed power of the installation to be connected, S_i, and the fundamental reactance at the PCC, $x_{1:i}$.

The emission allocation limit for non-triplen harmonics of order h for the i^{th} installation is given by (3.16) [15]:

$$E_{Ih:i} = k_h \cdot \frac{S_i^{1/\alpha}}{x_{1:i}^{1-1/\alpha}} \tag{3.16}$$

and k_h is given by (3.17) [15]:

$$k_h = \frac{L_{h:\text{LV}}}{h \cdot V_{\text{droop}}^{1/\alpha}} \tag{3.17}$$

where; V_{droop} is the maximum system voltage drop which is 30-40% [15] for typical Australian networks, S_i is the agreed power of the installation to be connected in per-unit and $x_{1:i}$ is the fundamental reactance at the PCC in per-unit. The voltage droop methodology does not provide emission limits for DGs, but rather relies on

maintaining a safety margin between the maximum harmonic voltage (that would occur when limits are derived from the VD methodology) and the planning limits, which could be used by DGs [16].

3.4.3 IEEE 519 - IEEE Recommended Practices and Requirements for Harmonic Control in Electrical Power Systems [38]

The IEEE 519 standard [38] provides harmonic current emission limits for large installations in terms of the ratio between the maximum short-circuit current, $I_{sc:i}$, at the PCC of the installation and the maximum demand load current, $I_{L:i}$, of the installation. These emission limits are based on (3.18) [124]:

$$I_h = \frac{V_h}{h \cdot Z_{sc} \cdot \sigma} \tag{3.18}$$

where; V_h is the maximum harmonic voltage allowed at the PCC [38] and Z_{sc} is the short-circuit impedance of the system at the PCC. The aggregation factor, σ, takes into account the maximum number of installations connected at a single point of connection, the ratio of the short-circuit current to the maximum demand customer load current, and the diversity between different order harmonics.

Harmonic current emission limits for installations connected to systems with nominal voltages between 120 V and 69 kV, are given in Table 3.3. It is recommended that $I_{L:i}$ be calculated using the maximum demand of the installation for the preceding 12 months. The limits given in Table 3.3 are to be observed under the worst case of normal operation (conditions lasting for longer than one hour) of the installation. However, the limits are allowed to exceed by 50% for shorter periods, during start-up and other unusual conditions. Even harmonics are restrained to 25% of the values indicated for odd harmonics in Table 3.3. Harmonic current emission limits for all DGs connected to LV networks are restricted to limits corresponding to $I_{sc:i}/I_{L:i} < 20$, regardless of the actual $I_{sc:i}/I_{L:i}$ at the PCC of the generators.

Table 3.3: Harmonic current distortion limits for general distribution systems 120 V through 69 kV [38]

Maximum Harmonic Current Distortion in Percent of I_L						
Individual Harmonic Order (Odd Harmonics)						
I_{sc}/I_L	$h < 11$	$11 \leq h < 17$	$17 \leq h < 23$	$23 \leq h < 35$	$35 \leq h$	TDD
< 20	4.0	2.0	1.5	0.6	0.3	5.0
$20 < 50$	7.0	3.5	2.5	1.0	0.5	8.0
$50 < 100$	10.0	4.5	4.0	1.5	0.7	12.0
$100 < 1000$	12.0	5.5	5.0	2.0	1.0	15.0
> 1000	15.0	7.0	6.0	2.5	1.4	20.0

3.4.4 Constrained Bus Voltage Method

The CBV method has been introduced in [12, 65] as an alternative methodology to the IEC methodology for managing harmonic emission in MV and HV networks. According to the CBV approach, the harmonic voltages at the network busbars are explicitly forced to be below the set planning levels when all loads inject their limits derived. The application of the CBV method can be demonstrated using the simple LV distribution network shown in Fig. 3.10.

Assume that the harmonic current emission limit of an installation is related to the apparent power in per-unit of the installations, S_i, as given by (3.19):

$$E_{Ih:i} = k_h \cdot \sqrt[\alpha]{S_i} \tag{3.19}$$

where; $E_{Ih:i}$ is the harmonic current emission limit for an installation that is connected to the i^{th} busbar and k_h is an allocation constant, which is dependent on the distribution network under consideration and yet to be determined.

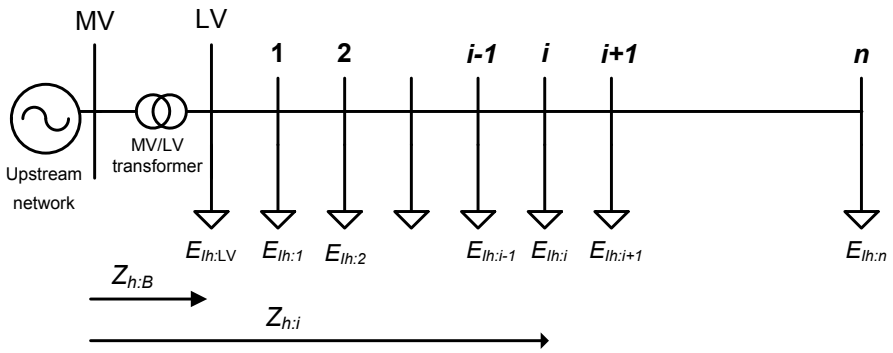

Figure 3.10: Simplified scheme of a radial LV system

Referring to (3.20) and Fig. 3.10, the total h^{th} harmonic voltage at the i^{th} busbar, $V_{h:i}^{\text{total}}$, is a result of:

- the harmonic voltage that propagates from upstream network, $V_{h:US}$,
- the harmonic voltage that propagates to the i^{th} busbar from the LV busbar due to the harmonic current emission from the installation connected to the LV busbar, $(Z_{h:\text{B}} \cdot E_{Ih:\text{B}})$,
- the harmonic voltage that propagates to the i^{th} busbar from all busbars which are upstream of the i^{th} busbar due to harmonic current emission from installations connected to those busbars, $\left(\sum_{m=1}^{i-1} [Z_{h:m} \cdot E_{Ih:m}]\right)$,
- the harmonic voltage due to the harmonic current emission from the installation connected at the i^{th} busbar, $(Z_{h:i} \cdot E_{Ih:i})$,
- the harmonic voltage that occurs at the i^{th} busbar due to harmonic current emission from installations connected to those busbars $\left(\sum_{m=i+1}^{n} [Z_{h:i} \cdot E_{Ih:m}]\right)$.

Hence, using the general summation law the total harmonic voltage at the i^{th} busbar, $V_{h:i}^{\text{total}}$, can be written as (3.20). Similarly, the total harmonic voltage at the MV busbar, $V_{h:\text{MV}}^{\text{total}}$, and total harmonic voltage at the n^{th} busbar, $V_{h:n}^{\text{total}}$, can be given by (3.21) and (3.22) respectively.

$$(V_{h:i}^{\text{total}})^{\alpha} = (V_{h:\text{US}})^{\alpha} + (Z_{h:\text{B}} \cdot E_{Ih:\text{B}})^{\alpha} + \sum_{m=1}^{i-1} [Z_{h:m} \cdot E_{Ih:m}]^{\alpha} + (Z_{h:i} \cdot E_{Ih:i})^{\alpha} + \sum_{m=i+1}^{n} [Z_{h:i} \cdot E_{Ih:m}]^{\alpha} \tag{3.20}$$

$$(V_{h:\text{MV}}^{\text{total}})^{\alpha} = (V_{h:\text{US}})^{\alpha} + (Z_{h:\text{B}} \cdot E_{Ih:\text{B}})^{\alpha} + \sum_{m=1}^{n} [Z_{h:\text{B}} \cdot E_{Ih:m}]^{\alpha} \tag{3.21}$$

$$(V_{h:n}^{\text{total}})^{\alpha} = (V_{h:\text{US}})^{\alpha} + (Z_{h:\text{B}} \cdot E_{Ih:\text{B}})^{\alpha} + \sum_{m=1}^{n} [Z_{h:m} \cdot E_{Ih:m}]^{\alpha} \tag{3.22}$$

where;

$(V_{h:i}^{\text{total}})$ is the magnitude of the total harmonic voltage at the i^{th} busbar in per-unit,

$(V_{h:\text{MV}}^{\text{total}})$ is the magnitude of the total harmonic voltage at the MV busbar in per-unit,

$(V_{h:n}^{\text{total}})$ is the magnitude of the total harmonic voltage at the n^{th} busbar in per-unit,

$Z_{h:\text{B}}$ is the magnitude of the harmonic impedance of the MV/LV transformer in per-unit,

$Z_{h:m}$ is the magnitude of the harmonic impedance of the system between the MV busbar and m^{th} busbar in per-unit and $m = 1, 2, 3, ..., i-1, i+1, ..., n$,

$Z_{h:i}$ is the magnitude of the harmonic impedance of the system between the MV busbar and i^{th} busbar in per-unit,

$E_{Ih:\text{B}}$ is the magnitude of the harmonic current emission by the installation connected to the transformer LV busbar in per-unit,

$E_{Ih:m}$ is the magnitude of the harmonic current emission by the load connected to the m^{th} busbar in per-unit,

$E_{Ih:i}$ is the magnitude of the harmonic current emission by the load connected to the i^{th} busbar in per-unit.

When the VA capacity of each installation and the harmonic impedance at each busbar is known in advance, and by substituting the harmonic current allocation given by (3.19) in (3.20)-(3.22), the harmonic voltages at each busbar can be evaluated as a function of the allocation constant, k_h. Considering that the harmonic voltage at any busbar should not exceed the set planning level for the distribution network, a suitable value for k_h can be determined. For example, when the value of k_h is increased from zero up to a certain value, the harmonic voltage at one of the busbars (called the critical busbar) will reach the chosen planning level for the network. Therefore, the value of k_h at which the critical busbar reached the planning levels can then be selected as the allocation constant for the network. Thereafter, the emission allocation limits for all installations can be calculated using (3.19).

If a large DG installation is connected to the distribution network, an emission allocation for the DG can be provided using (3.19). Note that (3.20)-(3.22) should be modified in order to take into account the presence of large DG installation. Assume that a DG installation with a VA capacity of S_{DG} in per-unit is now connected to the distribution network given in Fig. 3.10 at a busbar that is downstream to the i^{th} busbar. The harmonic current emission allocation for the DG installation, $E_{Ih:\mathrm{DG}}$, the total harmonic voltage at any i^{th} busbar, $V_{h:i}^{\mathrm{total}}$, and the total harmonic voltage at the n^{th} busbar, $V_{h:n}^{\mathrm{total}}$, can be given by (3.23), (3.24), (3.25) respectively.

$$E_{Ih:\mathrm{DG}} = k_h \cdot \sqrt[\alpha]{S_{\mathrm{DG}}} \tag{3.23}$$

$$\begin{aligned}(V_{h:i}^{\mathrm{total}})^{\alpha} = (V_{h:\mathrm{US}})^{\alpha} + (Z_{h:\mathrm{B}} \cdot E_{Ih:\mathrm{B}})^{\alpha} + \sum_{m=1}^{i-1} [Z_{h:m} \cdot E_{Ih:m}]^{\alpha} \\ + (Z_{h:i} \cdot E_{Ih:i})^{\alpha} + \sum_{m=i+1}^{n} [Z_{h:i} \cdot E_{Ih:m}]^{\alpha} + (Z_{h:i} \cdot E_{Ih:\mathrm{DG}})^{\alpha}\end{aligned} \tag{3.24}$$

$$(V_{h:n}^{\text{total}})^{\alpha} = (V_{h:\text{US}})^{\alpha} + (Z_{h:\text{B}} \cdot E_{Ih:\text{B}})^{\alpha} + \sum_{m=1}^{n} [Z_{h:m} \cdot E_{Ih:m}]^{\alpha} + (Z_{h:\text{DG}} \cdot E_{Ih:\text{DG}})^{\alpha} \tag{3.25}$$

where, $Z_{h:\text{DG}}$ is the magnitude of the harmonic impedance at the POC of the DG installation and k_h is a new allocation constant that needs to be re-calculated.

3.5 Comparison of Methodologies for Assessment of Harmonic Current Emission Limits for Large Installations

In this section, the application of harmonic current emission allocation methodologies discussed in Sections 3.2 and 3.4 are demonstrated through two case studies.

3.5.1 Case Study I

An office building with an agreed power of 100 kVA, consisting of linear and non-linear loads, is to be connected to a 3-phase LV feeder at a location 150 m from the MV/LV transformer[4]. The non-linear devices that will operate in the building are given in Table 3.4 [66].

The parameters of the LV network, which are based on a typical Australian LV system are as follows. The MV/LV transformer has a capacity of 315 kVA and an impedance of $(0.006 + j0.022)$ Ω referred to the LV side. The network consists of two feeders, each 250 m long. The phase and neutral conductor impedances are both $(0.315 + j0.259)$ Ω/km. The methodologies discussed in Sections 3.2 and 3.4 are used to determine the harmonic emission limits for the installation.

[4]POC of the installation is considered as the PCC/POE in the case study.

Table 3.4: Devices to be operated in the building

Devices/installation	kVA rating per unit	No. of units
Computers	0.5	18
Monitors	0.2	30
Terminals	0.3	15
Printers	0.8	5
Fax machines	0.5	1
UPS system	10	1
Lighting system	10	1
Lift	5	1
Air-conditioning	9	1

IEC 61000-3-14

Under Stage 1, the DNSP needs to specify the minimum size of a large installations. In the considered case, $S_{\min}$ is assumed to be 30 kVA. Since the agreed power of the considered installation exceeds 30 kVA, the ratio of the capacity of the installation to the short-circuit capacity at the PCC of the installation needs to be calculated in order to determine whether the installation can be accepted under Stage 1. The short-circuit power at the PCC, $S_{sc:i}$, is mainly determined by the impedance of the MV/LV transformer and LV line impedance. The $S_{sc:i}$ can be calculated as:

$$S_{sc:i} = \frac{U_n^2}{Z_i} = \frac{(0.4)^2}{(0.006 + j0.022) + (0.315 + j0.259) \cdot 0.150}$$

$$= 1.979\,\text{MVA}$$

Since the $S_i/S_{sc:i}$ ratio is greater than 1%, the connection of the installation cannot be accepted under Stage 1. Therefore, the DNSP will need to evaluate the emission limits based on Stage 2 methodology. The parameters given in Table 3.5 are used for evaluation of Stage 2 emission limits. Emission limits based on Stage 2 allocation methodology for the considered installation are given in Table 3.6.

Table 3.5: Parameters for application of the IEC 61000-3-14 Stage 2 allocation methodology

h	3	5	7	11	13
$L_{h:\mathrm{MV}}$[5] (%)	4.0	5.0	4.0	3.0	2.5
$L_{h:\mathrm{LV}}$ (%)	5.0	6.0	5.0	3.5	3.0
$T_{h:\mathrm{MV-LV}}$	1.0	1.0	1.0	1.0	1.0
α	1.0	1.4	1.4	2.0	2.0
$G_{h:\mathrm{LV}}$[6] (%)	1.0	2.1	2.0	1.8	1.7
K_{hB}[7]	0.22	0.53	0.53	0.53	0.53
$Z_{h:\mathrm{B}}$ (Ω)	0.066	0.110	0.154	0.242	0.286
$Z_{h:i}$[8] (Ω)	0.567	0.309	0.429	0.672	0.793

Table 3.6: Harmonic current limits based on IEC 61000-3-14, using (3.4)

h	3	5	7	11	13
$E_{Ih:i}$(A)	1.29	6.82	4.63	3.49	2.72

Technical Rules for the Assessment of Network Disturbances

The ratio of the short-circuit capacity at the PCC, $S_{sc,i}$, to the capacity of the installation, $S_{sc:i}$, can be calculated as:

$$\frac{S_{sc:i}}{S_i} = \frac{1979}{100} \leq 150$$

Since $S_{sc:i}/S_i$ ratio is less than 150, a comprehensive assessment is required. Therefore, each load within the installation is grouped according Table 3.7.

The total harmonic load of the installation $S_{OS:i}$ can be calculated using (3.13) as:

$$S_{OS:i} = 0.5 \cdot S_{\mathrm{Gr.1}} + S_{\mathrm{Gr.2}} = 53\,\mathrm{kVA}$$

The resulting harmonic load ratio, $S_{OS,i}/S_i = 0.53$, exceeds $0.082\sqrt{S_{sc,i}/S_i} = 0.378$. Therefore, the connection of the installation is accepted, only if remedial

[5]The MV and LV planning levels and MV to LV transfer coefficients are selected based on the indicative values given in IEC TR 61000-3-14 [2]

[6]Calculated using (3.1)

[7]Calculated using (3.8)

[8]For non-triplen harmonics $Z_{h:i} = |\boldsymbol{Z_{h:B}} + \boldsymbol{Z_{Lh:i}}|$, where; $\boldsymbol{Z_{h:B}}$ is the complex harmonic impedance of order h of the MV/LV transformer and $\boldsymbol{Z_{Lh:i}}$ is the complex harmonic impedance of order h for the line conductor at the PCC of the installation. For triplen harmonics, $Z_{h:i} = |\boldsymbol{Z_{h:B}} + \boldsymbol{Z_{Lh:i}} + 3 \cdot \boldsymbol{Z_{Nh:i}}|$, where; $\boldsymbol{Z_{Nh:i}}$ is the complex harmonic impedance of order h for the neutral conductor at the PCC of the installation.

Table 3.7: Harmonic load of the installation

Devices/installation	Group 1	Group 2
18 Computers		9 kVA
30 Monitors		6 kVA
15 Terminals		4.5 kVA
5 Printers		4 kVA
Fax machines		0.5 kVA
UPS system		10 kVA
Lighting system	10 kVA	
Lift		5 kVA
Air-conditioning		9 kVA
Sum	$S_{Gr.1} = 10\,\text{kVA}$	$S_{Gr.2} = 48\,\text{kVA}$

Table 3.8: Harmonic current limits based on Technical Rules for the Assessment of Network Disturbances, using (3.14)

h	3	5	7	11	13
$E_{Ih:i}$(A)	3.85 (11.55*)	9.63	6.42	3.21	2.57

$*$ corresponds to the current limit in the neutral conductor

measures are employed to limit the harmonic currents to values indicated in Table 3.8.

The admissible $\text{TDD}_{I:i}$ limit for the installation is given by:

$$\text{TDD}_{I:i} = \frac{20}{1000} \cdot \sqrt{\frac{S_{sc:i}}{S_i}} = \frac{20}{1000} \cdot \sqrt{19.79} = 8.90\%$$

Voltage Droop

The harmonic current limits derived based on the VD method are given in Table 3.9. The k_h values are determined subject to a maximum system VD of 30%, which is typical for Australian LV networks and LV compatibility levels as given by [62]. The reader should note that the harmonic current limits for triplen harmonics are not provided under VD method.

Table 3.9: Harmonic current limits based on VD methodology, using (3.16)

h	5	7	11	13
k_h	0.028	0.017	0.006	0.004
E_{Ihi}(A)	10.42	6.20	4.30	3.12

Table 3.10: Harmonic current limits based on IEEE Standard 519

h	3	5	7	11	13
Scaling factor	1.66	2.00	1.66	1.17	1.00
$E_{Ih:i}$(A)	9.62	11.55	9.62	3.37	2.89

IEEE Standard 519-1992

Harmonic voltage distortion limits specified by IEEE are different to the IEC compatibility values which are used in Australia. Therefore, the harmonic current emission limits given by Table 3.3 are adjusted using a scaling factor in order to determine the current emission limits for the considered installation [15]. The calculated current emission limits are given in Table 3.10. The maximum demand load current is calculated based on the agreed power of the installation. The scaling factor is calculated using the ratio of IEEE voltage distortion levels given in Table 2.2 and IEC compatibility levels given in Table 2.1 for h^{th} order in Section 2.5.1 .

A comparison of the harmonic current emission limits established using the various methodologies considered in this section is given in Fig. 3.11. The reader should note that IEC 61000-3-14 provides relatively stringent limits for 5^{th} and 7^{th} order harmonics, compared to those determined using Technical Rules for Assessment of Network Disturbances, VD and the IEEE 519 methodologies.

Fig. 3.12 compares the harmonic current emission limits derived using the four methodologies discussed, as the POC of the installation is moved from a location near the MV/LV transformer to the far end of feeder. Fig. 3.12 illustrates that the harmonic current emission limits for the installation are significantly higher if the installation is connected near the MV/LV transformer, than at the end of the feeder of the network. In addition, the reader should observe that the harmonic current limits for 3^{rd}, 5^{th} and 7^{th} order harmonics derived using the IEEE 519 standard, after adjusting them to be in line with IEC harmonic voltage compatibility levels are

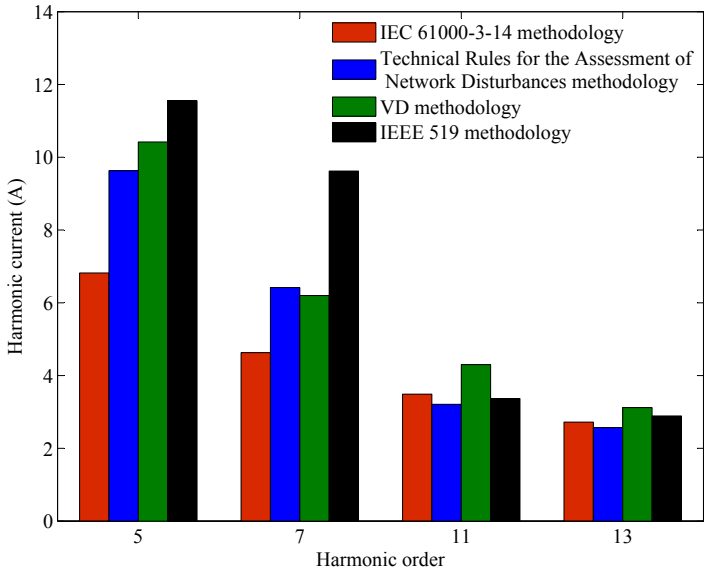

Figure 3.11: Comparison of harmonic current emission limits for the installation

significantly higher compared to the other methodologies discussed in this section.

Fig. 3.13 provides a comparison between the corresponding 5^{th} harmonic voltage, allocated to the installation as the POC of the installation is moved from a location near the MV/LV transformer to the end of feeder. The harmonic voltage emission given by IEC 61000-3-14 remains constant approximately at 0.01 pu, if the installation is connected at 75 m away from the MV/LV transformer or beyond. However, in the case of Technical Rules for Assessment of Network Disturbances and VD methodologies, the harmonic voltage emission gradually increases as the POC is varied from the MV/LV transformer to the end of feeder. In the case of IEEE 519, as the POC is moved, $I_{sc:i}/I_{L:i}$ ratio also changes, which leads to a step change in the harmonic current emission limit as shown in Fig. 3.12. These variations are reflected Fig. 3.13 as sudden drops in harmonic voltages. The highest 5^{th} harmonic voltage occurs if the installation is connected 150 m away from the MV/LV transformer and if the harmonic current emission allocation is conducted using IEEE 519 methodology. The harmonic voltage is also observed to exceed the maximum allowable 5^{th} harmonic voltage of 2.07%, which was assumed for the network under the IEC 61000-3-14 methodology.

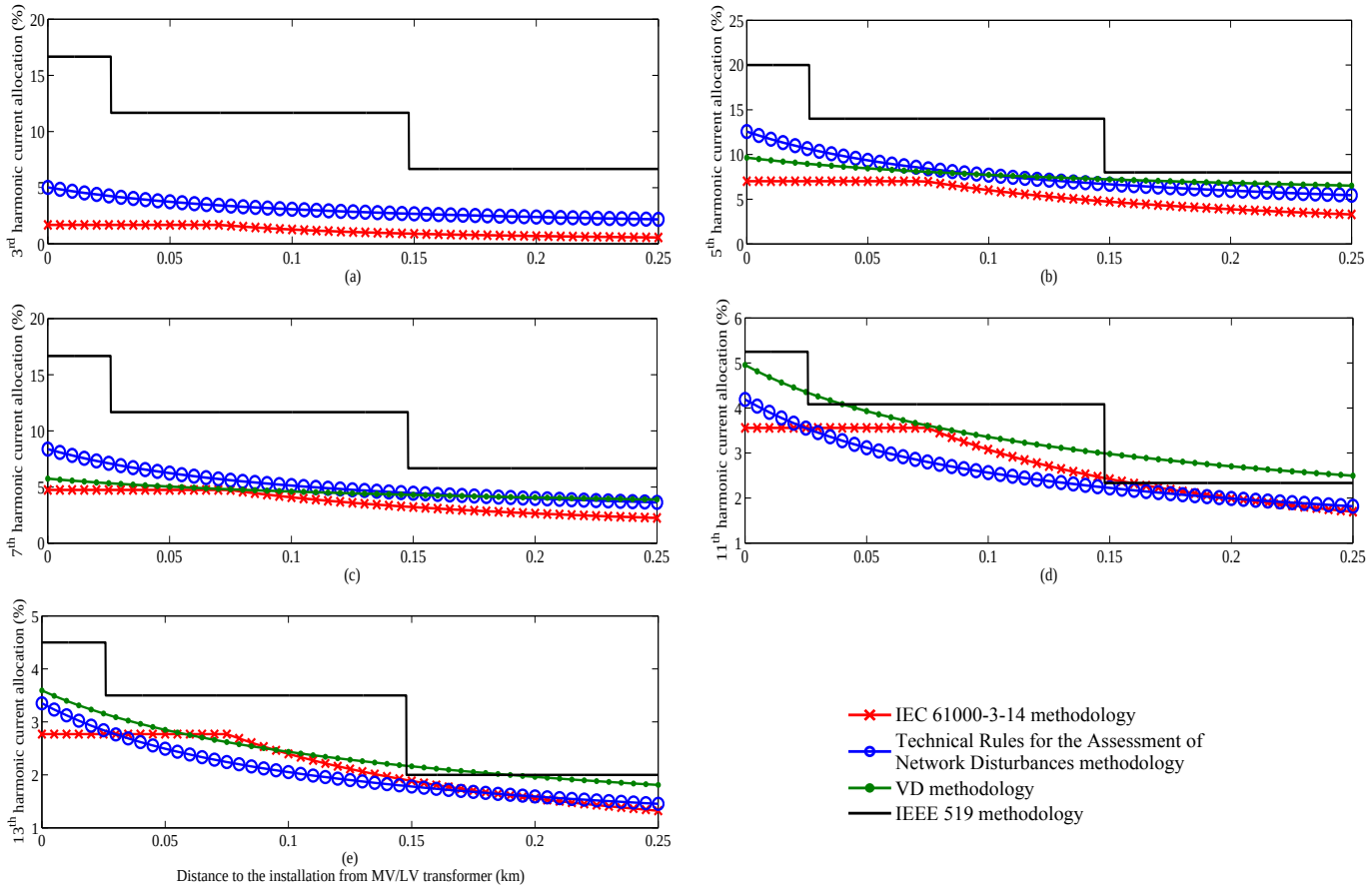

Figure 3.12: Harmonic current emission limits as a function of the distance to the installation from the MV/LV transformer (a) 3^{rd} harmonic current limit, (b) 5^{th} harmonic current limit, (c) 7^{th} harmonic current limit, (d) 11^{th} harmonic current limit, (e) 13^{th} harmonic current limit

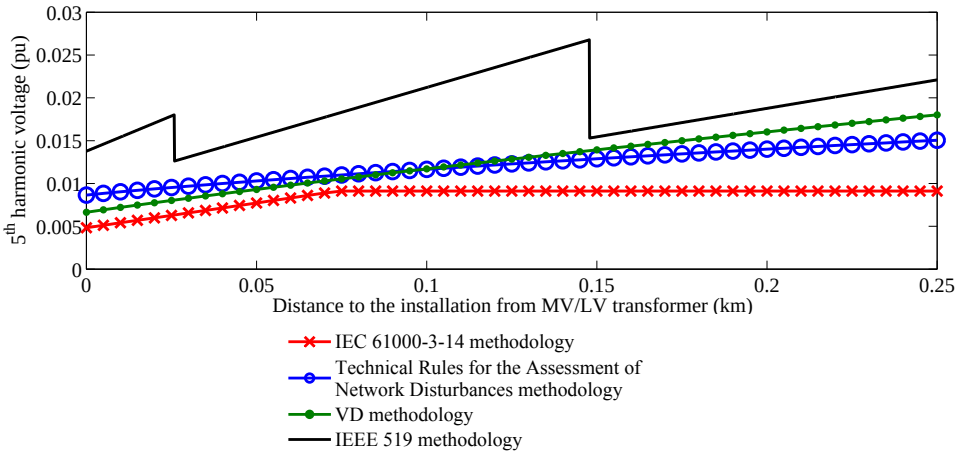

Figure 3.13: 5^{th} harmonic voltage allocated to the installation, as a function of the distance to the installation from the MV/LV transformer

3.5.2 Case Study II

In order to illustrate the application of harmonic emission allocation methodologies discussed in Section 3.4 to a distribution network, consider the LV distribution network feeder given in Fig. 3.14. The MV/LV transformer has a capacity of 400 kVA and an impedance of $(0.004 + j0.0155)\ \Omega$ referred to the LV side. The conductor impedance data are given in Appendix A. Note that the network consists of number of different conductors. The MV planning levels, LV planning levels and MV to LV transfer coefficient used in the example are given in Table 3.11. In this example, it is assumed that the MV network does not to have a neutral conductor. As a result, the 3^{rd} harmonic cannot exist in the MV network. Therefore, the corresponding MV to LV transfer coefficient for 3^{rd} harmonic is taken as zero.

The current emission limits of 3^{rd}, 5^{th}, 7^{th}, 11^{th} and 13^{th} harmonics which are calculated using IEC 61000-3-14, CBV, VD, and IEEE 519 methodologies respectively,

Table 3.11: Chosen planning levels and MV to LV transfer coefficients for the case study

h	3	5	7	11	13
$L_{h:\text{MV}}$ (%)	4.0	5.0	4.0	3.0	2.5
$L_{h:\text{LV}}$ (%)	5.0	6.0	5.0	3.5	3.0
$T_{h:\text{MV-LV}}$	0	1.0	1.0	1.0	1.0

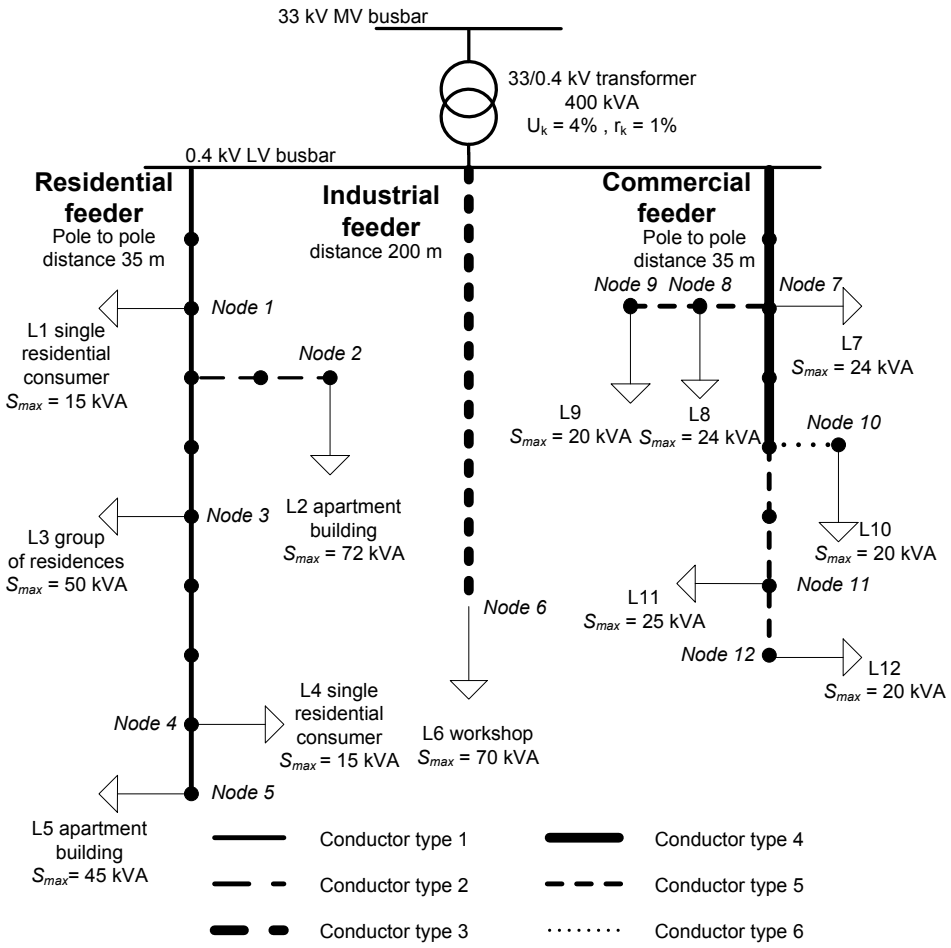

Figure 3.14: LV test distribution network

are given in Fig. 3.15[9]. Note that in relation to IEC 61000-3-14, all installations are considered as large installations, irrespective of their kVA capacity. Hence, all installations are provided with an emission limit considering the reduction factor as unity as explained in Section 3.3.3. Harmonic emission limits are expressed as a percentage of rated current of the installation.

Referring to Figs. 3.15 (a)-(e), the harmonic current emission limits established based on the IEC 61000-3-14 for installations connected near the MV busbar are relatively high compared to the limits for installations which are connected at the far end of the feeder. In contrast, the CBV methodology avoids such discrepancies by allocating emission limits which are lower than the IEC 61000-3-14 limits for installations connected near to the LV busbar and emission limits which are higher than the IEC 61000-3-14 limits for installations connected at the end of the feeder. For low order harmonics (e.g. 3^{rd}, 5^{th} and 7^{th} harmonics), the emission limits established by IEEE 519 methodology are significantly higher than other methodologies, whereas, the opposite is true for higher order harmonics (e.g. 11^{th} and 13^{th} harmonics). In addition, harmonic current emission limits given by the VD method are comparatively low across all harmonic orders. The reader should note that the 3^{rd} harmonic emission limits provided by IEC 61000-3-14 are significantly higher compared to the Case Study I, where 3^{rd} harmonic was assumed to be transferred to the LV network from the upstream MV network.

For comparison purposes, Table 3.12 lists the unused harmonic abortion capacity[10] (as a percentage of maximum acceptable global contribution of harmonic voltage of the LV level ($G_{h:\text{LV}}$)), when emission allocation is carried out based on the aforementioned methodologies. The unused absorption capacity values are calculated assuming that $G_{h:\text{LV}}$ given by (3.1) is valid, irrespective of the methodology

[9]As the harmonic current emission methodology given in Technical Rules for Assessment of Network Disturbances requires assessment of harmonic emission characteristics of each installation, the aforementioned methodology has not been considered in the example.

[10]The global contribution of all loads, to the harmonic voltage at the LV network was estimated using (3.20)-(3.21) in Section 3.4.4, where emission limits for individual installation is now give by limits in Fig. 3.15

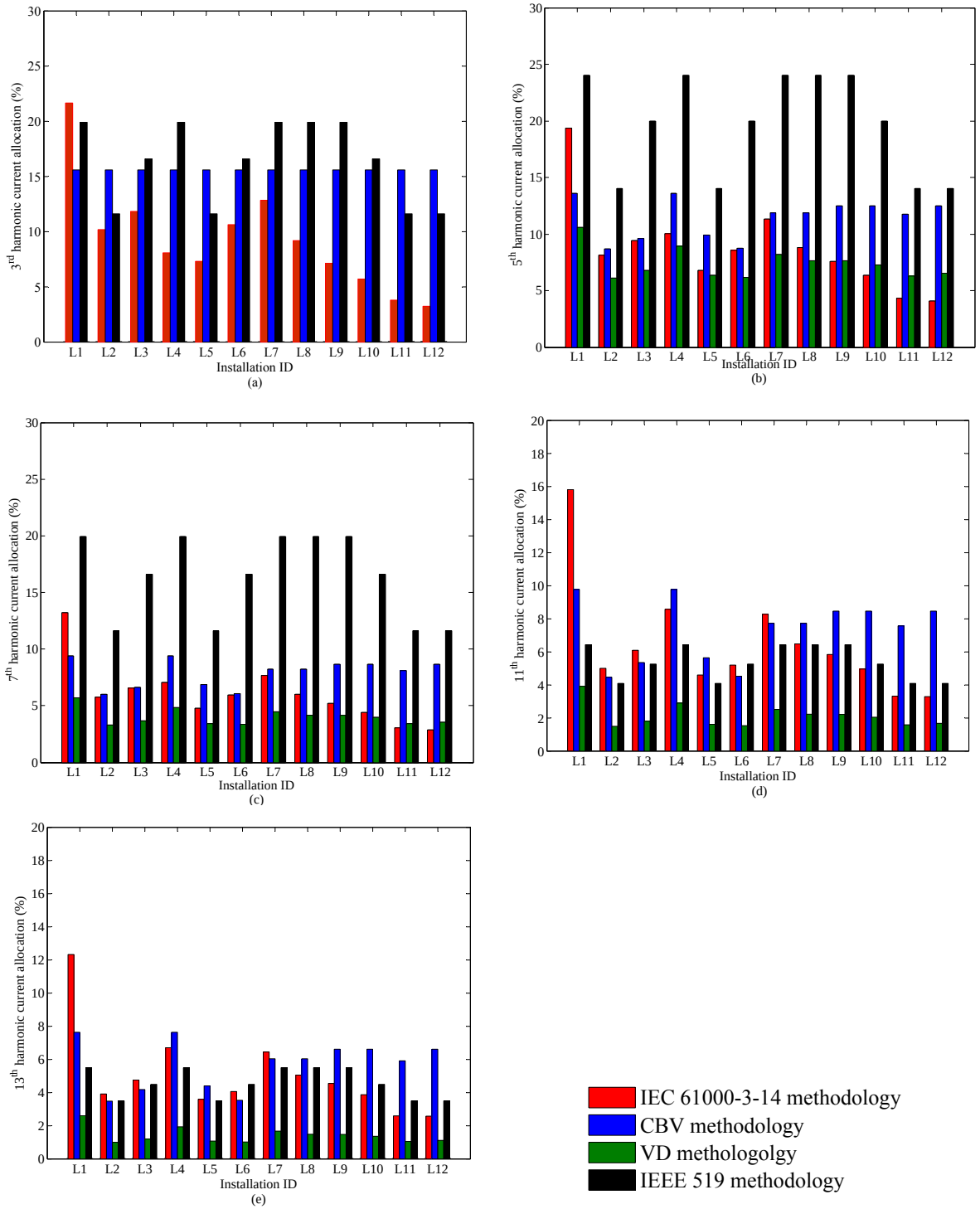

Figure 3.15: Harmonic current emission limits for (a) 3rd, (b) 5th, (c) 7th, (d)11th and (e) 13th individual installations connected to the test LV distribution network

Table 3.12: Unused harmonic absorption capacity of the network as a percentage of $G_{h:\mathrm{LV}}$

Harmonic order	3	5	7	11	13
IEC 61000-3-14 methodology	48.13%	33.84%	33.10%	28.90%	28.80%
CBV methodology	0	0	0	0	0
VD methodology	-	40.01%	52.90%	75.79%	79.32%
IEEE 519 methodology[11]	7.88%	-53.89%	-86.09%	35.62%	29.52%

used. However, the reader should note that such an assumption is not accurate for the VD and the IEEE 519 methods, as the allocation methodologies do not consider (3.1) in the allocation process.

According to the Table 3.12, the harmonic absorption capacity of the LV network is fully utilised in the case of the CBV methodology. Therefore, the CBV methodology provides a benchmark, in which other harmonic emission allocation methodologies can be compared, in relation to the availability of unused harmonic absorption capacity in the network. Accordingly, the limits established by IEC 61000-3-14 and VD methodologies can be seen to be conservative and leave some absorption capacity of the network unutilised. Such a safety margin is important, as it enables small DGs to be connected without causing the network harmonic voltage to exceed the planning levels. In the case of the IEEE methodology, the harmonic voltage contribution from all loads connected to the LV network has exceeded $G_{h:\mathrm{LV}}$ for 5^{th} and 7^{th} harmonics.

Furthermore, the allocation of harmonic current emission limits, when a large DG is connected to a distribution network is also investigated considering the test LV distribution network given in Fig. 3.14. A large DG installation with a capacity of 75 kVA is a connected to Node 5 of the distribution network. The harmonic emission allocation for large installations and the DG were calculated following the IEC 61000-3-14 and CBV methodologies. As the VD and IEEE methodologies do not provide dedicated procedures for evaluating the harmonic current emission allocation limits for DG installations, they were not considered in the investigation. Fig. 3.16

[11]The minus signs indicate that contribution of harmonic voltage to the LV level from all installations exceed ($G_{h:\mathrm{LV}}$).

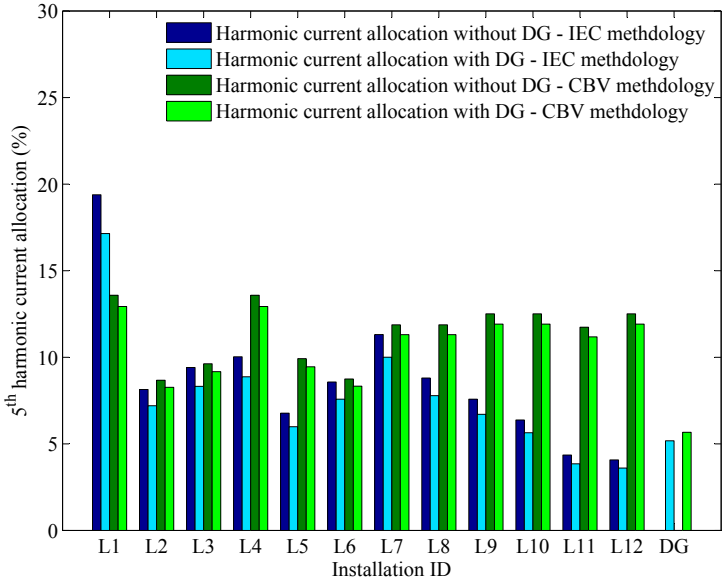

Figure 3.16: The 5^{th} harmonic current allocation with and without considering the connection of DG installation

compares the 5^{th} harmonic current emission allocation limits for each installation with and without considering the DG, for both the IEC and CBV methodologies. According to Fig. 3.16, the harmonic current allocation limits for installations L1 to L12 can be observed to reduce, when an emission limit is allocated to the DG. Table 3.13 provides the reduction of the harmonic current allocation (compared to the case when there is no DG connected to Node 5) calculated as a percentage for various harmonic orders under the IEC and CBV methodologies. In the case of IEC 61000-3-14 methodology, emission limits for each harmonic order shows a significant reduction compared to the CBV methodology.

Table 3.13: Reduction in the harmonic current allocation if a DG installation is connected to Node 5

Harmonic order	3	5	7	11	13
IEC 61000-3-14 methodology	11.55%	11.55%	11.55%	8.23%	8.23%
CBV methodology	5.38%	4.75%	4.90%	1.82%	1.84%

3.6 Comparison of Harmonic Current Emission Allocation Methodologies

In general, the harmonic current limits determined using the five methodologies discussed in this chapter are derived from the voltage quality targets such that when all installations emit their permissible emission levels, the net harmonic voltages in the network will be within the intended harmonic voltage limits. However, an exact agreement between the harmonic current limits cannot be expected, as the driving principles vary between the different methodologies. For instance, the IEC 61000-3-14, Technical Rules for the Assessment of Network Disturbances, CBV, and VD methods all rely on the compatibility level values [62], which decrease with the harmonic order. Voltage distortion limits in IEEE 519 are different from the IEC compatibility values and remain constant over a range of different harmonic orders.

The data requirements and ease of application varies between these methodologies. IEC 61000-3-14 provides a flexible methodology for assessment of harmonic limits. However, it requires the computation of various factors (e.g. the transfer coefficient and reduction factor) for the network under consideration, which could be problematic. For instance, the estimation of reduction factor for practical networks, similar to the network discussed in Section 3.5.2 requires a detailed knowledge with regard to load distribution in the network and harmonic current emission characteristics of installations connected to the network. When such data is not available, conservative values for these parameters should be used [2]. Thus, the emission limits could result in non-optimal values, leaving a considerable proportion of the harmonic absorption capacity of the network unused.

The methodology presented in Technical Rules for the Assessment of Network Disturbances takes into account an estimation of harmonic current emission of the considered installation. Thus, large installations which do not emit significant harmonic currents are exempted from application of harmonic current limits. Accordingly, higher harmonic current emissions are allowed for disturbing installations. The

data requirements are less compared to the IEC methodology and the required data can be conveniently obtained from utilities and the customers under consideration. The coefficients required to calculate the current limits can be directly obtained from [66], providing increased transparency between calculations. However, procedures to determine the coefficients are not given in [66], therefore, the application of the methodology for a specific situation would be difficult.

The VD methodology provides a more simplistic allocation methodology, requiring fewer computations and assumptions. However, for an LV network, the resistive component of the line impedance is significant. Accordingly, VD methodology only provides an approximation. Therefore, in such situations, the allocation equations should be adjusted to reflect the resistive component of the VD [15]. In addition, the VD method needs further development to assess the triplen-harmonic current limits, as the propagation of triplen-harmonic current is different from the propagation of non-triplen harmonics.

The methodology given in IEEE 519 provides a convenient approach to determine harmonic current emission limits compared to other methodologies discussed. However, the methodology is less flexible and difficult to be adopted to networks with different practices.

The CBV method is focused on utilising the network harmonic absorption capacity to the full extent. However, the major difficulty with the CBV approach is that the kVA capacity and harmonic impedance at the POC of all major loads, including future loads, are required to be known during the allocation process.

The methodologies discussed in this chapter do not take into consideration the possible resonance cases that could occur due to large cable networks or non-detuned capacitor banks in LV networks [2,123,124]. For cases where resonance might occur, a more detailed assessment or simulation is required for assessment of harmonic current emission limits.

With regard to harmonic current emission allocation for large DG installations,

each methodology provides a different approach. In the case of IEC 61000-3-14 and CBV methodologies, an emission allocation is provided for DG installations by modifying the emission allocation process as described in Sections 3.2 and 3.4.4, whereas Technical Rules for Assessment of Network Disturbances stipulates a 50 % emission limit determined according to the Section 3.4.1. The VD method does not consider large DG installations in the emission allocation process, but rather relies on maintaining a safety margin between the maximum harmonic voltage (that would occur when limits are derived from the VD methodology) and the planning limits, which could be used by DG [16]. With IEEE 519, the emission limits are relatively stringent compared to a disturbing installation with same agreed power.

3.7 Chapter Summary

This chapter presented a critical analysis and comparison of the harmonic emission limit allocation for large installations, including DG installations connected to LV distribution networks.

The theoretical bases for harmonic current emission allocation methodology given in IEC 61000-3-14 was established by employing a simple radial LV distribution network. Following major conclusions can be drawn from the study in Section 3.3.

- The harmonic current allocation methodology ensures that the contribution from small installations (for which emission limits are not governed by the Technical Report), is taken into account by introducing the concept of the reduction factor. Due to the harmonic current emission from such installations, the emission allocation for large installations is required to be restricted, in order to meet the stipulated planning levels.

- The reduction factor is dependent on the harmonic current emission from small installations and network configurations. Hence, when determining the reduction factor, the harmonic current emission assumed for small installations

should be based on field measurements. If all installations connected to the LV network are classified as large installations, the reduction factor value can be equated to unity.

- The estimation of reduction factor for a complex radial distribution network requires a detailed knowledge about the load distribution in the network and their harmonic characteristics. Therefore, the calculation of reduction factor should be based on individual network, in contrast to the recommended approach given in IEC 61000-3-14.

A comparison between the harmonic current emission limits given by IEC 61000-3-14, Technical Rules for Assessment of Network Disturbances, VD, IEEE 519 and CBV methodologies was conducted through two case studies. Although the assumptions and data requirements of each of these methodologies vary, all methodologies (except the IEEE 519 methodology) provided harmonic emission limits for large individual installation which are not too dissimilar. Harmonic emission allocation limits given by IEC 61000-3-14, Technical Rules for Assessment of Network Disturbances and VD methodologies were observed to be conservative for most cases; hence there is a safety margin between the maximum harmonic voltage observed in the network and its planning levels, which could be used by DGs. In contrast, the IEEE 519 methodology provided higher emission allocation, which could lead to harmonic voltages in exceedance of IEC compatibility levels given by [62].

In relation to harmonic emission allocation for large DGs, the IEC 61000-3-14 and CBV methodologies can be easily modified to incorporate DGs into the emission allocation process. In such situations, harmonic current emission limits for other disturbing installations are restricted, enabling an emission limit to be provided to DGs. However, such flexibility is not available with Technical Rules for Assessment of Network Disturbances, IEEE 519 and VD methodologies. Hence, for distribution networks with high levels of DG penetration, the application of Technical Rules for Assessment of Network Disturbances, IEEE 519 and VD methodologies may lead to situation where the harmonic voltage levels exceed the planning levels.

Chapter 4

Attenuation and Propagation of Voltage Unbalance in Radial Distribution Networks

4.1 Introduction

The recently published IEC Technical Reports IEC 61000-3-13 [5] and IEC 61000-3-14 [2] provide guidelines and recommendations for managing VU emission in electric power systems. The IEC Technical Report 61000-3-13 is mainly focused on VU emission allocation for unbalanced installations connected to MV, HV and EHV networks where the transmission lines are mainly asymmetrical in addition to loads. The IEC Technical Report IEC 61000-3-14 covers the provision of guiding principles on VU emission allocation to system operators in relation to large installations connected to LV distribution networks. The emission allocation methodologies presented in these Technical Reports follow a three stage allocation process similar to Technical Reports, IEC 61000-3-6 [3] for harmonics and IEC 61000-3-7 [4] for flicker in MV, HV and EHV networks, and IEC 61000-3-14 for harmonics and flicker for LV distribution networks.

According to IEC 61000-3-13, any three-phase installation that meets the criteria

given in (4.1), may be connected to the MV, HV or EHV network without further examination:

$$\frac{S_i}{S_{sc:i}} \leq 0.2\% \tag{4.1}$$

where; S_i is the single-phase power equivalent of the unbalanced installation i and $S_{sc:i}$ is the three-phase short-circuit power at the POE. For installations that do not comply with Stage 1, the VU emission allocation limits are provided under Stage 2. Considering an installation with an agreed power of S_i connected to an MV network, the VU emission allocation (in terms of voltage unbalance factor (VUF)) can be calculated by (4.2) and (4.3) respectively [5]:

$$G_{u:\mathrm{MV+LV}} = \sqrt[\alpha]{L_{u:\mathrm{MV}}^{\alpha} - (T_{u:\mathrm{MV-LV}} \cdot L_{u:\mathrm{HV}})^{\alpha}} \tag{4.2}$$

$$E_{u:i} = \sqrt[\alpha]{\mathrm{k_{uE}}}\ G_{u:\mathrm{MV+LV}}\ \sqrt[\alpha]{\frac{S_i}{S_t}} \tag{4.3}$$

where;

$L_{u:\mathrm{MV}}$ is the planning level for the MV network (%),

$L_{u:\mathrm{HV}}$ is the planning level for upstream HV network (%),

$T_{u:\mathrm{MV-LV}}$ is the VU transfer coefficient from the HV network to the MV network,

$E_{u:i}$ is the VUF emission limit for the installation i (%),

S_i is the agreed power of the installation i (MVA),

S_t is the total supply capacity of the considered MV and LV network (MVA),

k_{uE} is the fraction of global contribution to VU that can be allocated for emission from unbalanced installations in the MV and LV distribution system being considered. Hence, $(1 - k_{\mathrm{uE}})$ represent the fraction that accounts for system inherent VU,

α is a summation exponent,

$G_{u:\mathrm{MV+LV}}$ is the maximum acceptable global contribution to VU at MV level by the MV system inherent asymmetries and the total of MV and LV unbalanced installa-

tions that can be supplied from the considered MV busbar.

For installations, which require additional VU limits than permitted under Stage 2, the Stage 3 emission allocation process which was discussed in Section 2.7.1 is applicable.

At the LV distribution network, VU emission limits are provided using the three stage allocation process as given by IEC 61000-3-14. Large installations[1] that comply with (4.1) at the LV level, are allowed to connect without further investigations. If the installation fails to meet Stage 1 criteria, VU emission limits are provided using (4.4) and (4.5) respectively [2]:

$$G_{u:\mathrm{LV}} = \sqrt[\alpha]{L_{u:\mathrm{LV}}^{\alpha} - (T_{u:\mathrm{MV-LV}} \cdot L_{u:\mathrm{MV}})^{\alpha}} \tag{4.4}$$

$$E_{I_2:i} = \frac{V_n^2}{S_i} G_{u:\mathrm{LV}} \sqrt[\alpha]{\frac{S_i}{S_t}} \min\left(\frac{K_{uB}}{Z_B}, \frac{1}{Z_i}\right) \tag{4.5}$$

where;

$G_{u:\mathrm{LV}}$ is the maximum acceptable global contribution to the VU anywhere in the LV system due to all installations (including small installations as defined by IEC 61000-3-14) that can be supplied from the considered system,

$L_{u:\mathrm{LV}}$ is the planning level for the LV network (%),

$L_{u:\mathrm{MV}}$ is the planning level for upstream MV network (%),

$T_{u:\mathrm{MV-LV}}$ is the VU transfer coefficient from MV network to the LV network,

$E_{I_2:i}$ is the negative-sequence current emission limit for the installation i (as a % of rated current of the installation),

S_i is the agreed apparent power of the installation i (VA),

S_t is the total supply capacity of the considered LV system (VA),

Z_B is the modulus of the short-circuit impedance of the system at the LV substation

[1]If the installation agreed power S_i exceeds the $S_{\min}$ as defined by a DNSP, the installation is classified as a large installation. Any installation with agreed power less than $S_{\min}$ is allowed to be connected to the LV distribution network without any further investigations.

busbar (Ω),

Z_i is the modulus of the short-circuit impedance of the system at the POE of the installation i (Ω),

V_n is the nominal line to line voltage (V),

K_{uB} is the reduction factor for VU.

Higher VU emission limits are allowed under Stage 3 after a detailed examination, for installations that do not comply with Stage 2 allocation limits.

Note that in cases where DG installations are connected to the MV or LV network, the system capacity S_t in (4.3) and (4.5) needs to be adjusted, considering the MVA capacity of the DG installation and its effective contribution to the short-circuit power.

In (4.3), the factor k_{uE} is introduced to limit the allowable VU emission limits for installations, considering the VU which arises due to the asymmetry of the supply network. In LV distribution networks, the VU emission due to line asymmetry can be negligible [2, 125]; hence, k_{uE} is not taken into account in the emission allocation equation, (4.5). However, an additional factor K_{uB} is introduced in (4.5) to account for VU emission from small installations, following same principles for harmonics as discussed in Chapter 3.

As discussed in Section 2.8, a key deficiency in the IEC PQ emission allocation methodologies is that they fail to account for attenuation of PQ disturbances when propagating from downstream of the network to upstream of the network at the same voltage level. The CBV method which was discussed in Chapters 2 and 3 has been proposed in [12] and [65] as an alternative methodology for harmonic and flicker emission allocation, which address this deficiency. Using the CBV approach, the PQ emission levels at network busbars are explicitly forced to be set at a reference level when all installations are injecting their limits derived according to the CBV approach. By appropriately modifying the CBV methodology, VU emission

allocation in radial distribution networks can be carried out.

The focus of this chapter is to bridge the gap related to the knowledge of VU propagation and attenuation in relation to radial distribution networks. The outcomes of this chapter will be used in Chapter 5 to develop a revised VU emission allocation methodology based on the concept of CBV method.

The objectives of the work presented in this chapter are:

- to investigate the VU attenuation in radial distribution networks and to develop a methodology to quantify the VU attenuation from downstream to upstream network. A generalised theory which considers line asymmetries is initially presented. The outcomes are then simplified to accommodate distribution networks in which system inherent asymmetries are negligible [2]. The work carried out in this regard is presented in Section 4.2.

- to investigate the VU attenuation and propagation in radial distribution networks when multiple unbalanced installations are connected. This is covered in Section 4.3.

- to propose a methodology in relation to radial distribution networks, which can be used to estimate the VU when multiple unbalanced installations are operating simultaneously. This is covered in Section 4.4.

- to propose a methodology to quantify the VU attenuation provided by the three-phase induction motor, when an induction motor and a passive unbalanced installation are connected to the same distribution network. Modelling aspects and verification in this regard are given in Section 4.5.

Section 4.6 provides a summary of the work presented in the chapter, emphasising the major conclusions.

4.2 Voltage Unbalance Transfer in Radial Power Systems

4.2.1 Dependency of Voltage Unbalance Transfer Coefficient on Short-Circuit Capacity

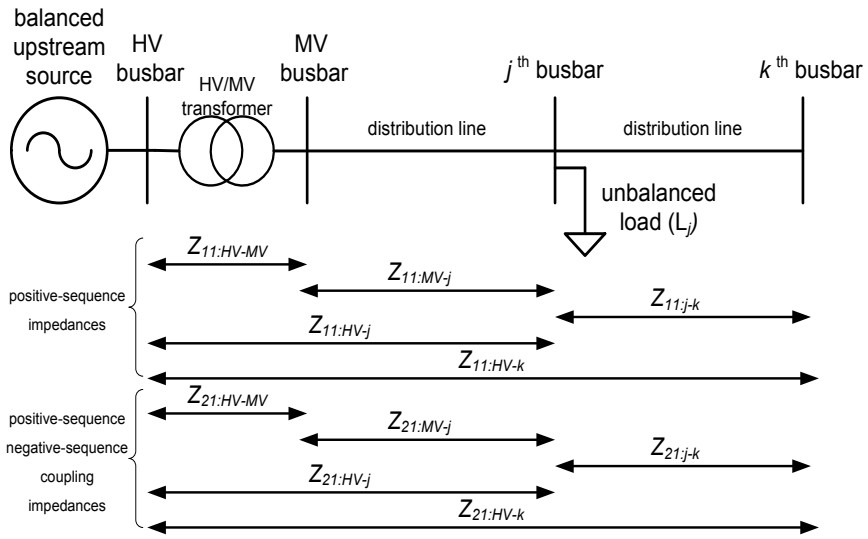

Figure 4.1: Radial distribution network with an unbalanced installation connected to the j^{th} busbar

Consider the radial HV/MV distribution network shown in Fig. 4.1. Two busbars, j and k respectively, are connected downstream of the MV busbar. The purpose is to assess the VU at each busbar, caused by the asymmetrical load connected at the j^{th} busbar, while the voltage at the upstream HV busbar is considered to be balanced. In order to develop a generic expression for VU at each busbar, the HV/MV transformer and the distribution line sections $\text{MV}-j$ and $j-k$ are assumed to be asymmetrical. The notations used in Fig. 4.1 are explained as follows:

$Z_{11:\text{HV}-\text{MV}}$ and $Z_{22:\text{HV}-\text{MV}}$ are the positive-sequence and negative-sequence impedances of the HV/MV transformer respectively,
$Z_{11:\text{MV}-j}$ and $Z_{22:\text{MV}-j}$ are the positive-sequence and negative-sequence impedances of the distribution line between the MV busbar and j^{th} busbar respectively,
$Z_{11:j-k}$ and $Z_{22:j-k}$ are the positive-sequence and negative-sequence impedances of the distribution line between the j^{th} busbar and k^{th} busbar respectively,

$Z_{11:\mathrm{HV}-j}$ and $Z_{22:\mathrm{HV}-j}$ are the positive-sequence and negative-sequence impedances of the system between the HV busbar and j^{th} busbar respectively,

$Z_{11:\mathrm{HV}-k}$ and $Z_{22:\mathrm{HV}-k}$ are the positive-sequence and negative-sequence impedances of the system between the HV busbar and k^{th} busbar respectively,

$Z_{21:\mathrm{HV}-\mathrm{MV}}$ is the negative-sequence positive-sequence coupling impedances[2] of the HV/MV transformer (generally equals to zero),

$Z_{21:\mathrm{HV}-j}$ is the negative-sequence positive-sequence coupling impedances of the system between the HV busbar and the j^{th} busbar.

Referring to Fig. 4.1, the positive-sequence voltages and negative-sequence voltages at the HV busbar, MV busbar, and j^{th} busbar are given in (4.6)-(4.9)[3]:

$$U_{1:\mathrm{HV}} = Z_{11:\mathrm{HV}-\mathrm{MV}} \cdot I_{1:L_j} + U_{1:\mathrm{MV}} \tag{4.6}$$

$$U_{1:\mathrm{HV}} = Z_{11:\mathrm{HV}-j} \cdot I_{1:L_j} + U_{1:j} \tag{4.7}$$

$$U_{2:\mathrm{HV}} = Z_{22:\mathrm{HV}-\mathrm{MV}} \cdot I_{2:L_j} + Z_{21:\mathrm{HV}-\mathrm{MV}} \cdot I_{1:L_j} + U_{2:\mathrm{MV}} \tag{4.8}$$

$$U_{2:\mathrm{HV}} = Z_{22:\mathrm{HV}-j} \cdot I_{2:L_j} + Z_{21:\mathrm{HV}-j} \cdot I_{1:L_j} + U_{2:j} \tag{4.9}$$

where;

$U_{1:\mathrm{HV}}$ and $U_{2:\mathrm{HV}}$ are the positive-sequence and negative-sequence voltages at the HV busbar respectively. Note that the $U_{2:\mathrm{HV}}$ is equal to zero, as the source connected at the HV busbar is balanced,

$U_{1:\mathrm{MV}}$ and $U_{2:\mathrm{MV}}$ are the positive-sequence and negative-sequence voltages at the MV busbar respectively,

$U_{1:j}$ and $U_{2:j}$ are the positive-sequence and negative-sequence voltages at the j^{th}

[2]When distribution lines and transformers are asymmetrical, unequal mutual impedances between individual phases cause unbalanced voltages across three phases. The presence of these unequal mutual impedances results in off-diagonal elements in the sequence domain impedance matrix. Z_{21} in the sequence domain is identified as the negative-sequence positive-sequence coupling impedance [126].

[3]In (4.6)-(4.9), the zero-sequence voltages are neglected. Refer to Appendix B for further discussion in this regard.

busbar respectively,

$I_{1:L_j}$ and $I_{2:L_j}$ are the positive-sequence and negative-sequence currents of the load which is connected at the j^{th} busbar respectively.

The positive-sequence load current, $I_{1:L_j}$, is given by (4.10):

$$I_{1:L_j} = \frac{U_{1:j}}{Z_{11:L_j}} \tag{4.10}$$

The negative-sequence current of the load, $I_{2:L_j}$, can be expressed in terms of the complex current unbalance factor[4] (CUF) of the load as (4.11):

$$I_{2:L_j} = \boldsymbol{CUF_{L_j}} \cdot \frac{U_{1:j}}{Z_{11:L_j}} \tag{4.11}$$

where; $\boldsymbol{CUF_{L_j}}$ and $Z_{11:L_j}$ are the complex CUF and the positive-sequence impedance of the load which is connected at the j^{th} busbar respectively.

Employing the fact that the negative-sequence impedance associated with distribution lines, transformers and passive loads are equal to their positive-sequence impedance, the negative-sequence impedance terms in (4.8) and (4.9) can be replaced by their corresponding positive-sequence impedance terms. Substituting (4.10) and (4.11), in (4.6)-(4.9), and considering that the voltage at the HV busbar is balanced (i.e. $U_{2:\text{HV}} = 0$), the voltage unbalance factor[5] (VUF) at the j^{th} busbar (VUF_j) can be evaluated as (4.12):

$$VUF_j = \left| -\frac{Z_{11:\text{HV}-j}}{Z_{11:L_j}} \cdot \boldsymbol{CUF_{L_j}} + \frac{Z_{21:\text{HV}-j}}{Z_{11:L_j}} \right| \tag{4.12}$$

[4]The CUF is defined as the magnitude of the ratio of negative-sequence current to positive-sequence current of the load [2]. The complex CUF is defined as the ratio of negative-sequence current (phasor) to positive-sequence current of the load (phasor).

[5]The VUF is defined as the magnitude of the ratio of negative-sequence voltage to positive-sequence voltage [5]. The complex VUF is defined as the ratio of negative-sequence voltage (phasor) to positive-sequence voltage.

Similarly, the VUF at the MV busbar (VUF_{MV}) can be expressed as (4.13):

$$VUF_{\mathrm{MV}} = \left| -\left(\frac{Z_{11:\mathrm{HV-MV}}}{Z_{11:L_j}} \cdot \boldsymbol{CUF_{L_j}} + \frac{Z_{21:\mathrm{HV-MV}}}{Z_{11:L_j}}\right) \cdot \frac{Z_{11:L_j}}{Z_{11:\mathrm{MV}-j} + Z_{11:L_j}} \right| \tag{4.13}$$

In (4.13), the term $\frac{Z_{11:L_j}}{Z_{11:\mathrm{MV}-j}+Z_{11:L_j}}$ can be re-written in-terms of the positive-sequence voltage at the MV busbar and j^{th} busbar as, $\frac{U_{1:j}}{U_{1:\mathrm{MV}}}$. Hence, VUF_{MV} in (4.13) can be re-expressed as (4.14):

$$VUF_{\mathrm{MV}} = \left| -\left(\frac{Z_{11:\mathrm{HV-MV}}}{Z_{11:L_j}} \cdot \boldsymbol{CUF_{L_j}} + \frac{Z_{21:\mathrm{HV-MV}}}{Z_{11:L_j}}\right) \cdot \frac{U_{1:j}}{U_{1:\mathrm{MV}}} \right| \tag{4.14}$$

The VU transfer coefficient from the j^{th} busbar to MV busbar, $T_{u:j-\mathrm{MV}}$, is defined as the ratio of VUF of the MV busbar, VUF_{MV}, to VUF of the j^{th} busbar, VUF_j, which can be expressed as (4.15):

$$T_{u:j-MV} = \left| \frac{Z_{11:\mathrm{HV}-MV} \cdot \boldsymbol{CUF_{L_j}} + Z_{21:\mathrm{HV}-MV}}{Z_{11:\mathrm{HV}-j} \cdot \boldsymbol{CUF_{L_j}} + Z_{21:\mathrm{HV}-j}} \cdot \frac{U_{1:j}}{U_{1:MV}} \right| \tag{4.15}$$

Generally, for three-phase transformers and symmetrical distribution lines, the associated negative-sequence positive-sequence coupling impedance is zero. Hence, the terms $Z_{21:\mathrm{HV}-MV}$ and $Z_{21:\mathrm{MV}-j}$ in (4.15) can be disregarded. Furthermore, assuming that $U_{1:j} \approx U_{1:\mathrm{MV}}$, (4.15) can be re-expressed as (4.16):

$$T_{u:j-\mathrm{MV}} \approx \left| \frac{Z_{11:\mathrm{HV-MV}}}{Z_{11:\mathrm{HV}-j}} \right| \tag{4.16}$$

Equation (4.16) implies that the transfer of VUF due to the asymmetry of a load from the j^{th} busbar to MV busbar can be approximated by the ratio of positive-sequence Thévenin impedances of the MV busbar and j^{th} busbar respectively; hence, related to short-circuit capacities of each busbar. Thus, the transfer coefficient can be expressed as in (4.17):

$$T_{u:j-\mathrm{MV}} \approx \frac{S_{sc:j}}{S_{sc:\mathrm{MV}}} \tag{4.17}$$

where; $S_{sc:\mathrm{MV}} = \frac{V_n^2}{|Z_{11:\mathrm{HV-MV}}|}$ is the short-circuit capacity (in MVA) at the MV busbar, $S_{sc:j} = \frac{V_n^2}{|Z_{11:\mathrm{HV}-j}|}$ is the short-circuit capacity (in MVA) at the j^{th} busbar and V_n is nominal line to line voltage of the network.

Equations (4.16) and (4.17) are independent of the load impedance, hence, they can facilitate the evaluation of the VU transfer coefficient irrespective of the type of load connected (i.e. constant impedance, constant power etc.) at the j^{th} busbar. The reader should note that in practical distribution networks, a voltage drop will occur between the MV busbar and j^{th} busbar, leading to $|\frac{U_{1:j}}{U_{1:\mathrm{MV}}}| < 1$. Therefore, referring to (4.15) and (4.16), $T_{u:j-\mathrm{MV}}$ given in (4.17), overestimates the VU propagation from j^{th} busbar to the MV busbar. A sensitivity analysis of $T_{u:j-\mathrm{MV}}$ in relation to the MVA capacities of the installation will be conducted in Section 4.2.2. In the case where a DG is connected to the j^{th} busbar, $U_{1:j}$ could be higher than $U_{1:\mathrm{MV}}$ if there is a power flow from j^{th} busbar to the MV busbar. Therefore, $|\frac{U_{1:j}}{U_{1:\mathrm{MV}}}|$ will be greater than unity. As a result, $T_{u:j-\mathrm{MV}}$ given in (4.17), underestimates the VU propagation from j^{th} busbar to the MV busbar.

Furthermore, the VUF at the downstream k^{th} busbar is equal to the VUF at the j^{th} busbar; hence, VU transfer coefficient from j^{th} busbar to k^{th} busbar is equal to unity.

4.2.2 Validation of Voltage Unbalance Transfer Model

In order to validate the mathematical formulation of the downstream to upstream VU transfer covered in Section 4.2.1, a 12.47 kV distribution network similar to that in Fig. 4.1 is utilised. The 138/12.47 kV HV/MV transformer is assumed to be symmetrical. An asymmetrical load, with a per-phase capacity of 4 MVA and lagging power factors of 0.6, 0.7 and 0.8 in phases A, B and C respectively, is connected at the j^{th} busbar. The distribution line which connects the j^{th} busbar to the MV busbar has a length of 1.6 km. The impedance data of the distribution line and the HV/MV transformer are given in Appendix A.

The VU transfer coefficients are evaluated using (4.15) and (4.17) for the follow-

ing four different cases.

- Case 1: The distribution line is asymmetrical and the load is of constant impedance type.
- Case 2: The distribution line is symmetrical (i.e. $Z_{21:\mathrm{MV}-j} = 0$) and the load is of constant impedance type.
- Case 3: The distribution line is asymmetrical and the load is of constant power type.
- Case 4: The distribution line is symmetrical and the load is of constant power type.

The resulting VU transfer coefficients from the j^{th} busbar to the MV busbar, $T_{u:j-\mathrm{MV}}$, is compared against the values obtained using unbalanced load-flow analyses using DIgSILENT PowerFactory software and the results are presented in Table 4.1.

Table 4.1: Comparison of VU transfer coefficient between the j^{th} busbar and the MV busbar ($T_{u:j-\mathrm{MV}}$) established using the mathematical model and load-flow analysis

	Case 1 (%)	Case 2 (%)	Case 3 (%)	Case 4 (%)
Load-flow analysis	0.34	0.51	0.31	0.50
Equation (4.15)	0.33	0.51	0.31	0.50
Equation (4.17)	-	0.53	-	0.53

According to results presented in Table 4.1, the VU transfer coefficient, $T_{u:j-\mathrm{MV}}$, established using the proposed formulation given by (4.15) are seen to be in close agreement with those established with unbalanced load-flow analyses. In the case of the balanced distribution line, the estimated VU transfer coefficient derived using (4.17) is slightly larger compared with that obtained from load-flow results. This over-estimation arises due to the approximation, $U_{1:j} \approx U_{1:\mathrm{MV}}$, made in the derivation of (4.16).

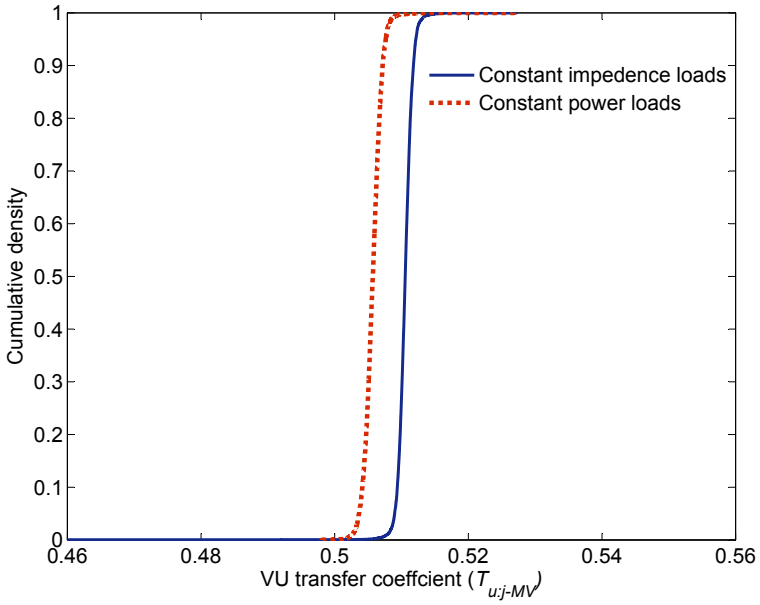

Figure 4.2: Cumulative distribution function of downstream to upstream VUF transfer coefficient for constant impedance and constant power loads for the case of symmetrical line

Fig. 4.2 illustrates the cumulative distribution function of $T_{u:j-\mathrm{MV}}$ for the test network when load-flow analysis was conducted for 5000 test cases, where the per-phase capacities of the load are randomly varied, while the distribution line is considered to be symmetrical and the POC of the load is fixed. The MVA capacities of each phase of the load were generated using a normally distributed random variable, with means of 3.40 MW and 2.12 MVAr and standard deviations of 0.26 MW and 0.16 MVAr. $T_{u:j-\mathrm{MV}}$ can be seen to remain approximately constant at 0.51 for constant impedance loads and at 0.505 for constant power loads irrespective of the random variation of per phase capacities of the load. These values are slightly smaller than 0.53 estimated using (4.17); hence, as predicted, (4.17) slightly overestimates the VU propagation from downstream to upstream network. A similar study was also carried out using a DG (represented by a constant power load), connected to the j^{th} busbar. The VU propagation from downstream to upstream network given by (4.17), slightly underestimated the observed value.

The cumulative distribution function of the VU transfer coefficient, when the distribution line is considered to be asymmetrical is given in Fig. 4.3. $T_{u:j-\mathrm{MV}}$ can

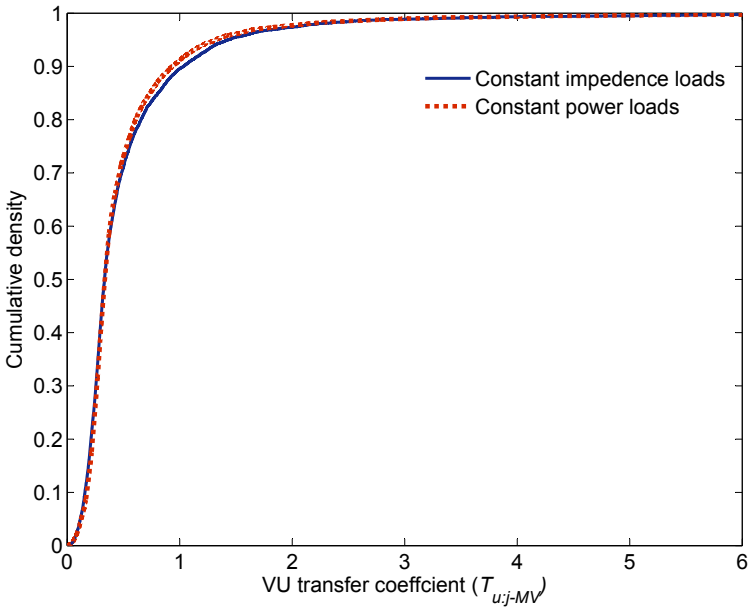

Figure 4.3: Cumulative distribution function of downstream to upstream VUF transfer coefficient for constant impedance and constant power loads for the case of asymmetrical line

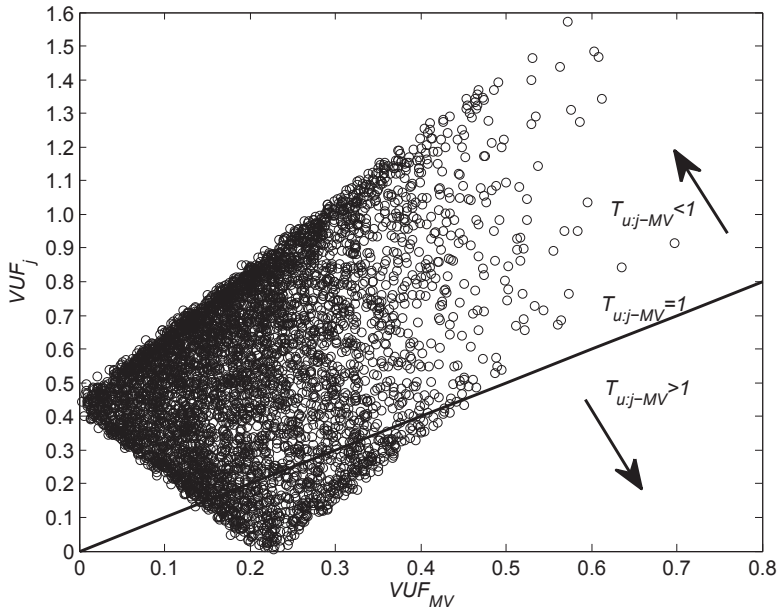

Figure 4.4: Variation of VUF_{MV} with VUF_j.

be seen to vary between zero and unity, and for a small number of cases (less than 10%) $T_{u:j-\mathrm{MV}} > 1$, which implies that the VUF at the MV busbar is larger than that of the j^{th} busbar. This can be attributed to the fact that in some instances, the VU caused by the load is compensated by the asymmetry of the distribution line, leading to less VU at the j^{th} busbar compared to that of the MV busbar. Fig. 4.4 illustrates the variation of VUF_{MV} with VUF_j, where VUF_{MV} can be observed to be larger than VUF_j. Thus, in the case of an asymmetrical distribution line, $T_{u:j-\mathrm{MV}}$ is highly dependent on the load asymmetry and line asymmetry; therefore, computation of $T_{u:j-\mathrm{MV}}$ needs to be undertaken on a case by case basis.

4.3 Analysis of Multiple Unbalanced Loads

In order to investigate the VU emission and propagation when multiple loads are connected to a radial distribution network, the radial network shown in Fig. 4.1 was modified by connecting an additional unbalanced passive load to the k^{th} busbar. Both distribution line sections were assumed to be symmetrical. Table 4.2 presents the expressions for the total VUF at the MV busbar, $\boldsymbol{VUF}_{\mathbf{MV}}^{\mathbf{total}}$, the j^{th} busbar, $\boldsymbol{VUF}_{\boldsymbol{j}}^{\mathbf{total}}$, and the k^{th} busbar, $\boldsymbol{VUF}_{\boldsymbol{k}}^{\mathbf{total}}$ respectively, when both loads are operating simultaneously. Note that $\boldsymbol{VUF}_{\mathbf{MV}}^{\mathbf{total}}$, $\boldsymbol{VUF}_{\boldsymbol{j}}^{\mathbf{total}}$, and $\boldsymbol{VUF}_{\boldsymbol{k}}^{\mathbf{total}}$ are expressed in terms of complex VUFs.

The derivations of the expressions given in Table 4.2 are given in Appendix C. Referring to Table 4.2, $\boldsymbol{VUF}_{\boldsymbol{L_j}}$ is identified as the VU emission from the unbalanced installation connected to j^{th} busbar and is equal to the complex VUF at the j^{th} busbar, when load L_j is operating in isolation. Similarly, $\boldsymbol{VUF}_{\boldsymbol{L_k}}$ represents the VU emission from the unbalanced installation connected to k^{th} busbar and is equal to the VUF at the k^{th} busbar, when load L_k is operating in isolation. Expressions for $\boldsymbol{VUF}_{\boldsymbol{L_j}}$ and $\boldsymbol{VUF}_{\boldsymbol{L_k}}$ are given in (4.18) and (4.19) respectively.

Table 4.2: Total VUFs at the MV, j^{th} and k^{th} busbars when both loads are operating simultaneously

$\boldsymbol{VUF}_{\mathbf{MV}}^{\mathbf{total}}$	$\boldsymbol{VUF}_{\boldsymbol{j}}^{\mathbf{total}}$	$\boldsymbol{VUF}_{\boldsymbol{k}}^{\mathbf{total}}$
$\frac{\frac{Z_{11:\mathrm{HV-MV}}}{Z_{11:j-k}}+\frac{Z_{11:\mathrm{HV-MV}}}{Z_{11:j-k}}\cdot\frac{Z_{11:\mathrm{HV}-k}}{Z_{11:\mathrm{HV}-j}}}{\frac{Z_{11:\mathrm{MV}-j}}{Z_{11:L_j}}+\frac{Z_{11:\mathrm{MV}-j}}{Z_{11:j-k}+Z_{11:L_k}}}\cdot\boldsymbol{VUF}_{\boldsymbol{j}}^{\mathbf{total}}+$	$\frac{Z_{11:j-k}}{Z_{11:\mathrm{HV}-k}}\cdot\boldsymbol{VUF}_{\boldsymbol{L_j}}$	$\frac{Z_{11:j-k}+Z_{11:L_k}}{Z_{11:\mathrm{HV}-j}}\boldsymbol{VUF}_{\boldsymbol{L_k}}$
$\frac{\frac{Z_{11:\mathrm{HV-MV}}}{Z_{11:j-k}+Z_{11:L_k}}-\frac{Z_{11:L_j}}{Z_{11:L_k}}\frac{Z_{11:\mathrm{HV-MV}}}{Z_{11:j-k}}}{\frac{Z_{11:\mathrm{MV}-j}}{Z_{11:L_j}}+\frac{Z_{11:\mathrm{MV}-j}}{Z_{11:j-k}+Z_{11:L_k}}}\cdot\boldsymbol{VUF}_{\boldsymbol{k}}^{\mathbf{total}}$	$+\frac{Z_{11:\mathrm{HV}-j}}{Z_{11:\mathrm{HV}-k}}\cdot\frac{Z_{11:L_k}}{Z_{11:L_k}+Z_{11:j-k}}\cdot\boldsymbol{VUF}_{\boldsymbol{k}}^{\boldsymbol{total}}$	$+\big(\frac{Z_{11:j-k}+Z_{11:L_k}}{Z_{11:L_k}}\big)\cdot\boldsymbol{VUF}_{\boldsymbol{j}}^{\mathbf{total}}$

$$\boldsymbol{VUF_{L_j}} = -\frac{Z_{11:\mathrm{HV}-j}}{Z_{11:L_j}} \cdot \boldsymbol{CUF_{L_j}} \tag{4.18}$$

$$\boldsymbol{VUF_{L_k}} = -\frac{Z_{11:\mathrm{HV}-k}}{Z_{11:L_k}} \cdot \boldsymbol{CUF_{L_k}} \tag{4.19}$$

According to Table 4.2, when both loads are operating simultaneously, VUFs at the j^{th} and k^{th} busbar can be expressed in terms of the VUF caused by the load connected to the particular busbar, and the VUF transferred to the same busbar from upstream and/or downstream busbars (i.e. VUF of the adjacent busbars). Similarly, the VUF at the MV busbar can be expressed in terms of the VUF that propagates to the MV busbar from both the j^{th} and k^{th} busbars. Furthermore, referring to (4.18), (4.19) and Table 4.2, both the VU emission from the load connected to a particular busbar and the VU propagation have been affected when both loads are operating simultaneously, compared to the situation in which individual loads are operating in isolation. Similar expressions can be developed for the VUF at each busbar when multiple loads are connected to the network. However, the complexity of such expressions will significantly increase; hence, the evaluation of the VU emission and propagation using a deterministic approach would be difficult. A statistical approach based on the general summation law discussed in Chapter 2, will be developed in Section 4.4 as a means for calculating the VU caused by multiple sources.

4.4 Estimation of Voltage Unbalance at Various Locations of a Radial Feeder

In order to establish a general expression for VUF at various locations along a feeder where multiple unbalanced installations are connected, consider the radial distribution network given in Fig. 4.5. The voltage at the upstream HV busbar is considered to be balanced. Multiple unbalanced installations are connected to

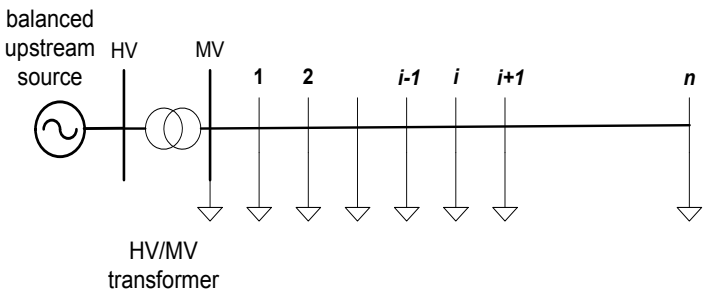

Figure 4.5: Radial distribution network with multiple installations

$$(VUF_i^{\text{total}})^\alpha = (VUF_{L_{\text{MV}}})^\alpha + \sum_{m=1}^{i-1} [VUF_{L_m}]^\alpha + [VUF_{L_i}]^\alpha + \sum_{m=i+1}^{n} \left[\frac{S_{sc:m}}{S_{sc:i}} VUF_{L_m}\right]^\alpha \tag{4.20}$$

the MV busbar and intermediate busbars 1 to n. The distribution line sections are assumed to be symmetrical. Considering one installation at a time, VU attenuation when it propagates upstream of the POC of the installation under consideration, can be expressed in terms of VU transfer coefficient. Referring to Section 4.3, the VU transfer coefficient from downstream to upstream of the network can be approximated using the ratio of short-circuit capacities of the two locations. The VU transfer coefficient from the POC of the installation to a downstream point of the network will be equal to unity as there are no further installations connected at downstream.

Following the aforementioned principles and summation law proposed in [2,5], a general expression for VUF at the i^{th} busbar can be formulated. Referring to (4.20) and Fig. 4.5, the total VUF at the i^{th} busbar, VUF_i^{total}, results from:

- the VU that propagates to i^{th} busbar from the MV busbar due to the VU emission from the unbalanced installation connected to the MV busbar, $VUF_{L_{\text{MV}}}$,
- the VU that propagates to the i^{th} busbar from all busbars which are upstream to i^{th} busbar due to VU emission from unbalanced installations connected to those busbars, $(\sum_{m=1}^{i-1} [VUF_{L_m}])$,

$$(VUF_i^{\text{total}})^\alpha = (VUF_{L_{\text{MV}}})^\alpha + \sum_{m=1}^{i} [VUF_{L_m}]^\alpha + \sum_{m=i+1}^{n} \left[\frac{S_{sc:m}}{S_{sc:i}} VUF_{L_m}\right]^\alpha \quad (4.21)$$

$$(VUF_{\text{MV}}^{\text{total}})^\alpha = (VUF_{L_{\text{MV}}})^\alpha + \sum_{m=1}^{n} \left[\frac{S_{sc:m}}{S_{sc:\text{MV}}} VUF_{L_m}\right]^\alpha \quad (4.22)$$

$$(VUF_n^{\text{total}})^\alpha = (VUF_{L_{\text{MV}}})^\alpha + \sum_{m=1}^{n} [VUF_{L_m}]^\alpha \quad (4.23)$$

- the VU emission from the installation connected at the i^{th} busbar, VUF_{L_i},
- the VU that propagates to i^{th} busbar from all other busbars located downstream of i^{th} busbar due to the VU emission from unbalanced installations connected to those busbars ($\sum_{m=i+1}^{n} \left[\frac{S_{sc:m}}{S_{sc:i}} VUF_{L_m}\right]$).

Hence, using the general summation law, the total VUF at the i^{th} busbar, VUF_i^{total}, can be written as (4.20).

Equation (4.20) can be further simplified as (4.21), where i is any busbar which is connected downstream to the MV busbar. Note that if there are parallel feeders, the term $VUF_{L_{\text{MV}}}$ also incorporates the VU emission from all installations connected to parallel feeders (except the feeder in which the busbar i is located), that gets transferred to the MV busbar. Following a similar approach, the VUF at the MV busbar, $VUF_{\text{MV}}^{\text{total}}$, and the VUF at the n^{th} busbar, VUF_n^{total}, can be given by (4.22) and (4.23) respectively.

In (4.20) to (4.23):
VUF_i^{total} is the magnitude resultant VUF at the i^{th} busbar (%),
VUF_n^{total} is the magnitude resultant VUF at the n^{th} busbar (%),
$VUF_{\text{MV}}^{\text{total}}$ is the magnitude resultant VUF at the MV busbar (%),
VUF_{L_m} is the magnitude of the VUF caused by the unbalanced installations connected m^{th} busbar and $m = 1, 2, 3, ..., i-1, i+1, ..., n$. Following (4.18), the complex VUF, $\boldsymbol{VUF_{L_m}}$, can be written as $\boldsymbol{VUF_{L_m}} = -\frac{Z_{11:\text{HV}-m}}{Z_{11:L_m}} \cdot \boldsymbol{CUF_{L_m}}$. Hence,

$|\boldsymbol{VUF_{L_m}}| = |-\frac{Z_{11:\mathrm{HV}-m}}{Z_{11:L_m}}| \cdot |\boldsymbol{CUF_{L_m}}|$. Considering that $S_{sc:m} = |\frac{V_n^2}{Z_{11:\mathrm{HV}-m}}|$ and $S_m \approx |\frac{V_n^2}{Z_{11:L_m}}|$, VUF_{L_m} can be written as (4.24):

$$VUF_{L_m} \approx \frac{S_{sc:m}}{S_m} \cdot CUF_{L_m} \tag{4.24}$$

where;

$S_{sc:m}$ is the short-circuit power at any intermediate m^{th} busbar (MVA),

S_m is the MVA capacity of the load connected to the m^{th} busbar (MVA),

CUF_{L_m} is the magnitude of the CUF of the load connected to the m^{th} busbar, which can be evaluated by either through a load flow analysis or by measurement[6] (%),

$VUF_{L_{\mathrm{MV}}}$ is the magnitude of the VUF caused by the unbalanced installations directly connected to the MV busbar and given by $\frac{S_{sc:\mathrm{MV}}}{S_{\mathrm{MV}}} \cdot CUF_{L_{\mathrm{MV}}}$ (%),

$S_{sc:\mathrm{MV}}$ is the short-circuit power at the MV busbar (MVA),

S_{MV} is the MVA capacity of the load connected to the MV busbar (MVA),

$CUF_{L_{\mathrm{MV}}}$ is the magnitude of the CUF of the load connected to the MV busbar (%),

VUF_{L_i} is the magnitude of the VUF caused by the unbalanced installations directly connected to the i^{th} busbar and can be given by $\frac{S_{sc:i}}{S_i} \cdot CUF_{L_i}$ (%),

$S_{sc:i}$ is the short-circuit power at the i^{th} busbar (MVA),

S_i is the MVA capacity of the load connected to the i^{th} busbar (MVA),

CUF_{L_i} is the magnitude of the CUF of the load connected to the i^{th} busbar (%).

Expressions given in (4.21)-(4.23) provide a simplified methodology, where the VU in a radial distribution network can be estimated using data such as MVA capacities of all distribution loads, their CUFs and short-circuit power at POCs.

[6]This may not necessarily be equal to the CUF of the load, when the load is operating independently. When multiple loads are connected, there exists some interaction which could affect the CUF of the load. However, such a discrepancy is minor and can be shown to be negligible through numerical examples.

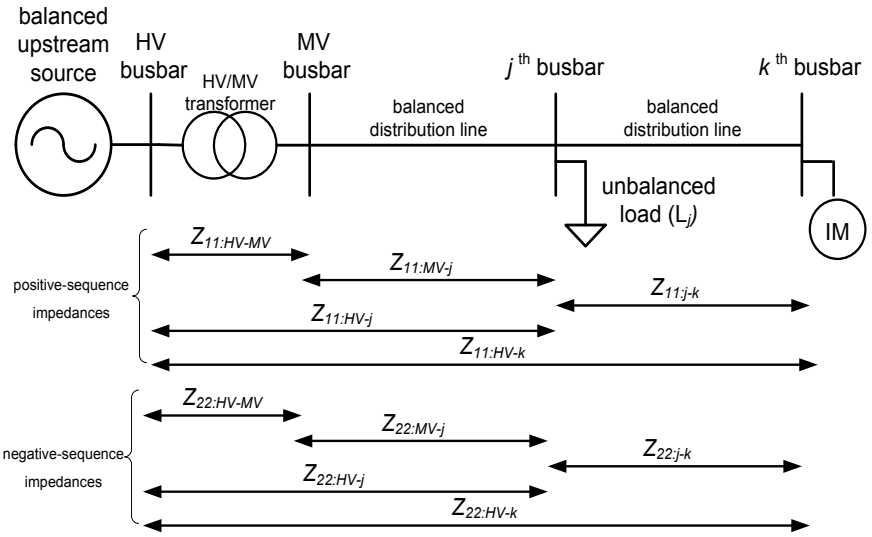

Figure 4.6: Radial distribution network with a passive load and an induction motor connected at j^{th} and k^{th} busbar respectively

4.5 Impact of Induction Motors on Voltage Unbalance Emission and Attenuation

Three-phase induction motors connected to distribution networks are known to attenuate VU, and therefore impact on VU emission and propagation in networks. Considering the radial distribution network in Fig. 4.1, the impact of induction motors on VU attenuation and propagation is examined in this section. Three scenarios are considered.

Scenario I: An unbalanced passive load and an induction motor are connected to the j^{th} and k^{th} busbars respectively (refer to Fig. 4.6). The VUF at the POC of the load connected to the j^{th} busbar, $VUF_{L_j|IM}$ (which is same as the VUF_j), and the VUF at the MV busbar, $VUF_{\text{MV}|IM}$, are given by (4.25) and (4.26) respectively.

$$VUF_{L_j|IM} = \left| K_1 \cdot \frac{Z_{11:\text{HV}-j}}{Z_{11:L_j}} \right| \cdot CUF_{L_j|IM} \tag{4.25}$$

$$K_1 = \frac{Z_{22:j-k} + Z_{22:m_k}}{Z_{22:\text{HV}-k} + Z_{22:m_k}}$$

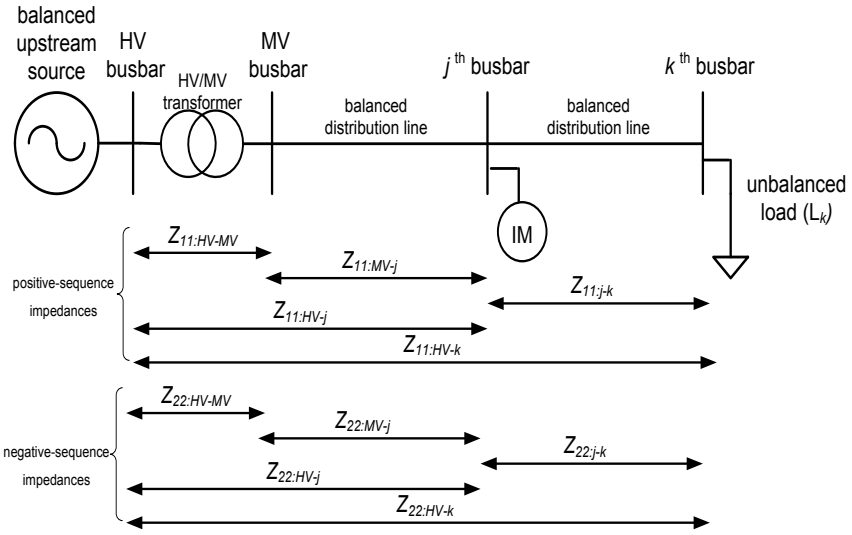

Figure 4.7: Radial distribution network with an induction motor and a passive load connected at j^{th} and k^{th} busbar respectively

$$VUF_{\text{MV}|IM} = \left| \frac{\left(\frac{(1-K_2)\cdot Z_{11:\text{MV}-j} - K_2 \cdot Z_{11:\text{HV}-\text{MV}}}{Z_{11:L_j}}\right)}{\frac{Z_{11:\text{MV}-j}+Z_{11:L_j}}{Z_{11:L_j}} + \frac{Z_{11:\text{MV}-j}}{Z_{22:j-k}+Z_{22:m_k}}} \right| \cdot CUF_{L_j|IM} \tag{4.26}$$

$$K_2 = \frac{Z_{22:\text{MV}-k} + Z_{22:m_k}}{Z_{22:\text{HV}-k} + Z_{22:m_k}}$$

where; $Z_{22:m_k}$ is the negative-sequence impedance[7] of the induction motor which is connected to the k^{th} busbar, and $CUF_{L_j|IM}$ is the magnitude of CUF of the load which is connected to the j^{th} busbar. The derivations of (4.25) and (4.26) are given in Appendix D.

Scenario II: The distribution network is modified by placing the induction motor at the j^{th} busbar and the unbalanced passive load at the k^{th} busbar (refer to Fig. 4.7). The resulting expressions for the VUF at the POC of the load connected to the k^{th} busbar, $VUF_{L_k|IM}$ (which is same as the VUF_k), and VUF at the MV busbar, $VUF_{\text{MV}|IM}$, are given by (4.27) and (4.28) respectively.

[7]In contrast to those of passive load, the negative-sequence impedance of an induction motor is different to its positive-sequence impedance.

$$VUF_{L_k|IM} = \left| \frac{K_3 \cdot (Z_{11:\mathrm{HV}-j}) + Z_{11:j-k}}{Z_{11:L_k}} \right| \cdot CUF_{L_k|IM} \tag{4.27}$$

$$K_3 = \frac{Z_{22:m_j}}{Z_{22:\mathrm{HV}-j} + Z_{22:m_j}}$$

$$VUF_{\mathrm{MV}|IM} = \left| \frac{\left(\frac{(1-K_4)\cdot Z_{11:\mathrm{MV}-j} - K_4 \cdot Z_{11:\mathrm{HV}-\mathrm{MV}}}{Z_{11:j-k}+Z_{11:L_k}}\right)}{\frac{Z_{11:\mathrm{MV}-j}+Z_{11:m}}{Z_{11:m}} + \frac{Z_{11:\mathrm{MV}-j}}{Z_{22:j-k}+Z_{22:L_k}}} \right| \cdot CUF_{L_k|IM} \tag{4.28}$$

$$K_4 = \frac{Z_{22:\mathrm{MV}-j} + Z_{22:m_j}}{Z_{22:\mathrm{HV}-j} + Z_{22:m_j}}$$

where; $Z_{22:m_j}$ is the negative-sequence impedance of the induction motor which is connected to the j^{th} busbar, and $CUF_{L_k|IM}$ is the magnitude of CUF of the load which is connected to the k^{th} busbar. The derivations of (4.27) and (4.28) are given in Appendix D.

Scenario III: The VUFs at the POC of the unbalanced load and the MV busbar when the induction motor and the unbalanced load are placed in two parallel feeders as shown in Fig. 4.8, are given by (4.29) and (4.30) respectively. Note that the j^{th} and k^{th} busbars are now connected to two parallel feeders.

$$VUF_{L_j|IM} = \left| \frac{K_5 \cdot Z_{11:\mathrm{HV}-\mathrm{MV}} + Z_{11:\mathrm{MV}-j}}{Z_{11:L_j}} \right| \cdot CUF_{L_j|IM} \tag{4.29}$$

$$VUF_{\mathrm{MV}|IM} = \left| \left(\frac{K_5 \cdot Z_{11:\mathrm{HV}-\mathrm{MV}}}{Z_{11:L_j}}\right) \cdot \frac{Z_{11:L_j}}{Z_{11:L_j} + Z_{11:\mathrm{MV}-j}} \right| \cdot CUF_{L_j|IM} \tag{4.30}$$

$$K_5 = \frac{Z_{22:\mathrm{MV}-k} + Z_{22:m_k}}{Z_{22:\mathrm{HV}-k} + Z_{22:m_k}}$$

The derivations of (4.29) and (4.30) are given in Appendix D.

Note that the magnitudes of the factors K_1, K_3 and K_5 are always less than

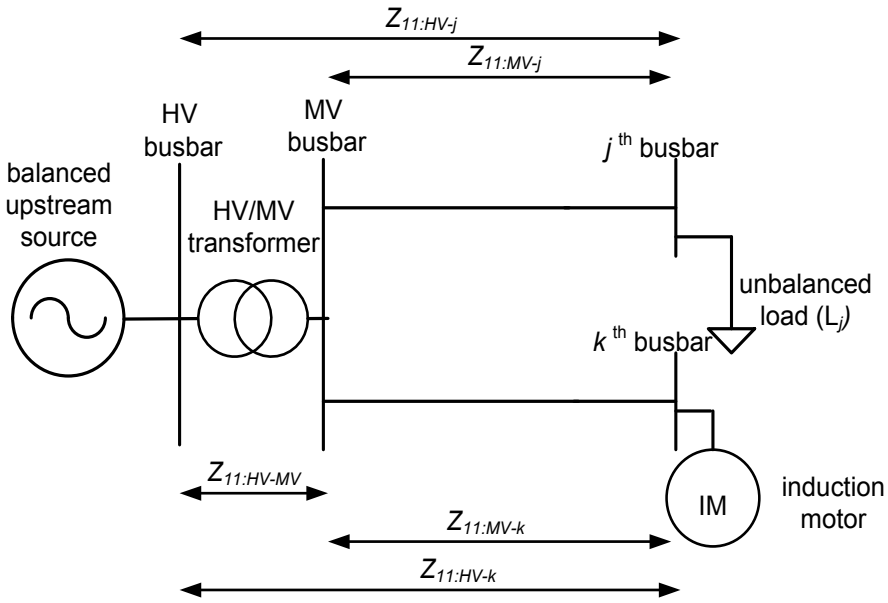

Figure 4.8: An induction motor and an unbalanced passive load connected to two parallel feeders

unity. Therefore, referring to (4.18), (4.19), (4.25), (4.27), (4.29) and assuming that the CUF of the passive load does not substantially change (i.e CUF_{L_j} in (4.18) and $CUF_{L_j|IM}$ in (4.25) are approximately equal in magnitude, and CUF_{L_k} in (4.19) and $CUF_{L_k|IM}$ in (4.27) are approximately equal in magnitude), the VUF at the POC of the load can be observed to decrease when induction motor is connected in the proximity of the load.

In order to verify (4.25), (4.27) and (4.29), four cases were considered.

- Case 1: Only a passive unbalanced load is connected to the j^{th} busbar of the MV distribution network discussed in Section 4.2.2 (refer to Fig. 4.1), and the length of the distribution line between the MV busbar and j^{th} busbar, $l_{\text{MV}-j} = 0.8$ km.

- Case 2: An unbalanced passive load and an induction motor load are connected to the j^{th} and k^{th} busbars of the MV distribution network given in Fig. 4.6, and $l_{\text{MV}-j} = 0.8$ km and $l_{j-k} = 0.4$ km.

- Case 3: An induction motor and an unbalanced passive load are connected to the j^{th} and k^{th} busbars of the MV distribution network given in Fig. 4.7, and

$l_{\text{MV}-j} = 0.4$ km and $l_{\text{MV}-k} = 0.8$ km.

– Case 4: An unbalanced passive load and an induction motor load are connected to j^{th} and k^{th} busbars respectively in two parallel feeders in the distribution network given in Fig. 4.8, and $l_{\text{MV}-\text{j}} = 0.8$ km and $l_{\text{MV}-k} = 0.4$ km.

Table 4.3: Comparison of results for $VUF_{\text{MV}|IM}$, $VUF_{L_{j/k}|IM}$ and $T_{u:L_{j/k}-\text{MV}|IM}$

Case	$VUF_{\text{MV}\|IM}$		$VUF_{L_{j/k}\|IM}$		$T_{u:L_{j/k}-\text{MV}\|IM}$	
	Load-flow analysis	Mathemat--ical formulation	Load-flow analysis	Mathemat--ical formulation	Load-flow analysis	Mathemat--ical formulation
1	0.43	0.44	0.63	0.64	0.68	0.68
2	0.402.84	0.412.83	0.592.72	0.602.72	0.67	0.68
3	0.40	0.41	0.602.71	0.60	0.67	0.68
4	0.41	0.42	0.61	0.62	0.67	0.67

The unbalanced loads have a per-phase MVA capacity of 4 MVA with lagging power factors of 0.6, 0.7 and 0.8 in phases A, B and C respectively. A 2.3 kV, 2250 hp induction motor which is connected to the distribution network through a 12.4/2.3 kV transformer is considered. The impedances of distribution lines, 138/12.47 kV transformer, 12.47/2.3 kV transformer and equivalent circuit parameters of the induction motor are given in Appendix A. The comparison of results for the VUFs at the MV busbar and the POC of the unbalanced load, $VUF_{L_{j/k}}$ and the VU transfer coefficient from load busbar to MV busbar, $T_{u:L_{j/k}-\text{MV}}$, obtained from the mathematical models in (4.25)-(4.30) and load-flow analyses using the DIgSILENT PowerFactory software are given in Table 4.3. Referring to Table 4.3, the VU emission from the unbalanced loads, $VUF_{L_{j/k}}$, in Cases 2, 3, and 4 have reduced (i.e. when an induction motor load is connected to the network), compared to Case 1, when there is no induction motor load. However, the VU transfer coefficient, $T_{u_{L_{j/k}-MV}}$, has remained approximately constant in Cases 1 to 4. Hence, the presence of induction motor loads is expected to have negligible impact to the

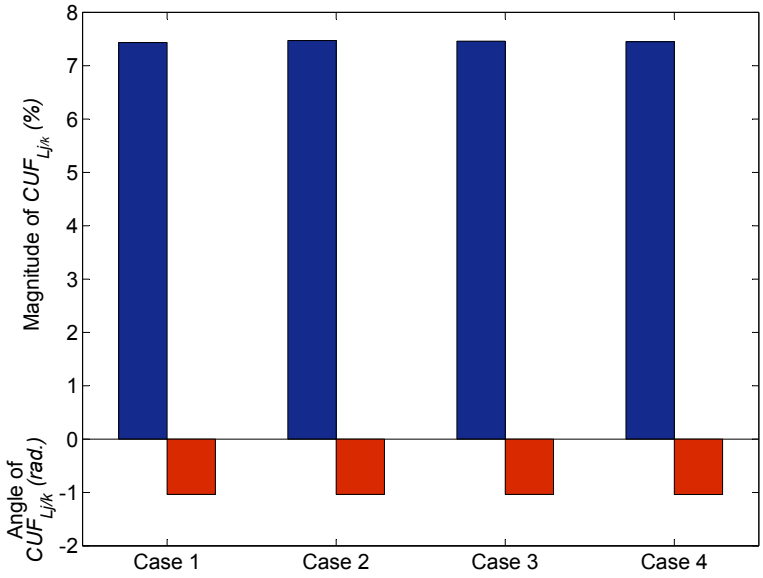

Figure 4.9: Variation of CUF of the unbalanced load for Cases 1-4.

VU propagation in the distribution network. Similarly, the complex CUFs of the passive load for Cases 1 to 4 given in Fig. 4.9 have remained constant in all four cases considered in the study. Hence, the sensitivity of the complex CUF of the load to the presence of the induction motor load is also considered to be negligible.

Fig. 4.10 illustrates the variation of the VUF at the POC of the unbalanced load while the position of the induction motor load is varied along the feeder. Assume the unbalanced load is connected at 0.8 km away from the MV busbar and (a) the induction motor is connected at the same feeder, (b) the induction motor is connected to a parallel feeder. According to Fig. 4.10, the VUF at the POC of the load has reduced from 0.63% to 0.61% when the induction motor is connected to a parallel feeder, but remains constant irrespective of the position of the induction motor in the parallel feeder. When the induction motor is connected to the same feeder where the unbalanced load is connected, the VU emission from the load further decreases from 0.61%, when the POC of the induction motor load is moved from the MV busbar towards the POC of the unbalanced load. The minimum value of 0.59% can be observed when the POC of the load and the POC of induction motor load coincide with each other. When the POC of the induction motor load

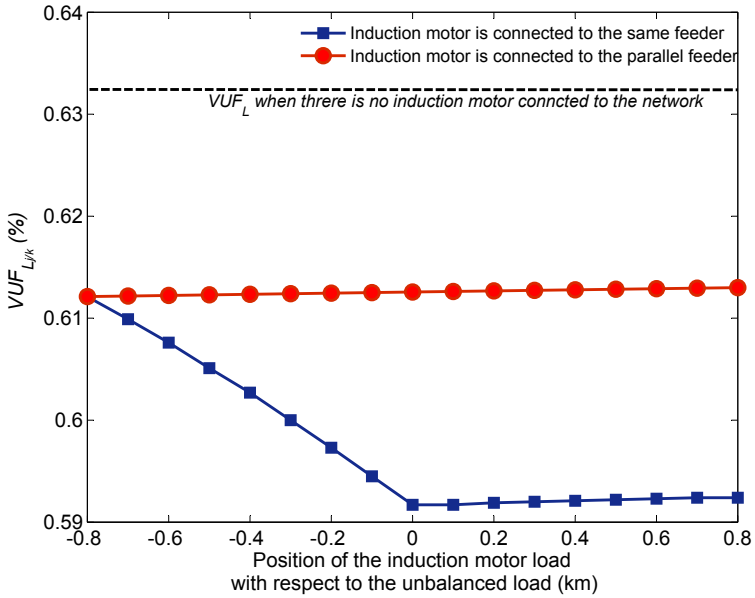

Figure 4.10: Variation of VU emission of the unbalanced load, with the position[9]of the induction motor

is moved further away from the passive load towards the end of the feeder, the VU emission from the passive load shows a negligible increase.

Based on the discussion of VU attenuation provided by induction motor loads, a factor termed the influence factor (γ) can be defined using (4.31) to quantify the VU attenuation provided by the induction motor at the POC of the unbalanced passive loads, when both loads are connected to a radial power system.

$$\gamma = \left| \frac{VUF_{\mathrm{L|IM}} \text{with the induction motor load}}{VUF_{\mathrm{L}} \text{without induction motor load}} \right| \tag{4.31}$$

Assuming that the CUF of the unbalanced passive load is not affected when induction motor load is connected, the influence factors for Scenarios I-III considered in this section are summarised in Table 4.4. Referring to Table 4.4, a DNSP can now evaluate the VU attenuation provided by an induction motor in a distribution network, and quantify the extra VU absorption capacity available in the distribution network due to the presence of the induction motor load. This aspect will be discussed in Chapter 5.

[9]The distance is measured with respect to the position of the unbalanced load.

Table 4.4: Influence coefficients

Scenario I (Unbalanced passive load and an induction motor are connected to j^{th} busbar and k^{th} busbar respectively as shown in Fig. 4.6)	$\gamma = \left\lvert \frac{Z_{22:j-k}+Z_{22:m}}{Z_{22:\text{HV}-k}+Z_{22:m}} \right\rvert$
Scenario II (Induction motor and an unbalanced passive load are connected to j^{th} busbar and k^{th} busbar respectively as shown in Fig. 4.7)	$\gamma = \left\lvert \frac{K\cdot(Z_{11:\text{HV}-j})+Z_{11:j-k}}{Z_{11:\text{HV}-\text{MV}}} \right\rvert$ where $K = \frac{Z_{22:m}}{Z_{22:\text{HV}-j}+Z_{22:m}}$
Scenario III (Unbalanced passive load and an induction motor are connected to j^{th} busbar and k^{th} busbar in two parallel feeder as shown in Fig. 4.8)	$\gamma = \left\lvert \frac{K\cdot Z_{11:\text{HV}-\text{MV}}+Z_{11:\text{MV}-j}}{Z_{11:\text{HV}-j}} \right\rvert$ where $K = \frac{Z_{22:\text{MV}-k}+Z_{22:m}}{Z_{22:\text{HV}-k}+Z_{22:m}}$

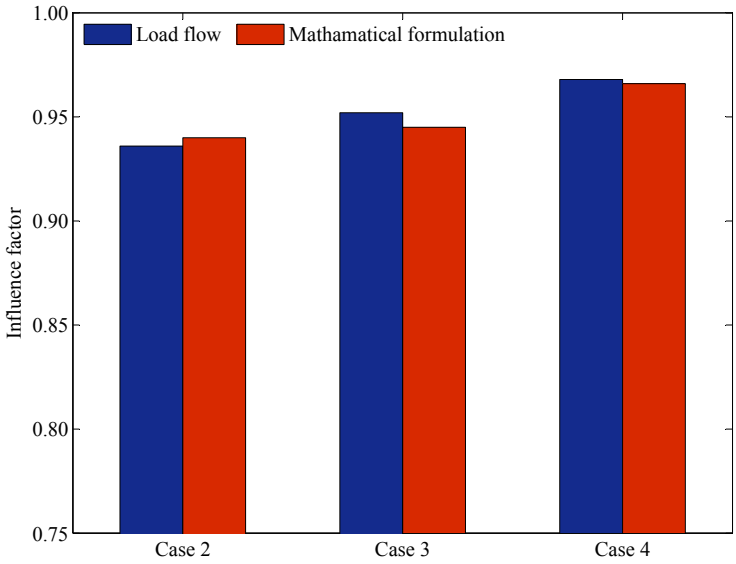

Figure 4.11: Comparison of influence factors derived from mathematical formulation and load-flow analysis.

A comparison of the influence factors evaluated using the formulations given in Table 4.4 and load-flow analyses for Cases 2 to 4 are given in Fig. 4.11. The magnitude of the influence factor estimated using the proposed formations in Table 4.4 is in close agreement with the load-flow results, hence, verifying the accuracy of the derivations in Table 4.4.

4.6 Chapter Summary

The main objective of this chapter was to examine the VU emission, propagation and attenuation in radial distribution networks, and to provide the theoretical background for Chapter 5.

Mathematical models were developed to characterise the VU propagation in distribution networks from downstream to upstream networks. The developed models were verified using unbalanced load-flow analysis. The investigations reveal that the attenuation of VU (caused by an unbalanced installation), when propagating from downstream network to upstream network can be approximated by the ratio of short-circuit capacities between the two locations of interest. This observation is accurate, even in the case where a DG is connected.

The VU propagation and attenuation, when multiple unbalanced loads are connected has also been discussed. Formulations suggest that the relationships between VU emission and propagation when multiple unbalanced installations are in operation, are complex, hence, deterministic approaches to estimate the net VU levels are difficult. Therefore, a statistical approach based on the general summation law has been proposed.

In addition, an influence factor was derived to quantify the impact that an induction motor has on the VU in radial distribution networks. A sensitivity analysis was carried out with respect to the position of the induction motor, and unbalanced installations, which showed that the highest attenuation occurs when both are connected at close proximity to each other.

Based on the proposed methodologies to evaluate VU propagation and attenuation, the VU emission allocation methodologies given in IEC 61000-3-13 and IEC 61000-3-14 can be further modified. This will be the focus of Chapter 5.

Chapter 5

Refined Voltage Unbalance Emission Allocation Methodologies

5.1 Introduction

Attenuation of VU when it propagates from downstream to upstream networks was investigated in Chapter 4 where it was shown that VU attenuation can be estimated using the ratio of short-circuit capacities between the two locations of interest. In addition, the VU attenuation provided by induction motor loads was quantified by introducing the concept of the influence factor.

As discussed in Chapter 2, the current IEC Stage 2 VU emission allocation methodologies fail to account for attenuation of VU when propagating from downstream to upstream network, and may lead to conservative emission limits for installations. The focus of this chapter is to develop alternative VU emission allocation methodologies which will address the deficiencies of the current IEC VU emission allocation techniques. Two alternative VU emission allocation methodologies are introduced in this chapter; the first is based on the CBV and the second is based on the VD [14, 16] method.

The CBV methodology, which was discussed in Chapters 2 and 3, is modified in this chapter to allocate VU emission limits for unbalanced installations, incorporating the VU attenuation aspects discussed in Chapter 4. Using the CBV methodology, emission levels at each network busbar are explicitly forced to be at or below a reference level when all installations are injecting their full allocation levels derived under the same methodology, allowing the compatibility levels for the network to be met.

Both IEC and CBV methodologies are data and computational intensive; hence, would be difficult to apply in practical distribution networks. The harmonic emission allocation methodology based on the VD method presented in Chapter 2 and Chapter 3 provides a pragmatic emission allocation methodology, which utilises data that are easily available with DNSPs (such as line impedance data). Hence, the applicability of the VD method in relation to VU emission allocation will also be investigated in this chapter.

The chapter is organised as follows. The theoretical bases of VU emission allocation methodology based on the CBV methodology and application examples are discussed in Section 5.2. The VU emission allocation in distribution networks with induction motor loads is investigated in Section 5.3. A new VU emission allocation methodology based on the concept of VD is presented in Section 5.4. A comparison of VU emission limits established by IEC methodologies and the proposed methodologies in relation to MV and LV distribution networks respectively are given in 5.5. Conclusions are given in Section 5.6

5.2 Voltage Unbalance Emission Allocation Methodology Based on the Constrained Bus Voltage Method

Considering the radial distribution network given in Fig. 5.1, the general principles in relation to VU emission allocation methodology can be established. The network consists of $(n+1)$ number of busbars including the MV busbar and an installation is

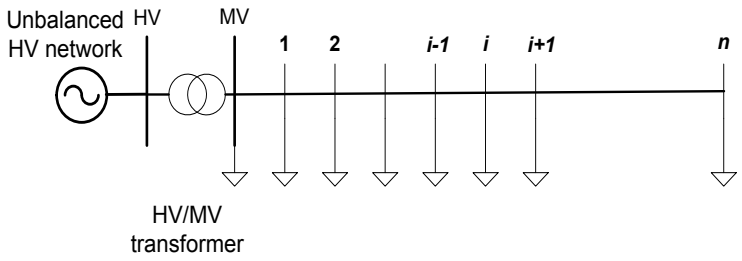

Figure 5.1: Radial distribution network with multiple installations

$$(VUF_i^{\text{total}})^\alpha = (VUF_{\text{HV}})^\alpha + (E_{u:\text{MV}})^\alpha + \sum_{m=1}^{i} [E_{u:m}]^\alpha + \sum_{m=i+1}^{n} \left[\frac{S_{sc:m}}{S_{sc:i}} E_{u:m}\right]^\alpha \quad (5.2)$$

$$(VUF_{\text{MV}}^{\text{total}})^\alpha = (VUF_{\text{HV}})^\alpha + (E_{u:\text{MV}})^\alpha + \sum_{m=1}^{n} \left[\frac{S_{sc:m}}{S_{sc:\text{MV}}} E_{u:m}\right]^\alpha \quad (5.3)$$

$$(VUF_n^{\text{total}})^\alpha = (VUF_{\text{HV}})^\alpha + (E_{u:\text{MV}})^\alpha + \sum_{m=1}^{n} [E_{u:m}]^\alpha \quad (5.4)$$

connected to each busbar. By closely following the CBV methodology for harmonics and flicker in which the emission allocation of the installation is derived based on the apparent power of the installation, the VU emission allocation limit for an installation connected to i^{th} ($i \leq n$) busbar can be given by (5.1):

$$E_{u:i} = k_u \cdot \sqrt[\alpha]{S_i} \quad (5.1)$$

where; $E_{u:i}$ is the VU emission allocation limit for an installation that is connected to the i^{th} busbar (VUF), α is the general summation exponent for VU which is equal to 1.4, S_i is the apparent power of the installation in per-unit and k_u is an allocation constant, which is yet to be determined.

Equations (4.21)-(4.23) can be modified as (5.2)-(5.4), where the VU emission of each installation is now given by VU emission allocation limit in (5.1). The reader should note that the VU contribution from the upstream HV network is taken into account using the term VUF_{HV}.

In (5.2) to (5.4):

$VUF_{\mathrm{MV}}^{\mathrm{total}}$ is the magnitude of resultant VUF at the MV busbar (%),

VUF_{i}^{total} is the magnitude of resultant VUF at the i^{th} busbar (%),

VUF_{n}^{total} is the magnitude of resultant VUF at the n^{th} busbar (%),

VUF_{HV} is the magnitude of VUF transferred from the upstream HV network (%),

$E_{u:\mathrm{MV}}$ is the VU emission allocation limit for the unbalanced installations directly connected to the MV busbar, which is given by (5.1) (%),,

$E_{u:m}$ is the VU emission allocation limit for the installations connected to downstream of the MV busbar, which is given by (5.1) and $m = 1, 2, 3, ..., i, i+1, ..., n$ (%),,

$S_{sc:m}$ is the short-circuit capacity at any intermediate busbar m (p.u.),

$S_{sc:\mathrm{MV}}$ is the short-circuit capacity at the MV busbar (p.u.).

Note that in the case of a multi-feeder network, the term $E_{VUF:\mathrm{MV}}$ also includes the VU that transfers to the MV busbar, from unbalanced installations that are connected to parallel feeders.

When the MVA capacity of each installation and the short-circuit capacity of each busbar is known in advance, the net VUF at each busbar can be estimated using (5.2)-(5.4) as a function of allocation constant k_u. Considering that the VUF at any busbar (e.g. end of the feeder) should not exceed the set planning level for the distribution network, a suitable value for k_u can be determined. For example, when the value of k_u is increased from zero up to a certain value in (5.2)-(5.4), the VUF at one of the busbars will reach the set planning level (hence, called as the critical busbar). The value of k_u for which the critical busbar reaches its planning level can be selected as the allocation constant. Thereafter, the emission allocation limits for all installations can be calculated using (5.1).

The acceptable negative-sequence current allocation limit ($E_{I_2:i}$) for the instal-

lation under consideration can be determined using (5.4) [5]:

$$E_{I_2:i} = \frac{E_{u:i}}{Z_{22:i}} \tag{5.4}$$

where; $Z_{22:i}$ is the negative-sequence impedance at the i^{th} busbar (per-unit), for converting voltage to current unbalance emission limits as given by [127]. When the system impedance is mainly dominated by transformer and line impedances, the negative-sequence impedance can be approximated by the positive-sequence impedance [5].

In relation to large DG installations, the CBV approach can be modified to provide VU emission limit. Assume that a large DG installation is connected to a busbar, which is downstream to i^{th} busbar. VU emission limit for the DG installation can be provided using (5.1) as (5.5):

$$E_{u:\text{DG}} = k_u \cdot \sqrt[\alpha]{S_{\text{DG}}} \tag{5.5}$$

where; $E_{u:\text{DG}}$ is the VU emission limit for the DG installation, S_{DG} is the agreed power of the DG installation in per-unit, and k_u is the VU allocation constant, which needs to be determined for the network. Following the principles of (5.2), the total VUF at the i^{th} busbar, (VUF_i^{total}), can be estimated as (5.6):

$$\begin{aligned}(VUF_i^{\text{total}})^\alpha = (VUF_{\text{HV}})^\alpha + (E_{u:\text{MV}})^\alpha + \sum_{m=1}^{i} [E_{u:m}]^\alpha + \\ \sum_{m=i+1}^{n} \left[\frac{S_{sc:m}}{S_{sc:i}} E_{u:m}\right]^\alpha + \left[\frac{S_{sc:\text{DG}}}{S_{sc:\text{i}}} E_{u:\text{DG}}\right]^\alpha\end{aligned} \tag{5.6}$$

where; $S_{sc:\text{DG}}$ is the short-circuit capacity at the POC of the DG installation. Following a similar approach as discussed previously, the allocation constant k_u can be determined using (5.6) such that the VUF at the critical location of the network to be within the planning level of the network.

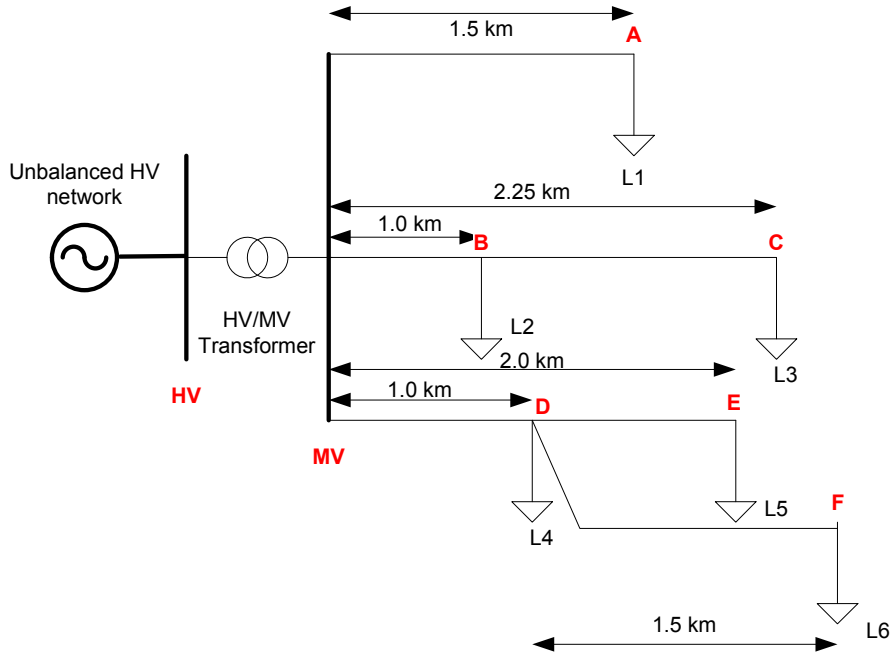

Figure 5.2: Test MV distribution network

5.2.1 Application Example of the Proposed Methodology

In this section, the application of the CBV methodology is demonstrated through two case studies, considering the radial MV distribution network given in Fig. 5.2.

Case I

The radial distribution network given in Fig. 5.2 consists of six unbalanced installations (L1 to L6) with MVA capacities as given in Table 5.1, connected via balanced distribution lines to the HV/MV transformer. The impedance data of the distribution lines and of the HV/MV transformer are given in Appendix A. The calculation procedure of emission limits for each unbalanced installation, using the proposed methodology is described in the following steps.

A HV planning level ($L_{u:\mathrm{HV}}$) of 1.35%, MV planing level ($L_{u:\mathrm{MV}}$) of 1.75% and a HV to MV transfer coefficient ($T_{u:\mathrm{HV-MV}}$) of unity are assumed for the network

Table 5.1: Emission allocation limit for each installation in Case I ($k_u = 0.01$, $S_{\text{base}} = 20$ MVA)

Bus ID - Load ID	Capacity of the installation connected to the bus	Total VUF at the busbar (%)	Allocated VUF to the installation (%)
MV	-	1.6091	-
A - L1	2.0 MVA	1.6424	0.1932
B - L2	5.0 MVA	1.7028	0.3717
C - L3	3.5 MVA	1.7437	0.2881
D - L4	2.5 MVA	1.6997	0.2266
E - L5	5.0 MVA	1.7500	0.3717
F - L6	2.0 MVA	1.7259	0.1932

[5][1]. Hence, the VU that propagates from the HV network to the MV network can be calculated as, $VUF_{\text{HV}} = T_{u:\text{HV}-\text{MV}} \cdot L_{u:\text{HV}}$. Each installation is given a VU emission allocation defined according to (5.1) as a function of k_u, which is yet to be determined. Employing (5.1) and (5.2), the VUF at the POC of each installations can be calculated for various values of k_u. The resultant VUF at each busbar when $k_u = 0.01$ with a base MVA of 20 MVA is given in Table 5.1.

According to Table 5.1, the resultant VUF at the POC of the installation L5 (Bus E) can be observed to reach the planning level of 1.75% for the network. Hence, the limiting value for the allocation constant k_u can be selected to 0.01. Accordingly, each installation can be given an allocation using (5.1), while maintaining the net VU levels within the planning level for the network. The resulting VU emission limit for each installation are given in Table 5.1 Column 4.

[1]The values for HV and MV planning levels are selected based on the indicative values given in IEC TR 61000-3-13 for HV and MV networks. The HV to MV transfer coefficient is selected as unity as there are no induction motor loads directly connected to the MV network.

Case II

In certain situations, allocation of VUF solely based on the unbalanced component of the installation, instead of the entire agreed power of the load would be reasonable. This enables the system operator to provide an increased VUF emission limit to other unbalanced installations connected to the same network, while maintaining the net VU of the network within the network planning levels. Thus, the VU allocation in (5.1) for an installation can be modified as (5.7):

$$E_{u:i} = k_u \cdot \sqrt[\alpha]{U_f \cdot S_i} \tag{5.7}$$

where; U_f is the ratio of MVA capacity of the unbalanced component ($S_{i:\text{unbalanced}}$) of the installation to the agreed power of the installation (S_i) (i.e. $U_f = S_{i:\text{unbalanced}}/S_i$)[2].

Assume that that installation L3 connected to the distribution network given in Fig. 5.2 to be fully balanced and unbalanced components of installation L1, installation L4 and installation L5 equal to 0.5. The VU emission allocation limit for each installation in the distribution network of Fig. 5.2, when allocation is made based on unbalanced MVA capacity of the installation, is given in Table 5.2. The limiting value of k_u is equal to 0.0144 in 20 MVA base.

Referring to Table 5.2, Busbar F now reaches the planing level of the network. The installation connected to Busbar C was considered to be a balanced load, hence, no emission allocation is required for this installation. As expected, the VU emission limits for installations L2 and L6 have increased to 0.53% and 0.28% respectively, compared to 0.37% and 0.19% in Case I.

[2]As an example, if an installation consists of balanced three-phase loads such as heating loads with MVA rating of $S_{\text{three-phase}}$ and single-phase loads distributed across three phases (with a total MVA rating of $S_{\text{single-phase}}$), U_f can be selected as $U_f = \frac{S_{\text{single-phase}}}{S_{\text{single-phase}}+S_{\text{three-phase}}}$. U_f can vary from 0 to 1.

Table 5.2: Emission allocation limits for each installation in Case II ($k_u = 0.0144$, $S_{\text{base}} = 20$ MVA)

Bus ID - Load ID	U_f	Installation capacity connected to the bus	Total VUF at the busbar (%)	Allocated VUF to the installation (%)
MV	-	-	1.6091	-
A - L1	0.5	2.0 MVA	1.6474	0.1689
B - L2	1.0	5.0 MVA	1.7291	0.5330
C - L3	0.0	3.5 MVA	1.7291	0
D - L4	0.5	2.5 MVA	1.7067	0.1981
E - L5	0.5	5.0 MVA	1.7484	0.3250
F - L6	1.0	2.0 MVA	1.7500	0.2771

5.2.2 The Impact of Single-phase/Two-phase Installations

The proposed CBV methodology can be modified in order to estimate the VU emission limits in situations where there is a special installation such as a single-phase or two-phase installation connected to the distribution network. The VUF at the POC of a single-phase or two-phase installation is given by (5.8):

$$E_{u:i} \approx \frac{S_i}{S_{sc:i}} \cdot CUF_i \tag{5.8}$$

where;

$E_{u:i}$ is the VUF at the i^{th} busbar where the load is connected,

CUF_i is the magnitude of CUF of the installation,

S_i is MVA capacity of the single or two-phase installation,

$S_{sc:i}$ is the three-phase short-circuit capacity at the i^{th} busbar.

The CUFs for different configurations of single and two-phase installations are given in Table 5.3 [128].

To demonstrate the application of the proposed methodology in the presence of single-phase or two-phase installations, the distribution network in Fig. 5.2 was modified by replacing the 3.5 MVA installation with a single-phase installation (without neutral) with an MVA capacity of 0.5 MVA. The VU emission from the single-phase installation was determined as 0.5586% using (5.8). Allocation of VU for the re-

Table 5.3: CUF for different configurations of single and two-phase installations

Configuration	$\lvert CUF_i \rvert$
1-phase connection with neutral[3]	1
2-phase connection with neutral	0.5
1-phase connection without neutral	1
2-phase connection without neutral	0.5

Table 5.4: Emission allocation for each three-phase installation (k_u = 0.0058, $S_{\text{base}} = 20$ MVA)

Bus ID - Load ID	Installation capacity connected to the bus	Total VUF at the busbar (%)	Allocated VUF to the installation (%)
MV	-	1.5442	-
A - L1	2.0 MVA	1.5600	0.1121
B - L2	5.0 MVA	1.6461	0.2158
C - L3	0.5 MVA single-phase installation	1.7500	-
D - L4	2.5 MVA	1.5874	0.1316
E - L5	5.0 MVA	1.6116	0.2158
F - L6	2.0 MVA	1.6000	0.1121

maining three-phase installations can be made using (5.1), while the VU emission limit for the single phase load is replaced by its VUF emission previously calculated using (5.8). Following the proposed methodology in Section 5.2 and (5.2), the allocation constant for the network is calculated as 0.0058. The resulting VU emission limits for three-phase installations are tabulated in Table 5.4.

Referring to Table 5.4, the VU at the POC of the single-phase installation (Busbar C), can be observed to reach the planning level of 1.75%. If there are more than one single or two-phase installations connected to the network across different phases, the application of the general summation law can lead to conservative results, hence, the specific characteristics of the connection scheme should be taken into account.

[3]Note that in the case of MV distribution networks, there is no neutral connection. Only for the completeness, the $|CUF_i|$ for installation with neutral connections are replicated from here.

5.2.3 Application of VUF Allocation for LV Networks

In this section, the CBV methodology is employed to calculate the emission limits for installations connected to an LV distribution network. In line with the IEC 61000-3-14 methodology, emission limits are provided to three-phase installations only. The responsibility to manage with VU produced by single-phase installations rests with the DNSPs.

The schematic of the test LV network, which is based on a network used in [129] is given in Fig. 5.3. The distribution network consists of three parallel feeders classified as residential feeder, industrial feeder and commercial feeder. The impedance of different conductors and underground cables are given in Appendix A. An MV planning level of 1.75% and an LV planning level of 2.0% are assumed[4]. For simplicity, the three residential installations L1, L3 and L4 are assumed to have three-phase connections or for the case where they are single-phase installations, the load is assumed to be distributed among the three phases. All other installations are assumed to be three-phase installations. The VU emission limits for each installation (including an allowance for residential installations L1, L3 and L4) and the net VU at each node, calculated using the proposed CBV methodology are given in Table 5.5. The value of the allocation constant calculated using the CBV methodology is equal to 0.01 with a base kVA of 400 kVA.

With reference to Table 5.5, the total VU at the Node E is observed to reach the planning level for the network.

5.3 Analysis of the Impact of Induction Motor Installations

As demonstrated in Chapter 4, the VU levels can improve in the presence of induction motor installations in a radial network. Due to the VU attenuation provided by induction motor installations, the net VU absorption capacity of the networks

[4]The values for MV and LV planning levels and MV to LV transfer coefficient are selected based on the indicative values given in IEC TR 61000-3-14 for LV networks.

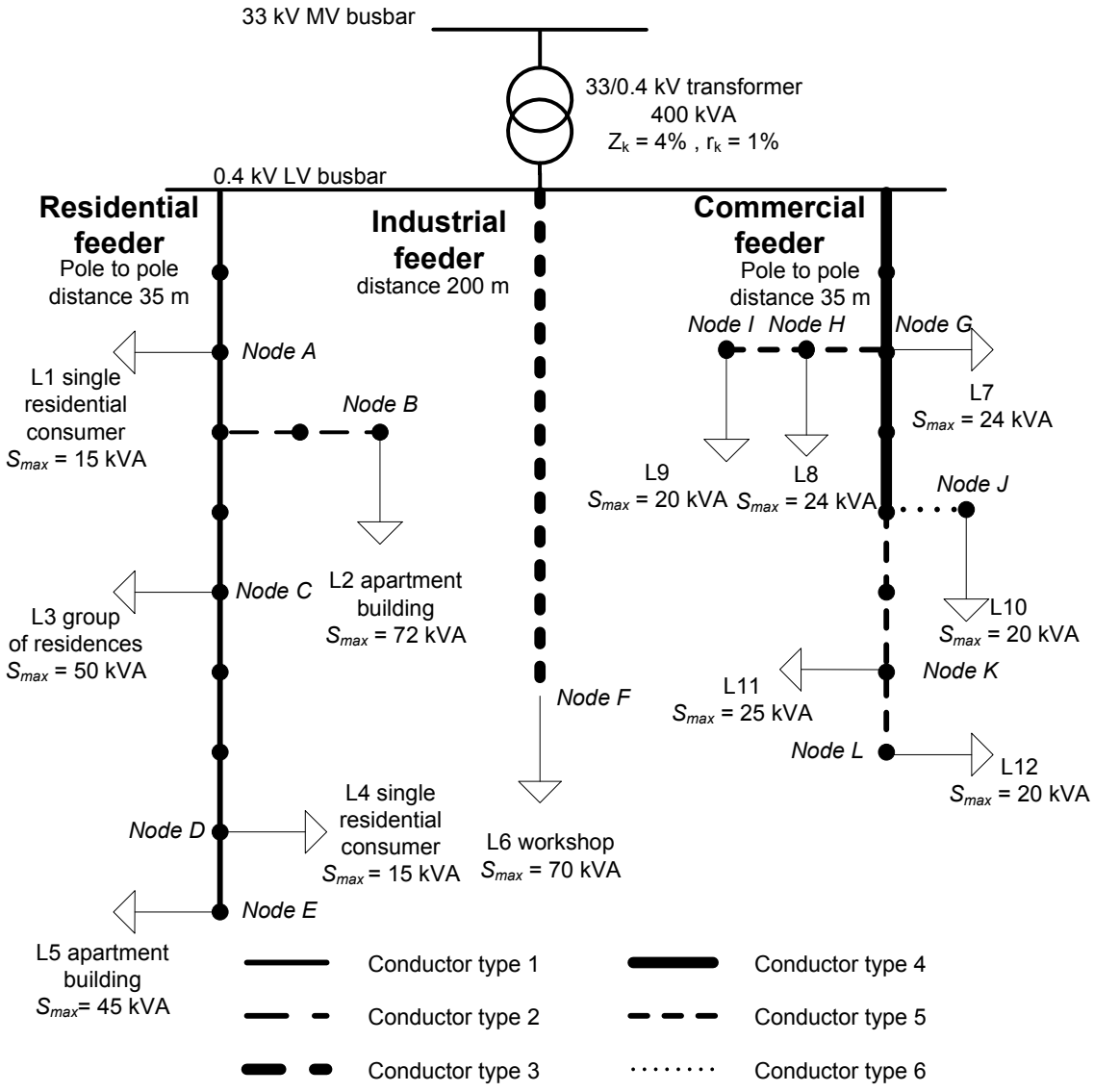

Figure 5.3: Test LV network

Table 5.5: VU emission allocation for three-phase installations connected to the LV distribution network

Node ID - Load ID	Capacity of the installation (kVA)	Total VUF at the node	Allocated VUF to the installation
A - L1	15	1.8811	0.0953
B - L2	72	1.9690	0.2923
C - L3	50	1.9603	0.2253
D - L4	15	1.9917	0.0953
E - L5	45	2.0000	0.2090
F - L6	70	1.9045	0.2865
G - L7	24	1.8813	0.1334
H - L8	24	1.9018	0.1334
I - L9	20	1.9104	0.1171
J - L10	20	1.9092	0.1171
K - L11	25	1.9375	0.1373
L - L12	20	1.9438	0.1171

will increase, which could be used to allocate VU to other unbalanced installation connected to the same network. The IEC Technical Reports IEC 61000-3-13 and IEC 61000-3-14 address the impact of induction motor installations on VU emission allocation process by proposing an upstream to downstream VU transfer coefficient which is less than unity. In this section, a new approach based on the concept of influence factor which was defined in Chapter 4, is proposed.

In order to allocate the additional VU absorption capacity that exists due to the presence of induction motor installations, the VU emission allocation equation given in (5.7) can be modified to give (5.9):

$$E_{u:i-\text{effective}} = \gamma \cdot E_{u:i} \tag{5.9}$$

where; $E_{u:i-\text{effective}}$ is the effective VUF emission from the unbalanced installation considering the attenuation provided by the induction motor installation, γ is the influence factor as defined in Chapter 4 and $E_{u:i}$ is the VU emission limit for the installation and equals $k_u \cdot \sqrt[\alpha]{S_i}$. Considering the installation i and the induction motor installation only, γ can be calculated using the formulation given in Table 4.4 for radial distribution networks. Substituting $E_{u:i}$ in (5.2)-(5.4) with $E_{u:i-\text{effective}}$,

Table 5.6: Influence factors

Installation ID	β
L1	0.9136
L2	0.9689
L3	0.9790
L4	0.9689
L5	0.9775
L6	0.9803

and following the methodology as given in Section 5.2, the allocation constant for a radial distribution network can be calculated.

A case study was conducted by employing the test MV network given in Fig. 5.2, in order to estimate the additional VU emission allocation limits allowed for unbalanced installations when a large induction motor load is connected to the same network. The test MV network was modified by connecting a 2.3 kV/2250 hp induction motor installation through a 12.47/2.3 kV transformer at busbar A. The impedance of the 12.47/2.3 kV transformer and equivalent circuit parameters of the induction motor are given in Appendix A. Table 5.6 provides the influence factors that were estimated using the methodology given in Chapter 4, considering one installation at a time with the induction motor connected at busbar A.

Referring to Table 5.6, highest attenuation of VU can be observed when the induction motor installation and the unbalanced installation are connected to the same POC (i.e. busbar A).

In the VU emission allocation process, all installations were considered to be totally unbalanced ($U_f = 1$) and no allocation was made to the induction motor installation. The VU that propagates from the HV network to the MV network was calculated as, $VUF_{\mathrm{HV}} = T_{u:\mathrm{HV-LV}}.L_{u:\mathrm{HV}}$, with $T_{u:\mathrm{HV-LV}}$ equal to unity. This is necessary, as any effect that the inductor motor installation has on the VU levels in the network is now addressed using the influence factor. The VU emission limits for each installation were allocated using (5.9), and the allocation constant was calculated using the methodology given in Section 5.2. A comparison of the

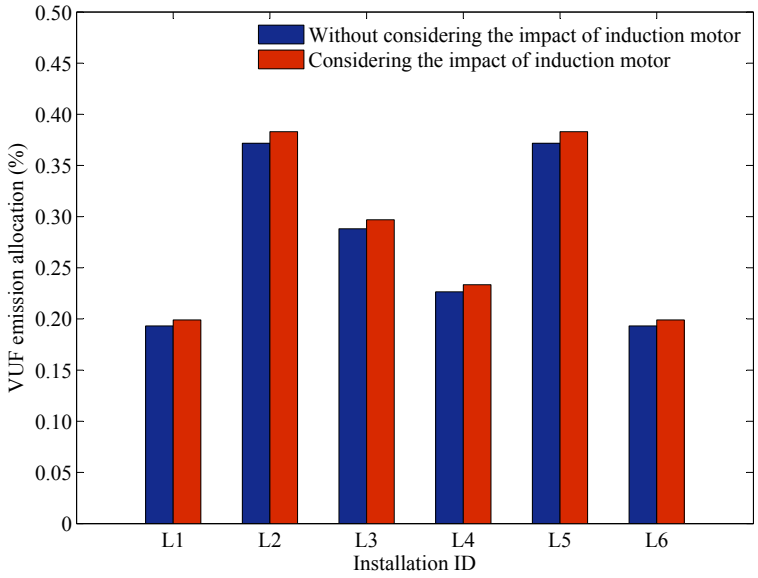

Figure 5.4: The increase in the VU emission limits in the presence of an induction motor

resulting VU emission limits for an unbalanced installation at each location with and without considering the attenuation of induction motor installation are given in Fig. 5.4. As expected, the allocation limits have sightly increased when induction motor installation is connected compared to the case without it.

5.4 Voltage Unbalance Emission Allocation Based on Voltage Droop Method

In this section, a general approach for VU emission allocation for customers connected to radial distribution networks is developed based on the concept of VD.

Consider an installation connected to an unloaded feeder at a point where the positive-sequence Thévenin impedance is $Z_{11:i}$. The positive-sequence VD, $U_{1,\text{droop}:i}$, at the POC of the installation can be given by (5.10):

$$U_{1,\text{droop}:i} = Z_{11:i} \cdot I_{1:Li} \tag{5.10}$$

where; $I_{1:Li}$ is the positive-sequence current drawn by the installation.

The agreed power of the load S_i in per-unit can be written in terms of sequence voltages and currents as (5.11):

$$\begin{aligned} S_i &= V_s^T \cdot I_s^* \\ &= U_{0:Li} \cdot I_{0:Li}^* + U_{1:Li} \cdot I_{1:Li}^* + U_{2:Li} \cdot I_{2:Li}^* \end{aligned} \tag{5.11}$$

where, $U_{0:Li}$, $U_{1:Li}$ and $U_{2:Li}$ are the zero-sequence, positive-sequence and negative-sequence voltages at the POC of the installation respectively. $I_{0:Li}$, $I_{1:Li}$ and $I_{2:Li}$ are the zero-sequence, positive-sequence and negative-sequence currents of the installation respectively.

For a 3-phase installations with no neutral, $I_{0:Li} = 0$ and $|U_{1:Li} \cdot I_{1:Li}| >> |U_{2:Li} \cdot I_{2:Li}|$. Hence, S_i in per-unit can be further simplified as (5.12):

$$S_i = U_{1:Li} \cdot I_{1:i}^* \tag{5.12}$$

Assuming $U_{1:Li} \approx 1$ pu, S_i can be written as (5.13):

$$S_i = I_{1,i} \tag{5.13}$$

Substituting (5.13) in (5.10), $U_{1,\text{droop:}i}$ can be written as (5.14):

$$U_{1,\text{droop:}i} = Z_{11:i} \cdot S_i \tag{5.14}$$

Initially, in order to develop the VU emission allocation methodology, the diversity among installations is neglected. Assuming that every installation is allocated a negative-sequence current emission proportional to its MVA capacity in per-unit, the negative-sequence current emission allocation, $E_{I_2:i}$, can be given by (5.15):

$$E_{I_2:i} = k_u \cdot S_i \tag{5.15}$$

where; k_u is identified as an allocation constant and S_i is the MVA capacity of the installation in per-unit.

Assuming that the distribution line is balanced, the negative-sequence voltage drop contribution of the installation, $U_{2:i}$ can be given by (5.16):

$$U_{2:i} = Z_{22:i} \cdot E_{I_2:i} \tag{5.16}$$

When the system impedance is mainly dominated by transformer and distribution line impedances, the negative-sequence Thévenin impedance $Z_{22:i}$ can be approximated by the positive-sequence Thévenin impedance $Z_{11:i}$. Hence, referring to (5.14) and (5.15), (5.16) can be re-written as (5.17):

$$\begin{aligned} U_{2:i} &= Z_{22:i} \cdot (k_u \cdot S_i) \\ &= Z_{11:i} \cdot (k_u \cdot S_i) \\ &= k_u \cdot (Z_{11:i} \cdot S_i) \\ &= k_u \cdot U_{1,\text{droop}:i} \end{aligned} \tag{5.17}$$

Therefore, according to (5.17), the negative-sequence voltage contribution of the installation to the network is equal to k_u times the load positive-sequence VD contribution.

When aggregated across all customers, the total negative-sequence voltage contributions of all loads, $\sum U_{2:i}$, becomes limited by k_u times the maximum network positive-sequence VD, $U_{1,\text{droop}}$. Hence, $\sum U_{2:i}$ can be written as (5.18):

$$\begin{aligned} \sum U_{2:i} &= k_u \cdot \sum U_{1,\text{droop}:i} \\ &= k_u \cdot U_{1,\text{droop}} \end{aligned} \tag{5.18}$$

where $U_{1,\text{droop}}$ is maximum positive-sequence VD of the power system.

In order to ensure that the maximum negative-sequence voltage at the extremity of the feeder is acceptable, the total contribution from all the loads to the negative-sequence voltage, $\sum U_{2:i}$, should be less than the planning level of the network (i.e. $\sum U_{2:i} \leq L_{u:\text{LV}}$). Hence, k_u can be evaluated as (5.19). Note that the planning levels are expressed in terms of VUF. However, VUF can be approximated by the per unit negative-sequence voltage $\frac{U_2}{U_n}$ [2, 5].

$$k_u \leq \frac{L_{u:\mathrm{LV}}}{U_{1,\mathrm{droop}}} \tag{5.19}$$

Once k_u is determined, the negative-sequence current emission allocation, $E_{I_2:i}$, in per-unit can be calculated using (5.15).

In order to consider the diversity among different loads, the negative-sequence current emission allocation in (5.15) can be modified as (5.20):

$$E_{I_2:i} = k_u \cdot \frac{S_i^{1/\alpha}}{Z_{11:i}^{1-1/\alpha}} \tag{5.20}$$

where; α is the general summation exponent for VU. Note that the positive-sequence Thévenin impedance at the POC of installation, $Z_{11:i}$, is mainly dependent on the transformer and line impedances at the considered voltage level (i.e. if the installation is connected to an MV network, $Z_{11:i}$ is mainly dependent on the HV/MV transformer impedance and MV line impedance) .

The corresponding negative-sequence voltage contribution of the load at the POC and at any point downstream of the network is given by (5.21):

$$U_{2:i} = Z_{22:i} \cdot E_{I_2:i} \tag{5.21}$$

Substituting (5.20) and (5.14) in (5.21), $U_{2:i}$ can be written as (5.22),

$$U_{2:i} = k_u \cdot U_{1,\mathrm{droop}:i}^{1/\alpha} \tag{5.22}$$

When aggregated across all loads, the negative-sequence voltage contribution of all loads connected to the network, $\sum U_{2:i}$, can be expressed using the general summation law as (5.23):

$$\sum U_{2:i} = k_u \cdot \left[\sum U_{1,\mathrm{droop}:i}^{\alpha}\right]^{1/\alpha} \tag{5.23}$$

Considering the fact that negative-sequence voltage contribution of all loads, $\sum U_{2:i}$, is limited to the VU planning level for the network, $L_{u:\mathrm{LV}}$, and positive-

sequence VD of all loads is limited to the maximum positive-sequence VD[5], $U_{1,\text{droop}}$, the allocation constant can be evaluated as (5.24):

$$k_u \leq \frac{L_{u:\text{LV}}}{U_{1,\text{droop}}^{1/\alpha}} \tag{5.24}$$

For typical Australian networks, system VD is observed to be 30% [14]. The same value can be used as the positive-sequence VD $U_{1,\text{droop}}$.

When an unbalanced installation is connected to a distribution network having asymmetrical distribution lines, VU can arise due to installation asymmetry as well as network asymmetry. Hence, when allocating an emission limit for the installation, the VU arising due to network asymmetry is required to be taken into account to ensure the compliance with network planning levels. The derivation of VU emission allocation methodology using the VD concept for distribution network with asymmetrical distribution lines is given in Appendix E.

In order to illustrate the application of the VU emission allocation method discussed here, two case studies were conducted employing the radial MV distribution network discussed in Case I of Section 5.2.1, and the radial LV distribution network discussed in Section 5.3. Assuming a positive-sequence VD of 30%, and an LV planning level of 2%, the allocation constant for the distribution network can be calculated for using (5.20) as 0.0473.

The negative-sequence current emission limit for each individual installation for the MV and LV network, which are calculated using (5.20), are given in Tables 5.7 and 5.8 respectively.

[5]The positive sequence voltage droops of the installations are assumed to be added, using the general summation law. Such an assumption can be justified, considering that the behaviour of installations are inherently random.

Table 5.7: Negative-sequence current allocation for installations connected to MV distribution network as a percentage of installation rated current

Installation ID	Negative-sequence current allocation (%)
L1	14.8563
L2	11.9869
L3	11.9328
L4	14.6122
L5	10.9775
L6	13.7606

Table 5.8: Negative-sequence current allocation for installations connected to LV distribution network as a percentage of installation rated current

Installation ID	Negative-sequence current allocation (%)
L1	12.9159
L2	6.4687
L3	7.5964
L4	9.5494
L5	6.7695
L6	6.8198
L7	10.4079
L8	9.3942
L9	9.1636
L10	8.4526
L11	6.8252
L12	6.8925

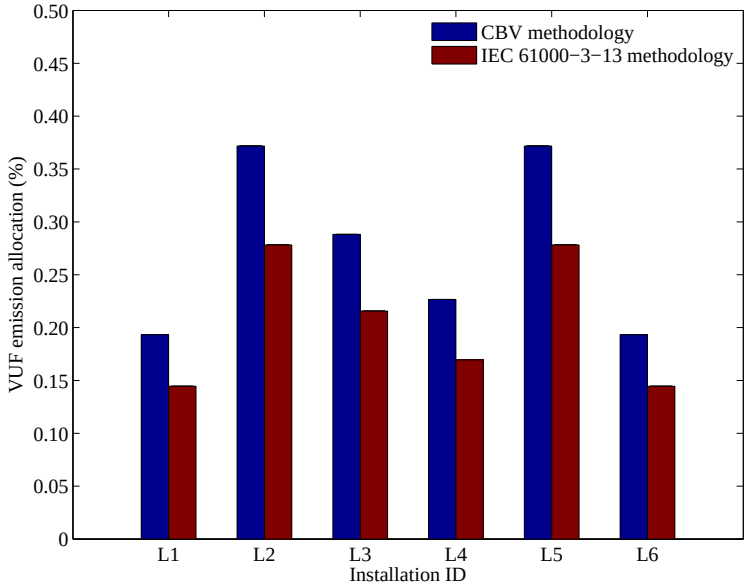

Figure 5.5: Comparison of VU emission limits based on the CBV and IEC 61000-3-13 methodologies for the test MV network

5.5 Comparison of Proposed VU Emission Allocation Methodology with Other Methodologies

The CBV and VD methodologies are proposed in this chapter as alternative VU emission allocation methodologies to the IEC VU emission allocation techniques. In order to compare the emission limits established by different approaches, consider the radial MV distribution network given in Fig. 5.2. The reader should note that the both CBV and IEC methodologies provide emission allocation in terms of VUF, whereas the VD approach provides VU emission limits in terms of negative-sequence currents.

Fig. 5.5 provides a comparison of the VU emission limits established using the IEC 61000-3-13 Stage 2 and CBV VU allocation methodologies for installations connected to the MV distribution network. In calculating the IEC 61000-3-13 Stage 2 VU emission allocations limits, the k_{uE} factor was assumed to be equal to unity considering the symmetrical distribution lines. The HV planning level, MV planning level and HV to MV VU transfer coefficient were selected according to Section 5.2.1.

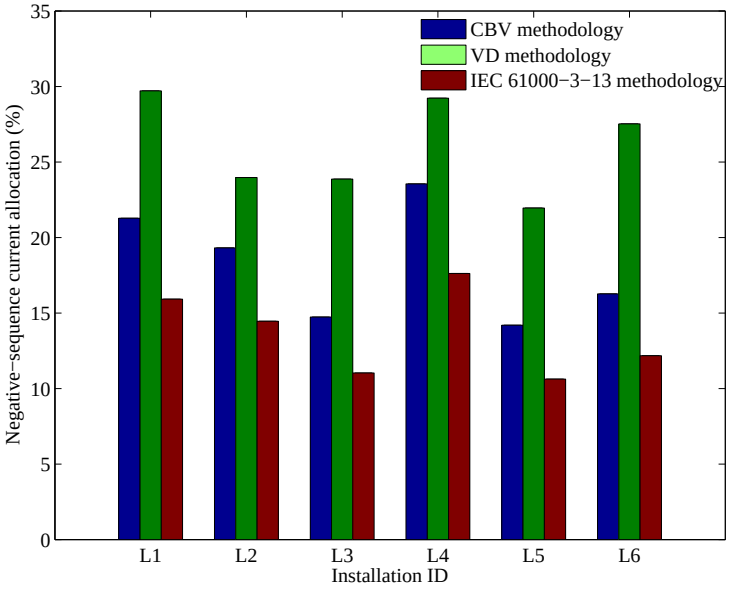

Figure 5.6: Comparison of negative-sequence current emission limits between the CBV, VD and IEC 61000-3-13 methodologies for the test MV network

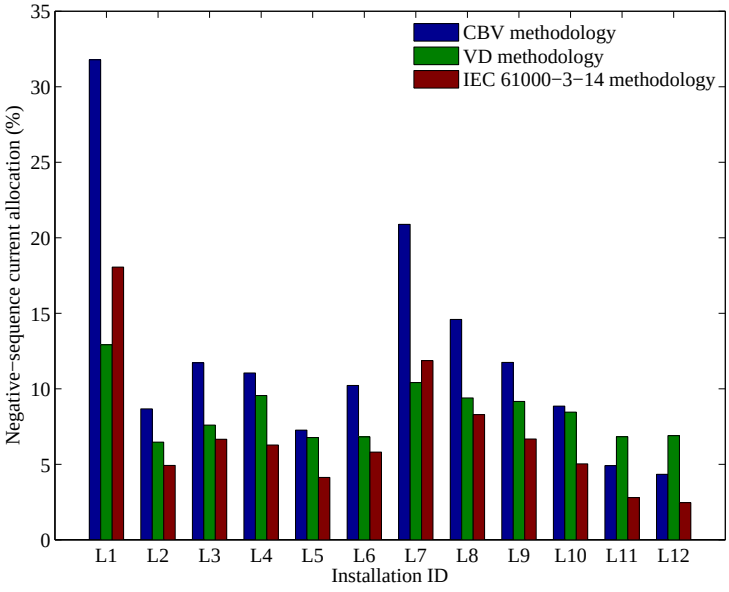

Figure 5.7: Comparison of negative-sequence current emission limits between the CBV, VD, and IEC 61000-3-14 methodologies for the test LV network

Referring to Fig. 5.5, VU emission allocation limits calculated using the CBV approach can be observed to be higher than those determined by IEC 61000-3-13 methodology.

Fig. 5.6 provides a comparison between the negative-sequence current emission limits established using IEC 61000-3-13, CBV, and VD methodologies respectively. The negative-sequence current emission limits proposed by the VD method are observed to be considerably high compared to CBV and IEC methodologies.

A similar comparison is made in relation to the LV distribution network of Fig. 5.3. For the IEC 61000-3-14 methodology, the reduction factor for the network under consideration was selected as unity, as all installations were considered as large installations. A comparison of negative-sequence currents established using the proposed methodologies and IEC 61000-3-14 is given in Fig. 5.7. Similar to the MV distribution network, the CBV methodology provides higher allocation limits compared to those using the IEC methodology. However, in contrast to the case of MV distribution network, the negative-sequence current emission limits established using VD method is less compared to the CBV methodology.

For comparison purposes, Tables 5.9 provides VUFs at the extremity of the network (which were calculated using (5.2)-(5.4) respectively) when each installation is injecting a VU emission limit as given by the aforementioned methodologies. An estimate of the unused VU absorption capacity as a percentage of maximum acceptable global contribution of VU at the MV level, $G_{u:\mathrm{MV+LV}}$, and LV level, $G_{u:\mathrm{LV}}$ (which are given by (4.2) and (4.4) respectively) is given in Table 5.10. The HV, MV and LV planning levels and HV to MV and MV to LV transfer coefficients considered in this comparison were as in Sections 5.2.1 and 5.3. Note that such assumptions are not valid for the VD methodology as its objective is to meet the compatibility level of the power system at the extremity of the network only, rather than meeting the planning level objectives at each voltage level.

Referring to Table 5.10, the CBV methodology can be observed to utilises the full

Table 5.9: VUF at the extremity of the radial feeder

	MV distribution network	LV distribution network
IEC methodology	1.6210%	1.8649%
CBV methodology	1.7500	2.0000
VD methodology	1.8526%	1.9342%

Table 5.10: Unused VU absorption capacity of the network as a percentage of of maximum acceptable global contribution to the MV level ($G_{u:\mathrm{MV+LV}}$) and LV level ($G_{u:\mathrm{LV}}$)

	MV distribution network	LV distribution network
IEC methodology	34.18%	29.58%
CBV methodology	0	0
VD methodology[6]	-37.54%	22.10%

VU absorption capacity of the network. In contrast, the emission limits established by the IEC 61000-3-13 and the IEC 61000-3-14 methodologies are conservative, leaving the VU emission absorption capacity of the network underutilised for MV and LV network respectively. As discussed previously, the attenuation of VU when propagating from downstream to upstream of the network has been taken in to account in the CBV approach, whereas such attenuations are disregards in the IEC methodologies. Therefore, IEC methodologies provide more conservative emission allocation limits compared to the CBV method, constraining the VU emission from unbalanced installations. In the case of the VD methodology, the VU emission level exceeds the selected planning level for the MV distribution network, but meets the compatibility level objective at the extremity of the network.

The three VU emission allocation methodologies discussed in this Chapter can vary in relation to the data requirements and ease of application. The Stage 2 VU emission allocation methodologies given in IEC Technical Reports IEC 61000-3-13 and IEC 61000-3-14 provide a flexible VU emission coordination process. However, the methodologies require computation of key coefficients such as k_{uE} factor, reduction factor and transfer coefficients, which is a non-trivial exercise. Such data requirements make the IEC methodologies less preferable, particularly for distribu-

[6]The minus signs indicate that contribution of VU to the LV level from all installations exceed G_{uMV+LV} and (G_{uLV}).

tion networks.

The CBV methodology overcomes such difficulties by estimating the net VU in the distribution network utilising readily available data such as short-circuit capacities at different points of the network. The main difficulty with the CBV methodology is that the POC and the MVA capacities of each installation are required to be known in advance. However, such difficulties can be overcome by intuitive, good engineering judgment and planning.

The VD approach is proposed as a less data and computation intensive alternative approach for VU coordination. The objective of the VD methodology is to meet the compatibility levels at the extremity of the network. Therefore, meeting the VU planning levels at each voltage level cannot be ensured. The main drawback of VD method is that it cannot be applied in relation to networks with large three-phase induction motor installations as the negative-sequence impedance of the network can vary from its positive-sequence impedance.

In relation to DG installations, both CBV and IEC methodologies can be modified to provide a VU emission limit as discussed in Sections 4.1 and 5.2. In VD method, VU emission limits are not provided for DG installations.

5.6 Chapter Summary

This chapter examined VU emission allocation methodologies for installations connected to MV and LV distribution networks. Similar to harmonic emission allocation as demonstrated in Chapter 3, the IEC VU emission allocation methodologies also lead to underutilisation of network VU absorption capacity.

In order to address such a discrepancy, a revised VU emission allocation methodology which was based on the concept of CBV was presented in this chapter. Based on the CBV methodology, the VU emission levels at network busbars are explicitly forced to be at the network planning levels, when all loads are injecting their pre-

scribed VU emission limits. Appropriate modifications were also proposed to the CBV methodology, in order to allocate VU in the presence of single and two-phase installations or induction motor loads.

In addition, a new VU emission allocation methodology based on the concept of VD was developed. The VD approach provides a simplistic and less computational and data intensive alternative methodology to both IEC and CBV methodologies.

Chapter 6

Characterisation of Flicker Emission and Propagation in Distribution Networks with Bi-directional Power Flows

6.1 Introduction

Voltage fluctuations leading to lamp flicker are a power quality concern for DNSPs [1]. The existing literature provides a comprehensive understanding on flicker propagation and attenuation in radial networks, essentially related to fluctuating loads where the active and reactive power flows are unidirectional, i.e upstream to downstream [83, 84, 130, 131]. Coordination of voltage fluctuations and flicker produced by fluctuating loads connected to MV and LV distribution networks are addressed in relevant standards and technical reports [2, 4]. However, the widespread integration of intermittent renewable energy generators (REGs) to the distribution network and resulting bi-directional power flows, could make the flicker coordination process in distribution networks difficult. Therefore, further investigations are required to understand flicker emission and propagation under such circumstances.

Existing studies on flicker emission and propagation due to REGs such as DFIG wind turbines are largely based on their unity power factor operation [87, 88, 93, 95–98, 132, 133]. Modern REGs such as DFIGs have reactive power capabilities [17] which enable them to operate in various control modes such as power factor control and voltage control operation. In the future, REGs may be required to operate under different control strategies in order to provide ancillary services such as reactive power support and system voltage control to the power network [134]. Only limited studies presently exist on the impact on flicker emission when REGs operating under such control strategies [104].

In addition, different loads connected to distribution networks can also influence flicker propagation and attenuation. Although flicker propagation and attenuation associated with induction motors have been well researched [135, 136], the flicker propagation and attenuation due to other load types such as constant power and constant current loads has not been adequately addressed. A comprehensive understanding of the flicker propagation and attenuation features associated with such loads can help in the effective planning and management of distribution networks which may have high levels of integrated REGs.

The main objective of the work presented in this chapter is to provide a comprehensive analysis on the impact of reactive power control strategies of REGs when they provide ancillary services to the network. In addition, the influence of different distribution system loads on flicker emission and propagation in radial distribution networks where there is bi-directional power flow is investigated. Mathematical models are developed and are verified using a simulation model of a wind farm in DIgSILENT PowerFactory software [17, 99, 100, 137].

The rest of this chapter is structured as follows: a theoretical analysis on the flicker emission and propagation under power factor control and voltage control modes of operation of a REG in general is given in Section 6.2. Section 6.3 presents a case study distribution system verifying the conclusions of Section 6.2. The response

of distribution system loads to voltage fluctuations; hence, flicker and its relationship with flicker emission of the REG is discussed in Section 6.4 through appropriate mathematical models. The simulation model of Section 6.3 is further extended in Section 6.5 to characterise the influence of distribution system loads on flicker emission and propagation. Conclusions are given in Section 6.6.

6.2 Dependency of Flicker Emission and Propagation on REG Control Strategies

In order to investigate the impact of a reactive power control strategy on flicker emission from a REG, a radial network model shown in Fig. 6.1 is considered.

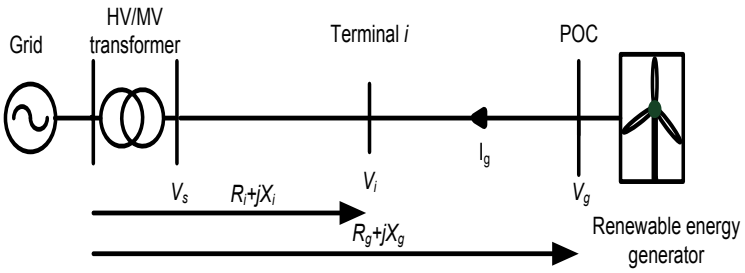

Figure 6.1: Renewable energy generator connected to a radial network

V_s, V_i and V_g denote the grid voltage, voltage at an intermediate terminal i and the voltage at the POC of the REG respectively. Due to the intermittent nature of the renewable energy sources, the active and reactive power output of the REG is considered to fluctuate, which leads to fluctuations in the POC voltage. The phasor representation of the voltage fluctuation at the POC is illustrated in Fig. 6.2. The convention used in the context of the chapter is as follows: when the REG is supplying both active and reactive power to the network at the POC, the REG is said to operate at a leading power factor (as shown in Fig. 6.2). When the REG is supplying active power while absorbing reactive power, the REG is said to operate at a lagging power factor.

Referring to Fig. 6.2, $V_{\text{pre:}g}$ and $V_{\text{post:}g}$ are the voltages at the POC of the gen-

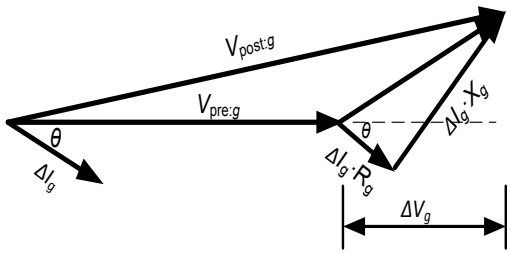

Figure 6.2: Phasor representation of the voltage fluctuation due to generator output power fluctuation [66]

erator pre- and post-power fluctuation, ΔI_g is the fluctuation in generator current, R_g and X_g are the Thévenin resistance and reactance at the POC of the REG, θ is the angle of generator real power fluctuation, ΔP, and reactive output power fluctuation, ΔQ, (i.e. $\arctan(\frac{\Delta Q}{\Delta P})$). The voltage fluctuation at the POC of the REG, ΔV_g, can be approximated by (6.1):

$$\Delta V_g \approx \Delta I_g \cdot (R_g \cdot \cos\theta + X_g \cdot \sin\theta) \tag{6.1}$$

The relative voltage fluctuation at the POC of the REG can be approximated in terms of ΔP and ΔQ as (6.2):

$$\left|\frac{\Delta V_g}{V_g}\right| \approx \left|\frac{\Delta P \cdot R_g + \Delta Q \cdot X_g}{V_g^2}\right| \tag{6.2}$$

Similarly, considering the intermediate terminal i in the radial distribution system given in Fig. 6.1, the relative voltage fluctuation, ΔV_i, due to changes in of active and reactive power outputs of the REG can be given by (6.3):

$$\left|\frac{\Delta V_i}{V_i}\right| \approx \left|\frac{\Delta P \cdot R_i + \Delta Q \cdot X_i}{V_i \cdot V_g}\right| \tag{6.3}$$

where; R_i and X_i are the Thévenin resistance and reactance at the i^{th} terminal of the network respectively.

Hence, the relative voltage fluctuation transfer coefficient between the POC and

intermediate terminal i, $T_{\Delta V:g-i}$ can be written as (6.4):

$$T_{\Delta V:g-i} \approx \frac{|\Delta V_i/V_i|}{|\Delta V_g/V_g|} = \left| \frac{\Delta P \cdot R_i + \Delta Q \cdot X_i}{\Delta P \cdot R_g + \Delta Q \cdot X_g} \cdot \frac{V_g}{V_i} \right| \tag{6.4}$$

Since the performance of the flickermeter is linear for voltage fluctuations of identical waveform shapes, the relative voltage fluctuations and relative voltage fluctuation transfer coefficient can be correlated to flicker and flicker transfer coefficient. Therefore, the flicker transfer coefficient from the POC of REG to terminal i of the network can be approximated by (6.4).

According to (6.2) and (6.4), flicker emission from the REG and flicker propagation to upstream of a radial network are dependent on active and reactive power fluctuations and network impedance. The active power fluctuations depend on the renewable energy source while the reactive power fluctuations depend on the control strategy of the REG.

The impact of (a) power factor control, (b) voltage control, and (c) reactive power dispatch of the REG on flicker emission and propagation are discussed in the following sections.

6.2.1 Power Factor Control Mode

Power factor control can be implemented in a REG, in which its operating power factor is maintained at a fixed value irrespective of output power fluctuations. Assuming an operating power factor of cos ϕ, where ϕ is the power factor angle, the fluctuation in real and reactive power will satisfy (6.5):

$$\Delta Q = \Delta P \cdot \tan\phi \tag{6.5}$$

By substituting (6.5) in (6.2), the relative voltage fluctuation at the POC of the

REG can be obtained as (6.6):

$$\left|\frac{\Delta V_g}{V_g}\right| \approx \left|\frac{\Delta P \cdot (R_g + \tan\phi \cdot X_g)}{V_g^2}\right| \tag{6.6}$$

Note that the angle of the REG output active and reactive power fluctuation θ in Fig. 6.2 is equal to the operating power factor angle ϕ of the REG in power factor operation mode, as the pre- and post-power fluctuation power factors of the REG are identical. Equation (6.6) can be further simplified to (6.7):

$$\left|\frac{\Delta V_g}{V_g}\right| \approx \frac{\Delta S}{S_{sc:g}} \cdot \cos(\varphi - \phi) \tag{6.7}$$

where; ΔS, $S_{sc:g}$, and φ are the VA output fluctuation of the REG, short-circuit capacity at the POC of the REG and the grid impedance angle ($\arctan(\frac{X_g}{R_g})$) as seen by the REG respectively. According to (6.7), the flicker emission by a REG is dependent on its operating power factor. If the operating power factor is maintained such that $\phi = -\pi/2 + \varphi$, the relative voltage fluctuation at the POC in (6.7) would be zero. This ideal observation results from the approximation made in the derivation of (6.1), however in practice, some flicker will exist. In unity power factor operation, the relative voltage fluctuation at the POC of the generator will only depend on the active power change, ΔP, and the grid resistance, R_g. Therefore, $|\frac{\Delta V_g}{V_g}|$ can be written as (6.8):

$$\left|\frac{\Delta V_g}{V_g}\right| \approx \frac{\Delta S}{S_{sc:g}} \cdot \cos(\varphi) \tag{6.8}$$

The relative voltage fluctuation at the intermediate terminal i in power factor operation mode is given by (6.9):

$$\left|\frac{\Delta V_i}{V_i}\right| \approx \left|\frac{\Delta P \cdot (R_i + \tan\phi \cdot X_i)}{V_i \cdot V_g}\right| \tag{6.9}$$

The flicker transfer coefficient between the POC of the REG and intermediate

terminal i can be written as (6.10):

$$T_{\Delta V:g-i} \approx \left| \frac{R_i + \tan(\phi) \cdot X_i}{R_g + \tan(\phi) \cdot X_g} \cdot \frac{V_g}{V_i} \right| \tag{6.10}$$

Assuming $V_i \approx V_g$, (6.10) can be approximated as (6.11):

$$T_{\Delta V:g-i} \approx \left| \frac{R_i + \tan(\phi) \cdot X_i}{R_g + \tan(\phi) \cdot X_g} \right| \tag{6.11}$$

According (6.11), flicker propagation from the POC of the REG to upstream of the network is dependent on the operating power factor of the REG. Note that in (6.11), a greater error will occur when applied for lagging power factor cases compared to leading power factor cases because of the cancellation which takes place in both the numerator and denominator of the RHS of (6.11).

6.2.2 Voltage Control Mode

A voltage control strategy associated with reactive power can also be employed in REGs for voltage stability improvement and network voltage profile management. In the voltage control mode, the relative voltage fluctuations at the POC ideally should be of zero magnitude. However, due to fast variations of the power levels associated with a REG, its voltage controller may not be capable of achieving zero relative voltage fluctuations; hence, leading to some flicker at the POC.

To achieve zero voltage fluctuation levels at the POC of the REG, the required theoretical level of ΔQ can be determined as given in (6.12):

$$\left| \frac{\Delta V_g}{V_g} \right| \approx \left| \frac{\Delta P \cdot R_g + \Delta Q \cdot X_g}{V_g^2} \right| \approx 0 \Rightarrow \Delta Q \approx \frac{-R_g}{X_g} \cdot \Delta P \tag{6.12}$$

Substituting (6.12) in (6.3), the relative voltage fluctuation at the intermediate terminal i of the network can be written as (6.13):

$$\left| \frac{\Delta V_i}{V_g} \right| \approx \left| \Delta P \cdot \frac{R_i - \frac{R_g}{X_g} \cdot X_i}{V_i \cdot V_g} \right| \tag{6.13}$$

According to (6.13) and referring to Fig. 6.1, there will be no voltage fluctuations at the POC when $R_i = R_g$ and $X_i = X_g$. As the location of interest (i.e. termincal i) moves away from the POC towards to the HV/MV transformer, the term $|R_i - \frac{R_g}{X_g} \cdot X_i|$ increases in magnitude up to a certain point along the feeder (e.g. transformer secondary) leading to increased flicker levels. Beyond that point (e.g. on the HV side of the transformer), the term $|R_i - \frac{R_g}{X_g} \cdot X_i|$ reduces to a smaller value, due to sudden reduction of X_i (e.g. transformer reactance). Hence, flicker levels would decrease to a relatively low value.

6.2.3 Reactive Power Dispatch Mode

In the reactive power dispatch mode, the REG will dispatch a fixed amount of reactive power, irrespective of active power fluctuations. Hence, the voltage fluctuations will be dependent only on active power fluctuations. This is similar to the unity power factor operation discussed in Section 6.2.1, because there are no reactive power fluctuations. Therefore, no further analysis is required.

6.3 Impact of Wind Farm Control Strategies on Flicker Emission and Propagation: Case Study

The flicker emission from a wind farm and the associated propagation of flicker to the upstream network, under varying wind conditions [17] is investigated using a network model as shown in Fig. 6.3. The wind farm consisting of 13, 1.5 MW DFIG generators connected to a 33 kV, 15 km long distribution line was modelled in DIgSILENT PowerFactory. The network and DFIG machine parameters are given in Appendix A. A wind profile with a mean wind speed of 7.5 m/s and turbulence intensity of 0.1 was used in the simulations. For a typical wind turbine, the cut in, cut out and rated wind speed are 3.5 m/s, 25 m/s and 12 m/s respectively [138]. The wind speed of 7.5 ms^{-1} was selected in the simulation considering the reactive power capabilities of the grid side and rotor side converters of the DFIG [17]. The

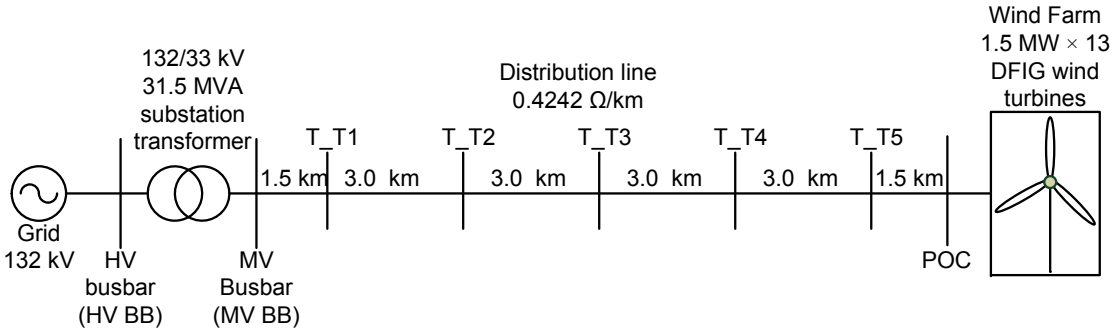

Figure 6.3: Single line diagram of the MV network

selected wind speed ensures that the reactive power capabilities of the DFIG are not exceeded under high wind gust situations, therefore, the wind farm can be operated under the investigated reactive power control strategies. The short-term flicker severity levels at the POC of the wind farm and at the intermediate terminals in the network T_T1 to T_T5, MV busbar and HV busbar were measured using the DIgSILENT PowerFactory flickermeter [139].

6.3.1 Power Factor Control Mode

Fig. 6.4 (a) and (b)[1] illustrate the flicker emission from the wind farm, when the wind farm is operating over a range of power factors considering the future requirements, where wind farms are required to provide reactive power support to the network. This operational requirement may occur due to the reduced number of synchronous generators in future networks. Flicker emission at unity power factor in which most of the existing wind farms are operated, is significantly less compared to leading power factor operation as shown from Fig 6.4 (a)-(b). Furthermore, according to Fig. 6.4 (a), dependency of flicker emission from the wind farm on the operating power factor and distribution line X/R ratio as suggested by (6.7) is evident. For a distribution line having a unity X/R ratio, the short-term flicker severity

[1]Fig. 6.4 (a) illustrates the flicker emission from the wind farm when the distribution line impedance was maintained constant at 0.4242 Ω/km, while the X/R ratio of the distribution line varies. Fig. 6.4 (b) illustrates the flicker emission from the wind farm when the distribution line impedance was maintained constant at $(0.3 + j0.3)$ Ω/km, while the short-circuit capacity of the HV distribution network varies.

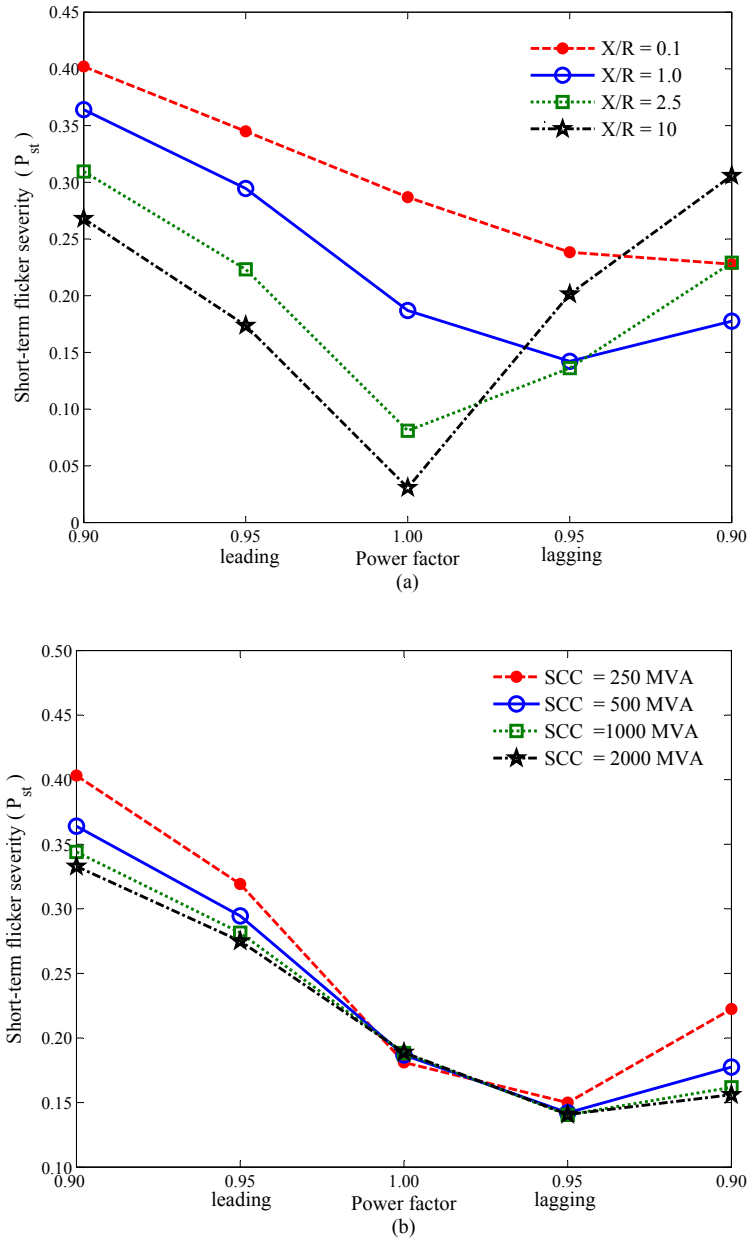

Figure 6.4: Short-term flicker severity at the POC of the wind farm for different power factors when, (a) distribution line X/R ratio varies; (b) short-circuit capacity of the HV grid varies;

reaches 0.36 when the wind farm is operating at 0.90 leading power factor. For the same line, the short-term flicker severity is 0.19 if operated at unity power factor, which further reduces to 0.14 at an operating power of 0.95 lagging. This characteristic can be explained referring to (6.6). For a leading power factor, the term $(\Delta P \cdot R_g)$ associated with real power fluctuations and the term $(\Delta P \cdot \tan(\phi) \cdot X_g)$ associated with reactive power fluctuations reinforce each other. On the contrary, for lagging power factors, the influence of active power fluctuations on voltage is counteracted by the voltage fluctuations associated with reactive power, thus reducing the resultant relative voltage fluctuations; hence, the flicker emission. According to (6.7), the voltage fluctuations caused by the active power fluctuations completely nullify the voltage fluctuations caused by the reactive power fluctuations when the operating power factor angle of the wind farm ϕ is equal to $-\pi/2 + \varphi$. Hence, the relative voltage fluctuations would be zero, thus giving rise to zero flicker. However, this is an ideal outcome that results from the approximation made in deriving (6.1). For a wind farm operating power factor of 0.90 lagging, the short-term flicker severity has increased from 0.14 to 0.18 which results from the dominance of the voltage fluctuations associated with reactive power fluctuations compared to the same corresponding to real power fluctuations (i.e. $\Delta P \cdot \tan(\phi) \cdot X_g > \Delta P \cdot R_g$).

Further observations can be made with respect to other distribution line X/R ratios from which it can be seen that the power factor at which the minimum flicker emission occur depends on the X/R ratio of the distribution line. Due to the gains and time delays associated with the DFIG control system, the instantaneous power factor of the wind farm can slightly vary from the fixed value. This aspect is not considered in the derivation of (6.7). Therefore, the power factor at which minimum flicker occurs will be slightly different from the theoretical value obtained from (6.7).

When the wind farm is operating at leading or unity power factors, flicker emission will decrease in relation to lines having higher X/R ratios. In contrast, at lagging power factors the flicker emission can be observed to increase with the distribution line X/R ratio. For instance, the short-term flicker levels are 0.30, 0.23 and

0.18 respectively for distribution lines with X/R ratios of 10, 2.5 and 1.0 when the wind farm is operating at a lagging power factor of 0.90. This characteristic is due to the increased dependency of voltage fluctuations on reactive power fluctuations interacting with line reactance.

Fig. 6.4 (b) illustrates that if the wind farm is connected to a weak HV grid, the flicker levels at the POC become marginally higher for a fixed power factor, compared to the case of a strong HV grid, resulting from the relatively higher grid impedance in the former case. Moreover, the HV grid impedance is mainly reactive. Therefore, short-term flicker severity levels do not appreciably change at unity power factor (because the voltage fluctuations are independent of line reactance at unity power factor) as the short-circuit capacity of the HV grid increases.

Fig. 6.5 (a) and (b) illustrate the flicker levels at different terminals of the network for various distribution line X/R ratios for a leading power factor of 0.95 and a lagging power factor of 0.95. For operation at the leading power factor, flicker levels decrease as the point of observation moves away from the POC of the wind farm towards the HV grid, irrespective of the distribution line X/R ratio, as expected. However, for operation at lagging power factor, flicker levels do not reduce as the point of observation gets closer to the HV grid. For instance, when the wind farm is operating at a lagging power factor of 0.95 with the distribution line having unity X/R ratio, slightly higher flicker levels can be observed at the MV busbar compared to downstream intermediate terminals. Minimum levels of flicker can be observed at the terminal T_T2. For lagging power factor operation, the voltage fluctuations at the terminal T_T2 due to active power fluctuations ($\Delta P \cdot R_i$) is counteracted by the voltage fluctuations due to reactive power fluctuations ($\Delta P \cdot \tan(\phi) \cdot X_i$) resulting in minimum flicker (according to (6.9)). However, at the MV busbar, the dependency of voltage fluctuations on reactive power fluctuations is greater than that due to active power fluctuations as $R_i < X_i$. Accordingly, the flicker levels at the MV busbar will be greater compared to that at terminal T_T2. In contrast,

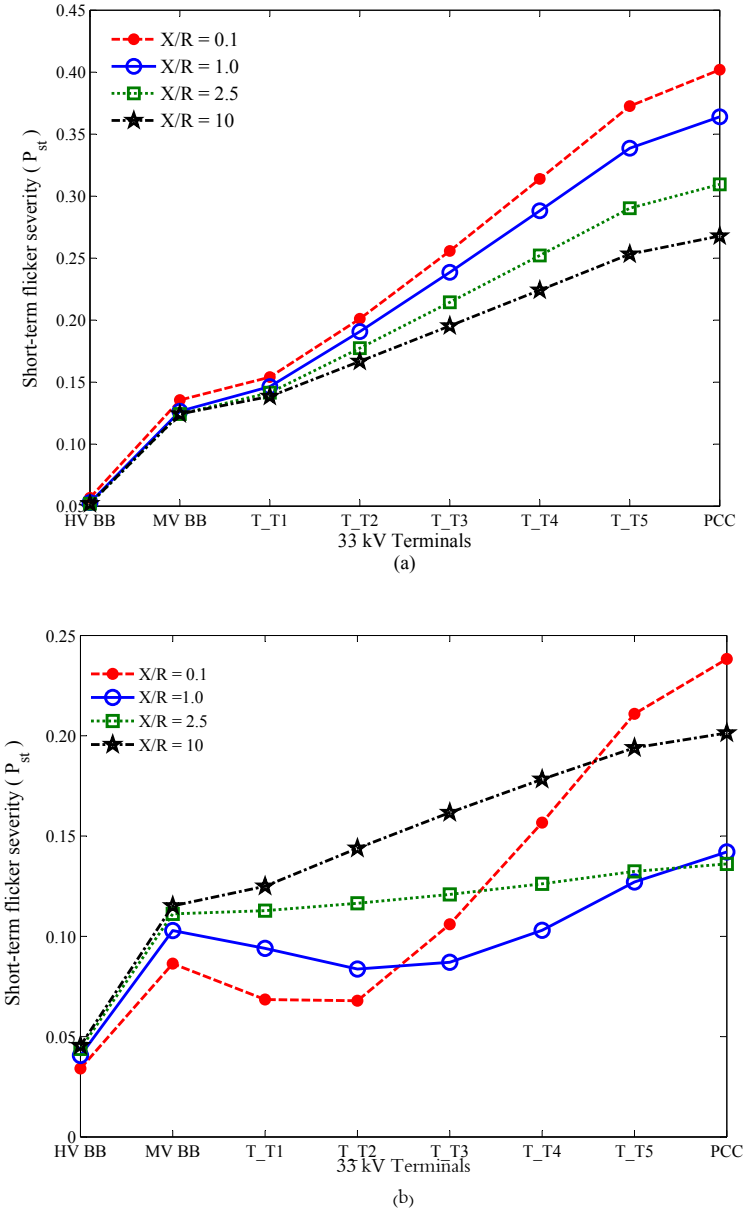

Figure 6.5: Short-term flicker severity at different terminals of the network when the wind farm is operating in a (a) leading power factor of 0.95; (b) lagging power factor of 0.95;

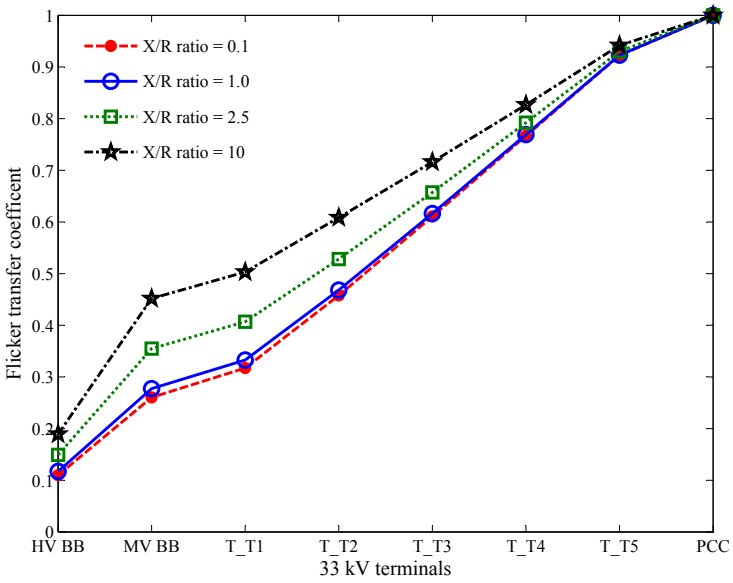

Figure 6.6: Comparison between the estimated values and simulation results of flicker transfer coefficient

with higher distribution line X/R ratios, the voltage fluctuations at intermediate points of the network are mainly dependent on reactive power fluctuations and the effective reactances at those points. Hence, flicker levels shows a gradual decrease, as the point of observation move towards the HV grid following the gradual decrease in effective reactance.

Fig. 6.6 provides a comparison of the flicker transfer coefficients estimated using (6.10) with the values obtained through simulations, for the wind farm operating with a distribution line having a unity X/R ratio. The estimated flicker transfer coefficients are marginally larger than those obtained from simulations for unity power factor operation where these coefficients are essentially governed only by the Thévenin resistance associated with the short-circuit capacity at the locations under consideration. This discrepancy arises as a result of the small amount of reactive power injection/absorption associated with the wind farm even at unity power factor operation (due to reactive power controller of the DFIG not being fast enough to respond to the active power fluctuations) thus affecting the flicker values.

6.3.2 Voltage Control Mode

Operation of the wind farm while maintaining a POC voltage of 1.05 p.u. is considered. According to Fig. 6.7 (a), higher flicker levels are observed at the POC of the wind farm when it is connected to a distribution line with a low X/R ratio. As an example, the flicker severity at the POC of the wind farm decreases from 0.08 to 0.04 when the distribution line X/R ratio changes from 0.1 to 2.5.

Fig 6.7(b) illustrates that the flicker emission from the wind farm (measured at the POC) has marginally increased for the HV grid with a greater short-circuit capacity. For instance, flicker level increased from 0.02 to 0.04 (although very small), when the short-circuit capacity of the HV grid increases from 250 MVA to 1000 MVA. The reason for this being that the HV grid will influence the reactive power fluctuations required to maintain the POC voltage at the reference value. For the considered case, the reactive power fluctuations associated with the wind farm to maintain the POC voltage are greater when the short-circuit capacity of the HV grid is 1000 MVA than in comparison to a short-circuit capacity of 250 MVA.

In addition, Fig. 6.7 (a) and (b) illustrate that the flicker level increases as the point of observation moves away from the POC of the wind farm towards the HV/MV transformer. The flicker level reaches a maximum value at the MV busbar and then decreases. This characteristic behaviour was explained in Section 6.2.2. As expected, the propagation of flicker to the upstream network significantly reduces when strong HV grids are utilised for the connection of wind farms as illustrated in Fig. 6.7 (b).

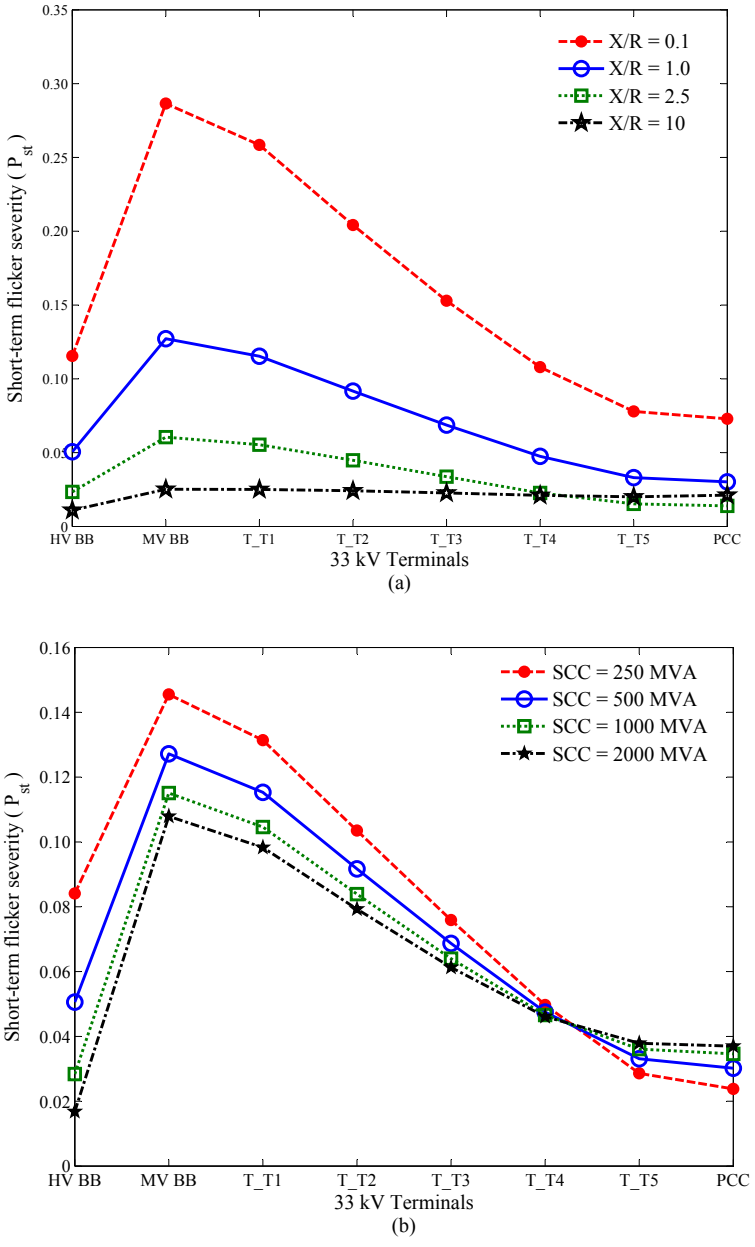

Figure 6.7: Short-term flicker severity at different terminals of the network when the wind farm is operating in voltage control mode when, (a) distribution line X/R ratio varies; (b) short-circuit capacity of the HV grid varies;

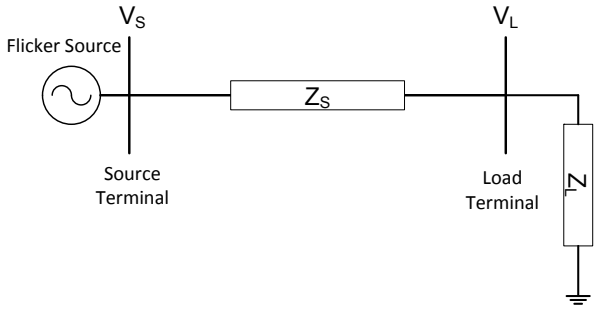

Figure 6.8: Radial power system

6.4 Dependency of Flicker Propagation on Distribution System Loads

6.4.1 Impact of Distribution System Load Types on Flicker Propagation

In radial power systems, the upstream to downstream flicker transfer is dependent on downstream load composition [83]. Consider a radial distribution network as shown in Fig. 6.8 where a distribution system load is connected to a fluctuating source by a network impedance. The voltage fluctuation transfer coefficient between the source and the load, $T_{\Delta \mathrm{V:S-L}}$, for the network can be expressed as (6.14) [83]:

$$T_{\Delta \mathrm{V:S-L}} \approx \frac{\left|\frac{\Delta V_L}{V_L}\right|}{\left|\frac{\Delta V_S}{V_S}\right|} = \frac{\left|1+\frac{Z_s}{Z_L}\right|}{\left|1+\frac{Z_s}{Z'_L}\right|} \tag{6.14}$$

where V_S and V_L are the magnitudes of the steady-state voltages at source and load terminals, ΔV_S and ΔV_L are voltage fluctuations at source and load terminals, Z_L is the steady-state impedance of the load, Z'_L is the dynamic impedance of the load to small voltage fluctuations and Z_S is the impedance of the supply system (i.e. sum of the steady-state impedances of the transformers and the distribution line). The dynamic impedance of an R-L type load (i.e. constant impedance load) is approximately equal to its steady-state impedance, whereas for an induction motor, the dynamic impedance is less than the steady-state impedance [83]. However, based on the load characteristics (i.e. constant power load, constant current load),

the dynamic impedance of a load can vary from its steady-state impedance value. In the following sections, the flicker attenuation characteristics of constant power (P), constant current (I), constant impedance (Z) and ZIP loads are briefly discussed.

Constant Power Loads (P)

Assume that a constant power load with an MVA capacity of $P_L + jQ_L$ is connected to a fluctuating voltage source via a line having an impedance of $R_S + jX_S$. The steady-state source voltage phasor ($\mathbf{V_S}$) and load voltage phasor ($\mathbf{V_L}$) can be given by (6.15):

$$\mathbf{V_S} = \mathbf{V_L} + (R_S + jX_S)\mathbf{I_L} \tag{6.15}$$

$$\mathbf{I_L} = (P_L - jQ_L)/\mathbf{V_L^*} \tag{6.16}$$

Now assume that $\mathbf{V_S}$ fluctuates by $\mathbf{\Delta V_S}$. Accordingly, the load voltage fluctuates by $\Delta\mathbf{V_L}$. Therefore,

$$\mathbf{V_S} + \mathbf{\Delta V_S} = \mathbf{V_L} + \mathbf{\Delta V_L} + (R_S + jX_S)\mathbf{I'_L} \tag{6.17}$$

$$\mathbf{I'_L} = (P_L - jQ_L)/(\mathbf{V_L} + \mathbf{\Delta V_L})^* \tag{6.18}$$

Take $\mathbf{V_L^*}$ as the reference, therefore, $\mathbf{V_L^*} = \mathbf{V_L} = V_L$. Assuming that $\mathbf{V_L}$, $\mathbf{V_S}$, $\Delta\mathbf{V_S}$ and $\Delta\mathbf{V_L}$ are in phase, ΔV_S can be written as (6.19):

$$\Delta V_S = \Delta V_L + Re((R_S + jX_S)\mathbf{\Delta I_L}) \tag{6.19}$$

where $\mathbf{\Delta I_L}$ can be written as (6.20):

$$\mathbf{\Delta I_L} = \mathbf{I_L} - \mathbf{I'_L} = \frac{P_L - jQ_L}{V_L} - \frac{P_L - jQ_L}{V_L + \Delta V_L} \tag{6.20}$$

Since $V_L \gg \Delta V_L$, $(V_L^2 + V_L \cdot \Delta V_L) \approx V_L^2$. Hence,

$$\mathbf{\Delta I_L} = (P_L - jQ_L)(\frac{-\Delta V_L}{V_L^2}) \tag{6.21}$$

Since ΔV_S and ΔV_L are assumed to being in-phase, (6.19) can be rewritten following the substitution of (6.21) as:

$$\left|\frac{\Delta V_L}{\Delta V_S}\right| = \left|\frac{1}{1 - \frac{P_L \cdot R_S + Q_L \cdot X_S}{V_L^2}}\right| \tag{6.22}$$

Furthermore, substituting (6.16) in (6.15) and rearranging (6.15) as:

$$\left|\frac{V_S}{V_L}\right| = \left|1 + \frac{P_L \cdot R_S + Q_L \cdot X_S}{V_L^2}\right| \tag{6.23}$$

Therefore, the relative voltage fluctuation coefficient can be written as (6.24):

$$T_{\Delta \mathrm{V:S-L}} = \frac{\left|\frac{\Delta V_L}{V_L}\right|}{\left|\frac{\Delta V_S}{V_S}\right|} = \left|\frac{1 + \frac{P_L \cdot R_S + Q_L \cdot X_S}{V_L^2}}{1 - \frac{P_L \cdot R_S + Q_L \cdot X_S}{V_L^2}}\right| \tag{6.24}$$

Examination of (6.24) indicates that $T_{\Delta \mathrm{V:S-L}} \geq 1$, for constant power loads with a lagging power factor. Hence, constant power loads will exacerbate the flicker levels at the load terminals when connected to a fluctuating upstream source via a network impedance.

Constant Current Loads (I)

Constant current loads will maintain the magnitude of the current constant, irrespective of the load terminal voltage. Thus,

$$\Delta V_L = \Delta V_S \tag{6.25}$$

Hence $T_{\Delta \mathrm{V_{S,L}}}$ can be written as (6.26):

$$T_{\Delta \mathrm{V:S-L}} = \left|1 + \frac{P_L \cdot R_S + Q_L \cdot X_S}{V_L^2}\right| \tag{6.26}$$

Referring to (6.26), $T_{\Delta \mathrm{V:S-L}} \geq 1$ for constant current loads with lagging power factor; hence, the upstream flicker levels will exacerbate at the load terminal as in the case of constant power loads.

Constant Impedance Loads (Z)

If a constant impedance load with an MVA capacity of $P_L + jQ_L$ is connected to the load terminal, the fluctuation of load current ΔI_L can be written as (6.27):

$$\Delta I_L \approx (P_L - jQ_L)\frac{\Delta V_L}{V_L^2} \tag{6.27}$$

Hence, $\Delta V_L/\Delta V_S$ can be written as (6.28):

$$\left|\frac{\Delta V_L}{\Delta V_S}\right| = \left|\frac{1}{1+\frac{P_L \cdot R_S + Q_L \cdot X_S}{V_L^2}}\right| \tag{6.28}$$

Therefore, considering (6.28) and (6.23), $T_{\Delta \mathrm{V:S-L}}$ can be found to be equal to unity. Therefore, the flicker levels at the load terminal will remain equal to that of the source terminal as expected.

ZIP Loads

Assume a mix of parallel connected constant power, constant current and constant impedance loads connected at the load busbar. In this case, $T_{\Delta \mathrm{V:S-L}}$ can be written as (6.29):

$$T_{\Delta \mathrm{V:S-L}} = \frac{\left|\frac{\Delta V_L}{V_L}\right|}{\left|\frac{\Delta V_S}{V_S}\right|} = \left|\frac{1+\frac{P_L \cdot R_S + Q_L \cdot X_S}{V_L^2}}{1-\frac{(K_1-K_3)\cdot(P_L \cdot R + Q_L \cdot X)}{V_L^2}}\right| \tag{6.29}$$

where K_1, K_2 and K_3 are ratios of capacity of constant power, constant current and constant impedance loads to the total capacity of the load respectively and $K_1 + K_2 + K_3 = 1$. The derivation of (6.29) is given in Appendix F. Therefore, upstream to downstream flicker propagation will depend on K_1, K_2 and K_3. Furthermore, when $K_1 = K_3$, flicker attenuation characteristics of a ZIP load will be similar to that of a constant current load.

Induction Motor Loads

The flicker attenuation characteristics of induction motors are well documented in [135,136] where the flicker transfer coefficient has been shown to be less than unity for

most modulation frequencies in a sinusoidally modulated flicker scenario. However, when the modulation frequency is extremely low, flicker levels at the source terminals can be magnified marginally [136].

6.4.2 Impact of Distribution Systems Loads on Flicker Emission from a REG

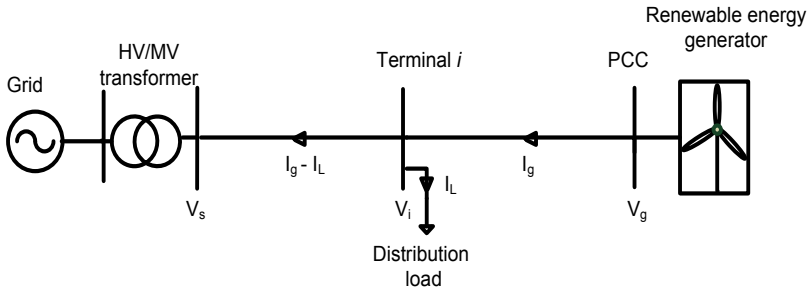

Figure 6.9: REG and distribution system load connected to a radial network

In order to examine the flicker emission and propagation associated with a REG in the presence of loads distributed along a feeder, consider the radial feeder given in Fig. 6.9. A distribution system load with a capacity of $P_L + jQ_L$ ($P_L < P_g$ and $Q_L < Q_g$, where P_g and Q_g are generator rated active power and reactive power output respectively) is connected to the intermediate terminal i in Fig. 6.9. If the operating power factor angle of the REG and load are ϕ_g and ϕ_L respectively, the steady-state voltage at the POC can be written as (6.30):

$$\begin{aligned} V_g \approx & V_s + I_g \cdot (R_g \cdot \cos\phi_g + X_g \cdot \sin\phi_g) \\ & - I_L \cdot (R_i \cdot \cos\phi_L + X_i \cdot \sin\phi_L) \end{aligned} \tag{6.30}$$

where I_L and I_g are steady-state load and generator currents. V_g and V_s are assumed to be in phase. Assuming that the operating power factor of the generator and load do not change, voltage fluctuation at the POC of the REG due to fluctuation of active power ΔP and reactive power ΔQ of the REG can be given by (6.31):

$$\begin{aligned}\Delta V_g \approx & \Delta I_g \cdot (R_g \cdot \cos\phi_g + X_g \cdot \sin\phi_g) \\ & - \Delta I_L \cdot (R_i \cdot \cos\phi_L + X_i \cdot \sin\phi_L)\end{aligned} \tag{6.31}$$

where; ΔI_L, ΔI_g are fluctuations of load current and generator current respectively. If the distribution system load is of constant current type, $\Delta I_L \approx 0$. Hence, the relative voltage fluctuation can be expressed in a simplified form taking ΔP and ΔQ into account given in (6.32):

$$\left|\frac{\Delta V_g}{V_g}\right| \approx \left|\frac{R_g \cdot \Delta P + X_g \cdot \Delta Q}{V_g^2}\right| \tag{6.32}$$

However, according to (6.30), the steady-state generator voltage will be less compared to the case where no distribution system loads are connected. Thus, the relative voltage fluctuation at the POC of the REG as given by (6.32) would be higher compared to that given by (6.2), leading to an increased flicker emissions when constant current loads are connected to the feeder. If the distribution system load is of the constant power type, ΔI_L will not be zero as $|\Delta V_i| \geq 0$. Therefore, according to (6.21) and (6.31), ΔV_g will be significant compared to the case of the constant current load; hence, flicker levels will exacerbate further when a constant power load is connected to i^{th} terminal. If the distribution system load is of constant impedance type, flicker level will be less in comparison to a constant current load (according to (6.31) and (6.27)), but will be higher compared to the case where there is no load connected to terminal i. Following a similar argument, the flicker level at the i^{th} terminal can be shown to increase when a load is connected to terminal i.

In voltage controlled operation of the REG, its reactive power output required to maintain the POC voltage at the reference value will vary when local distribution system loads are connected to the feeder. Therefore, the flicker emission of the REG will be affected. However, due to the closed loop control in voltage controlled operation, a general conclusion regarding the impact of distribution system load on

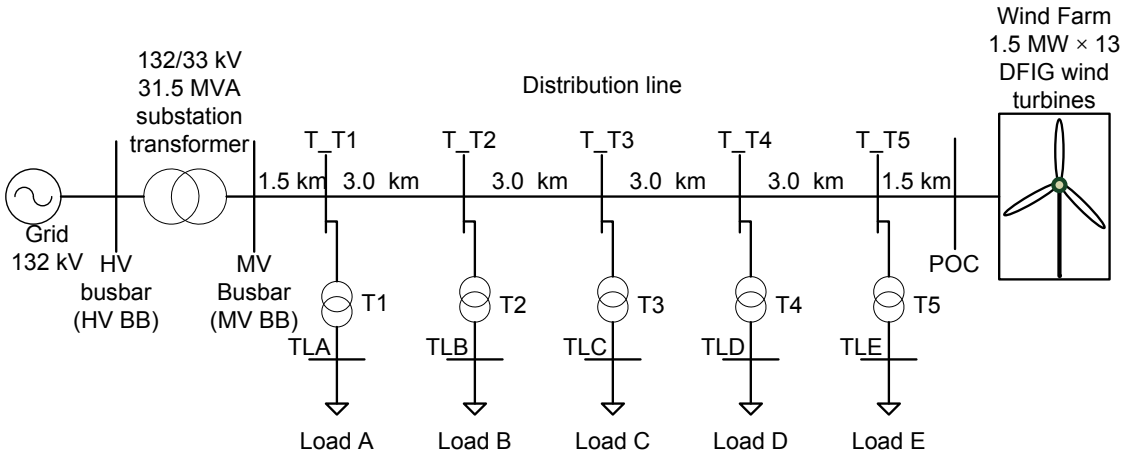

T1, T2, T3, T4, T5 - 33/11kV 10 MVA transformers

T_T1, T_T2, T_T3, T_T4, T_T5 – 33 kV terminals of T1, ..., T5 transformers respectively

TLA, TLB, TLC, TLD, TLE – 11 kV terminals of T1, ..., T5 transformers respectively

Figure 6.10: Single line diagram of the MV network with distribution system loads

flicker level cannot be made.

6.5 Impact of Distribution System Loads on Flicker Emission and Propagation in a Wind Farm

In order to demonstrate the impact of distribution system loads on flicker emission and propagation in a distribution network with REGs, the MV network of Fig. 6.3 was modified by connecting five 11 kV distribution system loads to intermediate terminals T_T1 to T_T5 using five 33/11 kV transformers as shown in Fig. 6.10. The HV network short-circuit capacity and the distribution line impedance was selected as 500 MVA and $(0.3 + \mathrm{j}0.3)\ \Omega$/km respectively.

Initially, the wind farm was set to operate with a leading power factor of 0.95 in order to maintain the voltage along the feeder within acceptable levels [140]. Flicker level at each busbar was obtained with various load types connected to intermediate terminals of Fig. 6.10. The following five scenarios were considered; (a) with no distribution system loads connected to the feeder, (b) constant power loads, (c) constant current loads, (d) constant impedance loads, (e) ZIP loads ($K_1 = K_2 =$

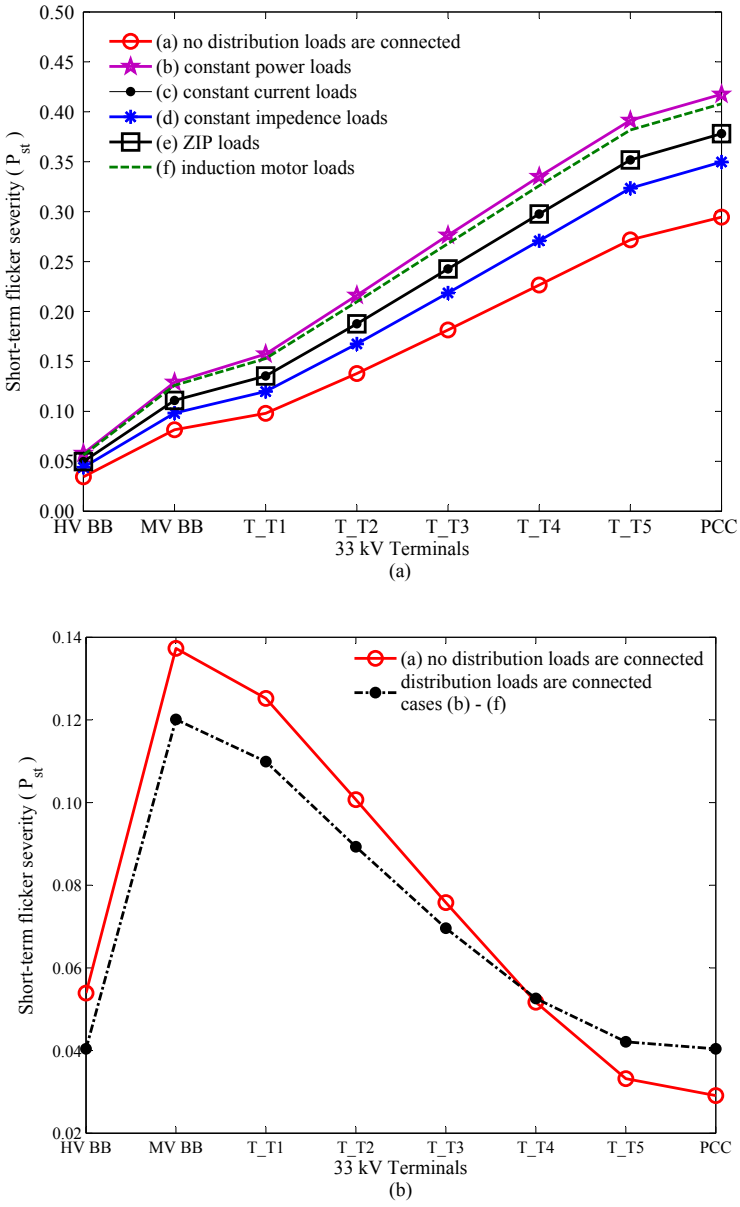

Figure 6.11: (a) Short-term flicker severity at different terminals when the wind farm is operating at a leading 0.95 power factor for cases (a) - (f); (b) Short-term flicker severity at different terminals when the wind farm is operating in voltage control mode for cases (a) - (f);

$K_3 = 33.33\%$), each with a capacity of 3.3 MW at 0.9 lagging power factor and, (f) induction motors rated at 3.3 MW at 0.9 lagging power factor. Both active and reactive power demands of the loads are greater than the wind power generation, hence, there will be active and reactive power flows from the HV grid. A similar study was conducted, when the wind farm was operating in voltage control mode with a reference voltage of 1.0 p.u.

Fig. 6.11 (a) illustrates that the flicker emission from the wind farm has exacerbated under power factor control operation when the distribution system loads are connected to the network for reasons explained in Section 6.4. Furthermore, the flicker levels at intermediate terminals have also increased. For instance, the flicker levels at all terminals show a 30-40% increase when constant power loads are connected to the distribution network. The highest flicker levels can be observed in the presence of constant power loads in the network followed by cases of the induction motor loads, constant current loads and constant impedance loads. When ZIP loads are connected to the feeder, flicker levels are observed to be equal to that of a constant current load as $K_1 = K_3$, reconfirming the conclusions in Section 6.4. Furthermore, in contrast to the common understanding that induction motors aid in attenuating flicker, flicker levels are seen to increase when induction motors are connected. This is due to the fact that voltage variations induced by the wind farm are of low modulation frequencies (generally less than 0.5 Hz), of which flicker is generally not attenuated by induction motors.

The flicker level for cases (a)-(f), when the wind farm is operating in voltage control mode is given in Fig. 6.11 (b). Flicker emission from the wind farm has slightly increased when the distribution system loads are connected to the feeder due to the increased reactive power requirement (hence, increased reactive power fluctuation) to maintain the POC voltage, compared to that of case (a). However, there is no distinguishable difference in flicker levels for cases (b)-(f). This is because, the voltage fluctuations arising at the POC and other terminals do not appreciably differ for cases (b)-(f).

In contrast to the power factor control mode of operation, the flicker levels at upstream terminals MV busbar, T_T1, and T_T2, have slightly reduced compared to the case when the wind farm is operating in voltage control operation. In both operation modes, there is a flow of the active and reactive power from the HV grid to the distribution network to cater for the deficiency between the load demand and wind power generation. Hence, the steady-state voltage at the upstream terminals (i.e. MV busbar, T_T1, T_T2) will be slightly higher compared to case (a). In power factor control mode, the voltage fluctuations due to power fluctuations will increase when distribution system loads are connected as explained in Section 6.4.2. Therefore, the relative voltage fluctuation, hence flicker, will increase when distribution system loads are connected, compared to that of case (a), irrespective of the increased steady-state voltages at the upstream terminals. However, compared to that of case (a), the relative voltage fluctuations have reduced in voltage control mode of operation, leading to less flicker at the MV busbar and T_, T1, T_T2 and T_T3 terminals, .

6.6 Chapter Summary

This chapter presented a detailed analysis on the impacts of reactive power control strategy of a REG and distribution system loads, in relation to flicker emission and propagation. The study developed mathematical models to exemplify the flicker emission and propagation which were verified through simulations. The flicker emission from REG, under power factor control operation would exacerbate when operating at both leading and lagging power factors depending on the grid impedance angle. The flicker propagation when a REG is operating at power factor control mode is also dependent on the operating power factor, and grid impedance angle at the point of interest. Furthermore, when the REG is operating in voltage control mode, flicker observed at the POC of the wind farm would be minimum, however, the flicker levels at upstream of the network would exacerbate. In the power factor

control mode, the connection of distribution system loads to the local feeder can influence flicker emission from the REG. However, in voltage control mode, the impact of the distribution system loads is largely negated by the closed loop controller of the REG. Although, the current research is mainly focused on wind energy generation, the general conclusions would be applicable to any fluctuating generating source connected to distribution feeders.

In the future, distributed generating sources may be required to provide increased ancillary services to the network. Therefore, existing flicker standards may need to be augmented to facilitate these services from distributed generators, and in this regard the outcome of this chapter can become applicable.

Chapter 7

Power Quality Emission and Propagation due to Small Scale Photovoltaic Systems

7.1 Introduction

As discussed in Chapter 2, the proliferation of DG systems in LV distribution networks can impact on the PQ [1]. The recently published IEC Technical Report IEC 61000-3-15 [10] focuses on proposing PQ emission limits for individual DGs up to 75 A per phase and providing guidelines on the assessment of PQ emission of such DGs under controlled conditions, in order to ascertain that DGs maintain adequate voltage quality in distribution networks in which they are connected. The PQ concerns addressed in [10] include low order harmonic emission, voltage fluctuations and flicker, DC injection, short and long duration over voltages and switching frequency harmonic emission. In the case of harmonics and flicker, the proposed emission limits and test procedures are mainly based on the corresponding equipment standards [6–9].

PV systems are the most common type of DGs that are connected to LV distribution networks. The increase in the penetration level of PV inverters (PVIs)

in a distribution network happens over time, resulting in connection of PVIs with various technologies that have different PQ characteristics. In spite of various field measurements and simulation work carried out in relation to PQ disturbance emission from PV systems [18–20], only limited research outcomes are available in the public domain [21] in which controlled experiments are carried out in a laboratory environment to investigate the PQ behaviour. The unavailability of realistic information in relation to PQ performance of different types of PVIs is a concern for DNSPs, in evaluating the impacts of PVIs on their distribution networks. Thus, the objective of the work presented in this chapter is to evaluate the PQ behaviour of PV systems in relation to harmonics and flicker emission by conducting PQ emission tests on PVIs in a laboratory, following the procedures detailed in the IEC Technical Report [10].

This chapter is organised as follows; Section 7.2 provides a general overview of the experimental setup used, which is based on the IEC Technical Report IEC 61000-3-15. The methodology, measurements and results of laboratory experiments carried out in relation to harmonic emission from PVIs are given in Section 7.3. Section 7.4 investigates the voltage fluctuations and flicker emission from PVIs under normal operation. The effects of varying irradiance on harmonics and flicker emission are investigated in Section 7.5. Section 7.6 examines the impacts of multiple PVIs on network harmonics and flicker levels by extending the experimental setup given in Section 7.2 to accommodate a model distribution feeder and two commercial inverters. Conclusions are given in Section 7.7.

7.2 Experimental Setup

The IEC Technical Report IEC 61000-3-15 [10] categorises all DGs into two main types as; DGs with rated current up to 16 A and DGs with rated current above 16 A and less than 75 A. The test setup and test conditions can vary based on the rated current of the DG. The general schematic of the test setup used in the

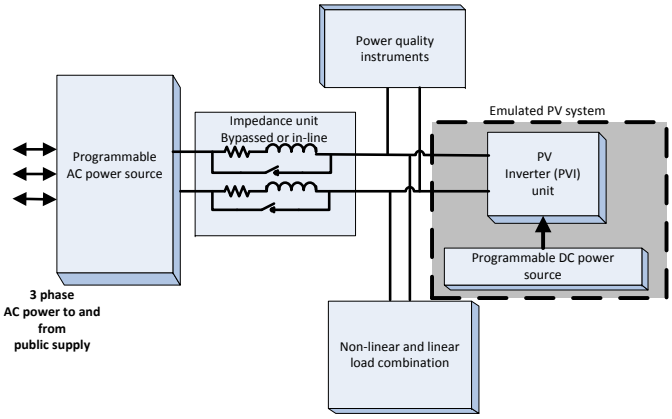

Figure 7.1: Experimental setup for PQ emission tests [10]

current research to evaluate the PQ emission from PV systems (i.e. PVIs) is given in Fig. 7.1.

The key components of the test setup are:

- AC power source - California Instrument MX30 programmable AC power source was used to emulate the public supply. The source is capable of absorbing active and reactive power supplied by the PVI and emulating various pre-distortion levels required for test conditions specified in [10],

- Programmable DC power source - The purpose of the DC source is to emulate the PV array which feeds power to the PVI under test. An AMATEK TerraSAS PV emulator ETS 1000/10 was used as the DC power source in the experimental setup. The PV emulator is capable of simulating the variation in power output of a PV array under varying irradiance and panel temperature conditions,

- Impedance unit[1] - The impedance network consisting of phase impedance of (0.15+j0.15) Ω and neutral impedance of (0.10+j0.10) Ω which can be in-line

[1]For all DGs with rated current up to 16 A, the test impedance proposed in [10] corresponds to the IEC 60725 reference impedance, which is (0.4+j0.25) Ω consisting of phase impedance of (0.24+j0.15) Ω and neutral impedance of (0.16+j0.10) Ω; whereas, for all DGs with rated current below 75 A (and above 16 A) the test impedance is (0.25+j0.25) Ω consisting of phase impedance of (0.15+j0.15) Ω and neutral impedance of (0.1+j0.1) Ω. However, due to the unavailability of the IEC 60725 reference impedance all test cases were conducted using the test impedance of (0.25+0.25j) Ω.

or by-passed was used in the test setup. When used in-line any non-linear current flowing to and from the PVI or load will cause voltage distortion on the inverter side of impedance,

- Linear and non-linear loads - Chroma programmable AC/DC electronic load (model number 63804) was used to simulate linear and non-linear loads,

- A Hioki PW3198 PQ analyser was used to record power quality data including the harmonic currents, harmonic voltages and flicker levels. In addition, an Agilent Technologies DS07034A four channel oscilloscope was used to capture current and voltage waveforms,

- Two commercial single-phase PVI units of which the details are given below were tested.

  - PVI 1 - 3600 W transformerless PVI operating at unity power factor, with nominal input DC voltage of 360 V and maximum input current of 10 A per array. A maximum of two solar arrays can be connected to the PVI[2].

  - PVI 2 - 2100 W transformer based PVI operating at unity power factor, with nominal input DC voltage of 200 V and maximum input current of 20 A.

7.3 Assessment of Harmonic Current Emission from a PVI

In order to verify that PV systems[3] do not significantly exacerbate either current or voltage distortion levels in a distribution network, the Technical Report IEC

[2]According the manufacturers' data, the PVI complies with limits established by IEC 61000-3-11 and IEC 61000-3-12. Hence, the PVI was considered to belong to the category of DGs with rated current above 16 A and below 75 A.

[3]In the context of this chapter, PV system refers to both the PVI and PV array. The harmonic emission from a PV system is mainly dependent on the characteristics of the PVI. However, the flicker emission can depend on the characteristics of the PVI as well as due to the fluctuations from power output from PV array (as a result of variations in incident irradiance levels).

61000-3-15 [10] proposes two different tests to be carried out on the PVI. In the first test, named the 'product test', PVIs are tested for harmonic current emission under simulated public supply network conditions [10]. The product test method utilises the test set up given in Fig. 7.1 with the impedance unit bypassed. If the PVI meets the stipulated emission limits in [10], the PV system is deemed to function properly in normal operation conditions.

The network in which the PV system is connected may not be ideal and have pre-existing voltage distortion levels; hence, the additional voltage distortion caused by the operation of PVI is required to be limited. In addition, the effects that high crest factor loads[4] such as TVs, computers and microwave ovens have on PVIs should be known. Therefore, a supplementary test named the 'system test' is proposed in [10] in which the increase in voltage THD due to the connection of a PVI is compared against a prescribed value. The system test method utilises the same experimental setup as in the product test with the impedance unit connected in-line with the test setup. Linear and non-linear loads are used to generate, the specified pre-existing distortion levels, which emulate actual conditions of the public supply networks.

In the following section, the aforementioned tests were conducted on the two PVIs introduced in Section 7.2 and the corresponding results are presented.

7.3.1 Harmonic Emission of PVIs Connected to a Simulated Public Supply - The Product Test

Each PVI was connected to the test setup as shown in Fig. 7.1 with the AC source voltage set to a nominal value of 230 V. Based on the PVI rated current, the corresponding pre-distortion levels as given by Clause 7.2.4 of [10] were introduced to the AC source voltage in-order to emulate the public power supply. As some PVIs with DC/AC current control will use open loop control for low power levels and closed loop control for high power levels [10] (which in turn affects their harmonic

[4]Crest factor is defined as the ratio of peak value to the RMS value of the current waveform.

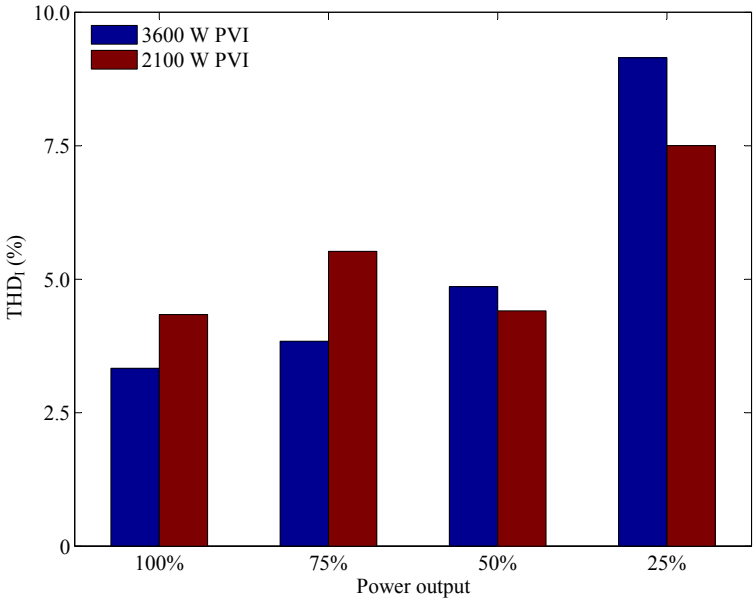

Figure 7.2: THD of current of each PVI for power outputs of 100%, 75%, 50% and 25% of its nominal power respectively

behaviour), each PVI was tested at 100%, 75%, 50% and 25% of their rated power by adjusting the irradiance and temperature input levels to the PV emulator (hence, the available output power of the PV emulator). The harmonic current emission of each PVI was recorded using the PQ analyser following the procedures specified in [6]. Fig. 7.2 illustrates the current THD[5] of each PVI for various power levels.

According to Fig. 7.2, the current THD of PVIs increase when they are operated at a substantially lower power level than the nominal power. In the case of the 3600 W PVI, the current THD increases from 3.33% to 9.15% when the power output of the PVI is reduced from 100% to 25% of its nominal power output respectively. However, for the 2100 W PVI, the current THD has slightly reduced when the power output is reduced from 75% to 50% but increased to 8.23% for 25% of power output. The increase in the current THD due to decreasing power output could also be attributed to a limitation in the inverter control as measurement resolution thresholds are approached at lower power levels [18], in addition to the changes in control methodology [10].

The harmonic current emission levels of both PVIs are given in Fig. 7.3. The

[5]Current THD is defined as a percentage of fundamental current output.

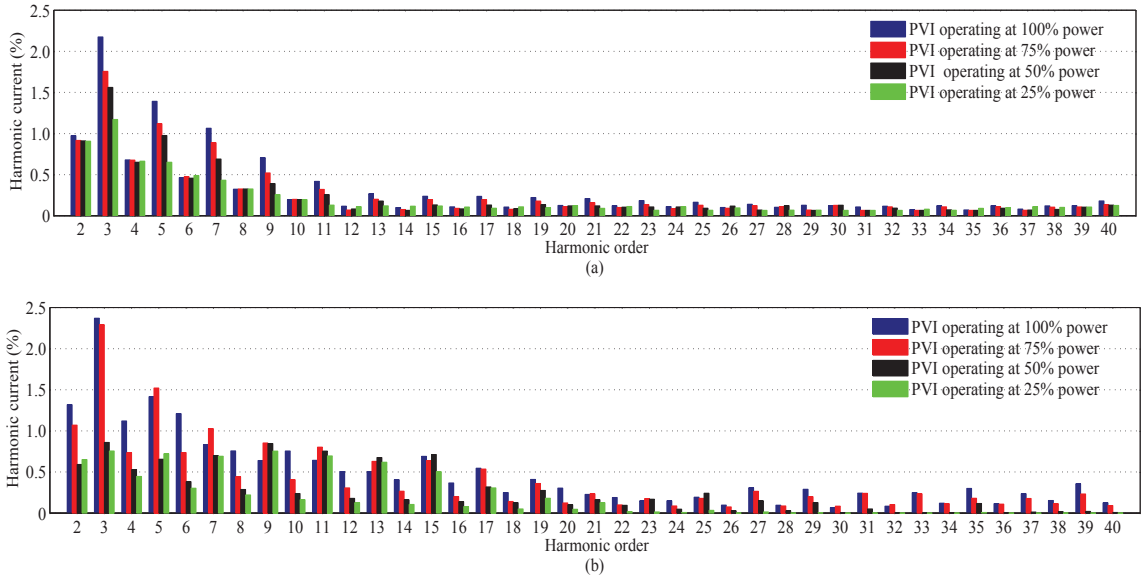

Figure 7.3: Harmonic current emission levels for power outputs of 100%, 75%, 50% and 25% of (a) 3600 W PVI (b) 2100 W PVI

levels given are derived as a percentage of the average RMS current of the PVI when each PVI is operating at 100% nominal power. Table 7.1 provides the proposed harmonic current emission limits for DGs with a VA capacity of greater than 600 W as given in [10]. With reference to Fig. 7.3, although the current THD of each PVI increases when the output power decreases, the harmonic current emission level in Amperes can be observed to decrease for most cases. In addition, the harmonic current emission of each PVI can be observed to comply with the odd harmonic current emission limits specified in Table 7.1. However, for the 2100 W PVI, the 2^{nd}, 4^{th} and 6^{th} harmonics are in excess of limits stipulated in Table 7.1.

Fig. 7.4 illustrates the harmonic phase angle variations for 3^{rd}, 5^{th}, 7^{th} and 9^{th} order harmonics for different output power levels of the 3600 W PVI. The corresponding harmonic phase angle diversity of each harmonic is observed to be small and is clustered around a particular phase angle irrespective of the variation of output power. Similar observations were made with respect to higher order odd harmonics and even order harmonics.

Table 7.1: Harmonic current emission limits for DGs up to 75 A/phase (in percent of I_{rms}) [10]

Harmonic order	Limit
2	1.0%
3	21.6%
5	10.7%
7	7.2%
9	3.8%
11	3.1%
13	2.0%
15-39 odd harmonics	1.0%
4-40 even harmonics	1.0%

7.3.2 Harmonic Emission of a PVI under Distorted Grid Conditions - The System Test

The system test utilises the same test setup discussed in Section 7.2 with the addition of an impedance network and additional linear and non-linear loads. Six test cases, as given by Table 7.2, were conducted on the two PVIs. Cases 2 to 6 are part of the system test specified by [10]. In Case 1, a linear load with an active power capacity equal to that of the PVI nominal power was connected to the AC source through the test impedance and the AC source was programmed to produce a pure sinusoidal waveform. The voltage THD in the load side of the test impedance was measured. Thereafter, the PVI operating at its rated power was connected to the load side of the test impedance and the increase in the voltage THD was recorded. Similar steps were followed for Cases 2 and 3, however, the AC source was programmed to produce a flat-top waveform and a peaky waveform (as specified by clause 7.5.2 [10]) with a voltage THD of 4%. For Cases 4 to 6, the AC source was programmed to produce a pure sinusoidal waveform, however, the voltage THD at the load side of the test impedance was set using linear and non-linear load combinations with active power capacities as given by Table 7.2. This combination replicates high crest factor loads commonly found in LV distribution networks [141]. The increment of the voltage THD at the load side of the impedance and the current THD of the PVI for all six cases for each PVI are given in Fig 7.5-(a) and 7.5-(b) respectively.

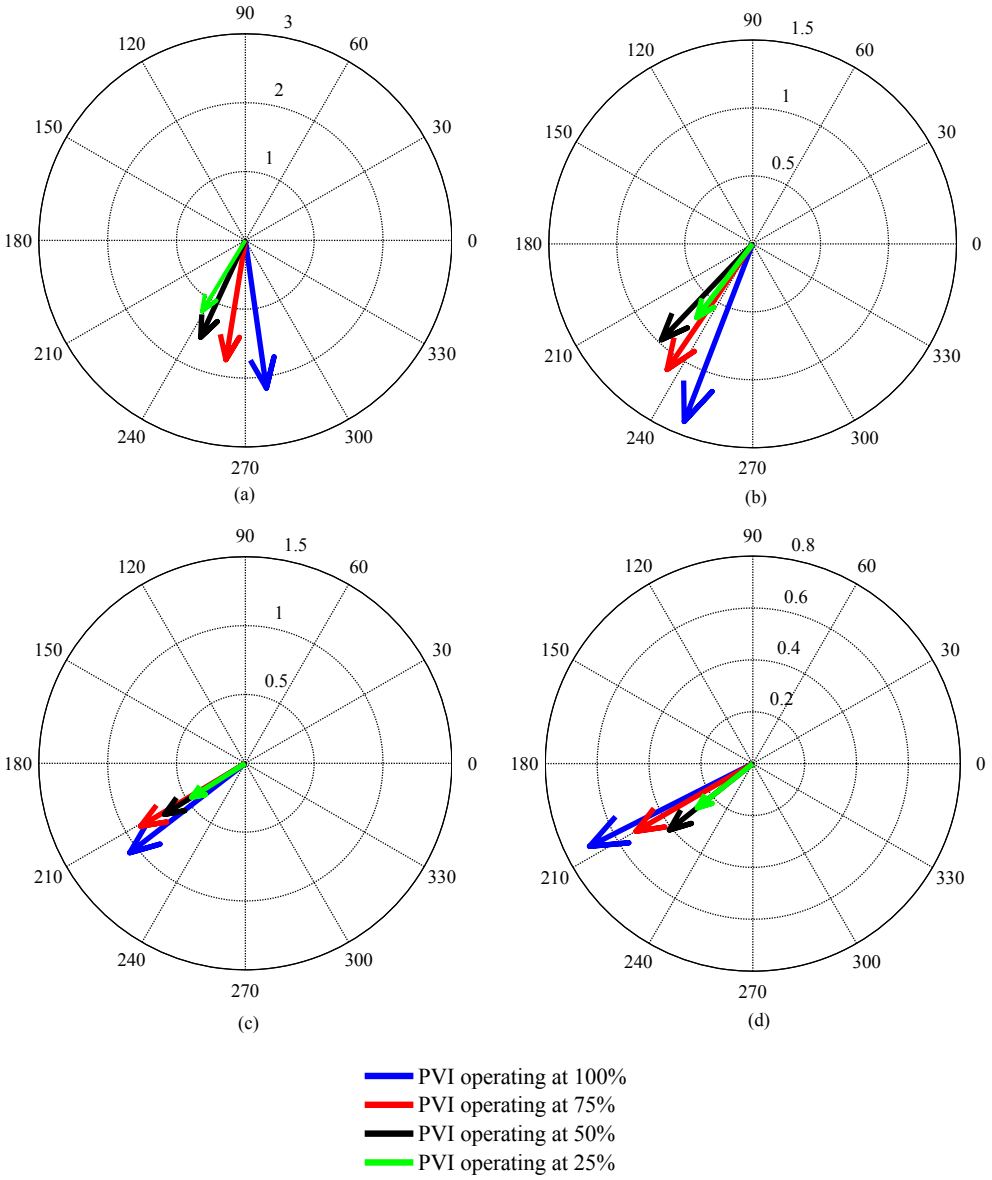

Figure 7.4: Phase angle diversity of (a) 3^{rd} (b) 5^{th} (c) 7^{th} (d) 9^{th} harmonic currents of 3600 W PVI for power outputs of 100%, 75%, 50% and 25% of its nominal power

If the voltage THD before the connection of the PVI is less than 5% and the increment of the voltage THD after the connection of the PVI is less than 1% absolute, the PVI is deemed to pass the system test (provided that they pass the product test) and is expected to function satisfactorily when connected to the actual distribution network [10]. According to the test results given in Fig. 7.5, the increment of the voltage THD is less than 1% for most cases, except in Case 5 for the 3600 W PVI where the increment of the voltage THD is 1.2%. The post-connection voltage THD

Table 7.2: Test cases for system test

Case	Load	DG Supply	Pre-distortion Limit
1	100% linear load	100%	pure sine wave
2	100% linear load	100%	4 ±0.2% set by the source
3	100% linear load	100%	4 ±0.2% set by the source
4	50% linear load 50% non-linear load	100%	4 ±0.2% set by the the loads
5	25% linear load 25% non-linear load	100%	2.5 ±0.2% set by the the loads
6	25% linear load 25% non-linear load	50%	4 ±0.2% set by the the loads

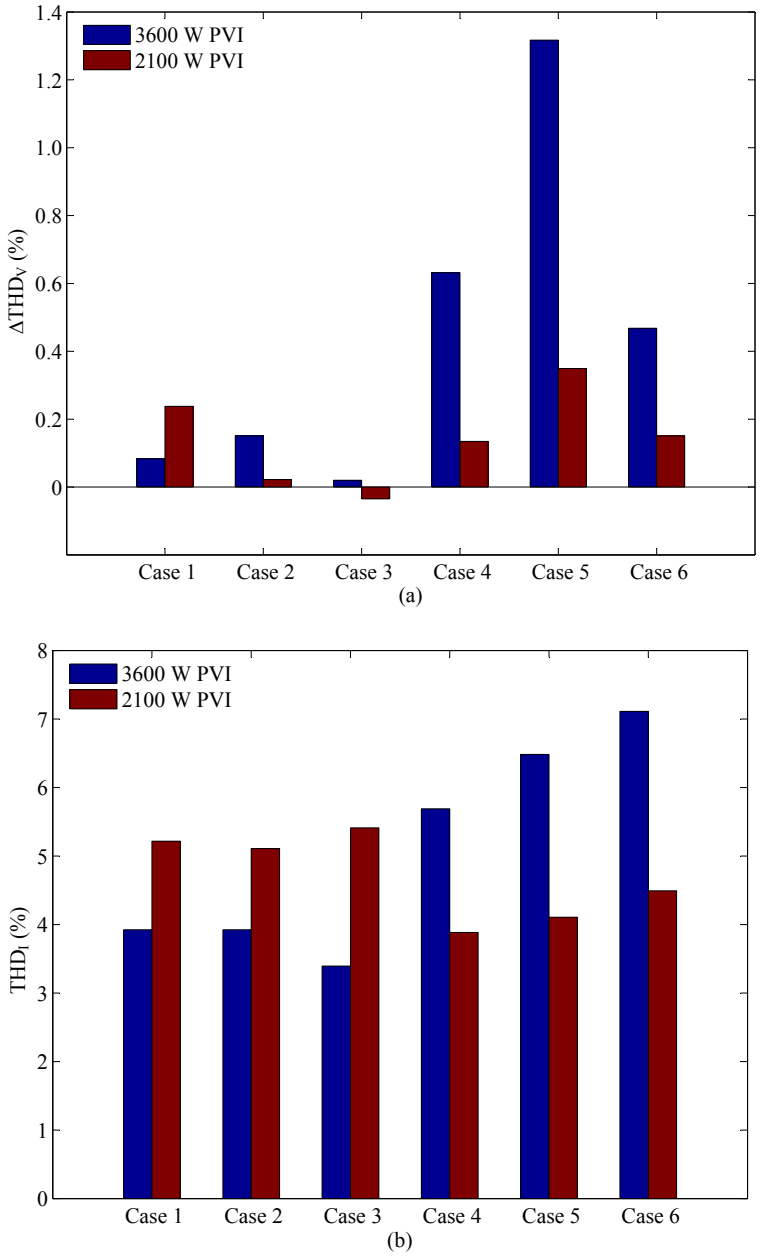

Figure 7.5: (a) Increase in the voltage THD for cases 1-6 (b) Current THD of the PVI for cases 1-6

can be observed to be less than the pre-connection voltage THD value for Case 3 of the 2100 W PVI[6]. Referring to Fig. 7.5, the current THD of the PVIs for Cases 1 to 3 show only a marginal variation. However, when the 3600 W PVI is connected together with a high crest factor load (replicated by the non-linear load), the current THD has increased. The opposite behaviour is observed in the case of the 2100 W PVI.

7.4 Voltage Fluctuations and Flicker Under Normal Operation

In this section, both PVIs were tested for their flicker emission using the test conditions specified by [10] and [8]. The short-term flicker severity index (P_{st}) was used as the metric for flicker emission. The experimental setup given in Section 7.2 was used, with a test impedance of $(0.25 + j0.25)\ \Omega$ connected between the AC source and the PVI. The source voltage was maintained at the nominal value of 230 V, frequency of 50 Hz, the THD of the supply voltage at 0.18% and a flicker value of P_{st} equals to 0.039, in-order to meet the requirements specified by [8].

A 10 minute test was performed on each PVI operating at 100%, 75%, 50% and 25% of their respective nominal power output levels and flicker emission in the inverter side of the impedance were recorded using an IEC flickermeter. Fig. 7.6 illustrates the half-cycle relative voltage change characteristics in the inverter side of the test impedance for a period of 0.2 s, when both PVIs are operating at the 100% power output. Note that the observations were made during the normal operation of the PVIs[7] (i.e. while the PVIs remain connected to the test network). During normal operation of the PVI, the irradiance and temperature inputs to the PV emulator were maintained at constant values. Hence, the output power of the emulated PV

[6]Note that the direct comparison of the increase in voltage THD should not be made with the prescribed value in [10] in the case of 2100 W PVI, as the proposed test impedance value in [10] is different to the test impedance used in the experiment

[7]This is in contrast to the switching operations, where PVIs are switched on and off. The switching operation of a PVI will affect the flicker reading.

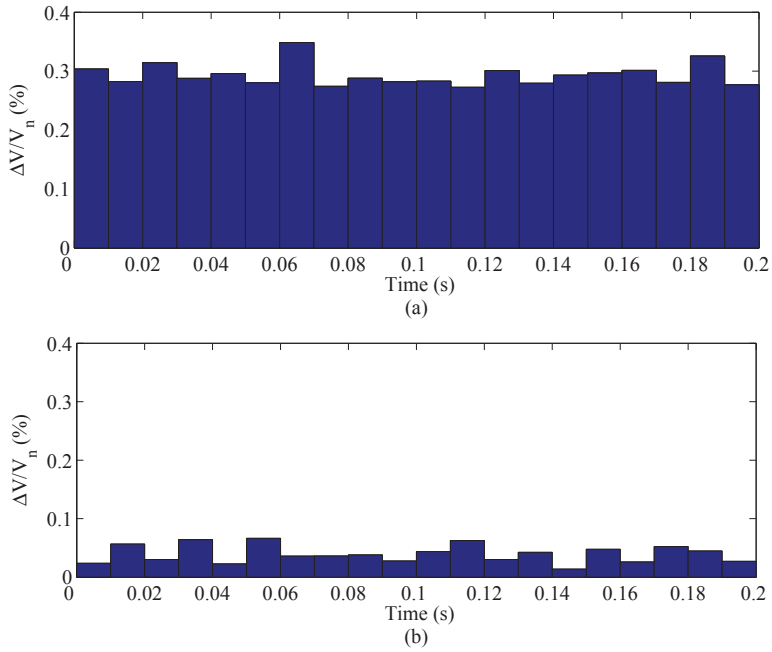

Figure 7.6: Relative voltage change characteristics on the inverter side of the impedance for (a) 3600 W PVI, (b) 2100 W PVI

array was held at a constant value. Referring to Fig. 7.6, the magnitudes of relative voltage fluctuations exhibited by the 3600 W PVI are relatively greater than that of the 2100 W PVI. A possible reason for the voltage fluctuations measured could be the effect of PVI control functions, including the maximum power point tracking operation.

Fig. 7.7 illustrates the increase in the flicker emission levels of each PVI for output power levels of 100%, 75%, 50% and 25% respectively. The results presented in Fig. 7.7 have been rescaled for the reference impedance value in the case of 2100 W PVI as specified by [9]. The flicker emission from the 3600 W PVI is greater compared to the 2100 W PVI. Furthermore, the flicker emission can be observed to reduce with the output power of each PVI. According to the limits stipulated by [10], if the increase in the flicker measurements is less than 0.5, PVIs are expected to function satisfactorily when connected to the actual distribution network. Accordingly, the flicker emission from each PVI given in Fig. 7.7 can be observed to be insignificant, compared to the limits established by [10].

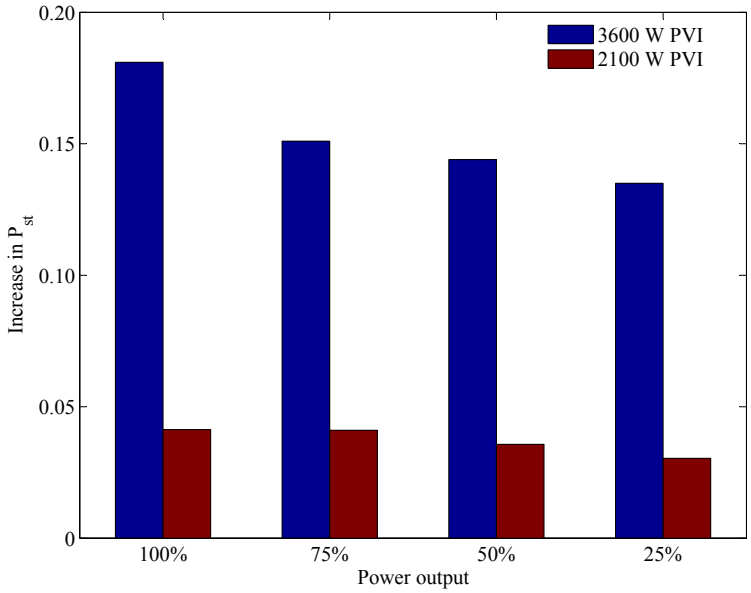

Figure 7.7: Flicker emission from PVIs when operating at 100%, 75%, 50% and 25% of their nominal power

7.5 Power Quality Assessment of PVIs Under Varying Irradiance and Temperature

PV arrays are subjected to a range of conditions including dynamic irradiance and panel temperature during their operation. These variations could affect the PQ performance of PVIs to which they are connected. In this section, the PQ performance of the two PVIs introduced in Section 7.2 were analysed when PV arrays connected to the PVIs were subjected to fluctuating irradiance levels and panel temperature conditions, using the test setup of Section 7.2. Two cases were considered; in the first case, the PV emulator was programmed to emulate the output of a PV array when subjected to a fluctuating irradiance pattern associated with a four hour time window of a heavy cloudy day as given in Fig. 7.8. In the second case, the irradiance pattern associated with a sunny day as given by Fig. 7.8 was considered. The fluctuation of panel temperature is also considered in each test case. For brevity, only the outcomes associated with the 3600 W PVI are presented. The associated active power output of the PVI, the voltage at the inverter side of

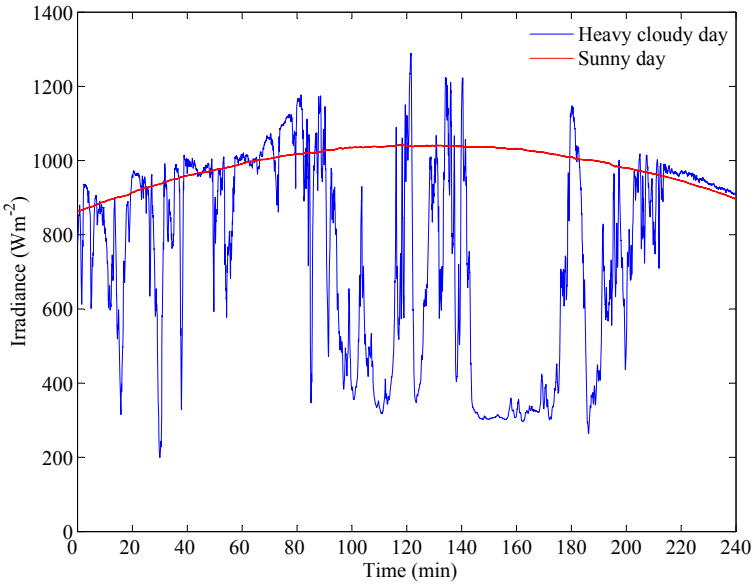

Figure 7.8: Fluctuation of incident irradiance of a PV array during a heavy cloudy day and a sunny day during a four hour window

the impedance unit, the current THD of the PVI, for the four hour time window corresponding to heavy cloudy day and sunny day are given in Fig. 7.9 (a), Fig. 7.9 (b) and Fig. 7.10 respectively.

According to Fig. 7.8 and Fig. 7.9, the output power of the PVI can be seen to correlate well with the incident irradiation levels on the PV array for both test cases. An approximate linear relationship between the power output and irradiance was observed, which is only slightly affected by the panel temperature. The voltage fluctuations on the PVI side of the test impedance are observed to follow the variation of the PVI output power. As presented in Section 7.3.1, the current THD of the PVI was observed to increase under low irradiance conditions.

Fig. 7.11 illustrates the flicker emission levels of the 3600 W and 2100 W PVIs for a four hour time window during a heavy cloudy day and a sunny day. The flicker emission levels are observed to be relatively insignificant. Flicker levels for both cloudy and sunny days can be observed to be higher in the case of 3600 W PVI, compared to that of the 2100 W PVI. For the 3600 W PVI, the flicker emission during the cloudy day and sunny day show only a negligible difference, whereas for the 2100 W PVI, the flicker emission levels during the cloudy day are higher than the

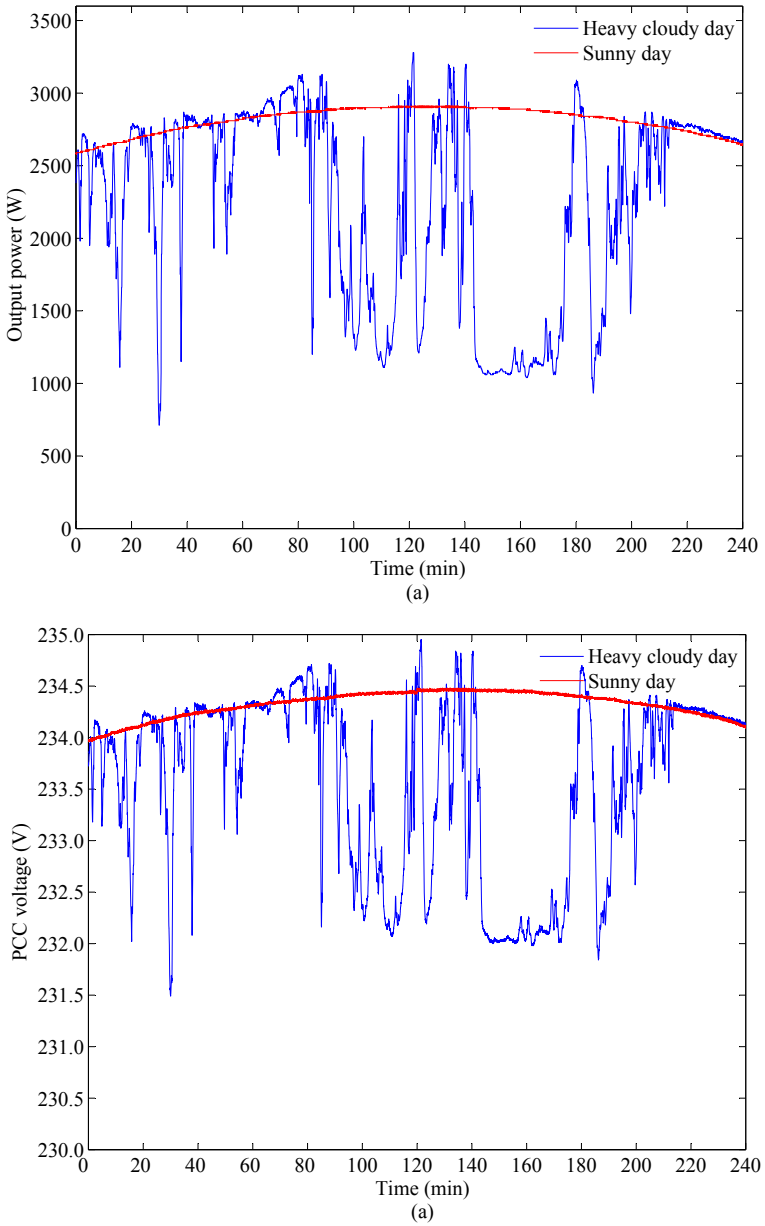

Figure 7.9: (a) Power output fluctuations of the 3600 W PVI during a heavy cloudy day and a sunny day, (b) Voltage fluctuations in the inverter side of the impedance of the 3600 W PVI during a heavy cloudy day and a sunny day

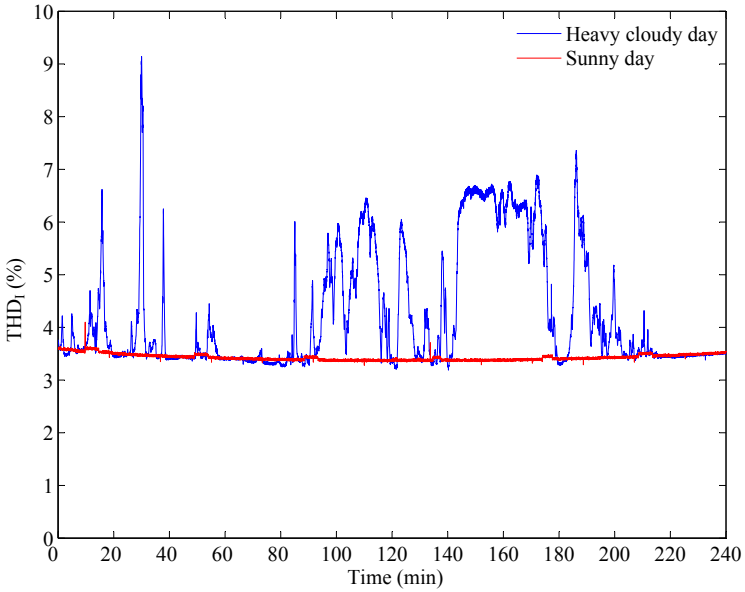

Figure 7.10: Variation of the current THD of the 3600 W PVI during a heavy cloudy day and a sunny day

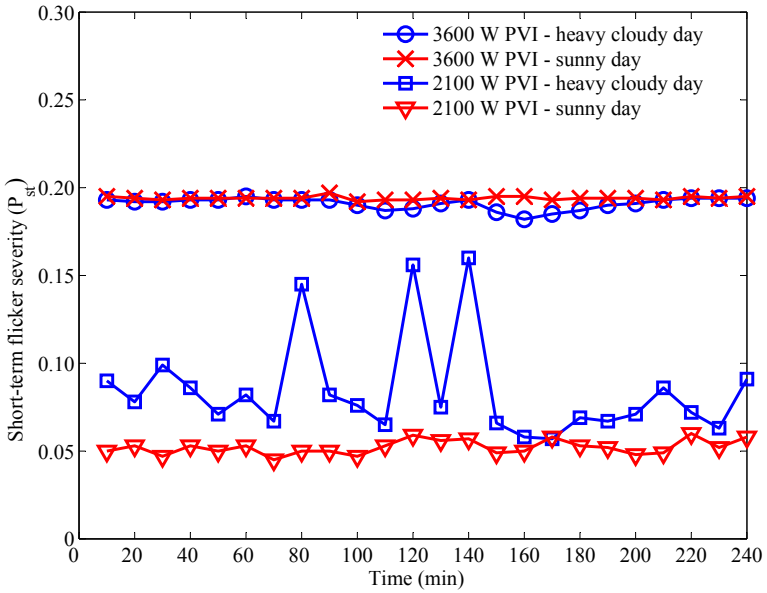

Figure 7.11: Flicker emission of the 3600 W and 2100 W PVI during a heavy cloudy day and a sunny day

flicker emission from the same PVI during a sunny day. Accordingly, the influence of the internal controls on flicker emission levels are predominant in the case of the 3600 W, whereas the flicker emission from the 2100 W PVI is more susceptible to the changes in the incident irradiation on the PV array.

7.6 PQ Disturbance Emission from Multiple PVIs

Even though a single PV system can comply with the prescribed PQ disturbance emission limits, a possibility exists that when multiple systems are operating simultaneously, the network PQ disturbance levels may exceed the planning levels for the network. Hence, PQ behaviour of multiple PV systems needs to be investigated. In this section, the PQ disturbance emission from two PV systems connected to a model distribution network is investigated. Two cases are considered.

1. Two PVIs are connected to two different POCs (refer to Fig. 7.12 (a)).
2. Both PVIs are connected to the same POC at the end of the modelled feeder (refer to Fig. 7.12 (b))

Two identical, 2600 W, commercially available PVIs were selected for the experiments, as such a combination is expected to produce most undesirable PQ levels, due to their similar characteristics (such as harmonic current magnitudes and phase angles). The two PVIs were connected to the modelled distribution feeder as given in Fig. 7.12 (a) and (b). In the model feeder each impedance segment corresponds to $(0.120 + j0.083)\ \Omega$ respectively[8]. Hence, the total impedance between the source and the first PVI (total of phase and neutral impedances) and total impedance between the source and second PVI are $(0.235 + j0.166)\ \Omega$ and $(0.470 + j0.322)\ \Omega$ respectively. Thus, the first PVI can be considered as connected to a strong POC (in-terms of short-circuit power) and the second PVI is connected to a weak POC. In the second experimental setup illustrated in Fig. 7.12 (b), the total impedance

[8]The impedance values were selected based on the reference impedance given in IEC 60725 and availability of components in the laboratory.

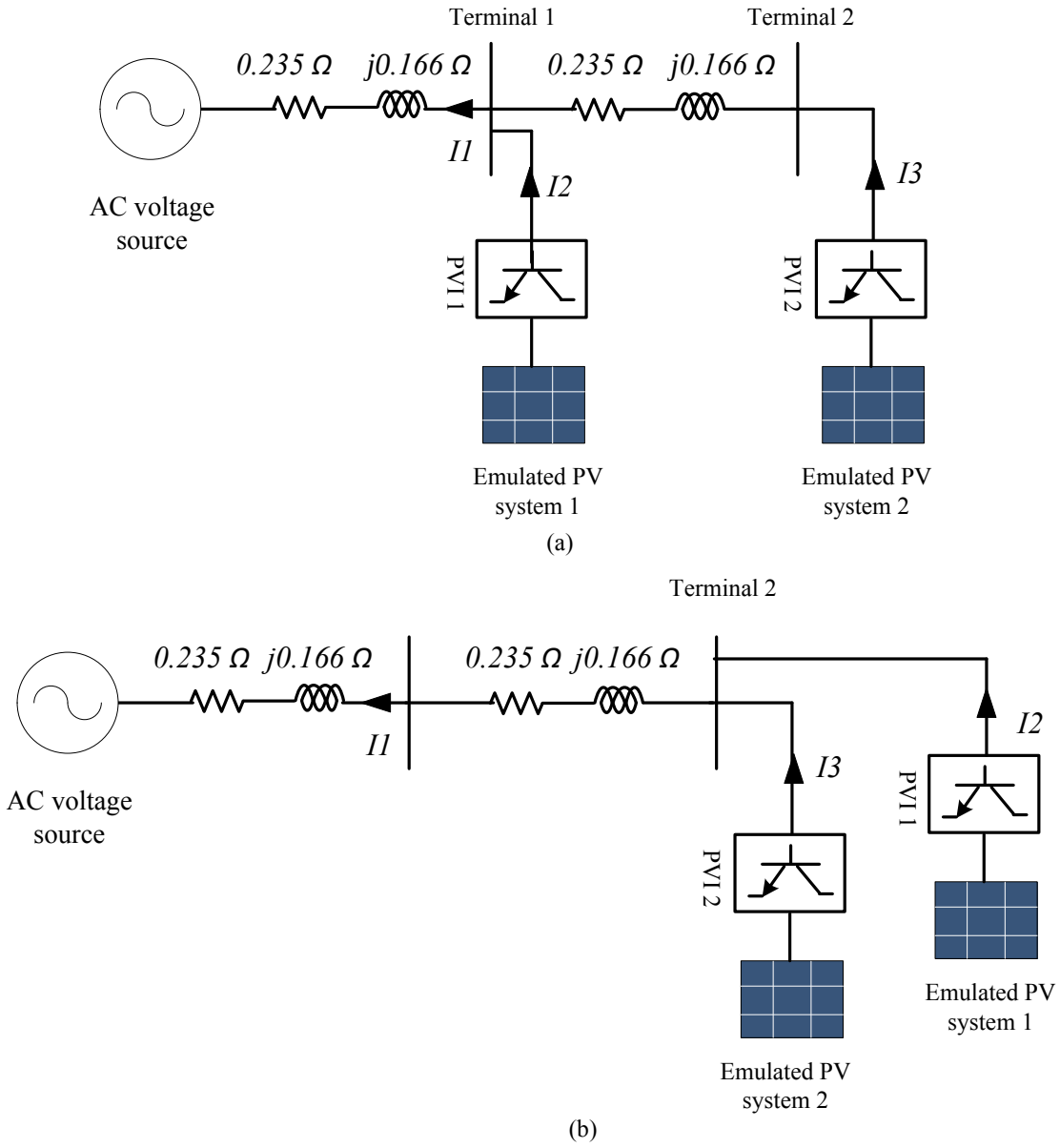

Figure 7.12: Experimental setup for PQ emission tests from multiple PVIs

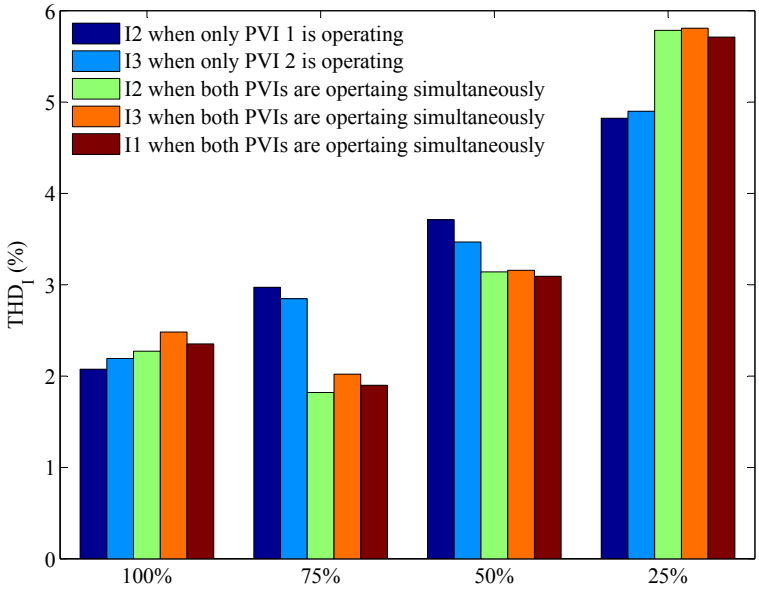

Figure 7.13: Variations of THD of current with respect to power output when both PVIs are connected to two different POCs

between the source and the POC of both PVIs corresponds to $(0.47 + j0.322)\ \Omega$ respectively. Thus, both PVIs can be considered to be connected to a weak POC.

7.6.1 Harmonic Emission Due to Multiple PVIs

Generally, harmonic distortion is characterised by harmonic voltages. However, the harmonic voltages generated are dependent on harmonic current emission and the network impedance. Therefore, the focus of this section is to analyse the harmonic current emission in relation to multiple PVIs.

Case I - Inverters Connected to Two Different POCs

Fig. 7.13 illustrates the total harmonic distortion of currents, I1, I2, and I3 (refer to Fig. 7.12 (a)) when each PVI was operated at 100%, 75%, 50% and 25% of rated power. For reference, the THD values of I2 and I3, when each PVI was operated in isolation were recorded and are given in Fig. 7.13. Similar to Section 7.3.1, the current THD of both PVIs have increased with decreasing power output, when PVIs are operating in isolation.

Referring to Fig. 7.13, at 100% rated power, the THD of I2 and I3 shows a slight increase when the PVIs are operating simultaneously compared to the scenario when they are operating in isolation. However, when each PVI is operating at 75% and 50% of their rated power, the THD of I2 and I3 have reduced when operating together. The highest level of current THD can be observed when the PVIs are operating at 25% of their rated power.

Fig. 7.14 illustrates the 3^{rd}, 5^{th}, 7^{th} and 9^{th} harmonic current emission levels and their phase angles from PVIs under simultaneous and isolated operation respectively (PVI output set to 100 % rated power). The harmonic currents are expressed as a percentage of the corresponding average RMS current. Note that voltage distortion level experienced by each PVI in its POC is different when multiple PVIs are connected to the same feeder, compared to the case when it operate in independently. The 3^{rd} harmonic current emission from each PVI has slightly increased when PVIs are operating simultaneously, due to the change in the POC voltage distortion. A similar observation can be made with respect to 5^{th}, 7^{th} and 9^{th} harmonics. The harmonic phase angles of I2 and I3, under isolated operation and simultaneous operation can be observed to be clustered around a particular phase angle irrespective of the voltage distortion at the POC. Consequently, the 3^{rd}, 5^{th} and 7^{th} harmonic currents of I1 also show a slight increase[9]. However, the 9^{th} harmonic current showed a significant reduction due to the phase angles of I2 and I3 being opposite to each other, under simultaneous operation.

Case II - Both Inverters Connected to the Same POC

The THD of I1, I2, and I3 (refer to Fig. 7.12 (b)) when both inverters were operated simultaneously (at 100%, 75%, 50% and 25% of inverter rated power respectively) are given in Fig. 7.15. The THD of I2 and I3 remain approximately equal

[9]Due to clustered phase angles of I2 and I3, the harmonic current expressed in terms of Amperes shows a significant increase. However, when normalised to the RMS current, the increase in not significant.

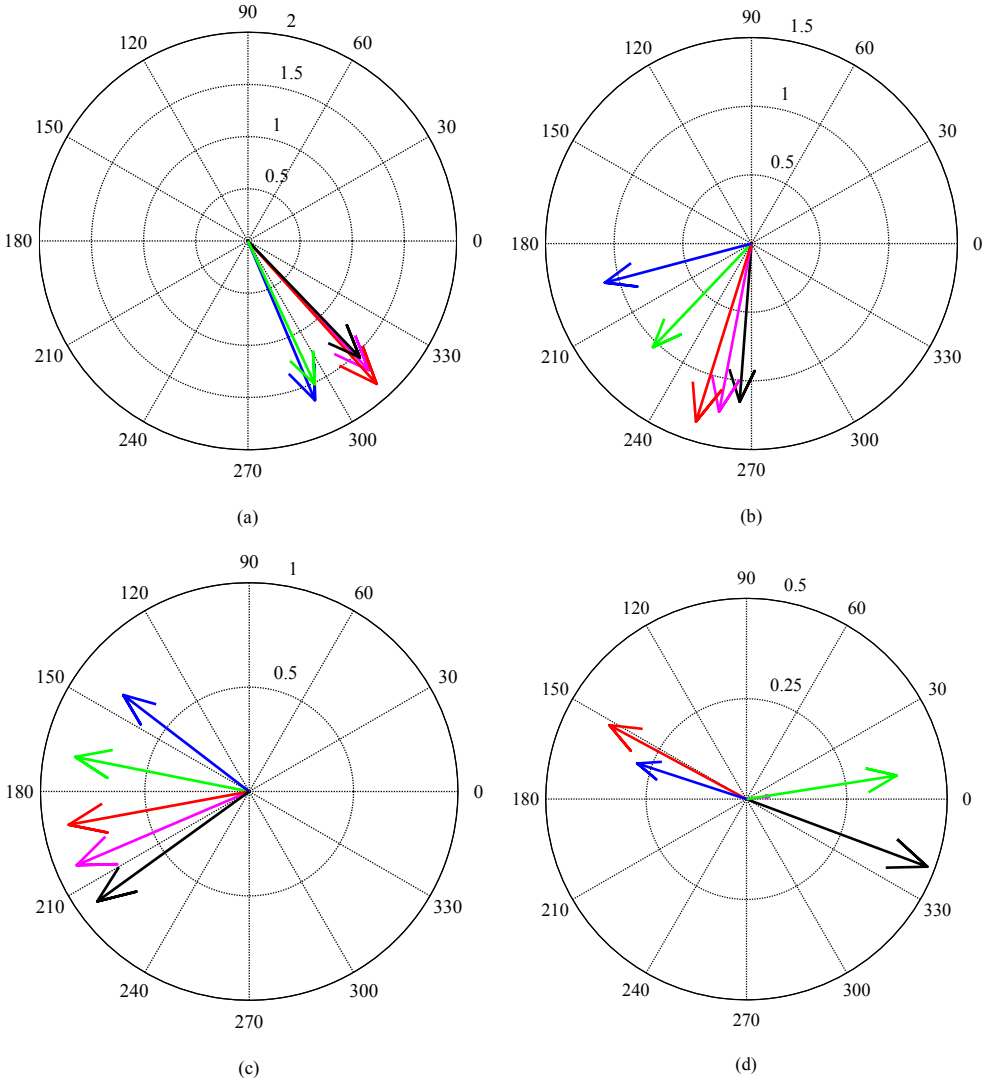

Figure 7.14: (a) 3rd (b) 5th (c) 7th (d) 9th harmonic currents of 2600 W PVIs when both are connected to the different POCs and operating at 100% of rated power

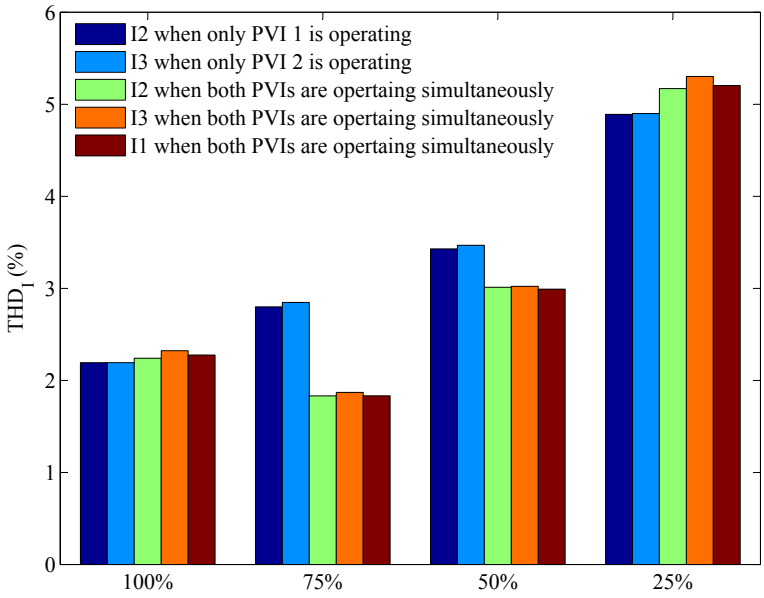

Figure 7.15: Variations of THD of current with respect to power output when both PVIs are connected to the same POC

when each PVI is operating in isolation, irrespective of their power output. This is expected due to the similar characteristics of the PVIs and the similar POC voltage. When both inverters are operating at 100% power simultaneously, THD values of I1, I2 and I3 show only a minor increase. However, for power levels of 50% and 75%, there is a significant reduction in the THD of I1, I2 and I3, compared to THD of I2 and I3 when PVIs are operating in isolation. Furthermore, only a minor variation between THD of I1, I2 and I3 are observed when PVIs are operating simultaneously.

Fig. 7.16 provides a comparison of 3^{rd} and 5^{th} harmonic current emission levels from PVIs. When operating simultaneously, the phase angles of I2 and I3 are equal, as expected. Therefore, I1 which is the vector summation of I2 and I3, has the same phase angle. However, when each harmonic current is expressed as a percentage of corresponding RMS current, the magnitude of I1 is approximately equal to that of I2 and I3. Similar observations can be made with respect to other harmonic orders. However, in the case of 75% rated power levels (as given in Fig. 7.17), a significant reduction of the 5^{th} harmonic current components of I1, I2 and I3 can be observed when PVIs are operating simultaneously. This observation which results due to change in the POC voltage distortion, when both inverters operating

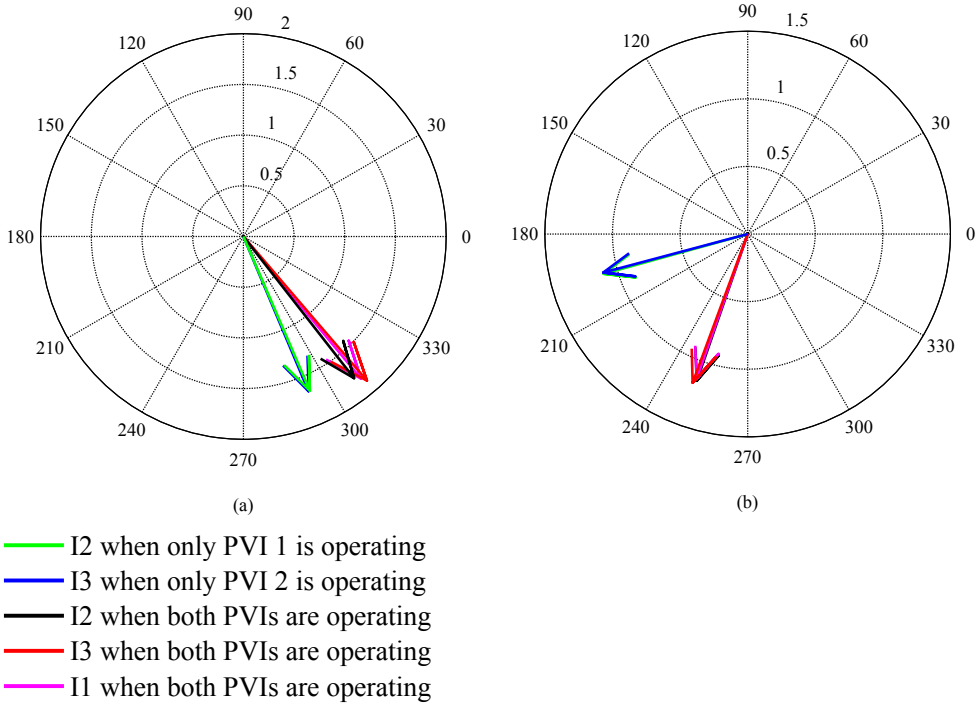

Figure 7.16: (a) 3rd (b) 5th harmonic currents in 2600 W PVIs when both PVIs are connected to the same POC and PVIs are operating at 100% rated power

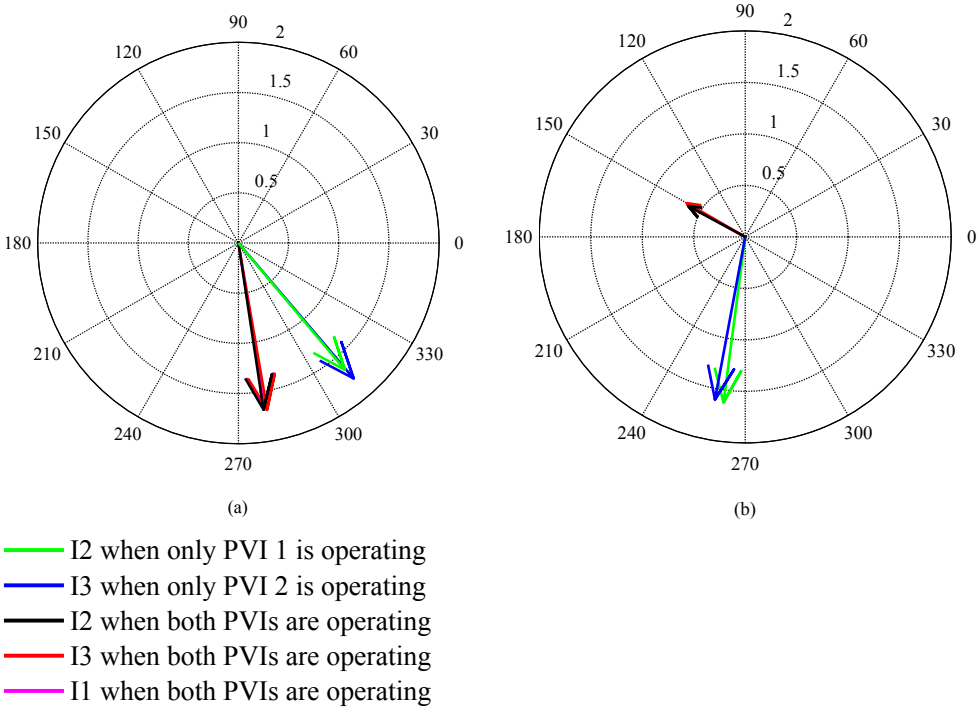

Figure 7.17: (a) 3rd (b) 5th harmonic currents in 2600 W PVIs when both PVIs are connected to the same POC and PVIs are operating at 75% rated power

simultaneously at 75% of their rated power (compared to 100%), was identified as the cause for lower THD for I1, I2 and I3 at 75 % rated power.

7.6.2 Flicker Emission Due to Multiple PVI

Flicker emission from multiple PV systems were investigated using the same experimental setup given in Fig. 7.12 (a) and (b). The following three cases were considered.

Case 1 - PVI Connected to Two Different POCs

Flicker levels at Terminal 1 and Terminal 2 (refer to Fig. 7.12 (a)) caused by PVIs operating in isolation are given in Fig. 7.18 (a) and (b) respectively for 100%, 75%, 50% and 25% power levels. When PVI 1 is operating independently, the flicker levels observed at Terminal 2 are approximately equal to the flicker levels recorded at Terminal 1, implying that flicker has propagated to the downstream terminal without any attenuation. In addition, when PVI 2 is operating in isolation, the flicker levels have significantly attenuated when propagating to Terminal 1.

Fig. 7.18 also provides the flicker levels at each terminal when both PVIs are operating simultaneously. Similar to harmonics, the measured flicker levels were found to combine, with some attenuation, when both PVIs were operating simultaneously. However, no cancellation of flicker levels were observed for all power levels in the case under investigation.

Case 2 - Both PVIs Connected to the Same POC

Fig. 7.19 illustrates the flicker levels at Terminal 2 when both PVIs are connected to the Terminal 2. Flicker levels have increased only by approximately 20% when both PVIs are operating simultaneously at 100% of their rated power, in comparison to the situation when PVIs are operating in isolation. Similar observations can be made with respect to other power levels, except at 75% power where flicker levels

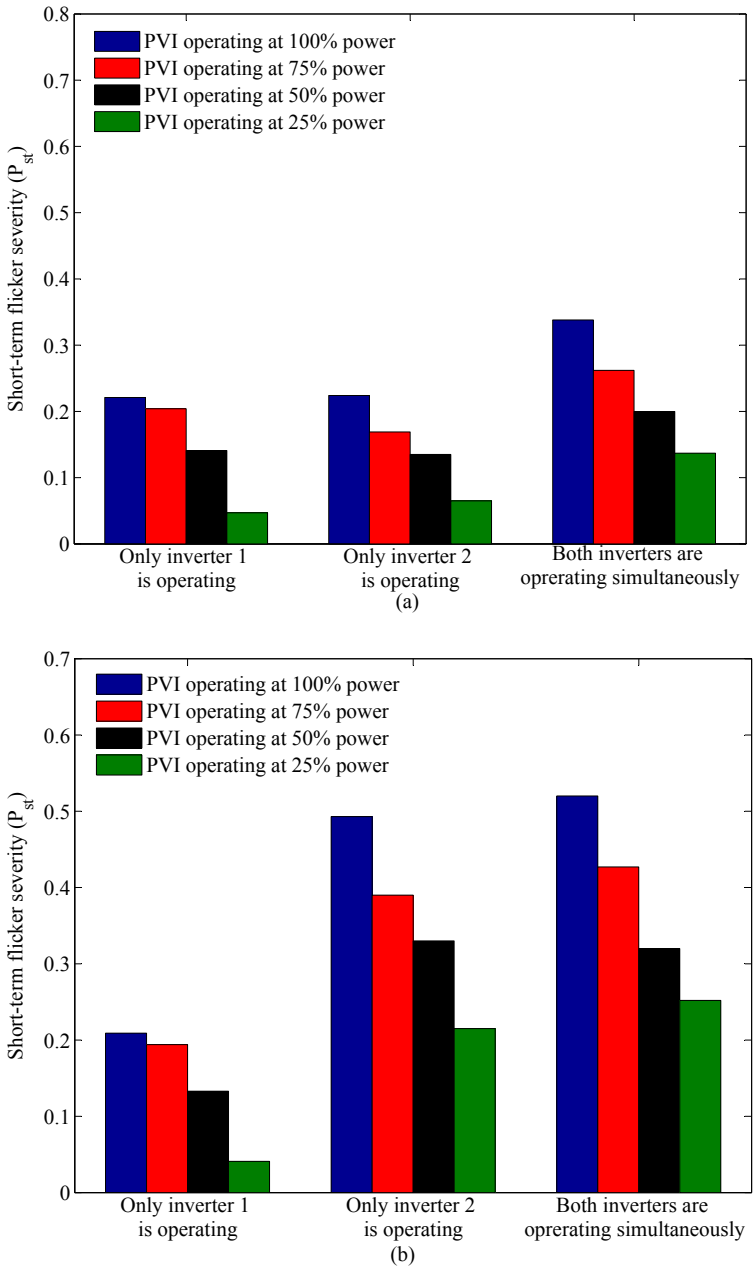

Figure 7.18: (a) Flicker levels at Terminal 1 (refer to Fig. 7.12 (a)) when PVIs are operated at 100%, 75%, 50% and 25% power levels (b) Flicker levels at Terminal 2 (refer to Fig. 7.12 (a)) when PVIs are operated at 100%, 75%, 50% and 25% power levels, when PVIs are connected to two different POCs

have increased approximately by 40%. The observations are in agreement with the Case 1, in which flicker levels from both PVIs have combined with some attenuation.

Case 3 - Flicker Emission Under Varying Irradiance Levels

In order to simulate the flicker emission under varying irradiance levels, the DC sources connected to PVI 1 and PVI 2 were programmed to follow the irradiance pattern corresponding to a cloudy day given in Fig. 7.8[10]. The flicker levels at Terminal 1 and Terminal 2 are given in Fig. 7.20. Similar to the Case 1 and 2, flicker levels are observed to be combined with some attenuation.

7.7 Chapter Summary

This chapter reported on the results of an experimental study carried out on commercial PVIs in order to evaluate harmonic and flicker emissions. A series of tests, as specified by the IEC Technical Report IEC 61000-3-15 were performed using two PVIs, and the results were compared against the stipulated limits. Both PVIs complied with the prescribed limits for harmonics, except for even harmonics, where excessive 2^{nd}, 4^{th} and 6^{th} order harmonics were observed in the case of the smaller rated PVI. In general, the THD of the output current was observed to increase with decreasing power levels. In relation to flicker, the short-term flicker severity index at the POC was observed to reduce with decreasing power outputs of the PVI. In addition, harmonic and flicker emissions from the PVIs were measured when the PV arrays were subjected to fluctuations in irradiance and panel temperature associated with a heavy cloudy day and a sunny day. Although the flicker emission from the smaller rated PVI was affected due to the passing clouds, recorded flicker emission levels were insignificant. Thus, any substantial increase in the flicker emission from the PVI, due to the passing clouds, was not identified. .

[10]Two hour time window corresponding to 40-160 mins. of the irradiance and temperature variations of a cloudy day given in Fig. 7.8 was selected for the experiment. In order to simulate the physical distance between each PVI, a 30 seconds time difference was introduced between PVI1 and PVI2.

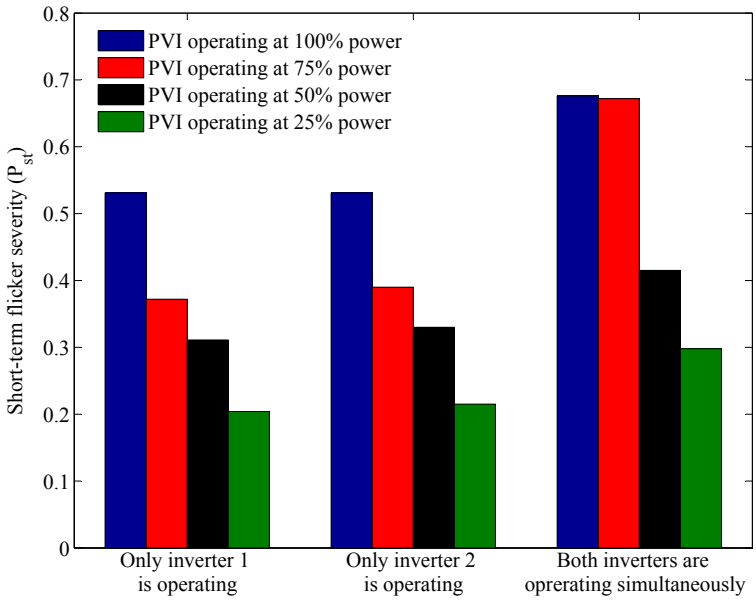

Figure 7.19: (a) Flicker levels at Terminal 2 (refer to Fig. 7.12 (b)) when PVIs are operated at 100%, 75%, 50% and 25% power levels and both PVIs are connected to the same POC.

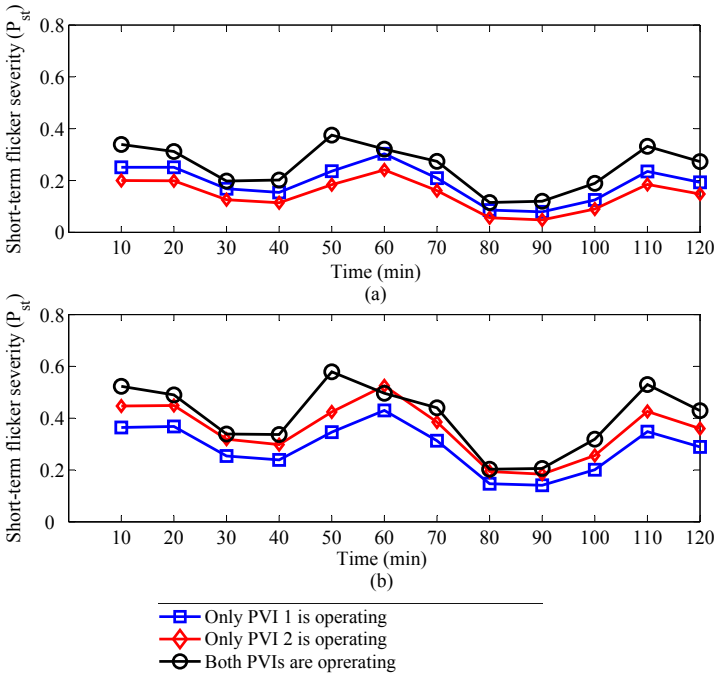

Figure 7.20: (a) Flicker levels at Terminal 1 (refer to Fig. 7.12) (b) Flicker levels at Terminal 2 (refer to Fig. 7.12) when both PVIs are operated at varying irradiance conditions

In addition, harmonic and flicker emissions from multiple PV systems were also investigated employing a model LV feeder and two commercial PVIs. With regard to harmonics, inverter interactions were observed which lead to a reduction in the THD of inverter currents, when both PVIs are operating simultaneously. When both PVIs are connected to the same POC, an increase in the harmonic currents were observed. However, the increase in the THD was observed to be marginal due the increase in fundamental current. In relation to flicker, emission levels from both PVIs were observed to combine with some attenuation. The highest flicker levels were observed while the inverters were connected to the same POC. The results warrant further experimental work employing greater number of PVIs, in order to accurately model the impact of PVIs on network PQ.

The results obtained from the experimental work presented in this chapter can be used by DNSPs to accurately modelling the impact of PVIs in distribution networks, considering the characteristics of their networks. Some preliminary work with this regard considering flicker emission is presented in Appendix G.

Chapter 8

Conclusions and Recommendations for Future Work

8.1 Conclusions

This Thesis investigated key issues related to the management of PQ in distribution networks, with an emphasis on harmonics, voltage fluctuations and flicker and VU. The outcomes and findings are expected to contribute to further development of relevant IEC Technical Reports and Standards. The key conclusions and recommendations based on the work undertaken are summarised as follows.

IEC 61000-3-14 Harmonic Current Emission Allocation Methodology:

One of the main objectives of this Thesis was to develop the theoretical background in relation to the PQ disturbance emission allocation methodologies presented in IEC Technical Report 61000-3-14. The methodologies presented in the aforementioned Technical Report contains several concepts that do not provide a clear approach for the allocation of emission limits to customer installations. In this regard, its

harmonic current emission allocation methodology was critically examined, in order to clarify these ambiguities. The concept of a reduction factor, which is proposed in the Technical Report, was utilised in order to take into account the harmonic voltage contributions from small installations for which emission limits are not governed by the Technical Report. The reduction factor was shown to be dependent on the harmonic current emission from small installations, in contrast to the assumptions made in the IEC Technical Report. Hence, an approach where a fixed harmonic emission limit is assumed for small installations was proposed in order to calculate the reduction factor. In addition, the IEC approach for estimating the reduction factor was found to be incomplete in cases such as LV distribution networks with spurs or distribution networks with different conductor types. In such situations, DNSPs need to estimate the reduction factor based on the first principles. Such difficulties undermine the applicability of the harmonic emission allocation methodology in relation to practical LV networks.

Alternative Harmonic Current Emission Methodologies

A critical analysis of alternative harmonic emission allocation methodologies was performed, employing two radial LV distribution networks as case studies. Other methodologies included the CBV methodology, VD methodology, IEEE 519 methodology and Technical Rules for Assessment of Network Disturbances methodology. These methods were compared using criteria such as allowable harmonic current emission limits, ease of application data requirements and etc.. The analyses have shown good correlation between the emission limits established by all methodologies. However, the emission limits established according to the IEC 61000-3-14, VD and Technical Rules for Assessment of Network Disturbances methodologies were observed to be conservative compared to the CBV methodology, hence, a safety margin exists between the maximum harmonic voltage observed in the network and its planning levels. In addition, the alternative harmonic emission allocation methodologies were found to be superior to that of IEC 61000-3-14, in terms of

ease of application, data and computational requirements. The streangth of the IEC 61000-3-14 methodology was its flexibility in applying to specific distribution network, when all required data are readily available.

Harmonic Current Emission for Distributed Generators

In relation to harmonic emission allocation for DGs, the IEC 61000-3-14 and CBV methodologies can be easily modified to incorporate DGs into the emission allocation process. However, such flexibility is not available with Technical Rules for Assessment of Network Disturbances, IEEE 519 and VD methodologies. Hence, for distribution networks with high levels of DG penetration, the application of Technical Rules for Assessment of Network Disturbances, IEEE 519 and VD methodologies may lead to situation where the harmonic voltage levels exceed the planning levels.

Voltage Unbalance Emission Allocation Based on Constrained Bus Voltage Method

A revised VU emission allocation methodology based on the CBV allocation principles was developed for radial distribution networks. In the CBV allocation technique, emission levels at network busbars are explicitly forced to be at or below the set planning level when all loads inject their limits allocated under the CBV approach. This revised allocation technique was examined by employing MV and LV test systems, and emission levels at all network busbars were observed to remain within the planning levels selected for the network. By appropriately modifying the CBV methodology, VU emission allocation in situations where single and two-phase installations and induction motor installation are present can be accomplished.

Voltage Unbalance Emission Allocation Based on Voltage Droop Method

A key deficiency of the CBV approach was that prior knowledge of the MVA capacities and short-circuit capacities at the POC of all installation is required. In order to address such difficulties, a new VU emission allocation methodology based on the concept of VD was developed. Using the VD methodology, VU level at the extremity of the network can be maintained below the chosen planning level. This approach eliminates the requirement for individual planning levels at each voltage level of the network. The application of the VD methodology for VU emission allocation was demonstrated using LV and MV test networks, where it was shown to be simplistic and less computational and data intensive, compared to both IEC and CBV approaches. The CBV methodology is shown to be superior in comparison to the IEC VU allocation methodologies, as it enables the network VU absorption capacity to be fully utilised.

Voltage Fluctuations due to Renewable Energy Generators

Voltage fluctuations and flicker emission and propagation from REG connected to radial distribution networks operating in different control modes (i.e. power factor control operation, voltage control mode and reactive power dispatch mode) were examined using mathematical models. The results suggest that the flicker emission from a REG, under power factor control operation would increase when operating at both leading and lagging power factors compared to unity power factor operation, depending on the grid impedance angle. In addition, the flicker propagation when a REG is operating in power factor control mode was also shown to be dependent on the operating power factor and grid impedance angle at the point of interest. When the REG is operating in voltage control mode, flicker observed at the POC of a wind farm would be minimum, however, the flicker levels at upstream of the network would increase. These observations were supported through a simulation studies consisting

of a model of a wind farm connected to an MV distribution network. The study emphasised on the requirement for proper planning from DNSPs in relation to flicker emission and propagation, considering the reactive power control strategy employed in the REG, when connecting REG to distribution networks.

Flicker Propagation in Distribution Networks

The propagation of voltage fluctuations and flicker from an upstream network to a downstream network, in terms of transfer coefficients, was initially examined using mathematical models, with four basic load types connected to the downstream network. (i.e. constant impedance, constant current, constant power and ZIP loads). A flicker transfer coefficient of unity which has been assumed for upstream to downstream flicker propagation in the presence of passive loads was observed to be conservative in relation to some passive load types such as constant power loads and constant current loads. The mathematical models were then extended to investigate the flicker emission and propagation from a REG operating in power factor control and voltage control modes, when distribution system loads are connected to the same feeder. In power factor control mode, the connection of distribution system loads to the same feeder was observed to influence flicker emission from the REG. However, in voltage control mode, the impact of the distribution system loads is largely negated by the closed loop controller of the REG.

Experimental Studies to Understand the Power Quality Behaviour of Photovoltaic Systems

The final objective of this Thesis was to examine the characteristics of PV systems in relation to harmonic and flicker emission, using a laboratory experimental setup. The results obtained from these experiments are expected to assist DNSPs in assessing the PQ impact of PVIs on distribution networks. The experiments were conducted using a number of PVIs from different manufacturers. The results indi-

cate that the low-order odd-harmonic emission from PVIs used in the experiment were within the stipulated limits in IEC standards. Even order harmonics observed in some cases were in excess of limits prescribed by IEC 61000-3-15. In relation to flicker emission, PVI control operations may be identified as a source of flicker. However, the observed flicker levels were insignificant and were well within the stipulated limits. Furthermore, flicker emission from the PVIs were measured when the PV arrays were subjected to fluctuations in irradiance and panel temperature associated with a heavy cloudy day and a sunny day. Recorded flicker emission levels were negligible. These results warrant further investigation, in relation to impacts of PVIs on network PQ.

8.2 Recommendations for Future Work

The Technical Report IEC/TR 61000-3-14, has recently been adopted as an Australian Standard, to provide guidelines for DNSPs in Australia in the management of PQ emission limits for large installations connected to LV distribution networks. As demonstrated in Chapter 3, the PQ disturbance emission allocation methodologies require the computation of key factors and coefficients, which are specific to networks under consideration. Hence, further work is required in order to assist DNSPs in the implementation of the IEC 61000-3-14 in their networks. Verification of the PQ disturbance emission allocation methodologies proposed in Chapters 3 and 5 through field measurements are also encouraged.

The VU emission allocation methodologies discussed in the Thesis primarily focused on radial distribution networks, as most distribution networks are radial in nature. However, some meshed distribution networks are located in inner city locations, where a strongly supply is required. Further work is required to extend the VU emission allocation methodologies discussed in this Thesis to meshed distribution networks.

The work presented in relation to VU in this Thesis does not consider the

zero-sequence VU and assumed that zero-sequence VU can be mitigated through proper system design and maintenance. However, with the increasing penetration of single-phase REGs such as PVIs in the distribution networks, management of zero-sequence VU emission through system design and maintenance may become difficult. Hence, additional work is required to propose methodologies for management of zero-sequence VU emission in distribution networks.

Practical verification of the mathematical and simulation outcomes presented in Chapter 6 in relation to the impact of reactive power control strategy employed on a REG on flicker emission and propagation using laboratory experiments or field measurements is encouraged. In addition, the load models proposed with regard to flicker attenuation need to be extended by incorporating their time constant of responses.

The work conducted in Chapter 7 demonstrated the possibility of the presence of even harmonics in distribution networks caused by PVIs. With an increasing number of PVIs in distribution networks, even harmonic voltage levels in the distribution network would be expected to increase. Hence, the applicability of harmonic coordination approaches given in this Thesis needs to be investigated in relation to even harmonics. In addition, further work is required to examine the levels of harmonics related to switching frequencies of PVIs as such units increase in numbers in the LV distribution networks.

References

[1] M. H. J. Bollen and F. Hassan. *Intergration of Distributed Generation in the Power System*. John Wiley and Sons, 2011.

[2] IEC/TR 61000-3-14: Electromagnetic compatibility (EMC) - Part 3-14: Assessment of emission limits for the connection of disturbing installation to LV power systems, Ed. 1. Technical report, International Electrotechnical Commission, 2011.

[3] IEC/TR 61000-3-6: Electromagnetic compatibility (EMC) - Limits - Assessment of emission limits for distorting loads in MV and HV power systems, Ed. 1. Technical report, International Electrotechnical Commission, 1996.

[4] IEC/TR 61000-3-7: Electromagnetic compatibility (EMC) - Limits - Assessment of emission limits for fluctuating loads in MV and HV power systems, Ed. 1. Technical report, International Electrotechnical Commission, 1996.

[5] IEC/TR 61000-3-13: Electromagnetic compatibility (EMC) - Limits - Assessment of emission limits for the connection of unbalanced installations to MV, HV and EHV power systems, Ed. 1. Technical report, International Electrotechnical Commission, 2008.

[6] IEC 61000-3-2:Electromagnetic compatibility (EMC) - Part 3-2: Limits - Limits for harmonic current emissions (equipment input current (16 A per phase),Ed. 3.0. Technical report, Inernational Electrotechnical Committee, 2005.

[7] IEC 61000-3-12:Electromagnetic compatibility (EMC) - Part 3-12: Limits - Limits for harmonic currents produced by equipment connected to public low-voltage systems with input current $\geq$ 16 A and $\leq$ 75 A per phase, Ed. 3.0. Technical report, Inernational Electrotechnical Committee, 2004.

[8] IEC 61000-3-3:Electromagnetic compatibility (EMC) - Part 3-3: Limits - Limitation of voltage changes, voltage fluctuations and flicker in public low-voltage supply systems, for equipment with rated current $\leq$ 16 A per phase and not subject to conditional connection, Ed. 1.2. Technical report, Inernational Electrotechnical Committee, 2005.

[9] IEC 61000-3-11:Electromagnetic compatibility (EMC) - Part 3-11: Limits - Limitation of voltage changes, voltage fluctuations and flicker in public low-voltage supply systems equipment with rated current less than or equal to 75 A and subject to conditional connection, Ed. 1.2 . Technical report, Inernational Electrotechnical Committee, 2000.

[10] IEC 61000-3-15:Electromagnetic compatibility (EMC) - Part 3-15: Limits - Assessment of low frequency electromagnetic immunity and emission requirements for dispersed generation systems in LV network, Ed. 1. Technical report, International Electrotechnical Commission, 2011.

[11] P. Paranavithana. *Contribution Towards the Development of the Technical Report IEC/TR 61000-3-13 on Voltage Unbalance Emission Allocation.* PhD thesis, School of Electrical, Computer and Telecommunications Engineering, University of Wollongong, Wollongong, Australia, March 2008.

[12] T. J. Browne. *Harmonic Management in Transmission Networks.* PhD thesis, School of Electrical, Computer and Telecommunications Engineering, University of Wollongong, Wollongong, Australia, March 2008.

[13] Handbook HB264: Power Quality - Recommendations for the Application of AS/NZS 61000.3.6 and AS/NZS 61000.3.7. Technical report, Standards Australia, 2003.

[14] R. A. Barr and V. J. Gosbell. Introducing Power System Voltage Droop as a New Concept for Harmonic Current Allocation. In *Proc.* 14$^{\text{th}}$ *Int. Conf. on Harmonics and Quality of Power*, 26-29 Sept. 2010.

[15] V. J. Gosbell and R. A. Barr. Harmonic Allocation Following IEC Guidelines Using the Voltage Droop Concept. In *Proc.* 14th *Int. Conf. on Harmonics and Quality of Power*, 26-29 Sept. 2010.

[16] V. J. Gosbell and R. A. Barr. A New Approach to Harmonic Allocation for MV Installations. In *Proc.* 20th *Australasian Universities Power Engineering Conf.*, 5-8 Dec. 2010.

[17] L. Meegahapola and S. Perera. Impact of Wind Generator Control Strategies on Flicker Emission in Distribution Networks. In *Proc.* 15th *Int. Conf. on Harmonics and Quality of Power*, 17-20 June 2012.

[18] D. G. Infield, P. Onions, A. D. Simmons, and G. A. Smith. Power Quality from Multiple Grid-connected Single-phase Inverters. *IEEE Trans. on Power Delivery*, 19(4):1983–1989, 2004.

[19] S. B. Kjaer. Flicker and Photovoltaic Power Plants. In *Proc.* 25th *European Photovoltaic Solar Energy Conf. and Exhibition*, pages 545–550, 6-10 Sept. 2010.

[20] J. H. R. Enslin and P. J. M. Heskes. Harmonic Interaction Between a Large Number of Distributed Power Inverters and the Distribution Network. *IEEE Trans. on Power Electronics*, 19(6):1586–1593, 2004.

[21] M. van den Bergh. Solar Inverter Testing per IEC 61000-3-15. In *Proc. Int. Conf. on Electricity Distribution*, 6-9 June 2011.

[22] R. C. Dugan, M. F. McGranaghan, and H. W. Beaty. *Electrical Power Systems Quality*. New York: McGraw-Hill, 1996.

[23] M. H. J. Bollen. *Understanding Power Quality Problems - Voltage Sags and Interruptions*. Institute of Electrical and Electronics Engineers, 2000.

[24] IEC 60050: International Electrotechnical Vocabulary (IEV) - Chapter 161-Electromagnetic Compatibility. Technical report, International Electrotechnical Commission, 1990.

[25] J. Arrillaga, N. R. Watson, and S. Chen. *Power System Quality Assessment*. John Wiley and Sons, 2000.

[26] T. Keppler. *Flicker Measurements and Propagation in Power Systems*. PhD thesis, Electrical and Electronic Engineering, University of Canterbury, Christchurch, New Zealand, Sept. 1998.

[27] AS/NZS 61000.4.15:2005 Electromagnetic Compatibility (EMC) Part 4.15: Testing and Measurement Techniques - Flickermeter-Function and Design Specifications. Technical report, Standards Australia, 2005.

[28] AS/NZS 4376:1996, Flickermeter-Functional and Design Specifications. Technical report, Standards Australia/Standard New Zealand, 1996.

[29] M. B. Hughes. Revenue Metering Error Caused by Induced Voltage from Adjacent Transmission Lines. *IEEE Trans. on Industry Applications*, 7(2):741–745, Apr. 1992.

[30] M. T. Bina and E. P. Javid. A Critical Overview on Zero Sequence Component Compensation in Distorted and Unbalanced Three-phase Four-wire Systems. In *Proc. Int. Power Engineering Conf. (IPEC 2007)*, pages 1167–1172, Dec. 2007.

[31] J. E. Parton and Y. K. Chant. The Three-Limbed Phase Transformer with Controlled Zero Sequence Effect. *IEEE Trans. on Power Apparatus and Systems*, 90(5):2019–2029, Sept. 1971.

[32] A. von Jouanne and B. Banerjee. Assessment of Voltage Unbalance. *IEEE Trans. on Power Delivery*, 16(4):782–790, Oct. 2001.

[33] IEC 61000-4-30: Electromagnetic Compatibility (EMC) - Part 4-30 - Environment - Testing and Measurement Techniques - Power Quality Measurement Methods, Ed. 1. Technical report, International Electrotechnical Commission, 2003.

[34] U. Jayatunga, S. Perera, and P. Ciufo. Voltage Unbalance Emission Assessment in Radial Power Systems. *IEEE Trans. on Power Delivery*, 27(3):1653–1661, July 2012.

[35] U. Jayatunga, S. Perera, P. Ciufo, and A. P. Agalgaonkar. Voltage Unbalance Emission Assessment in Interconnected Power Systems. *IEEE Trans. on Power Delivery*, 28(4):2383–2393, Oct. 2013.

[36] NEMA MG1: Motors and Generators . Technical report, National Electricity Manufacturer's Association, 1993.

[37] J. Radatz. *IEEE 100: Standard Dictionary of Electrical and Electronics Terms*. Institute of Electrical and Electronics Engineers, 1996.

[38] IEEE 519: IEEE Recommended Practice for Harmonic Control in Electrical Power Systems. Technical report, Institute of Electrical and Electronics Engineers, 1992.

[39] M. De Witte, C. Pirenne, S. Magnus, P. Lauwers, and E. De Jaeger. Connection Rules for Possibly Disturbing Loads in LV Networks. In *Proc.* 14$^{\text{th}}$ *Int. Conf. on Electricity Distribution*, volume 3, pages 189–192, 5-8 May 2007.

[40] T. H. Chen. Criteria to Estimate the Voltage Unbalances due to High-Speed Railway Demands. *IEEE Trans. on Power Systems*, 9(3):1672–1678, Aug. 1994.

[41] T. H. Chen and H. Y. Kuo. Analysis on the Voltage Unbalances due to High-Speed Railway Demands. In *Proc. Int. Conf. on Energy Management and Power Delivery (EMPD '95)*, volume 2, pages 657–661, Nov. 1995.

[42] P. Vinicius, S. Valois, C. M. V. Than, N. Kagan, and H. Arango. Voltage Unbalance in Low Voltage Distribution Networks. In *Proc.* 14th *Int. Conf. on Electricity Distribution*, June 2001.

[43] W. R. Bullard, H. L. Lowe, and H. W. Wahlquist. Calculation of Unbalanced Voltage in Distribution Circuits with Particular Reference to Multi-Grounded Neutrals. *AIEE Trans. on Electrical Engineering*, 63:145–148, 1944.

[44] E. T. B. Gross and S. W. Nelson. Electromagnetic Unbalance of Untransposed Transmission Lines. *AIEE Trans. on Power Apparatus and Systems*, 74(3):887–893, 1955.

[45] R. H. Brierley, A. S. Morched, and T. E. Grainger. Compact Right-of-ways with Multi-voltage Towers. *IEEE Trans. on Power Delivery*, 6(4):1682–1689, Oct. 1991.

[46] P. V. Santos Valois, C. M. Vieira Tahan, N. Kagan, and H. Arango. Voltage Unbalance in Low Voltage Distribution Networks. In *Proc. Int. Conf. on Electricity Distribution (CIRED2001)*, June 2001.

[47] Z. Emin and D. S. Crisford. Negative Phase-sequence Voltages on E&W Transmission System. *IEEE Trans. on Power Delivery*, 21(3):1607–1612, July 2006.

[48] A. Ametani, D. Van Dommelen, and I. Utsumi. Study of Super-Bundle and Low Reactance Phasings on Untransposed Twin-Circuit Lines . In *IEE Proc. Generation, Transmission and Distribution*, volume 137-4, pages 245–253, July 1990.

[49] P. G. Cummings. Estimating Effect of System Harmonics on Losses and Temperature Rise of Squirrel-Cage Motors. *IEEE Trans. on Industry Applications*, IA-22(6):1121–1126, Nov. 1986.

[50] A. Vamvakari, A. Kandianis, A. Kladas, S. Manias, and J. Tegopoulos. Analysis of Supply Voltage Distortion Effects on Induction Motor Operation. In *Proc. Int. Conf. on Electric Machines and Drives*, May 1999.

[51] V. E. Wagner, J. C. Belda, and T. M. Barnes. Effects of Harmonics on Equipment. *IEEE Trans. on Power Delivery*, 8(2):672–680, Apr. 1993.

[52] W. Chen and Z. Cheng. An Experimental Study of the Damaging Effects of Harmonics in Power Networks on the Capacitor Dielectrics. In *Proc.* 2nd *Int. Conf. on Properties and Applications of Electrical Materials*, volume 2, pages 645–648, 1988.

[53] K. Zhao, P. Ciufo, and S. Perera. Rectifier Capacitor Filter Stress Analysis when Subject to Regular Voltage Fluctuations. *IEEE Trans. on Power Electronics*, 28(7):3625–3635, July 2013.

[54] D. Mirabbasi, G. Seifossadat, and M. Heidari. Effect of Unbalanced Voltage on Operation of Induction Motors and Its Detection. In *Proc. Int. Conf. on Electrical and Electronics Engineering*, volume 3, pages 189–192, Nov. 1997.

[55] C. Y. Lee, B. K. Chen, W. Lee, and Y. F. Hsu. Effects of Various Unbalanced Voltages on the Operation Performance of an Induction Motor Under the Same Voltage Unbalance Factor Condition. In *Proc. IEEE Industrial and Commercial Power Systems Technical Conf.*, volume 4, pages 51–59, May 1997.

[56] C. Y. Lee. Effects of Unbalanced Voltage on the Operation Performance of a Three-phase Induction Motor. *IEEE Trans. on Energy Conversion*, 14(2):202–208, June 1999.

[57] AS 1359.101: Rotating Electrical Machines - General Requirements - Rating and Performance. Technical report, Standards Australia, 1997.

[58] A. von Jouanne, J. G. Rangel, P. Enjeti, and W. Gray. Harmonics Generated by Variable Speed AC Motor Drives: Case Studies. pages 342–355, Sept. 1994.

[59] D. P. Manjure and E. B. Makram. Impact of Unbalance on Power System Harmonics. In *Proc.* 10^{th} *Int. Con. on Harmonics and Quality of Power (ICHQP 2002)*, pages 328–333, 2002.

[60] Edited by Angelo Baggini. *Handbook of Power Quality*. John Wiley and Sons, 2008.

[61] J. Kuang and S. A. Boggs. Pipe-type Cable Losses for Balanced and Unbalanced Currents. *IEEE Trans. on Power Delivery*, 17(2):313–317, April 2002.

[62] IEC 61000-2-2: Electromagnetic compatibility (EMC) - Part 2.2 - Environment - Compatibility levels for low-frequency conducted disturbances and signalling in public low-voltage power supply systems, Ed. 2. Technical report, International Electrotechnical Commission, 2002.

[63] IEC 61000-2-12: Electromagnetic compatibility (EMC) - Part 2.2 - Environment - compatibility levels for low-frequency conducted disturbances and signalling in public medium-voltage power supply systems, Ed. 1. Technical report, International Electrotechnical Commission, 2003.

[64] National Electricity Code Australia, Version 1.0 - Amendment 9.0. Technical report, National Electricity Code Administrator Limited, Australia, 2004.

[65] HB 264: Power Quality - Recommendation for the Application of AS/NZS 61000.3.6 and AS/NZS 61000.3.7. Technical report, Standards Australia/New Zealand, 2003.

[66] Technical Rules for the Assessment of Network Disturbances, Ed. 2. Technical report, 2007.

[67] Modeling and Simulation of the Propagation of Harmonics in Electric Power Networks. II. Sample Systems and Examples. *IEEE Trans. on Power Delivery*, 11(1):466–474, 1996.

[68] K. Wada, H. Fujita, and H. Akagi. Analysis of Harmonic Propagation in a Power Distribution System: An Application of a Distributed Constant-Circuit Model. *Electrical Engineering in Japan*, 139(1), 2002.

[69] A. I Maswood and J. Z. Jun. Attenuation and Diversity Effect in Harmonic Current Propagation Study. In *Proc. IEEE Power Engineering Society General Meeting*, volume 3, pages 1480–1485, July 2003.

[70] Modeling and Simulation of the Propagation of Harmonics in Electric Power Networks. I. Concepts, Models, and Simulation Techniques. *IEEE Trans. of Power Delivery*, 11(1):466–474, 1996.

[71] W. Xu, J. R. Jose, and H. W. Dommel. A Multiphase Harmonic Load Flow Solution Technique. volume PS-6, pages 174–182, Feb. 1991.

[72] R. Yacamini and J.C. de Oliveira. Harmonics in Multiple Convertor Systems: A Generalized Approach. volume 127, pages 96–106, March 1980.

[73] J. A. Ghijselen, W. A. Ryckaert, and J. A. Melkebeek. Distribution System Parameters and Their Influence on Harmonic Propagation. In *Proc.* 17$^{\text{th}}$ *Int. Conf. on Electricity Distribution*, 2003.

[74] J. A. Ghijselen, W. A. Ryckaert, and J. A. Melkebeek. Influence of Electric Power Distribution System Design on Harmonic Propagation. *Electrical Engineering*, 86(4):181–190, 2004.

[75] M. F. Abdullah, N. H. Hamid, Z. Baharudin, and M. F. I. Khamis. Triplen Harmonics Currents Propagation Through Medium Voltage Distribution Network. In *Proc.* 4$^{\text{th}}$ *Int. Conf. on Modeling, Simulation and Applied Optimization (ICMSAO)*, pages 1–5, April 2011.

[76] S. Tennakoon. *Flicker Propagation in Radial and Interconnected Power Systems*. PhD thesis, School of Electrical, Computer and Telecommunications Engineering, University of Wollongong, Wollongong, Australia, March 2008.

[77] E. De Jaeger, G. Borloo, and W. Vancoetsem. Flicker Transfer Coefficients from HV to MV and LV Systems. In *Proc.* 14th *Int. Conf. on Electricity Distribution (CIRED97)*, pages 101–102, Birminhgam, UK, June 1997.

[78] S. Perera, D. Robinson, S. Elphick, D. Geddey, N. Browne, V. Smith, and V. Gosbell. Synchronised Flicker Measurement for Flicker Transfer Evaluation in Power Systems. *IEEE Trans. on Power Delivery*, 21(3):1477–1482, July 2006.

[79] D. Stade, H. Schau, and A. Novitskiy. Flicker Analsyis in the HV Transmission System. In *Proc.* 10th *Int. Conf. on Harmonics and Quality of Power*, volume 2, pages 541–546, Oct. 2002.

[80] M. C. Simöes and S. M. Deckmann. Flicker Propagation and Attenuation. In *Proc.* 10th *Int. Conf. on Harmonics and Quality of Power*, volume 2, pages 644–648, Oct. 2002.

[81] M. Couvreur, E. De Jaeger, and A. Robert. The Voltage Fluctuations and the Concept of Short-Circuit Power. In *Session 2000 CIGRE*, pages Report 13/1436–08, 2000.

[82] M. Couvreur, E. De Jaeger, P. Goossens, and A. Robert. The Concept of Short-Circuit Power and the Assessment of the Flicker Emission Level. In *Proc.* 16th *Int. Conf. on Electricity Distribution (CIRED)*, volume 2, pages 2.36/1–2.36/7, June 2001.

[83] S. Perera, D. Robinson, S. Elphick, D. Geddey, N. Browne, V. Smith, and V. Gosbell. Synchronized Flicker Measurement for Flicker Transfer Evaluation in Power Systems. *IEEE Trans. on Power Delivery*, 21(3):1447–1982, July 2006.

[84] Review of Flicker Objectives for LV, MV and HV Power Systems. Technical report, CIGRE C4.108 Technical Brochure, 2011.

[85] H. Renner and M. Sakulin. Flicker Propagation in Meshed High Voltage Networks. In *Proc.* 9th *Int. Conf. on Harmonics and Quality of Power*, volume 3, pages 1023–1028, Oct. 2000.

[86] P. Paranavithana, S. Perera, and R. Koch. An Improved Methodology for Determining MV to LV Voltage Unbalance Transfer Coefficient. In *Proc.* 13th *Int. Conf. on Harmonics and Quality of Power*, pages 1–6, 2008.

[87] B. Fox, D. Flynn, L Bryans, N. Jenkins, D. Milborrow, M. O'Malley, R. Watson, and O. Anaya-Lara. *Wind Power Integration: Connection and System Operational Aspects*. IET Power and Engineering Series 50, 2007.

[88] M. P. Papadopoulos, S. A. Papathanassiou, S. T. Tentzerakis, and N. G. Boulaxis. Investigation of the Flicker Emission by Grid Connected Wind Turbines. In *Proc.* 8th *Int. Conf. on Harmonics and Quality of Power*, 14-18 Oct. 1998.

[89] S. Das, N. Karnik, and S. Santoso. Time-Domain Modeling of Tower Shadow and Wind Shear in Wind Turbines. *ISRN Renewable Energy*, pages 1–11, 2011.

[90] D. Dolan and P.W. Lehn. Simulation Model of Wind Turbine 3P Torque Oscillations due to Wind Shear and Tower Shadow. *IEEE Trans. Energy Conversion*, pages 717–724, 2006.

[91] T. Thiringer and J. A. Dahlberg. Periodic Pulsations from a Three-Bladed Wind Turbine. *IEEE Trans. Energy Conversion*, 16(2):128–133, 2001.

[92] X. Liu, D. McSwiggan, T. B. Littler, and L. Kennedy. Measurement-Based Method for Wind Farm Power System Oscillations Monitoring. *Renewable Power Generation*, 4(2):198–209, 2010.

[93] A. Larsson. Flicker Emission of Wind Turbines During Continuous Operation. *IEEE Trans. Energy Conversion*, pages 114–118, March 2002.

[94] A. Lazkano, K. Redondo, P. Saiz, J. J. Gutierrez, I. Azcarate, L. A. Leturiondo, and J. Barros. Case study: Flicker Emission and 3P Power Oscillations on Fixed-Speed Wind Turbines. In *Proc.* 13th *Int. Conf. on Harmonics and Quality of Power*, pages 268–273, 2012.

[95] T. Sun, Z. Chen, and F. Blaabjerg. Flicker Study on Variable Speed Wind Turbines with Doubly Fed Induction Generators. *IEEE Trans. on Energy Conversion*, 20(4):896–905, Dec. 2005.

[96] G. Chicco, P. Di Leo, I. S. Ilie, and F. Spertino. Operational Characteristics of a 27-MW Wind Farm from Experimental Data. In *Proc.* 14th *IEEE Mediterranean Electrotechnical Conf.*, 5-7 May 2008.

[97] G. Chicco, P. Di Leo, P. Scapino, and F. Spertino. Experimental Analysis of Wind Farms Connected to the High Voltage Grid: The Viewpoint of Power Quality. In *Proc.* 1st *Int. Symp. on Environment Identities and Mediterranean Area*, 9-12 July 2006.

[98] L. S. Christensen, P. E. Sørensen, T. S. Sørensen, and H. K. Nielsen. Evaluation of Measuring Methods for Flicker Emission from Modern Wind Turbine. In *Proc. AEE TECHWINDGRID09-Grid Integration Seminar*, 2009.

[99] L. Meegahapola, T. Littler, B. Fox, J. Kennedy, and D. Flynn. Voltage and Power Quality Improvement Strategy for a DFIG Wind Farm During Variable Wind Conditions. In *Proc. Int. Symp. of Modern Electric Power Systems (MEPS)*, pages 1–6, 2010.

[100] L. Meegahapola, B. Fox, and D. Flynn. Flicker Mitigation Strategy for DFIGs During Variable Wind Conditions. In *Proc. IEEE Power Engineering Society General Meeting*, pages 1–8, July 2010.

[101] C. Vilar, J. Usaola, and H. Amaris. A Frequency Domain Approach to Wind Turbines for Flicker Analysis. *IEEE Trans. on Energy Conversion*, 18(2):335–341, 2003.

[102] M. Wilch, V. S. Pappala, S. N. Singh, and I. Erlich. Reactive Power Generation by DFIG Based Wind Farms with AC Grid Connection. pages 1–10, Sept. 2007.

[103] I. Erlich, W. Winter, and A. Dittrich. Advanced Grid Requirements for the Integration of Wind Turbines into the German Transmission System. In *Proc. IEEE Power and Energy Society General Meeting*, 2006.

[104] Y. S. Kim and D. Won. Mitigation of the Flicker Level of a DFIG Using Power Factor Angle Control. *IEEE Trans. on Power Delivery*, 24(4):2457–2458, OCt. 2009.

[105] M. Armstrong, D. J. Atkinson, C. M. Johnson, and T. D. Abeyasekera. Low Order Harmonic Cancellation in a Grid Connected Multiple Inverter System via Current Control Parameter Randomization. *IEEE Trans. on Power Electronics*, 20(4):885–892, 2005.

[106] A. Kulkarni and V. John. Mitigation of Lower Order Harmonics in a Grid-connected Single-phase PV Inverter. *IEEE Trans. on Power Electronics*, 28(11):5024–5037, Nov. 2013.

[107] J. Schlabbach. Harmonic Current Emission of Photovoltaic Installations Under System Conditions. In *Proc.* 5$^{\text{th}}$ *Int. Conf. on European Electricity Market*, pages 1–5, 2008.

[108] J. Schlabbach, A. Grob, and G. Chicco. Influence of Harmonic System Voltages on the Harmonic Current Emission of Photovoltaic Inverters. In *Proc. Int. Conf. on Engineering, Energy and Electrical Drives*, pages 545–550, 2007.

[109] I. T. Papaioannou, A. S. Bouhouras, A. G. Marinopoulos, M. C. Alexiadis, C. S. Demoulias, and D. P. Labridis. Harmonic Impact of Small Photovoltaic Systems Connected to the LV Distribution Network. In *Proc.* 5th *Int. Conf. on European Electricity Market*, pages 1–6, 2008.

[110] F. Batrinu, G. Chicco, J. Schlabbach, and F. Spertino. Impacts of Grid-connected Photovoltaic Plant Operation on the Harmonic Distortion. In *Proc. IEEE Mediterranean Electrotechnical Conf.*, pages 861–864, 2006.

[111] H. Laukamp E. Caamao-Martn, M. Jantsch, T. Erge, J. Thornycroft, H. De Moor, S. Cobben, D. Suna, and B. Gaiddon. Interaction Between Photovoltaic Distributed Generation and Electricity Networks. *Progress on Photovoltaic: Research and Applications*, 16(7):629–643, 2008.

[112] W. Enders, C. Halter, and P. Wurm. Investigation of Typical Problems of PV-Inverters. In *Proc.* 17th *European Solar Energy Conf. Exhibition*, pages 22–26, 2001.

[113] A. Kempe and U. Schonwandt. EMC of PV-Plants with Line-Commutated Inverters. pages 1343–1346, 13-17 May 1996.

[114] J. Stevens. The Issue of Harmonic Injection from Utility Integrated Photovoltaic Systems: Part 1. The Harmonic Source. *IEEE Trans. on Energy Conversion*, 3(3):507–510, 1988.

[115] J. Stevens. The Issue of Harmonic Injection from Utility Integrated Photovoltaic Systems: Part 2. Study Results. *IEEE Trans. on Energy Conversion*, 3(1):511–515, 1988.

[116] D. Cyganski, J. A. Orr, A. K. Chakravorti, A. E. Emanuel, E. M. Gulachenski, C. E. Root, and R. C. Bellemare. Current and Voltage Harmonic Measurements and Modeling at the Gardner Photovoltaic Project. *IEEE Trans. on Power Delivery*, 3(1):800–809, 1989.

[117] G. A. Vokas and A. V. Machias. Harmonic Voltages and Currents on Two Greek Islands with Potovoltaic Stations: Study and Field Measurements. *IEEE Trans. on Energy Conversion*, 2(2):302–306, 1995.

[118] S. Cobben, B. Gaiddon, and H. Laukamp. Impacts of Photovoltaic Generation on Power Quality in Urban Area with High PV Population . Technical report, PV Upscale, 1990.

[119] R. Yan and T. K. Saha. Voltage Variation Sensitivity Analysis for Unbalanced Distribution Networks due to Photovoltaic Power Fluctuations. *IEEE Trans. on Power Systems*, 27(2):1078–1089, 2012.

[120] K. H. Chua, Y. S. Lim, J. Wong, P. Taylor, E. Morris, and S. Morris. Voltage Unbalance Mitigation in Low Voltage Distribution Networks with Photovoltaic Systems. *Journal of Electronic Science and Technology*, 10(1):495–501, 2012.

[121] F. Shahnia, A. Ghosh, G. Ledwich, and F. Zare. Voltage Unbalance Reduction in Low Voltage Distribution Networks with Rooftop PVs. In *Proc.* 20$^{\text{th}}$ *Australasian Universities Power Engineering Conference (AUPEC)*, pages 1–5, 5-8 Dec. 2010.

[122] U. Ammeter, J. Hanzlik, J. Meyer, and J. Zierlinger. Methods for the Assessment of Emission Levels for Disturbing Installations Connected to Low and Medium Voltage Networks. In *Proc.* 20$^{\text{th}}$ *Int. Conf. on Electricity Distribution*, 8-11 June 2009.

[123] J. Meyer, U. Ammeter, J. Hanzlik, and J. Zierlinger. Methods for the Assesment of Network Disturbances in Distribution Networks. In *Proc.* 13$^{\text{th}}$ *Int. Conf. on Harmonics and Quality of Power*, 28$^{\text{th}}$ Sept. - 1$^{\text{st}}$ Oct. 2008.

[124] P. F. Ribeiro. Common Misapplications of the IEEE 519 Harmonic Standard: Voltage or Current Limits. In *Proc. IEEE Power Engineering Society General Meeting*, 20-24 July 2008.

[125] G. Beaulieu, R. Koch, M. Halpin, and L. Berthet. Recommended Methods of Determining Power Quality Emission Limits for the Installations Connected to EHV, HV, MV and LV Power Systems. In *Proc.* 19th *Int. Conf. on Electricity Distribution*, 21-24 May 2007.

[126] P. M. Anderson. *Analysis of Faulted Power Systems.* John Wiley and Sons, 1995.

[127] IEC 60909-1:Short-circuit currents in three-phase a.c. systems, Ed. 1.2. Technical report, International Electrotechnical Commission, 2001.

[128] Review of Disturbance Emission Assessment Techniques. Technical report, CIGRE/CIRED C4.109 WG Report 468, 2011.

[129] S. Papathanassiou, N. Hatziargyriou, and K. Strunz. A Benchmark Low Voltage Microgrid Network. In *Proc. CIGRE Symposium: Power Systems with Dispersed Generation*, Apr. 2005.

[130] M. C. Simoes and S. M. Deckmann. Flicker Propagation and Attenuation. In *Proc.* 10th *Int. Conf. on Harmonics and Quality of Power*, pages 644–648, 2012.

[131] E. De Jaeger, G. Borloo, and W. Vanceotsem. Flicker Transfer Coefficient from HV to MV and LV Systems. In *Proc.* 14th *Int. Conf. on Electricity Distribution, (CIRED97)*, pages 101–102, 1987.

[132] M. Machmoum, A. Hatoum, and T. Bouaouiche. Flicker Mitigation in a Doubly Fed Induction Generator Wind Turbine System. *Mathematics and Computers in Simulation*, pages 433–445, 2010.

[133] B. Chen, X. Yuan, Y. Xu, X. Wei, Q. Li, R. Sun, J. Song, and J. Zhao. Power Quality Measurement and Comparison Between Two Wind Farms Equipped with FSIG+PMSG and DFIG. In *Proc. Int. Conf. on Power System Technology*, 2010.

[134] R. Piwko, P. Meibom, H. Holttinen, S. Baozhuang, N. Miller, C. Yongning, and W. Weisheng. Penetrating Insights: Lessons Learned from Large-Scale Wind Power Integration. *IEEE Power and Energy Magazine*, 10(2):44–52, March 2012.

[135] S. Tennakoon, S. Perera, and D. Robinson. Flicker Attenuation Part I: Response of Three-phase Induction Motors to Regular Voltage Fluctuations. *IEEE Trans. on Power Delivery*, 23(2):1204–1214, April 2008.

[136] S. Tennakoon, S. Perera, and D. Robinson. Flicker Attenuation Part II: Transfer Coefficients for Regular Voltage Fluctuations in Radial Power Systems with Induction Motor Loads. *IEEE Trans. on Power Delivery*, 23(2):1215–1221, April 2008.

[137] A. D. Hansen, F. Iov, P. E. Sørensen, N. A. Cutululis, C. Jauch, and F. Blaabjerg. Dynamic Wind Turbine Models in Power System Simulation Tool DIgSILENT. Technical report, Risø report Risø-R-1400(EN), 2007.

[138] A. Kusiak, A. Verma, and X. Wei. Wind Turbine Frontier from SCADA. *Wind Systems Magazine*, 3(9):36–39, 2008.

[139] DIgSILENT GmbH. DIgSILENT PowerFactory Version 14.1 User's Manual Volume II. Technical report, DIgSILENT GmbH, May 2011.

[140] AS 60038: Standard Voltages. Technical report, Standards Australia, 2000.

[141] Comprehensive Test Solutions for Domestic Grid-tied Solar Inverters. Technical report, AMETEK Inc, 2010.

[142] P. C. Krause. *Analysis of Electric Machinery.* John Wiley & Sons Inc., 2002.

Appendix A

Network Parameters

The transformer and conductor impedance data for the distribution network discussed in Section 3.5.2

Transformer parameters

- 33/0.4 kV transformer: 400 kVA, (0.004+j0.0155) Ω refereed to LV side (0.01+j0.0387) pu

Conductors: Impedances are as given by Table A.1.

Table A.1: Conductor impedances data of the LV distribution network

Conductor ID	$R_{\text{phase}}/R_{\text{neutral}}$ (Ω/km)	$X_{\text{Phase}}/X_{\text{neutral}}$ (Ω/km)
1	0.284	0.083
2	0.497	0.086
3	0.264	0.071
4	0.397	0.279
5	0.574	0.294
6	1.218	0.318

The network parameters of the HV/MV distribution network in Section 4.2.1 and Section 4.5

Line Parameters:

- The phase impedance matrix ($[Z_{abc}]$/km) of the 12.47 kV asymmetrical distri-

bution line sections in Ω/km

$$\begin{matrix} 0.2494 + j0.8748 & 0.0592 + j0.4985 & 0.0592 + j0.4462 \\ 0.0592 + j0.4985 & 0.2494 + j0.8748 & 0.0592 + j0.4985 \\ 0.0592 + j0.4462 & 0.0592 + j0.4985 & 0.2494 + j0.8748 \end{matrix}$$

- The phase impedance matrix ($[Z_{abc}]$/km) of the 12.47 kV symmetrical distribution line sections in Ω/km

$$\begin{matrix} 0.2494 + j0.8748 & 0.0592 + j0.4811 & 0.0592 + j0.4811 \\ 0.0592 + j0.4811 & 0.2494 + j0.8748 & 0.0592 + j0.4811 \\ 0.0592 + j0.4811 & 0.0592 + j0.4811 & 0.2494 + j0.8748 \end{matrix}$$

Transformer parameters:

- 138/12.47 kV transformer: 20 MVA, 60 Hz, 0.0048+j0.09988 pu impedance
- 12.47/2.3 kV transformer: 5 MVA, 60 Hz, 0.01+j0.07937 pu impedance

Induction motor parameters [142]:

- 2.3 kV, 2250 hp, 60 Hz, r_s=0.0269 Ω, X_{ls}= 0.226 Ω, X_M = 13.04 Ω, X'_{lr} = 0.226 Ω, R'_r = 0.022 Ω and J = 63.87 kg.m^2

The network parameter of the MV distribution network in Section 5.2.1

Line Parameters:

- The phase impedance matrix of the 12.47 kV distribution line sections in Section 5.2.1 in Ω/km

$$\begin{matrix} 0.2494 + j0.8748 & 0.0592 + j0.4811 & 0.0592 + j0.4811 \\ 0.0592 + j0.4811 & 0.2494 + j0.8748 & 0.0592 + j0.4811 \\ 0.0592 + j0.4811 & 0.0592 + j0.4811 & 0.2494 + j0.8748 \end{matrix}$$

Transformer Parameters:

- 138/12.47 kV transformer: 20 MVA, 60 Hz, 0.0048+j0.09988 pu impedance

- 12.47/2.3 kV transformer: 5 MVA, 60 Hz, 0.01+j0.07937 pu impedance

Induction motor parameters:

- 2.3 kV, 2250 HP, 60 Hz, r_s=0.0269 Ω, X_{ls}= 0.226 Ω, X_M = 13.04 Ω, X'_{lr} = 0.226 Ω, R'_r = 0.022 Ω and J = 63.87 kg.m^2

The network parameters of the HV/MV distribution network in Section 6.3 and Section 6.5

Line parameters:

- impedance of the distribution line 0.4242 Ω/km
- length of the distribution line 15 km

Transformer parameters:

- 132/33 kV transformer: 31.5 MVA, 50 Hz, 0.0034+j0.1020 pu impedance
- 132/33 kV transformer: 5 MVA, 50 Hz, 0.0048+j0.0698 pu impedance

Induction motor parameters:

- 11 kV, 50 Hz, 3.3 MW, efficiency: 96.2%, rated speed: 1485 rpm, no. pole pairs: 2, torque at stalling point : 2.68041 p.u. , inertia: 227.8598 kg.m^2

Doubly-fed induction generator:

- 1.5 MW, rated stator voltage: 0.69 kV, rated rotor voltage: 1863 V, rated apparent power: 1667 kW; rated speed: 1800 rpm; no. pole pairs: 2; stator resistance: 0.01 pu; stator reactance: 0.1 pu; rotor reactance: 0.1 pu; rotor resistance: 0.01 pu; magnetizing reactance: 3.5pu; generator inertia: 75 kg.m^2 turbine inertia: 4,052,442 kg.m^2, shaft stiffness: 83,000,000 Nm/rad

Appendix B

Derivation of Equation (4.6)-(4.9)

For the radial distribution line given in Fig. 4.1, the positive-sequence and negative-sequence voltage at the HV busbar and j^{th} busbar are related as,

$$U_{1:\text{HV}} = Z_{10:\text{HV}-j} \cdot I_{0:L_j} + Z_{11:\text{HV}-j} \cdot I_{1:L_j} + Z_{12:\text{HV}-j} \cdot I_{2:L_j} + U_{1:j} \tag{B.1}$$

$$U_{2:\text{HV}} = Z_{20:\text{HV}-j} \cdot I_{0:L_j} + Z_{21:\text{HV}-j} \cdot I_{1:L_j} + Z_{22:\text{HV}-j} \cdot I_{2:L_j} + U_{2:j} \tag{B.2}$$

where; $Z_{10:\text{HV}-j}$ - positive-sequence zero-sequence coupling impedance of the system between the HV busbar and j^{th} busbar, $Z_{20:\text{HV}-\text{j}}$ - negative-sequence zero-sequence coupling impedance of the system between the HV busbar and j^{th} busbar, $Z_{12:\text{HV}-\text{j}}$ - negative-sequence positive-sequence coupling impedance of the system between the HV busbar and j^{th} busbar, and $I_{0:\text{L}_\text{j}}$ - zero-sequence current of the load. Other symbols have their usual meanings as defined in Section 4.2.

In general $Z_{10:\text{HV}-j}$ and $Z_{20:\text{HV}-j}$ are relatively small and $I_{0:L_j} = 0$. Therefore the voltage drop terms $Z_{10:\text{HV}-j} \cdot I_{0:L_j}$ and $Z_{20:\text{HV}-j} \cdot I_{0:L_j}$ can be neglected in (B.1) and (B.2) [128]. Furthermore as $I_{2:L_j}$ is relatively small compared to $I_{1:L_j}$, the voltage drop terms $Z_{11:\text{HV}-j} \cdot I_{1:L_j} >> Z_{12:\text{HV}-j} \cdot I_{2:L_j}$. Hence, $Z_{12:\text{HV}-j} \cdot I_{2:L_j}$ can be neglected in (B.1). Therefore (B.1) and (B.2) can be further simplified as given in (4.7) and (4.9). Similar relationships between the positive-sequence and negative-sequence voltages of HV busbar and MV busbar can be established and are given in (4.6) and

(4.8).

Appendix C

Derivation of Expression for VUF When Two Installations are Operating Simultaneously

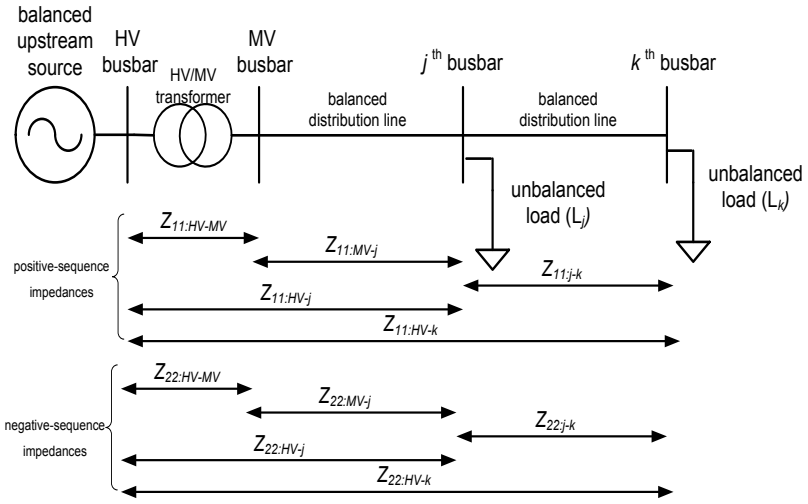

Figure C.1: Radial distribution network with two passive loads connected at j^{th} and k^{th} busbar respectively

Referring to Fig. C.1 the positive-sequence voltages and negative-sequence voltages at the HV busbar, MV busbar, j^{th} and k^{th} busbar are given in (C.1)-(C.6)[1]:

[1]In (C.1)-(C.6) the zero sequence voltages are neglected. Refer to Appendix A for further discussion in this regard.

$$U_{1:\mathrm{HV}} = Z_{11:\mathrm{HV-MV}} \cdot (I_{1:L_j} + I_{1:L_k}) + U_{1:\mathrm{MV}} \tag{C.1}$$

$$U_{1:\mathrm{MV}} = Z_{11:\mathrm{MV}-j} \cdot (I_{1:L_j} + I_{1:L_k}) + U_{1:j} \tag{C.2}$$

$$U_{1:j} = Z_{11:j-k} \cdot (I_{1:L_k}) + U_{1:k} \tag{C.3}$$

$$U_{2:\mathrm{HV}} = Z_{22:\mathrm{HV-MV}} \cdot (I_{2:L_j} + I_{2:L_k}) + U_{2:\mathrm{MV}} \tag{C.4}$$

$$U_{2:\mathrm{MV}} = Z_{22:\mathrm{MV}-j} \cdot (I_{2:L_j} + I_{2:L_k}) + U_{2:j} \tag{C.5}$$

$$U_{2:j} = Z_{22:j-k} \cdot (I_{2:L_k}) + U_{2:k} \tag{C.6}$$

where;

$U_{1:\mathrm{HV}}$ and $U_{2:\mathrm{HV}}$ are the positive-sequence and negative-sequence voltages at the HV busbar respectively. Note that the $U_{2:\mathrm{HV}}$ is equal to zero, as the source connected at the HV busbar is balanced,

$U_{1:\mathrm{MV}}$ and $U_{2:\mathrm{MV}}$ are the positive-sequence and negative-sequence voltages at the MV busbar respectively,

$U_{1:j}$ and $U_{2:j}$ are the positive-sequence and negative-sequence voltages at the j^{th} busbar respectively,

$U_{1:k}$ and $U_{2:k}$ are the positive-sequence and negative-sequence voltages at the k^{th} busbar respectively,

$I_{1:L_j}$ and $I_{2:L_j}$ are the positive-sequence and negative-sequence currents of the load which is connected at the j^{th} busbar respectively,

$I_{1:L_k}$ and $I_{2:L_k}$ are the positive-sequence and negative-sequence currents of the load which is connected at the k^{th} busbar respectively.

The positive-sequence load currents, $I_{1:L_j}$ and $I_{1:L_j}$, and the negative-sequence load currents, $I_{2:L_j}$ and $I_{2:L_k}$, can be given by (C.7)-(C.10):

$$I_{1:L_j} = \frac{U_{1:j}}{Z_{11:L_j}} \tag{C.7}$$

$$I_{2:L_j} = \boldsymbol{CUF_{L_j}} \cdot \frac{U_{1:j}}{Z_{11:L_j}} \tag{C.8}$$

$$I_{1:L_k} = \frac{U_{1:k}}{Z_{11:L_k}} \tag{C.9}$$

$$I_{2:L_k} = \boldsymbol{CUF_{L_k}} \cdot \frac{U_{1:k}}{Z_{11:L_j}} \tag{C.10}$$

where;

$Z_{11:L_j}$ and $Z_{11:L_k}$ are the positive-sequence impedances loads which are connected at the j^{th} and k^{th} busbar;

$\boldsymbol{CUF_{L_j}}$ and $\boldsymbol{CUF_{L_k}}$ are the complex CUFs of loads which are connected at j^{th} and k^{th} busbar.

Using (C.1)-(C.10), the total VUF at the MV, j^{th} and k^{th} busbars can be shown as given by Table 4.2.

Appendix D

Derivation of Equations (4.25)-(4.30)

D.1 Scenario I: An unbalanced passive load and an induction motor are connected to the j^{th} and k^{th} busbars respectively

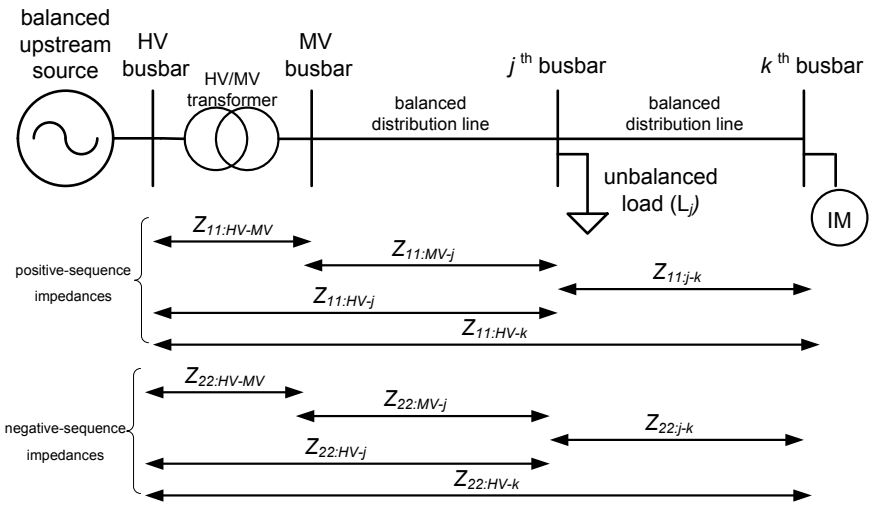

Figure D.1: Radial distribution network with an unbalanced passive load and an induction motor connected at j^{th} and k^{th} busbar respectively

Referring to Fig. D.1, the positive-sequence voltages and negative-sequence voltages at the HV busbar, MV busbar, j^{th} busbar, and k^{th} busbar are given in (D.1)-

(D.6):

$$U_{1:\mathrm{HV}} = Z_{11:\mathrm{HV-MV}} \cdot (I_{1:L_j} + I_{1:m_k}) + U_{1:\mathrm{MV}} \tag{D.1}$$

$$U_{1:\mathrm{MV}} = Z_{11:\mathrm{MV}-j} \cdot (I_{1:L_j} + I_{1:m_k}) + U_{1:j} \tag{D.2}$$

$$U_{1:j} = Z_{11:j-k} \cdot (I_{1:m_k}) + U_{1:k} \tag{D.3}$$

$$U_{2:\mathrm{HV}} = Z_{22:\mathrm{HV-MV}} \cdot (I_{2:L_j} + I_{2:m_k}) + U_{2:\mathrm{MV}} \tag{D.4}$$

$$U_{2:\mathrm{MV}} = Z_{22:\mathrm{MV}-j} \cdot (I_{2:L_j} + I_{2:m_k}) + U_{2:j} \tag{D.5}$$

$$U_{2:j} = Z_{22:j-k} \cdot (I_{2:m_k}) + U_{2:k} \tag{D.6}$$

where;

$U_{1:\mathrm{HV}}$ and $U_{2:\mathrm{HV}}$ are the positive-sequence and negative-sequence voltages at the HV busbar respectively. Note that the $U_{2:\mathrm{HV}}$ is equal to zero, as the source connected at the HV busbar is balanced,

$U_{1:\mathrm{MV}}$ and $U_{2:\mathrm{MV}}$ are the positive-sequence and negative-sequence voltages at the MV busbar respectively,

$U_{1:j}$ and $U_{2:j}$ are the positive-sequence and negative-sequence voltages at the j^{th} busbar respectively,

$U_{1:k}$ and $U_{2:k}$ are the positive-sequence and negative-sequence voltages at the k^{th} busbar respectively,

$I_{1:L_j}$ and $I_{2:L_j}$ are the positive-sequence and negative-sequence currents of the load which is connected at the j^{th} busbar respectively,

$I_{1:m_k}$ and $I_{2:m_k}$ are the positive-sequence and negative-sequence currents of the induction motor which is connected at the k^{th} busbar respectively.

The positive-sequence load current, $I_{1:L_j}$, the negative-sequence load current, $I_{2:L_j}$, the positive-sequence induction motor current, $I_{1:m_k}$, and the negative-sequence induction motor current, $I_{2:m_k}$, can be given by (D.7)-(D.10):

$$I_{1:L_j} = \frac{U_{1:j}}{Z_{11:L_j}} \tag{D.7}$$

$$I_{2:L_j} = \boldsymbol{CUF_{L_j|IM}} \cdot \frac{U_{1:j}}{Z_{11:L_j}} \tag{D.8}$$

$$I_{1:m_k} = \frac{U_{1:k}}{Z_{11:m_k}} \tag{D.9}$$

$$I_{2:m_k} = \frac{U_{2:k}}{Z_{22:m_k}} \tag{D.10}$$

where;

$Z_{11:m_k}$ is the positive-sequence impedance of the induction motor connected to the k^{th} busbar,

$Z_{22:m_k}$ is the negative-sequence impedance of the induction motor connected to the k^{th} busbar,

$Z_{11:L_j}$ is the positive-sequence impedance of the load which is connected at the j^{th} busbar,

$\boldsymbol{CUF_{L_j|IM}}$ is the complex CUF of the load which is connected at the j^{th} busbar, when an induction motor is connected to an adjacent busbar,

$CUF_{L_j|IM}$ is the magnitude of the CUF of the load which is connected at the j^{th} busbar, when an induction motor is connected to an adjacent busbar.

Substitute (D.10) in (D.6), and rearrange:

$$U_{2:j} = \frac{Z_{22:j-k} + Z_{22:m_k}}{Z_{22:m_k}} \cdot U_{2:k} \tag{D.11}$$

Considering $Z_{22:\text{HV}-\text{MV}} + Z_{22:\text{MV}-j} = Z_{22:\text{HV}-j}$ and $U_{2:\text{HV}} = 0$ (as the upstream HV

busbar is balanced), the addition of (D.4) in (D.5) can be written as (D.12)

$$U_{2:\mathrm{HV}} = Z_{22:\mathrm{HV}-j} \cdot (I_{2:L_j} + I_{2:m_k}) + U_{2:j} = 0 \tag{D.12}$$

Substitute $I_{2:L_j}$ and $I_{2:m_k}$ in (D.12) with (D.8)and (D.10), and rearrange:

$$0 = \frac{Z_{22:\mathrm{HV}-j}}{Z_{11:L_j}} \cdot \boldsymbol{CUF_{L_j|IM}} \cdot U_{1:j} + \frac{Z_{22:\mathrm{HV}-j}}{Z_{22:m_k}} \cdot U_{2:k} + U_{2:j} \tag{D.13}$$

Substitute (D.11) in (D.13), and rearrange:

$$VUF_{L_j|IM} = \left|\frac{U_{2:j}}{U_{1:j}}\right| = \left|\frac{Z_{22:j-k} + Z_{22:m_k}}{Z_{22:\mathrm{HV}-k} + Z_{22:m_k}} \cdot \frac{Z_{11:\mathrm{HV}-j}}{Z_{11:L_j}}\right| \cdot CUF_{L_j|IM} \tag{D.14}$$

Similarly, $VUF_{\mathrm{MV}|IM}$, can be shown as (D.15):

$$VUF_{\mathrm{MV}|IM} = \left|\frac{\left(\frac{(1-K_2)\cdot Z_{11:\mathrm{MV}-j} - K_2 \cdot Z_{11:\mathrm{HV}-\mathrm{MV}}}{Z_{11:L_j}}\right)}{\frac{Z_{11:\mathrm{MV}-j}+Z_{11:L_j}}{Z_{11:L_j}} + \frac{Z_{11:\mathrm{MV}-j}}{Z_{22:j-k}+Z_{22:m_k}}}\right| \cdot CUF_{L_j|IM} \tag{D.15}$$

$$K_2 = \frac{Z_{22:\mathrm{MV}-k} + Z_{22:m_k}}{Z_{22:\mathrm{HV}-k} + Z_{22:m_k}} \tag{D.16}$$

where;

$VUF_{L_j|IM}$ is the VUF at the POC of the load connected to the j^{th} busbar, when an induction motor is connected to k^{th} busbar,

$VUF_{\mathrm{MV}|IM}$ is the VUF of MV busbar, when an induction motor is connected to k^{th} busbar.

D.2 Scenario II: An induction motor and an unbalanced passive load are connected to the j^{th} and k^{th} busbars respectively

Referring to Fig. D.2, the positive-sequence voltages and negative-sequence voltages at the HV busbar, MV busbar, j^{th} and k^{th} busbar are given in (D.17)-(D.22):

$$U_{1:\mathrm{HV}} = Z_{11:\mathrm{HV}-\mathrm{MV}} \cdot (I_{1:m_j} + I_{1:L_k}) + U_{1:\mathrm{MV}} \tag{D.17}$$

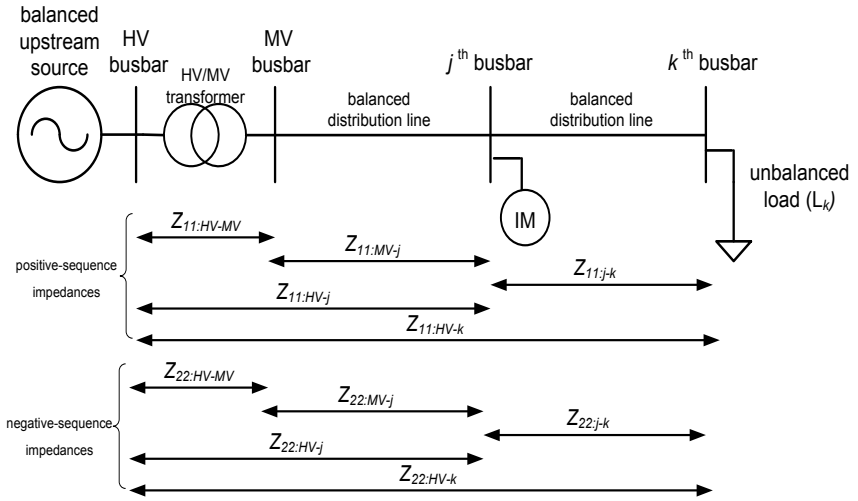

Figure D.2: Radial distribution network with an induction motor and an unbalanced passive load connected at j^{th} and k^{th} busbar respectively

$$U_{1:\text{MV}} = Z_{11:\text{MV}-j} \cdot (I_{1:m_j} + I_{1:L_k}) + U_{1:j} \tag{D.18}$$

$$U_{1:j} = Z_{11:j-k} \cdot (I_{1:L_k}) + U_{1:k} \tag{D.19}$$

$$U_{2:\text{HV}} = Z_{22:\text{HV}-\text{MV}} \cdot (I_{2:m_j} + I_{2:L_k}) + U_{2:\text{MV}} \tag{D.20}$$

$$U_{2:\text{MV}} = Z_{22:\text{MV}-j} \cdot (I_{2:m_j} + I_{2:L_k}) + U_{2:j} \tag{D.21}$$

$$U_{2:j} = Z_{22:j-k} \cdot (I_{2:L_k}) + U_{2:k} \tag{D.22}$$

The positive-sequence induction motor current, $I_{1:m_j}$, the negative-sequence induction motor current, $I_{2:m_j}$, positive-sequence load current, $I_{1:L_k}$ and the negative-sequence load current, $I_{2:L_k}$, can be given by (D.23)-(D.26):

$$I_{1:m_j} = \frac{U_{1:j}}{Z_{11:m_j}} \tag{D.23}$$

$$I_{2:m_j} = \frac{U_{2:j}}{Z_{22:m_j}} \tag{D.24}$$

$$I_{1:L_k} = \frac{U_{1:k}}{Z_{11:L_k}} \tag{D.25}$$

$$I_{2:L_k} = \boldsymbol{CUF_{L_j|IM}} \cdot \frac{U_{1:k}}{Z_{11:L_k}} \tag{D.26}$$

where;

$Z_{11:m_j}$ is the positive-sequence impedance of the induction motor connected to the j^{th} busbar,

$Z_{22:m_j}$ is the negative-sequence impedance of the induction motor connected to the j^{th} busbar,

$Z_{11:L_k}$ is the positive-sequence impedance of the load which is connected at the k^{th} busbar,

$\boldsymbol{CUF_{L_k|IM}}$ is the complex CUF of the load which is connected at the k^{th} busbar, when an induction motor is connected to an adjacent busbar,

$CUF_{L_k|IM}$ is the magnitude of CUF of the load which is connected at the k^{th} busbar, when an induction motor is connected to an adjacent busbar.

Using (D.17)-(D.26), VUF_{L_k} and VUF_{MV} can be shown as (D.27) and (D.29) respectively.

$$VUF_{L_k|IM} = \left| \frac{K_3 \cdot (Z_{11:\text{HV}-j}) + Z_{11:j-k}}{Z_{11:L_k}} \right| \cdot CUF_{L_k|IM} \tag{D.27}$$

$$K_3 = \frac{Z_{22:m_j}}{Z_{22:\text{HV}-j} + Z_{22:m_j}} \tag{D.28}$$

$$VUF_{\text{MV}|IM} = \left| \frac{\left(\frac{(1-K_4)\cdot Z_{11:\text{MV}-j} - K_4 \cdot Z_{11:\text{HV}-\text{MV}}}{Z_{11:j-k}+Z_{11:L_k}}\right)}{\frac{Z_{11:\text{MV}-j}+Z_{11:m}}{Z_{11:m}} + \frac{Z_{11:\text{MV}-j}}{Z_{22:j-k}+Z_{22:L_k}}} \right| \cdot CUF_{L_k|IM} \tag{D.29}$$

$$K_4 = \frac{Z_{22:\mathrm{MV}-j} + Z_{22:m_j}}{Z_{22:\mathrm{HV}-j} + Z_{22:m_j}} \tag{D.30}$$

where;

$VUF_{L_k|IM}$ is the VUF at the POC of the load connected to the k^{th} busbar, when an induction motor is connected to j^{th} busbar,

$VUF_{\mathrm{MV}|IM}$ is the VUF of MV busbar, when an induction motor is connected to j^{th} busbar.

D.3 Scenario III: An unbalanced passive load and an induction motor are connected to the j^{th} and k^{th} busbars which are located in parallel feeders

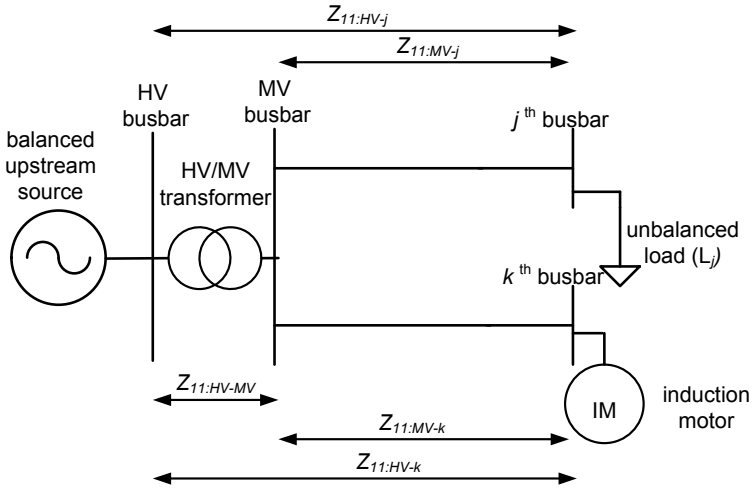

Figure D.3: An unbalanced passive load and an induction motor are connected to two parallel feeders.

Referring to Fig. D.3, the positive-sequence voltages and negative-sequence voltages at the HV busbar, MV busbar, j^{th} and k^{th} busbar are given in (D.31)-(D.40):

$$U_{1:\mathrm{HV}} = Z_{11:\mathrm{HV}-\mathrm{MV}} \cdot (I_{1:L_j} + I_{1:m_k}) + U_{1:\mathrm{MV}} \tag{D.31}$$

$$U_{1:\mathrm{MV}} = Z_{11:\mathrm{MV}-j} \cdot (I_{1:L_j}) + U_{1:j} \tag{D.32}$$

$$U_{1:\mathrm{MV}} = Z_{11:\mathrm{MV}-k} \cdot (I_{1:m_k}) + U_{1:k} \tag{D.33}$$

$$U_{2:\mathrm{HV}} = Z_{22:\mathrm{HV}-\mathrm{MV}} \cdot (I_{2:L_j} + I_{2:m_k}) + U_{2:\mathrm{MV}} \tag{D.34}$$

$$U_{2:\mathrm{MV}} = Z_{22:\mathrm{MV}-j} \cdot (I_{2:L_j}) + U_{2:j} \tag{D.35}$$

$$U_{2:\mathrm{MV}} = Z_{22:\mathrm{MV}-k} \cdot (I_{2:m_k}) + U_{2:k} \tag{D.36}$$

The positive-sequence load current, $I_{1:L_j}$, the negative-sequence load current, $I_{2:L_j}$, the positive-sequence induction motor current, $I_{1:m_k}$, and the negative-sequence induction motor current, $I_{2:m_k}$, can be given by (D.37)-(D.40):

$$I_{1:L_j} = \frac{U_{1:j}}{Z_{11:L_j}} \tag{D.37}$$

$$I_{2:L_j} = \boldsymbol{CUF_{L_j|IM}} \cdot \frac{U_{1:j}}{Z_{11:L_j}} \tag{D.38}$$

$$I_{1:m_k} = \frac{U_{1:k}}{Z_{11:m_k}} \tag{D.39}$$

$$I_{2:m_k} = \frac{U_{2:k}}{Z_{22:m_k}} \tag{D.40}$$

where;

$Z_{11:m_k}$ is the positive-sequence impedance of the induction motor connected to the k^{th} busbar,

$Z_{22:m_k}$ is the negative-sequence impedance of the induction motor connected to the k^{th} busbar,

$Z_{11:L_j}$ is the positive-sequence impedance of the load which is connected at the j^{th}

busbar,

$\boldsymbol{CUF_{L_j|IM}}$ is the complex CUF of the load which is connected at the j^{th} busbar, when an induction motor is connected to an adjacent busbar,

$CUF_{L_j|IM}$ is the magnitude of CUF of the load which is connected at the j^{th} busbar, when an induction motor is connected to an adjacent busbar.

Using (D.31)-(D.40), VUF_{L_k} and VUF_{MV} can be shown as (D.41) and (D.42) respectively.

$$VUF_{L_j|IM} = \left| \frac{K_5 \cdot Z_{11:\text{HV}-\text{MV}} + Z_{11:\text{MV}-j}}{Z_{11:L_j}} \right| \cdot CUF_{L_j|IM} \tag{D.41}$$

$$VUF_{\text{MV|IM}} = \left| \frac{K_5 \cdot Z_{11:\text{HV}-\text{MV}}}{Z_{11:L_j}} \cdot \frac{Z_{11:L_j}}{Z_{11:L_j} + Z_{11:\text{MV}-j}} \right| \cdot CUF_{L_j|IM} \tag{D.42}$$

$$K_5 = \frac{Z_{22:\text{MV}-k} + Z_{22:m_k}}{Z_{22:\text{HV}-k} + Z_{22:m_k}} \tag{D.43}$$

where;

$VUF_{L_j|IM}$ is the VUF at the POC of the load connected to the j^{th} busbar, when an induction motor is connected to k^{th} busbar,

$VUF_{\text{MV}|IM}$ is the VUF of MV busbar, when an induction motor is connected to k^{th} busbar.

Appendix E

VU Emission Allocation Methodology Based on Voltage Droop for Asymmetrical Distribution Lines

A general approach for VU emission allocation for customers connected to asymmetrical radial distribution networks is developed following the concept of voltage droop in this section. For an unbalanced load i connected to an asymmetrical distribution network, the negative-sequence voltage drop at the PCC $U_{2:i}$, can be written as:

$$U_{2:i} = Z_{22:i} \cdot I_{2:i} + Z_{21:i} \cdot I_{1:i} \tag{E.1}$$

where;

$Z_{11:i}$ is the positive-sequence Thévenin impedance at the POC of the installation

$Z_{22:i}$ is the negative-sequence Thévenin impedance at the POC of the installation

$Z_{21:i}$ is the negative-sequence positive-sequence coupling impedance the POC of the installation

$I_{1:i}$ is the positive-sequence current of the installation

$I_{2:i}$ is the negative-sequence current of the installation

Assuming no diversity, the negative-sequence current emission allocation, $E_{I_2:i}$, can be given by (E.2):

$$E_{I_2:i} = k_u \cdot \frac{S_i}{Z_{11:i}} - \frac{Z_{21:i}}{Z_{11:i}} \cdot S_i \tag{E.2}$$

Substituting (E.2) and (5.13) in (E.1) and considering positive-sequence impedance $Z_{11:i}$ is equal to the negative-sequence impedance $Z_{22:i}$, $U_{2:i}$, can be expressed as (E.7):

$$\begin{aligned} U_{2:i} &= k_u \cdot (Z_{11:i} \cdot S_i) \\ &= k_u \cdot U_{1,\text{droop}:i} \end{aligned} \tag{E.3}$$

where; k_u is termed the allocation constant and S_i is the MVA capacity of the installation.

When aggregated across all customers the total negative-sequence voltage at the extremity of the power system becomes limited by the maximum positive-sequence voltage droop. The total contribution from all the loads to the negative-sequence voltage in the network $\sum V_{2:i}$ can be written as (E.4),

$$\sum U_{2:i} = k_u \cdot U_{1,\text{droop}} \tag{E.4}$$

where $U_{1,\text{droop}}$ is positive-sequence voltage droop of the power system.

In order to to ensure that the maximum negative-sequence voltage at the extremity of the power system is acceptable, the total contribution from all the loads to the negative-sequence voltage $\sum U_{2:i}$, should be less than the planning level of the network (i.e. $\sum U_{2:i} \leq L_{u:\text{LV}}$). Hence, k_u can be evaluated, subjected to (E.5):

$$k_u \cdot U_{1:\text{droop}} \leq L_{u:\text{LV}} \tag{E.5}$$

In order to consider the diversity among different loads, the negative-sequence current emission allocation in (5.15) can be modified as (E.6):

$$E_{I_2:i} = k_u \cdot \frac{S_i^{1/\alpha}}{Z_{11:i}^{1-1/\alpha}} - \frac{Z_{21:i}}{Z_{11:i}} \cdot S_i \tag{E.6}$$

Accordingly, the negative-sequence voltage drop at the POC of the installation can be written as (E.7):

$$U_{2:i} = k_u \cdot U_{1,\text{droop}:i}^{1/\alpha} \tag{E.7}$$

When aggregated across all loads, total negative-sequence voltage at the extremity ($\sum U_{2,i} = k_u \cdot U_{1,\text{droop}}^{1/\alpha}$) of the power system should be less than the planning level of the network. Hence, k_u can be evaluated as (E.8):

$$k_u \cdot U_{1,\text{droop}}^{1/\alpha} \leq L_{u:\text{LV}} \tag{E.8}$$

Application of the proposed VU emission allocation methodology can be demonstrated employing the radial distribution network discussed in Section 5.2.1. The distribution line is now assumed to be asymmetrical. The phase impedance matrix ($[Z_{abc}]$/km) of the 12.47 kV asymmetrical distribution line sections in Ω/km is as follows.

$$\begin{matrix} 0.2494 + j0.8748 & 0.0592 + j0.4811 & 0.0592 + j0.4811 \\ 0.0592 + j0.4811 & 0.2494 + j0.8748 & 0.0592 + j0.4811 \\ 0.0592 + j0.4811 & 0.0592 + j0.4811 & 0.2494 + j0.8748 \end{matrix}$$

Each installation is allocated a negative-sequence current emission according to (E.6) and the allocation constant is determined by (E.8). The system voltage droop is assumed to be 30%. Table E.1 provides the emission allocation limit for each installation connected to the radial distribution network.

Fig E.1 provides a comparison between the emission limits for each unbalanced installation connected to the distribution network given in Section 5.2.1 when; (a) the distribution line is assumed to be symmetrical and (b) the distribution line is assumed to be asymmetrical. As expected, the negative-sequence current allocation is less, when the distribution lines are asymmetrical compared to case where the

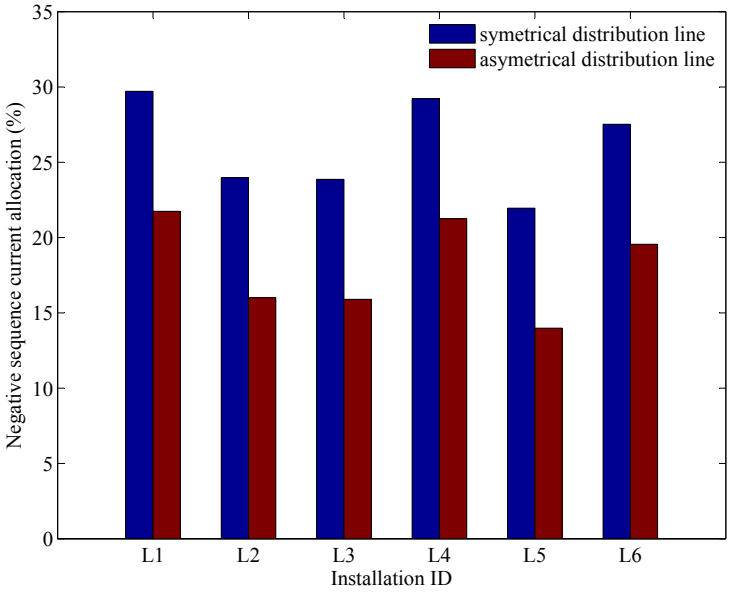

Figure E.1: VU emission limits for installations connected to radial distribution network given in Fig. 5.2 when (a) distribution lines are symmetrical (b) distribution lines are asymmetrical

distribution lines are symmetrical, due to the negative-sequence voltage contribution from line asymmetry.

Table E.1: Negative-sequence current allocation for installations connected to MV distribution network with asymmetrical distribution lines

Installation ID	Negative-sequence current allocation (%)
L1	21.7438
L2	16.0050
L3	15.8969
L4	21.2556
L5	21.9551
L6	19.5524

Appendix F

Derivation of Relative Voltage Fluctuation Transfer Coefficient for Distribution System Loads

F.1 Constant Power Load

Assume that a constant power load with a MVA capacity of $P_L + jQ_L$ is connected to a fluctuating voltage source via a line having an impedance of $R_S + jX_S$ as shown in Fig. F.1. The steady-state source voltage phasor, $\mathbf{V_S}$,) and load voltage phasor, $\mathbf{V_L}$, can be given by (F.1):

$$\mathbf{V_S} = \mathbf{V_L} + (R_S + jX_S)\mathbf{I_L} \tag{F.1}$$

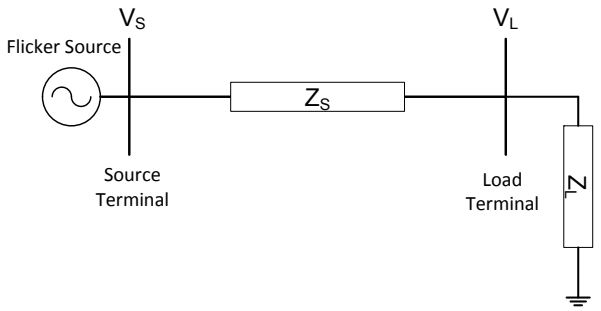

Figure F.1: Radial power system for relative voltage fluctuation transfer coefficient derivation

$$\mathbf{I_L} = (P_L - jQ_L)/\mathbf{V_L^*} \tag{F.2}$$

Now assume that $\mathbf{V_S}$ fluctuates by $\mathbf{\Delta V_S}$. Accordingly, the load voltage fluctuates by $\Delta\mathbf{V_L}$. Therefore,

$$\mathbf{V_S} + \mathbf{\Delta V_S} = \mathbf{V_L} + \mathbf{\Delta V_L} + (R_S + jX_S)\mathbf{I'_L} \tag{F.3}$$

$$\mathbf{I'_L} = (P_L - jQ_L)/(\mathbf{V_L} + \mathbf{\Delta V_L})^* \tag{F.4}$$

Take $\mathbf{V_L^*}$ as the reference, therefore, $\mathbf{V_L^*} = \mathbf{V_L} = V_L$. Assuming that $\mathbf{V_L}$, $\mathbf{V_S}$, $\mathbf{\Delta V_S}$ and $\Delta\mathbf{V_L}$ are in phase, ΔV_S can be written as (F.5):

$$\Delta V_S = \Delta V_L + Re((R_S + jX_S)\mathbf{\Delta I_L}) \tag{F.5}$$

where $\mathbf{\Delta I_L}$ can be written as (F.6):

$$\mathbf{\Delta I_L} = \mathbf{I_L} - \mathbf{I'_L} = \frac{P_L - jQ_L}{V_L} - \frac{P_L - jQ_L}{V_L + \Delta V_L} \tag{F.6}$$

Note that the active power and reactive power of the load do not change under pre and post voltage fluctuation conditions.

Since $V_L \gg \Delta V_L$, $(V_L^2 + V_L \cdot \Delta V_L) \approx V_L^2$. Hence,

$$\mathbf{\Delta I_L} = (P_L - jQ_L)(\frac{-\Delta V_L}{V_L^2}) \tag{F.7}$$

Substitute (F.7) in (F.5). Since ΔV_S and ΔV_L are in phase, (F.5) can be rearrange as:

$$\left|\frac{\Delta V_L}{\Delta V_S}\right| = \left|\frac{1}{1 - \frac{P_L \cdot R_S + Q_L \cdot X_S}{V_L^2}}\right| \tag{F.8}$$

Furthermore, substitute (F.2) in (F.1) and rearrange (F.1):

$$\left|\frac{V_S}{V_L}\right| = \left|1 + \frac{P_L \cdot R_S + Q_L \cdot X_S}{V_L^2}\right| \tag{F.9}$$

Therefore, the relative voltage fluctuation coefficient can be written as (F.10):

$$T_{\Delta \mathrm{V:S-L}} = \frac{\left|\frac{\Delta V_L}{V_L}\right|}{\left|\frac{\Delta V_S}{V_S}\right|} = \left|\frac{1 + \frac{P_L \cdot R_S + Q_L \cdot X_S}{V_L^2}}{1 - \frac{P_L \cdot R_S + Q_L \cdot X_S}{V_L^2}}\right| \tag{F.10}$$

F.2 Constant Current Load

If the load connected to the load busbar is a constant current load, from (F.5) the voltage at the load busbar, ΔV_L, will be equal to the voltage at the load busbar, ΔV_S, as $\mathbf{\Delta I_L} = 0$.

$$\Delta V_L = \Delta V_S \tag{F.11}$$

Hence, from (F.9) and (F.11), $T_{\Delta \mathrm{V_{S-L}}}$ can be written as (F.12):

$$T_{\Delta \mathrm{V:S-L}} = \frac{\left|\frac{\Delta V_L}{V_L}\right|}{\left|\frac{\Delta V_S}{V_S}\right|} = \left|1 + \frac{P_L \cdot R_S + Q_L \cdot X_S}{V_L^2}\right| \tag{F.12}$$

F.3 Constant Impedance Load

If the load connected to the load busbar is a constant impedance load, the change in the load current, $\mathbf{\Delta I_L}$, can be given by (F.13):

$$\mathbf{\Delta I_L} = \frac{P_L - jQ_L}{\mathbf{V_L}} - \frac{P'_L - jQ'_L}{\mathbf{V_L} + \mathbf{\Delta V_L}} \tag{F.13}$$

where; P'_L and Q'_L are the active power and reactive power of the load, after the voltage fluctuation. Take $\mathbf{V_L^*}$ as the reference, therefore, $\mathbf{V_L^*} = \mathbf{V_L} = V_L$. Assuming that $\mathbf{V_L}$, $\mathbf{V_S}$, $\mathbf{\Delta V_S}$ and $\mathbf{\Delta V_L}$ are in phase, $\mathbf{\Delta I_L}$ can be written as (F.14):

$$\mathbf{\Delta I_L} = \frac{P_L - jQ_L}{V_L} - \frac{P'_L - jQ'_L}{V_L + \Delta V_L} \tag{F.14}$$

Furthermore, P'_L and Q'_L can be given by (F.15) and (F.16):

$$\frac{P'_L}{P_L} = \left(\frac{V_L + \Delta V_L}{V_L}\right)^2 \tag{F.15}$$

$$\frac{Q'_L}{Q_L} = \left(\frac{V_L + \Delta V_L}{V_L}\right)^2 \tag{F.16}$$

Using (F.15) and (F.16), $P'_L - jQ'_L$ can be written as (F.17):

$$P'_L - jQ'_L = \left(\frac{V_L + \Delta V_L}{V_L}\right)^2 \cdot (P_L - jQ_L) \tag{F.17}$$

Substitute (F.17) in (F.14) and neglecting the second order terms, $\mathbf{\Delta I_L}$ can be written as (F.18):

$$\mathbf{\Delta I_L} = P_L - jQ_L \cdot \frac{\Delta V_L}{V_L} \tag{F.18}$$

Substitute (F.18) in (F.5), and rearrange:

$$\left|\frac{\Delta V_L}{\Delta V_S}\right| = \left|\frac{1}{1 + \frac{P_L \cdot R_S + Q_L \cdot X_S}{V_L^2}}\right| \tag{F.19}$$

Therefore, referring to (F.19) and (F.9), $T_{\Delta \mathrm{V_{S-L}}}$ for a constant impedance busbar can be written as (F.20):

$$T_{\Delta \mathrm{V:S-L}} = \frac{\left|\frac{\Delta V_L}{V_L}\right|}{\left|\frac{\Delta V_S}{V_S}\right|} = \left|\frac{1 + \frac{P_L \cdot R_S + Q_L \cdot X_S}{V_L^2}}{1 + \frac{P_L \cdot R_S + Q_L \cdot X_S}{V_L^2}}\right| = 1 \tag{F.20}$$

F.4 ZIP

Assume a mix of parallel connected constant power, constant current and constant impedance loads connected at the load busbar. The constant power, constant current and constant impedance of the load are $K_1 \cdot (P_L + jQ_L)$, $K_2 \cdot (P_L + jQ_L)$ and $K_3 \cdot (P_L + jQ_L)$ respectively. K_1, K_2 and K_3 are ratios of capacity of constant power, constant current and constant impedance loads to the total capacity of the load respectively and $K_1 + K_2 + K_3 = 1$. Now assume that $\mathbf{V_S}$ fluctuates by $\mathbf{\Delta V_S}$. Accordingly, the load voltage fluctuates by $\Delta \mathbf{V_L}$. The source voltage fluctutaion ΔV_S and the load current fluctuation, $\mathbf{\Delta I_L}$ can be given by (F.21) and (F.22) respectively.

$$\Delta V_S = \Delta V_L + Re((R_S + jX_S)\mathbf{\Delta I_L}) \tag{F.21}$$

$$\mathbf{\Delta I_L} = \mathbf{\Delta I_{PQ}} + \mathbf{\Delta I_I} + \mathbf{\Delta I_Z} \tag{F.22}$$

where; $\mathbf{\Delta I_{PQ}}$, $\mathbf{\Delta I_I}$ and $\mathbf{\Delta I_Z}$ are the fluctuation of current of the load corresponding to the constant power, constant current and constant impedance component of the load. Referring to Sections F.1-F.3, $\mathbf{\Delta I_{PQ}}$, $\mathbf{\Delta I_I}$ and $\mathbf{\Delta I_Z}$ can be written as (F.23)-(F.25) respectively.

$$\mathbf{\Delta I_{PQ}} = K_1 \cdot (P_L - jQ_L)(\frac{-\Delta V_L}{V_L^2}) \tag{F.23}$$

$$\mathbf{\Delta I_I} = 0 \tag{F.24}$$

$$\mathbf{\Delta I_Z} = K_1 \cdot (P_L - jQ_L)(\frac{\Delta V_L}{V_L^2}) \tag{F.25}$$

Substitute (F.23)-(F.25) in (F.21) and rearrange:

$$\left|\frac{\Delta V_L}{\Delta V_S}\right| = \left|\frac{1}{1 - \frac{(K_1 - K_3)\cdot(P_L \cdot R_S + Q_L \cdot X_S)}{V_L^2}}\right| \tag{F.26}$$

Therefore, referring to (F.26) and (F.9), $T_{\Delta \mathrm{V_{S-L}}}$ for a constant impedance busbar can be written as (F.27):

$$T_{\Delta \mathrm{V:S-L}} = \frac{\left|\frac{\Delta V_L}{V_L}\right|}{\left|\frac{\Delta V_S}{V_S}\right|} = \left|\frac{1 + \frac{P_L \cdot R_S + Q_L \cdot X_S}{V_L^2}}{1 - \frac{(K_1 - K_3)\cdot(P_L \cdot R + Q_L \cdot X)}{V_L^2}}\right| \tag{F.27}$$

Appendix G

Flicker Emission Analysis of Photovoltaic Systems Connected to Distribution Networks

With the increased growth of PV systems in the LV distribution networks, voltage fluctuations leading to flicker is expected to become a main power quality concern to DNSPs. In the work presented in this Appendix, voltage fluctuations and flicker emission from PV systems due to passing clouds and temperature variations are investigated employing a simulation model of a network feeder with multiple PV systems

G.1 Photovoltaic System Model

A simulation model of a PV system consisting of 27, 185 W PV panels, connected to a 6 kVA inverter was developed using DIgSILENT PowerFactory software. A schematic diagram of the PV system simulation model is shown in Fig. G.1 where, V_{array}, I_{array}, V_{dc}, V_{dc_ref}, I_{d_ref}, I_{q_ref}, V_{grid}, P_{grid}, Q_{grid}, E, and T are the output voltage of the PV array, output current of the PV array, DC-link voltage, DC-link reference voltage, d-axis current reference, q-axis current reference, AC voltage of the grid, active power output of the PV system, reactive power output of the

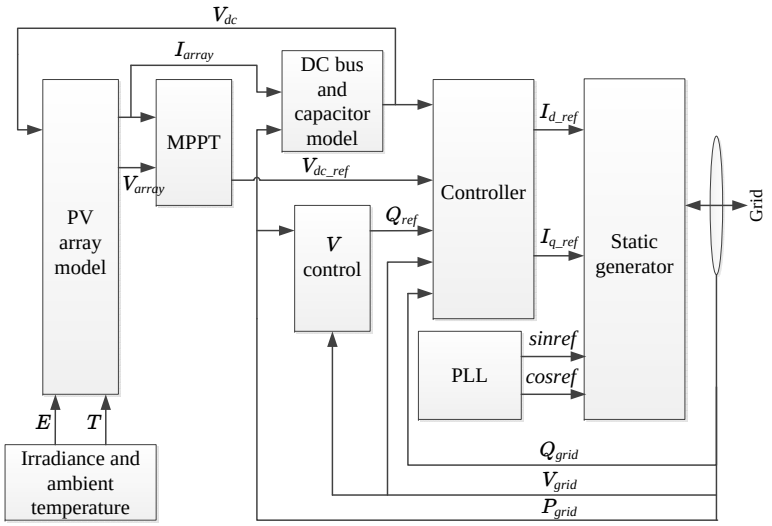

Figure G.1: Simulation model of the PV system.

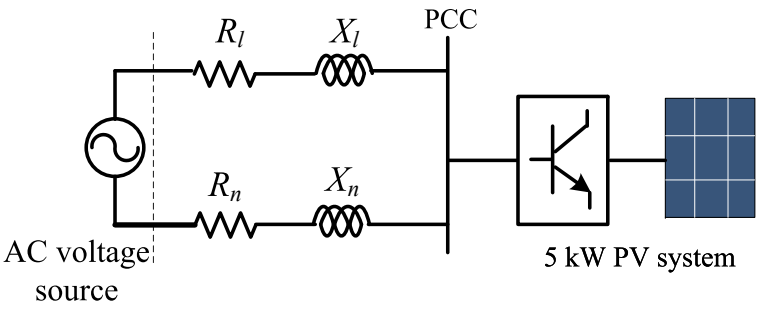

Figure G.2: PV system connected to a voltage source via the test impedance.

PV system, irradiance input and ambient temperature input respectively. $sinnref$ and $cosref$ are the outputs of the phase-locked-loop. The incremental conductance method was used as the MPPT algorithm in the simulation model.

G.2 Flicker Emission From a Single PV System

In order to investigate the flicker emission from a PV system under fluctuating irradiance and ambient temperature conditions, a PV system connected to an AC voltage source through an impedance of $(0.25 + j0.25)\ \Omega$, consisting of a phase impedance of $(0.15 + j0.15)\ \Omega$ and neutral impedance of $(0.1 + j0.1)\ \Omega$, as shown in Fig. G.2 was considered. The impedance values were selected in accordance to IEC Technical Report IEC 61000-3-15. Irradiance and panel temperature fluctuations corresponding to four hour time window of a heavy cloudy day (from 240 minutes to 480 minutes) as shown in Fig. G.3 were used for simulation case studies. The

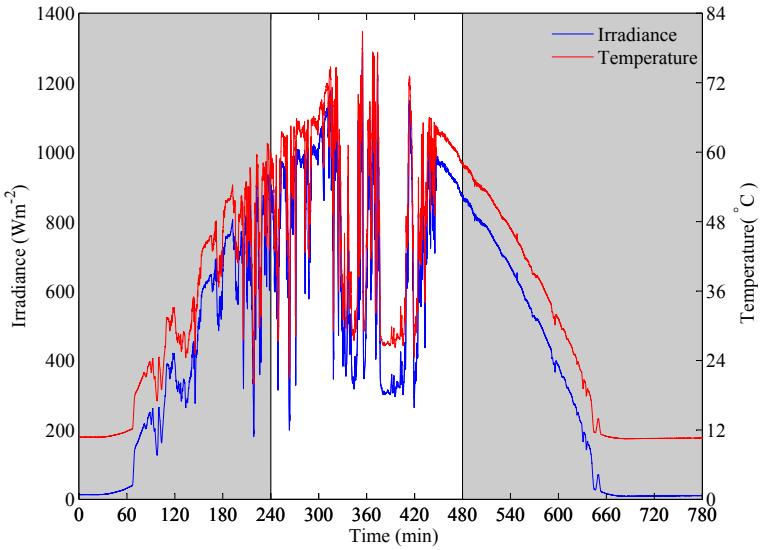

Figure G.3: Fluctuation of irradiation and ambient temperature corresponding to a heavy cloudy day.

short-term flicker severity index was used as the main index to analyse the flicker emission from the PV system. The flicker severity was measured in accordance with the IEC 61000-4-15, using the in-built flickermeter of DIgSILENT PowerFactory. The active power output of the PV system and the PCC voltage together with corresponding flicker emission levels of the PV system are illustrated in Fig. G.4.

According to Fig. G.3 and Fig. G.4 (a), the output power of the PV system can be seen to be co-related to the incident irradiation. An approximate linear relationship between the output power and irradiance was observed, which is slightly affected by the ambient temperature. With reference to Fig. G.4 (b), the voltage fluctuations at the PCC of the PV system can be observed to follow the variation of the output power of the PV system, as expected. The flicker emission from the PV system can be observed to be influenced by the fluctuations in the irradiation. However, the observed flicker severity values are negligible in comparison to the stipulated flicker emission limits for an individual DG unit as given in IEC TR 61000-3- 15[1].

[1]The IEC Technical Report IEC 61000-3-15 stipulates a flicker emission limit of $P_{st} = 0.5$ for all DG units connected to LV distribution networks.

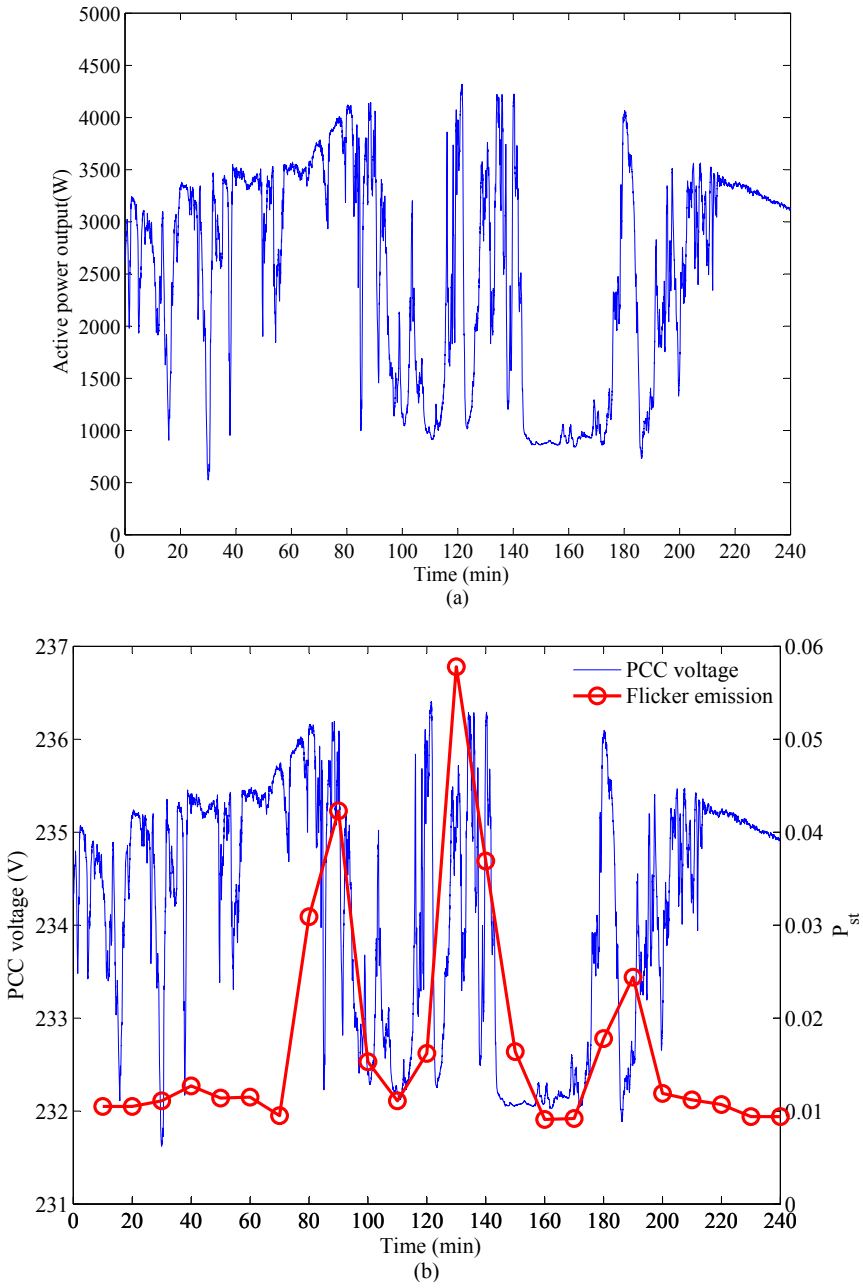

Figure G.4: (a) Active power output from the PV system; (b) Voltage fluctuations and flicker emission at the PCC of the PV system, corresponding to a four hour time window of a heavy cloudy day.

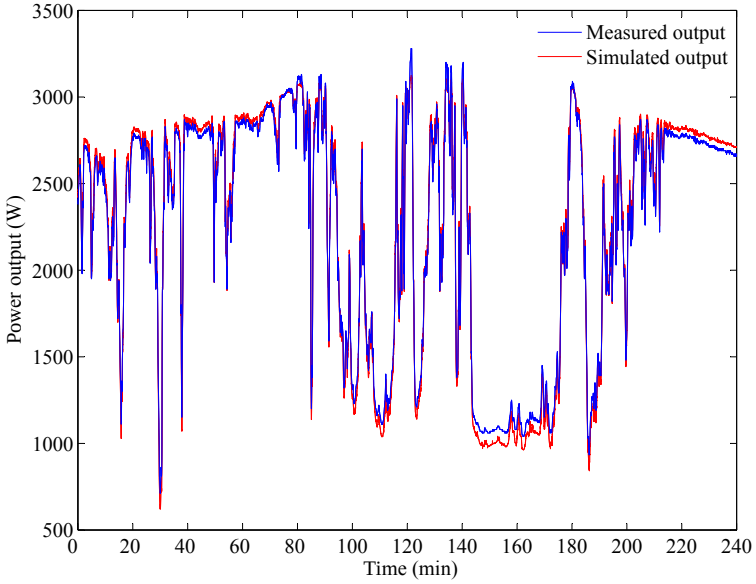

Figure G.5: Comparison of active power output of an actual PV system and the simulation model.

G.3 Comparison of Simulation Model with an Actual PV System

Following the guidelines and the experimental setup specified in IEC Technical Report IEC 61000-3-15, power output of a PV system consisting of a 3.6 kW commercial PV inverter, under fluctuating irradiance and temperature corresponding to the four-hour time window of a heavy cloudy day given in Fig. G.3 has been obtained in Chapter 7. Fig. G.5 provides a comparison between the active power output of the actual PV system and the simulation model developed in this Appendix, where a good correlation between the two systems can be observed. However, according to Fig. G.6, the flicker emission from the actual PV system is significantly different to the flicker values obtained using the simulation, which indicates that other pertinent factors such as the employed MPPT algorithm and control functions (e.g. grid impedance measurements) can also have a significant influence the flicker emission from a PV system.

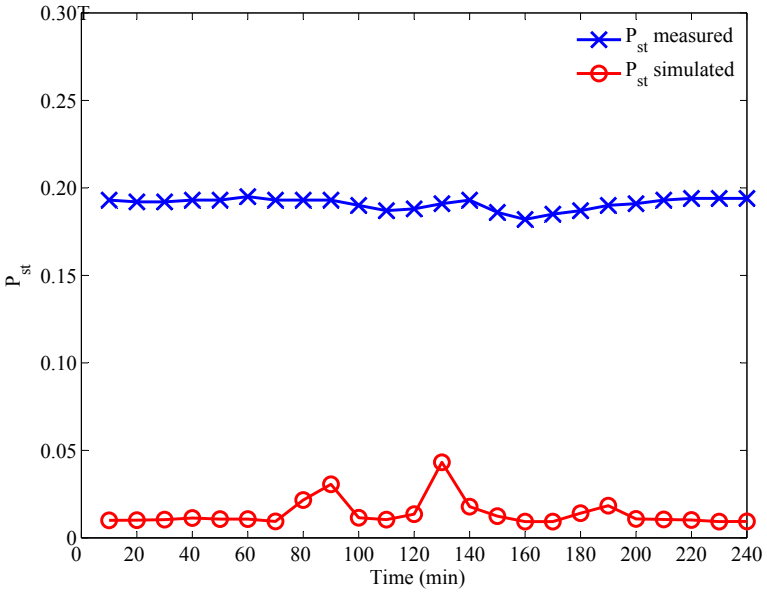

Figure G.6: Comparison of short-term flicker severity of an actual PV system and the simulation model.

G.4 Flicker Emission Investigation in Distribution Networks

In this section, the flicker emission from multiple PV systems distributed across an LV distribution network was investigated by employing the test distribution network given in Fig. G.7. Ten 5 kW PV systems connected across the LV distribution network between Phase A and neutral of the distribution network were considered. The MV/LV transformer has a kVA capacity of 315 kVA and an impedance of $(0.01 + j0.05)$ p.u. referred to the LV side. The impedance of the phase and neutral conductors of the distribution line were selected as $(0.3 + j0.3)$ Ω/km respectively. The length of the distribution line is 300 m. The phase and neutral impedance of the service wire were selected as $(0.054 + j0.038)$ Ω and $(0.01 + j0.01)$ Ω respectively, such that the total impedance in the LV network, experienced by the PV system connected to the end of feeder is equal to the test impedance used in Section G.2. Each PV system was subjected to the same irradiation and panle temperature fluctuations corresponding to the heavy cloudy day given in Fig. G.3 and the active power flow through the MV/LV transformer, voltage and short-term flicker severity index at each terminal of the distribution network were recorded for a period of four hours. Fig. G.8 illustrates the active power flow from the LV network to the MV

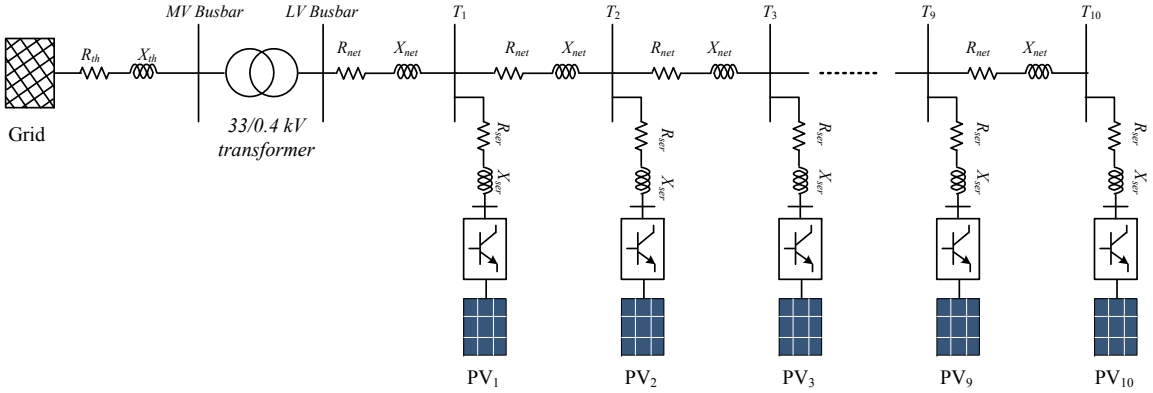

Figure G.7: Simulation model of the test LV distribution network.

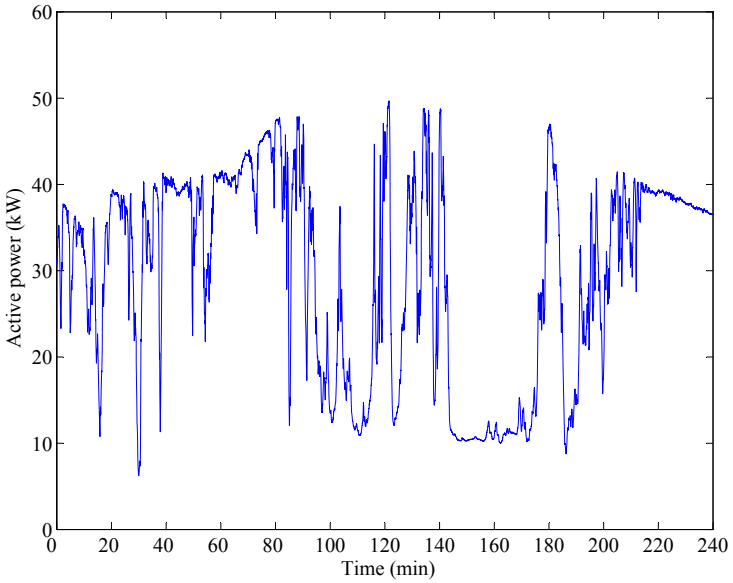

Figure G.8: Active power flow through the MV/LV transformer.

network through the MV/LV transformer. The voltage and the flicker levels at the terminal T_{10} and LV busbar are given in Fig. G.9.

Referring to Fig. G.9, the voltage fluctuation at the end of the feeder (terminal T_{10}) can be observed to be severe compared to the LV busbar. Hence, the flicker levels observed at the LV busbar are significantly less compared to the terminal T_{10}. In comparison to Fig. G.4 (b), the flicker levels at the end of the feeder have increased when multiple PV systems were connected to the distribution network. However, the increment in flicker levels were relatively small, which suggest that the

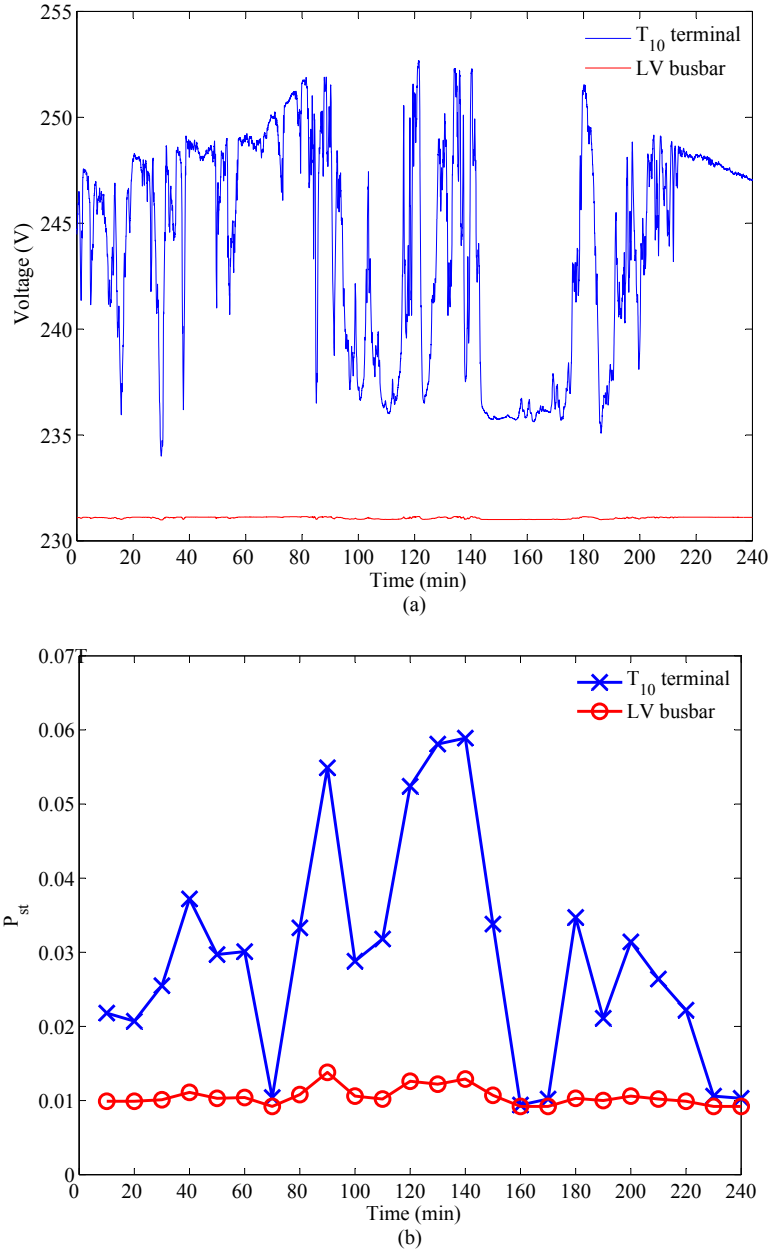

Figure G.9: (a) Voltage fluctuations at different terminals of the network (b) Short-term flicker severity at different terminals of the distribution network.

voltage fluctuations are considerably attenuated among each PV systems.

G.5 Summary

This Appendix investigates the flicker emission from a PV system under fluctuating irradiance and ambient temperature conditions using DIgSILENT PowerFactory. The Appendix reports that although the flicker emission of PV systems can be influenced by the varying irradiation, the recorded flicker levels are insignificant and well below the stipulated limits. In addition, when multiple PV systems are connected across a distribution feeder, flicker is extensively attenuated among different units. As a result, the net flicker level observed at the end of the feeder is significantly less than the flicker compatibility level for LV networks. Based on the observations made, it can be concluded that the fluctuation of irradiation and temperature due to passing clouds alone, may not produce flicker levels which are in excess of network compatibility levels.